Variability of the steering factors for extreme hydrometeorological events in Central Asia and its relation to the formation of mudflows in the piedmont areas of Uzbekistan

Gavkhar Mamadjanova

A thesis submitted to the University of Birmingham for the degree of

DOCTOR OF PHILOSOPHY

School of Geography, Earth and Environmental Sciences
College of Life and Environmental Sciences
University of Birmingham

December 2018

Per Ardua ad Alta

"Through efforts to heights"

Abstract

Mudflows are formed almost every year in Uzbekistan and neighbouring countries which present a major threat to human life and settlements and can significantly damage infrastructure. The central goal of this thesis is to understand mudflow risks that could potentially arise due to the hydrometeorological factors, such as precipitation patterns and precipitation driving mechanisms in synoptic and large scale over Uzbekistan. Empirically developed local synoptic classification (SWT, synoptic weather type) results show that the advection of westerly airflow initiates mudflows more frequently compared to other SWTs. Objective approach (CWT, circulation weather type) outputs show that cyclonic (C), westerly (W) and south-westerly (SW) are the main mudflow generating weather types in Uzbekistan. Statistical modelling of rainfall threshold triggering mudflows also proves that rainfall associated with the C, W and SW weather types group has sufficient magnitude to induce mudflow occurrences.

Risks of mudflows are discussed to increase in the future due to an increase in global population and enhanced anthropogenic activities in previously sparsely populated regions prone to hazardous mudflow events, specifically in mountainous areas. In addition to this, any future potential effect of anthropogenic climate change e.g. increased precipitation intensity and/or changes associated with atmospheric circulation characteristics will increase the potential of disastrous mudflows by impacting on respective triggering mechanisms. Applying well established weather typing and state-of-the-art reveal that mudflow generating large-scale circulation flows will increase by up to 5% to the end of the century. Applying the statistical-empirical transfer function for the important weather types (C, W and SW) inducing mudflows show that mudflow activity will increase in the selected region as precipitation values associated with the CWT C, W and SW flows in Coupled Model Inter-Comparison Project Phase 5 (CMIP5) projection are expected to increase for the target period of 2071-2100.

Dedicated to my beloved parents,

my dearest brothers and my precious sister

Author's declaration

Parts of the Chapters 1-4 are adapted from the following research article published in the Journal of Natural Hazards and Earth System Sciences.

Mamadjanova, G., Wild, S., Walz, M. A. & Leckebusch, G. C. 2018. The role of synoptic processes in mudflow formation in the piedmont areas of Uzbekistan. *Natural Hazards and Earth System Sciences,* 18**,** 2893-2919.

Data collection and analysis, visualisation and writing the initial manuscript were done by GM. GCL supervised and directed the research and contributed to the analysis and design of the findings of this work and participated in the revision process of the paper.

SW contributed to the Circulation Weather Types algorithm in FORTRAN programming language. MW constructed Logistic Regression function in R language.

Chapters 5 and 6 of this thesis is prepared for the publication in the Journal of Climate.

Data analysis performed in this thesis has been carried out by GM using Blue-BEAR (Linux HPC) service provided by University of Birmingham and LES-Linux-FS servers of the College of Life and Environmental Sciences at the University of Birmingham.

Acknowledgements

"When you are grateful, fear disappears and abundance appears."

Anthony Robbins

I am deeply grateful to Dr Gregor Leckebusch, who read my research proposal in early 2014 and accepted to be my lead supervisor. I am thankful to him for giving me enough time and freedom to explore the thesis subject, for his prompt feedbacks and inputs, for his major contribution on the subject matter, for the many subject related discussions, and patient supervision all these years.

My sincere thanks to all my PhD colleagues from Meteorology and Climate group namely Simon Wild, Mohammad Alharbi, Michael Walz, Daniel Befort and Nicolas Otto Kirchner for their respect and understanding and for supporting me when I was struggling with very basic practicalities in programming the climate data. I am also thankful to my co-supervisor Dr Martin Widmann for his inputs related to statistical methods. I am grateful to Simon Wilson from the IT Services of College of Life Sciences (LES), University of Birmingham, for his timely support and professionalism in troubleshooting with the Linux HPC when I could not run my scripts on LES-Linux servers in my final year of PhD study.

I would like to acknowledge Professor Lee Chapman and Dr Reinhard Schiemann for taking the time to examine this thesis and for their constructive feedbacks. I am also thankful to Gretchel Coldicott and Jamie Peart from the School of GEES for the excellent administrative support in the department.

My deepest gratitude is to the Islamic Development Bank (IDB) for awarding the PhD scholarship. I am also thankful to ECMWF, CEDA and CERA for the available reanalysis and climate model dataset used in this thesis. I am also very grateful to Uzhydromet (Centre of Hydrometeorological Service of the Republic of Uzbekistan) for sharing the mudflow and climate data.

I would also like to thank late Professor Gennady Nikolayevich Trofimov at the National University of Uzbekistan (NUUz), an expert par excellence in mudflow rheology and dynamics in Uzbekistan and Central Asia. Professor Trofimov continued to guide me on the subject till the last days of his life with cancer in 2015. Rest in peace dear Gennady Nikolayevich. The next appreciation goes to late Professor Takhir M Mukhtarov (NUUz) an experienced climatologist, who encouraged me to understand the subject of synoptic processes and weather circulation over the Central Asia. May his soul rest in peace.

I am indebted to Professor Boris K Tsarev from the Hydrometeorological Scientific and Research Institute at Uzhydromet for giving me the idea to investigate the link between mudflow occurrences and synoptic weather types while I was a MSc student

at NUUz. I want to express my deep gratitude to my experienced colleagues from Uzhydromet Irina Zaytseva, Fatima Kasimova, Lidiya Em, Lyudmila Nesterova, Nadezhda Belorussova for their endless encouragements and for sharing with me their knowledge which helped me to explore the weather and climate over Uzbekistan and Central Asia. I am also very grateful to all my generous friends and colleagues from Uzhydromet Mukaddam, Gulnoza, Raushana, Katya, Natasha, Victoria, Mahmuda and Sherzod for their constant support despite the restrictions on distance and time.

I am deeply grateful to Professor Fazliddin Hikmatov and Dr Zukhra Sirliboyeva from NUUz who took out the valuable time to discuss the hydrological aspects of the study area which enriched my work.

A few warm words for my great friend Indrani Mahapatra with whom I shared moments of my happiness and deep anxiety since the very first days of my PhD life. She showed me true friendship by encouraging me in every matter, the time of the day, she was there with me when I was sick or when I needed urgent financial help. I am also very grateful to her for reading my thesis so that major errors in compilation and representation could be minimised. Her constant support can never be forgotten.

I thank my kind and wonderful friends Marie, Priutchada and Hien who were sharing the corner in Geography Room 325 on my right and left sides and generously offered me to try vegan foods and traditional Thai and Vietnamese dishes and because of them I had some of the best lunch breaks in my PhD life. Their warm auras kept me happy and helped me to study peacefully.

I would like to thank Kefayat for taking the time to hike and explore the English heritage across the South East of the country, an amazing land of coastal castles. The most impressive and best preserved castles (Rochester Castle, Dover Castle, Walmer Castle, Leeds Castle) with their charming gardens, unique remains of Lullingstone Roman Villa, the world heritage Canterbury Cathedral, 1066 Battle of Hastings as the symbol of triumph, all this, and much more, inspired and enriched my PhD life. The breathtaking sea views with immensely significant and delightful places of England's history filled my heart with peace and ability to power through the difficulties.

Finally, none of this would have been possible without the endless support and love of my parents Akhmatkhon and Munojat, my siblings Ziyovuddin, Alisher and Gulnoz and their families. The unconditional love of my nieces, Naima and Rayona, and my sweet nephew Davronbek has given me the extra strength and motivation to complete this work despite the challenges.

Contents

List of Figures

List of Tables

Abbreviations

ADRM	Antecedent Daily Rainfall Model
AOGCM	Atmosphere-Ocean General Circulation Model
CA	Central Asia
CDO	Climate Data Operators
CEDA	Centre For Environmental Data Analysis
CERA	Climate and Environmental Retrieval and Archive
COSMO-CLM	Consortium for Small-scale Modelling – Climate Limited area Modelling
CMIP5	Couple Model Intercomparison Project 5
CWT	Circulation Weather Type
CORDEX	Coordinated Regional Climate Downscaling Experiment
ECMWF	European Centre For Medium-Range Weather Forecasts
GCMs	Global Circulation Models or Global Climate Models
LOCI	Local Intensity Scaling
LS	Linear Scaling
LRM	Logistic Regression Model
NCEP	National Centers for Environmental Prediction
PT	Power Transformation Method
RCMs	Regional Climate Models
RCP8.5	Representative Concentration Pathway High Emission Scenarios
SWT	Synoptic Weather Type
SRTM	Shuttle Radar Topographic Mission

Chapter 1 Introduction & Statement of Aim & Objectives

"Anyone can build a fast CPU. The trick is to build a fast system."

Seymour Cray

1.1. Introduction

1.1.1. Definition of mudflow

Why mudflows not landslides?

In English "landslide" is a generic term (Takahashi, 2007) for the variety of mass movement of soil associated with geologic, topographic, climatic (Clague and Roberts, 2012) and anthropogenic (Sidle and Ochiai, 2006) factors which can be further categorize according to failure mechanism, water content and flow speed (Varnes, 1958, Hungr et al., 2014).

The concept of landslide classification devised by Varnes (1958) has been found to be simple and the most used by worldwide researchers and geoengineers (Hungr et al., 2014, Takahashi, 2007). The definition of "landslide" in Varnes classification encompasses five main modes of slope

movement (falls, topples, slides, spreads, and flows) including three broad material divisions (rock, debris, and earth) (Table 1.1). Varnes created a sixth group of landslides - "complex slopes" which includes combinations of two or more different types of movement.

Poorly researched earthquake induced mass movement processes on the seabed or underwater known as submarine landslides (Prior et al., 1989, Yincan and et al., 2017) and which are responsible for causing tsunamis that damage coastal areas, is a type of landslide not classified by Varnes. Landslides have also been identified on terrestrial planets, such as Mercury, Venus and Mars (Bulmer, 2012).

This thesis will not detail on landslide types and characteristics, however, the ***terminology of mudflow*** which is related to the fifth group of Varnes classification will be defined here as the thesis is focused on this phenomenon and as they pose considerable risk to people and cause significant material losses in Uzbekistan (the thesis author's birth country).

Bull (1964) reported that the ***term of mudflow*** was used for the first time in McGee (1896) studies on Sonoran district slopes in US. Blackwelder (1928) in his studies on extreme flows in semiarid mountains in Utah described mudflow as a type of flow which was a phenomena in between landslide and ordinary stream-floods which contains enough water to swell the clay colloids

and silts reducing internal cohesion making the mass slippery. Nobles and Sharp (1953) proposed mudflow to be a type of debris flow in which the mud, even though not necessarily quantitatively predominant, has a specific nature of flowage and appearance depending on the factors which differ it from flows of debris devoid of mud. Authors report that the flowing nature of mudflow occurrence early May in 1941 at Wrightwood, Southern California, was *"light gray and mushy to soupy consistency just like freshly mixed concrete, much of it consisted of silt, sand, and pebbles less than 1 inch in diameter and with a rough surface velocities from 300 to 120 cm per second"* (Nobles and Sharp, 1953).

Table 1.1. Varnes classification system of landslides (adapted from Hungr et al. (2014)).

Group	Movement type		Rock	Debris	Earth
1	Fall		1. Rock fall	2. Debris fall	3. Earth fall
2	Topple		4. Rock topple	5. Debris topple	6. Earth topple
3	Slide	rotational	7. Rock slump	8. Debris slump	9. Earth slump
		translational	10. Block slide	11. Debris slide	12. Earth slide
4	Lateral spreading		13. Rock spread	-	14. Earth spread
5	Flow		15. Rock creep	16. Talus flow	21. Dry sand flow
				17. Debris flow	22. Wet sand flow
				18. Debris avalanche	23. Quick clay flow
				19. Solifluction	24. Earth flow
				20. Soil creep	25. Rapid earth flow
					26. Loess flow
6	Complex		27. Rock slide-debris avalanche	28. Cambering, valley bulging	29. Earth slump-earth flow

Rickmers (1913) gives excellent photos of mudflows in the Turkestan ranges of the Zerafshan valley (in modern day Central Asia) by describing them under the name "mudspates… which is frequently in Alai-Pamirs" (Figure 1.1). The author in his book "*The Duab of Turkestan"* (pp.194–195) says:

> *"When a gentle slope of grit and shingle has been soaked like a sponge by rain or melting snows there may come a time when it bulges out and slides off… Slipping into channels and gullies this mass is mixed with more water, attains a higher speed and carries away soft material as well as rocks which it finds on its way. It is during this descent that the mudspate generally acquires its characteristic composition, for only by movement can an even mixture of liquid and solids be maintained. It is neither dry nor is there much free water, but the whole mass appears like a rapid flush of mud, although frequently the rock waste is so rough as not to suggest what is popularly called mud."*

Iverson (2014) reports that Rickmers' term "mudspate" has faded from use in the English language over the past century and the author proposes the use of the term debris flow based on Rickmers' view to describe mudflow like phenomena.

Figure 1.1. Rickmers (1913) notes a steep channel as a "mudspate-track" within which mudflows move in surges down in Veshab (nowadays in Tajikistan) in the Zerafshan Valley (from "The Duab of Turkestan" page 199).

In some papers mudflows are also called mudslides (Figure 1.6 d-e) due to the phenomenon of movement of soil mass *"by shearing on slopes considerably flatter than those corresponding to limiting equilibrium for residual strength on the sliding surface and ground water coincident with and flowing parallel to the slope surface"* (Hutchinson and Bhandari, 1971). Large mudflows are referred by the Indonesian term "lahars" which may occur during volcanic activity ("hot lahars) or without eruption ("cold lahars") due to the hydroclimatic factors (Hungr et al., 2014) defined as pyroclastic flow (Yamao et al., 2016) in the literature.

In recent studies **mudflow** is considered as a subclass of debris flow containing mixture of water and grains of various sizes ranging from about 0.1μm to above 200 mm (Table 1.2) which flows in to mountain streams after heavy rainfall (Coussot, 1997) (Figure 1.6 a).

Table 1.2. Grain size classification based on data used by the International Society of Soil (from Coussot (1997)).

Clay	Silt	Fine sand	Coarse sand	Gravel	Pebbles	Boulders

2μm 20 μm 200 μm 2 mm 2 cm 0.2m

Increasing particle diameter ⟶

Hungr et al. (2014) use the term **mudflow** to describe a very rapid, sometimes extremely rapid, surging flow of saturated plastic soil in a steep channel involving significantly greater water content relative to the source material. Based on controlling parameter, i.e., the Plasticity Index (I_p) of the material, authors gradated the boundary between debris flow ($I_p < 0.05$) and mudflow ($I_p > 0.05$ and $I_p > 0.5$).

Based on information available in the literature relevant to the terminology of mudflow this thesis means mudflow to be a flowage in which the water content reaches up to 60% and has large amount of soil and silt particles that

moves down with a maximum velocity of 25-30 m/s depending on the terrain topography (Žic et al., 2015). The speed of the fluid is highly affected by the density and viscosity of particles and this reason will not allow a phenomenon to flow as far as a streamflow. Mudflows are most common in arid and semiarid regions (Blackwelder, 1928) and it causes great damage to life and property.

1.1.2. Mudflow studies in Uzbekistan

1.1.2.1. Soviet and post-Soviet period

Fleishman (1978) contributed the term "selevie potoki"[1] ("селевые потоки" in Russian) which means debris and mud flows in Soviet literature which is still used as the main terminology for hazard flows in post-Soviet countries including Uzbekistan. "Sel" cannot be fully equivalent to landslide as the author does not consider the mechanism of other types of landslide associated with topples, dry flows and falls which are included in Varnes classification. Fleishman (1978) classification is easy to understand as the author mainly focuses on velocity, concentration of solids and plasticity of the mass movement (Figure 1.2).

[1] "sel" ("сель" in Russian and Uzbek) originated from the Arabic word of "sayl" (turbulent flow)

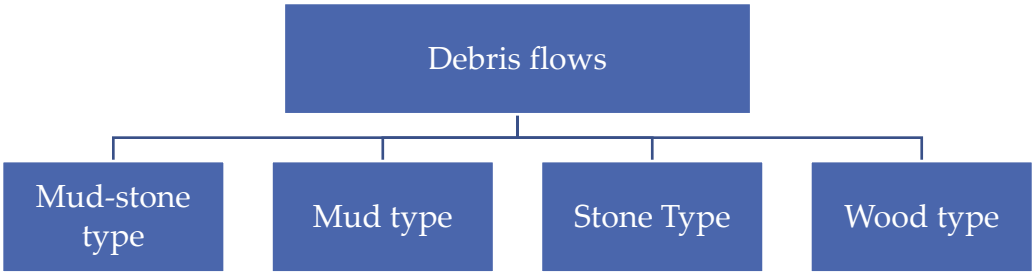

Figure 1.2. Fleishman classification of debris flows used in Soviet studies.

The first mudflow susceptibility mapping effort depicting the areas prone to mudflow occurrences in Uzbekistan was investigated by Kochergo in 1960. Such mudflow hazard zonation map (Figure 1.3) was included in the encyclopaedia of Soviet Uzbekistan in 1982 by Babko (Perov, 2012). Geographical information system (GIS) was widely used in the mudflow database and mapping stage (Figure 1.4) by the next generation of scientists (Trofimov, 2006). A national database of mudflow occurrences was generated and published as catalogues during the Soviet (Kudishkin et al., 1967) and post-Soviet periods (Chub et al., 2007). Mudflow rheology, dynamics and various other hydrogeological characteristics of mudflow hazards in Uzbekistan were carried out by Karpov et al. (1976), Trofimov (2006), Chub et al. (2007) and others (e.g., Karpov and Pushkarenko (1968), Babko (1978), Tulyaganov (1988), Isakova et al. (2009), Niyazov and Nurtaev (2013), Niyazov and Nurtaev (2014), Juliev et al. (2017), Juliev et al. (2019)). Climatologists such as Salikhova (1975) and Lyakhovskaya (1989) predicted mudflow occurrences

in river basins and mountain areas of Uzbekistan based on analysis of synoptic circulation and remote sensing data. Mudflow occurrences under climate change conditions was investigated by Chub (2007).

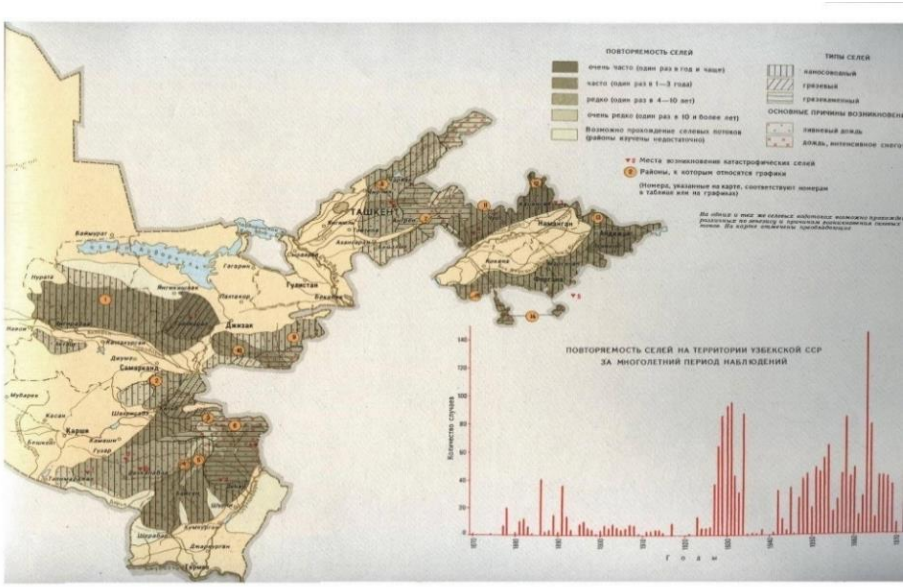

Figure 1.3. Mudflow map of Uzbekistan by Babko illustrated in 1982.

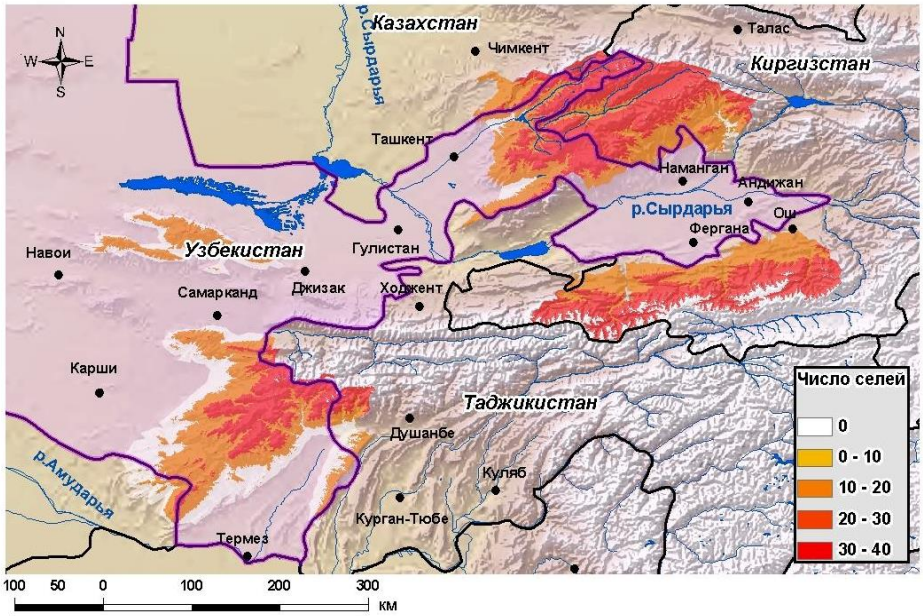

Figure 1.4. Mudflow susceptibility map of Uzbekistan using GIS tools (Trofimov, 2006).

1.1.2.2. Mudflow studies in this thesis

Mudflows are amongst the most damaging and deadly natural hazards in Uzbekistan. Data from the Centre of Hydrometeorological Service of the Republic of Uzbekistan (Uzhydromet) suggests that mudflows were responsible for over 38 deaths and damaged approximately 3000 households and 5000 ha of the agricultural crop over the decade (2005–2014) in Uzbekistan (Table 1.3, Figure 1.5). However, the incidence of damage may be much larger as these events commonly occur in mountainous areas, in incised valleys and in areas of otherwise low relief.

In the river basins of Uzbekistan, mudflows generally occur during the periods of intense rainfall or rapid snowmelt. The consistency of the mudflow is mainly water and mud (liquidity index >0.5, e.g. Hungr et al. (2001)) with loose rock and other fragments, which flows down the hills and through the mountain streams (Figure 1.6 a). The destructive power of a mudflow can be greatly increased moving downhill due to the accumulation of water and rocky mud. It can destroy riverbeds and banks of rivers, floodplains and even low terraces above the floodplain and other objects in its path (Chub et al., 2007) (Figure 1.6).

The period of historically documented mudflow events confirms that the areas with a high passage of mudflow occurrences in Uzbekistan can be divided into

five regions: Fergana Valley, the Zerafshan basin included in Zerafshan Valley, the Surkhandarya, the Kashkadarya and the Chirchik-Akhangaran rivers' basins (Figure 1.5). From a geological point of view, mountain ranges (western part of the Pamir-Alai system and western Tien-Shan) of the study area are mainly composed of Palaeozoic limestones, granites, schists, marbles, sandstones, conglomerates and partly igneous rocks (Petrov et al., 2017) as well as shale and loess deposits forming weak surfaces of the low relief hillslopes, especially in Fergana Valley, that are frequently prone to sliding due to the interaction with water.

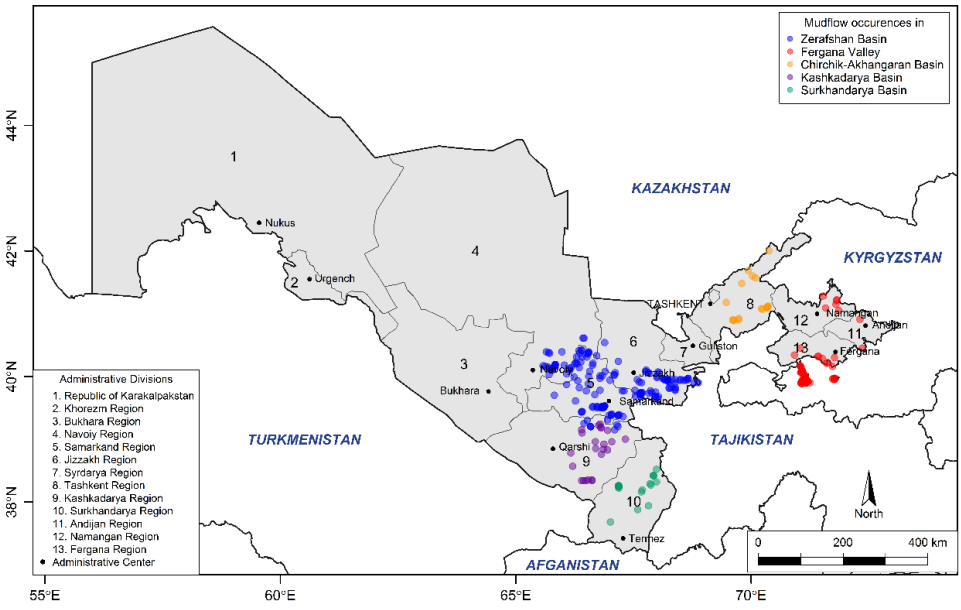

Figure 1.5. Mudflow occurrences for the years 2005-2014 in areas with high probability of mudflow passage in Uzbekistan: Zerafshan basin (blue dots) in central part of the country; Fergana Valley (red dots) in the east; Chirchik-Akhangaran basin (orange) in the north-east; Surkhandarya (green) and Kashkadarya (violet) rivers' basins in the south of Uzbekistan. Map also represents political administrative divisions and administrative centers/cities of the country.

Precipitation is an important mudflow trigger (Huggel et al., 2012) in Uzbekistan; however, snow cover and glaciers in mountain regions (Petrov et al., 2017), slope instability and temperature (Huggel et al., 2010) are additional factors. Other main factors such as antecedent rainfall (Glade et al., 2000, Sidle and Ochiai, 2006) and rapid snowmelt (Kim et al., 2004) may further reduce the slope stability, thereby enhancing potential of mud and debris flow occurrences.

Rainfall records in high mountain regions are limited, reflecting the limited number of meteorological stations in Uzbekistan; thus there are gaps in the rainfall and mudflow data due to missing spatial and temporal information. Furthermore, orographic effects on precipitation may not be captured adequately by a single (or a few) rain gauges (Huggel et al., 2012). In the Alps, precipitation is generally observed in mid- to high-elevation areas (Buzzi et al., 1998, Huggel et al., 2012), similar to the mountain ranges (Tien-Shan, Alai and Pamir) in Central Asia (CA); however, mudflows usually occur in lower to intermediate elevations. Reviews on precipitation thresholds triggering landslides indicate the magnitude of an extreme event (Glade, 1998, Guzzetti et al., 2008) depends on the rainfall intensity and duration (Caine, 1980), the local climate and orographic precipitation (Buzzi et al., 1998, Gheusi and Davies, 2004), the geomorphologic structure of the area (Rosi et al., 2016), soil

characteristics (Yamao et al., 2016) and land use (Sidle and Ochiai, 2006, Gravina et al., 2017).

Table 1.3 Mudflow disasters causing fatalities and other relative damages over the period 2005-2014 in Uzbekistan (Data source: Uzhydromet).

Year	Number of deaths	Number of households damages	Livestock head counts	Infrastructure damages					Agricultural crops			
				Highways (km)	Local bridges (count)	Hydrologic bridges or tools	Schools (count)	Other (count)	Cotton fields (ha)	Wheat fields (ha)	Gardens (ha)	Other (ha)
2005		860			1			2	200	69		
2006	7	175						2	152	165	118	22
2007		8	1	6	15	7		3		2		6
2008	7	413	1	0.3	5			49	747	261		123
2009	8	498	80		14	5	2		966	834	56	18
2010	8	41			6		2	7		5		3
2011	2	94	50	0.5		1		52	483.5	318.6	0.12	10.1
2012	5	773	3	2.7	25	6	1	55				
2013	1	31		0.012	2	6		3				200
2014								4				
Total	38	2893	135	10	68	25	5	177	2548	1655	174	382

Figure 1.6. Photographs show mudflow events occurred in Samarkand[2], Kashkadarya[3] and Surkhandarya[4] regions due to the intense rainfall between 13-14 May and 18-23 May 2018: mudflow passage in a small mountain river (a); damages in small scale agriculture after mudflow passages (b, c), mudslides (d, e), damages in a village road and bridge during the mudflow occurrence (f).

[2] https://kun.uz/uz/news/2018/05/20/surhondareda-emgir-korga-ajlandi-dareda-kizil-va-sarik-lojka-okmokda
[3] http://xs.uz/uz/post/qashqadaryo-viloyatida-yuz-bergan-sel-toshqinlari-talafotlari-foto
[4] https://fvv.uz/uz/news/sel-oqibatlari-bartaraf-etildi-/?&page=270

1.1.3. Climate Modeling

General Circulation Models also known as Global Climate Models (GCMs for both) represent fundamental global scale dynamic physical processes of the Earth's atmosphere, ocean and land surface. GCMs are based on equations of numerical weather prediction (NWP) used to simulate changes in global climate system due to temporal (annual to century) changes in greenhouse gas (GHG) concentrations. State-of-the-art GCMs are coupled atmosphere-ocean models (AOGCMs) representing key components of atmospheric system (such as water vapour, effects of aerosols) and ocean along with sea ice and land-surface.

GCMs are structured in a three-dimensional (more precisely four-dimensional) where dynamic core components of each system are parameterised. GCMs have a horizontal resolution between 1 and 5 degree in latitude and longitude (about 100-600 km) and 10-20 vertical atmospheric layers and up to 30 layers considering ocean. New generations of GCMs have improved the spatial resolution from about 500 km in 1990 (FAR - First Assessment Report) up to 110 km in 2007 (AR4 - Fourth Assessment Report). Moreover, state-of-the-art CMIP5 (Taylor et al., 2012) multi-model projection used in the IPCC (Intergovernmental Panel on Climate Change) Fifth Assessment Report (AR5) has a finest horizontal resolution in the atmosphere of around 70 km with 20-50 atmosphere levels. Average spatial resolution or horizontal size of grid cells of about 200km is used widely. In addition to horizontal resolution, GCMs have a temporal resolution

i.e., “virtual weather stations” located at grid intersections and are typically run with time steps in the range 0.5 - 3 hours.

Standard emissions scenarios presented in IPCC reports are used by the climate modelling community as input for GCM simulation and to make projections of possible future changes in climate system. These families of emissions scenarios have become more comprehensive with over the years. The SA90 original emission scenarios were replaced by the IS92 in the 1990s. Thereafter, the integrated assessment modeling community developed the Special Report on Emissions Scenarios in 2000 (SRES) which were in turn succeeded by the Representative Concentration Pathways (RCPs) in 2010 (Hayhoe et al., 2017).

The present generation of GCMs, though have the ability to predict climate change, are associated with significant uncertainty with regard to future climate projections, especially at the regional scale. There are three distinct sources of ***uncertainties*** in climate projections: 1) natural variability, 2) model-response, and 3) emission-scenario (Hawkins and Sutton, 2009, Knutti and Sedláček, 2012, Deser et al., 2012). ***Natural fluctuation*** of climate system is an unforced component of any evolution in climate and is irreducible for a decade or so for the longer-term trends (Hawkins and Sutton, 2009, Deser et al., 2012). ***Model uncertainty*** known as response uncertainty arise from incomplete understanding of natural processes and system and their representations in models (Knutti et

al., 2017). Therefore, multiple models are developed in various research institutions with the aim to simulate similar experiments (e.g. CMIP5 projection), where individual developer make different but plausible choices of the processes represented in their model (Parker, 2006, Knutti and Sedláček, 2012). ***Uncertainty in future emissions*** of greenhouse gases due to uncertainty in pathways of social and technological development thereby increasing uncertainty in future radiative forcing (Hawkins and Sutton, 2009). Such uncertainty is generally addressed by making projections (rather than predictions) conditional on an emission scenario (Knutti et al., 2017).

1.1.4. Downscaling of GCMs output and underlying assumptions

Atmosphere–ocean coupled Global Climate Models (GCMs) simulate the past, present and future global climate on the bases of different climate change scenarios. GCMs have typically coarse resolutions (~200 km) and hence they have limited in its capacity to account and capture sub-grid or convective scale parameters (Wilby et al., 1998, Kendon et al., 2017). Thus, downscaling techniques are needed to bridge the issue of representativeness from the large coarse spatial resolution of a GCM to the smaller scales (Maraun and Widmann, 2018) or even at the station scale (Kumar et al., 2014). Hence, different downscaling techniques have been developed and they are broadly grouped under statistical and dynamical approaches.

Statistical downscaling, also known as "empirical/statistical" or "statistical/dynamical" uses statistical relationships to transform a GCM data from large scale coarse resolution to finer resolution. The large scale atmospheric variables, e.g., sea level pressure, geopotential height, precipitation, temperature, solar radiation, humidity and wind are employed as "predictors" to regional or local climate variables named "predictands" (Maraun et al., 2010, Smid and Costa, 2018). The idea of statistical downscaling is expressed by Fowler et al. (2007) in the following equation:

$$R = F(X) \qquad (1.1)$$

where R is the local climate parameter which is subject to downscaling, X is the large-scale variable or GCM data, and F is a function related to *R* and *X* which is being validated by the use of observation or reanalysis data.

The performance of statistical downscaling approach depends on the choice of domain (Wilby and Wigley, 2000) and applied techniques which are generally classified into regression models, weather typing schemes and weather generators (Fowler et al., 2007) each covering a range of methods (Figure 1.7). Reyers et al. (2013) study is a good example of weather typing approach using statistical-dynamical downscaling in which authors evaluated future changes of large scale atmospheric circulation over Central Asia and its impact on rainfall pattern in mountain areas of the region.

Strengths and weaknesses of statistical downscaling methods have been discussed in Wilby et al. (1998), Fowler et al. (2007), Maraun and Widmann (2018), Smid and Costa (2018). The key strength of statistical downscaling approach is that is easily transferrable to other regions and can be used to derive climate parameters not available in RCMs. However, it requires a long-term and reliable observed data for bias correction. The main weakness of statistical downscaling is that it may underestimate the observed variance and represent extreme weather events poorly.

Dynamical downscaling rely on data and physical processes which are dynamic in nature and is similar in formulation to a global GCMs but at a higher resolution (from 25-50 km up to 5 km) which span a limited regions (Kendon et al., 2014). Dynamically downscaled data has been applied by Ozturk et al. (2012), Ozturk et al. (2017) and Altinsoy et al. (2013) to assess future changes in seasonal mean temperature and precipitation for the Central Asia domain using CORDEX (Giorgi et al., 2009) and RegCM4 (Giorgi et al., 2012) regional climate models.

Although dynamical downscaling allows the user to model very high resolution experiments and provide robust results for regional climate, the process entails increased computational cost, needs large and comprehensive dataset and high level of skills and expertise to interpret the results (Smid and Costa, 2018). Moreover, these experiments require high frequency GCM outputs for boundary

conditions. Due to these practical limitations, the regional dynamical downscaling models at kilometre-scale resolution remain out of reach for many researchers, especially researchers in developing countries. In such cases, statistical downscaling proves to be an advantageous and is useful alternative for impact studies where issues with computational capability, technical expertise or limited time exist (Trzaska and Schnarr, 2014).

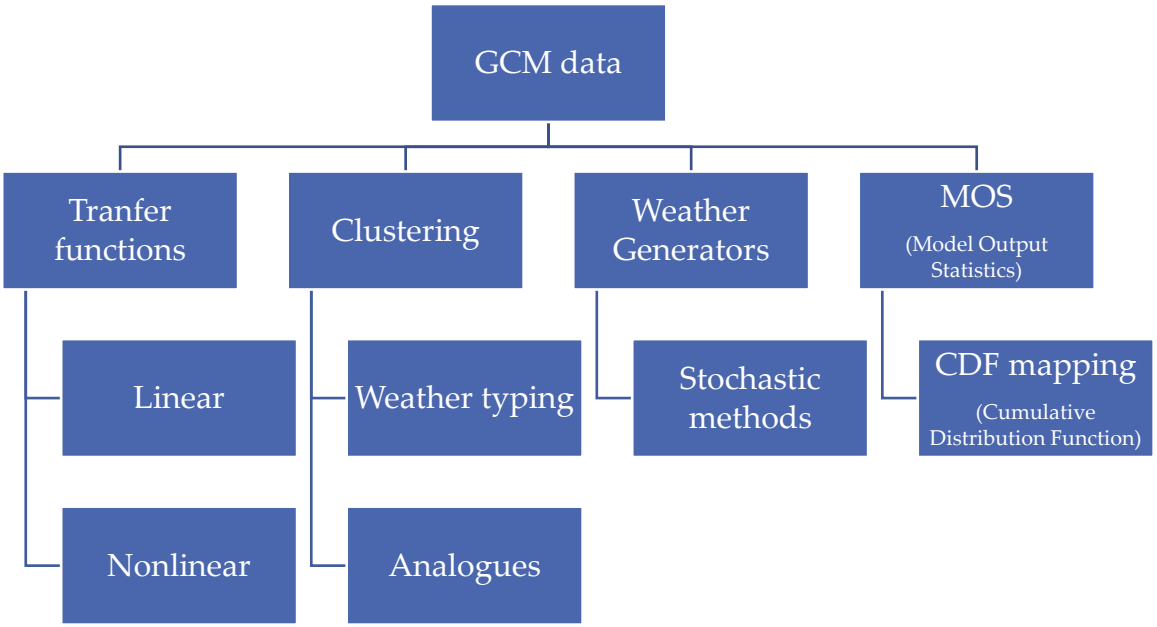

Figure 1.7. Statistical downscaling methods (adapted from Smid and Costa (2018)).

1.1.5. Manual and automatic weather circulation type classification

Classifications of large and synoptic scale circulation systems have more than a century long history; the earliest classification of the complete pressure pattern over the North Atlantic and Western Europe was developed in 1895 by Van Bebber and Köppen. Through subjective manual procedures, authors distinguished five main weather types and twenty subtypes in relation to the position of anticyclonic and cyclonic movements from the earlier studies of Van Bebber (Barry and Perry, 1973). Since then many regional synoptic classifications of pressure and circulation fields have been developed. Based on the major centre of action and pressure distribution at the surface (Baur, 1936; 1951) and in the middle troposphere (Hess and Brezowsky, 1952), the concept of Grosswetterlagen (GWL, Hess and Brezowsky, 1969) was developed and applied to areas in Europe and eastern part of North Atlantic Ocean. The Grosswetterlagen (GWL) catalogue has a set of 29 synoptic weather patterns each with a specific definition.

Yoshino, in 1968 depicted a weather catalogue including six main circulation types and a total of fifteen subtypes comparable to GWL catalogue for eastern Asia (Barry and Perry, 1973). Another very ambitious endeavour of defining weather circulation based on trajectory of anticyclones along three major axes (normal polar, ultra-polar and Azores normal) to the territory of post-soviet countries has been carried out by Mul'tanovski (1933). Lamb (1972) developed a

synoptic scheme calendar of 27 possible weather types and categorised them into seven principle types (anticyclonic, cyclonic, northerly, easterly, southerly, westerly and north-westerly) of weather regime over the British Isles (Jones et al., 2014).

A classification of eleven individual synoptic systems for the Central Asia prepared by Giorgio and Bugayev (1936) and Bugayev et al. (1957) based on overall movement of air masses associated with anticyclone and cyclone tracks in synoptic scale.

The advances in computing and increased sophistication in meteorological tools in recent decades have allowed for the development of global reanalysis datasets in a regular grid and these have played a significant role in transfer of manual schemes to automated synoptic classification methods (Sheridan, 2002, Vallorani et al., 2018). Huth et al. (2016) documented fifteen objective classification techniques that were collected in the COST (European Cooperation in Science and Technology) Action 733 database and evaluated the extent to which the classifications could be used to perform the weather system over the Europe. It is worth saying here that the wide range of automotive algorithms for classifications of weather regime is a key factor for the assessment of their potential applicability (Vallorani et al., 2018) in identification of frequencies of climate variables associated with weather system.

1.2. Research gap

Experts believe that mudflow and landslide risks will increase in the future due to the major reasons (Sidle and Ochiai, 2006, Clague and Roberts, 2012) of large increase in global population and widespread anthropogenic activities in previously sparsely populated mudflow and landslides prone regions, specifically in mountainous areas. These twin factors are postulated to significantly affect the magnitude, reactivation and frequency of landslide types that occur in many parts of the world. Furthermore, future potential effect of climate change characterised by increases in temperature, total precipitation and rainfall intensity associated with atmospheric circulation characteristics will increase the triggering mechanisms for landslides.

Population in Uzbekistan is forecasted to grow over the rest of this century (UN, 2017) with associated increase in human settlements and land use activities in piedmont and mountain zones. However, it is beyond the scope of this thesis to discuss in detail the whole mechanism of mudflow occurrences in Uzbekistan taking into the consideration socio-economic-behavioural and policy aspects. The focus of this thesis is mudflow response to atmospheric conditions notably, major weather types and its cross linkages with precipitation climatology initiating mudflow events in the study area. Moreover, there are relatively few studies or peer-reviewed publications from English literature that have

investigated atmospheric precursors of mudflow occurrences in Uzbekistan and Central Asia. To the best of knowledge, there is no study that examines the association between major weather patterns and mudflow occurrences in Uzbekistan and Central Asia under current and future climate conditions by running successive generations of atmospheric reanalysis and multiple climate models. The research presented in this thesis highlights the importance of studies investigating the association between atmospheric circulation and mudflow occurrences and how this relationship will change under future climate change scenarios.

1.3. Aim and objectives

The aim of this thesis is to investigate the relationship between extreme mudflow events and mudflow triggering factors from synoptic to large scales under the present climate for Uzbekistan and to explore the impacts of anthropogenic climate change on mudflow triggering mechanisms by the end of 21st century over the study area.

The aim will be achieved by addressing following research objectives:

Objective 1: To review the literature on mudflow events, to summarise relevant details on climate modelling approaches to help identify research needs.

Objective 2: To assess the main characteristics of the investigation area and mudflow variability and to compile and analyse related data and methodologies.

Objective 3: To identify the link between the potential effects of synoptic and large scale conditions and the occurrence of extreme hydro-meteorological mudflow events in Uzbekistan by manual assessment of Synoptic Weather Type (SWT) and automatic Circulation Weather Type (CWT) approaches.

Objective 4: To estimate the precipitation thresholds initiating mudflows considering data availability and limitations.

Objective 5: To project the potential impact of future anthropogenic climate change on major weather circulation patterns leading to the mudflow occurrences in Uzbekistan in the end of century (2071-2100) based on statistical downscaling of CMIP5 GCMs outputs.

Objective 6: To project the changes in precipitation thresholds inducing extreme mudflow occurrences in the investigation area under the consequences of increased GHGs scenarios (RCP8.5).

Objective 7: To summarise the findings and limitations of the study and discuss future areas of research.

Objectives 3-6 are illustrated as a methodological flowchart in Figure 1.8.

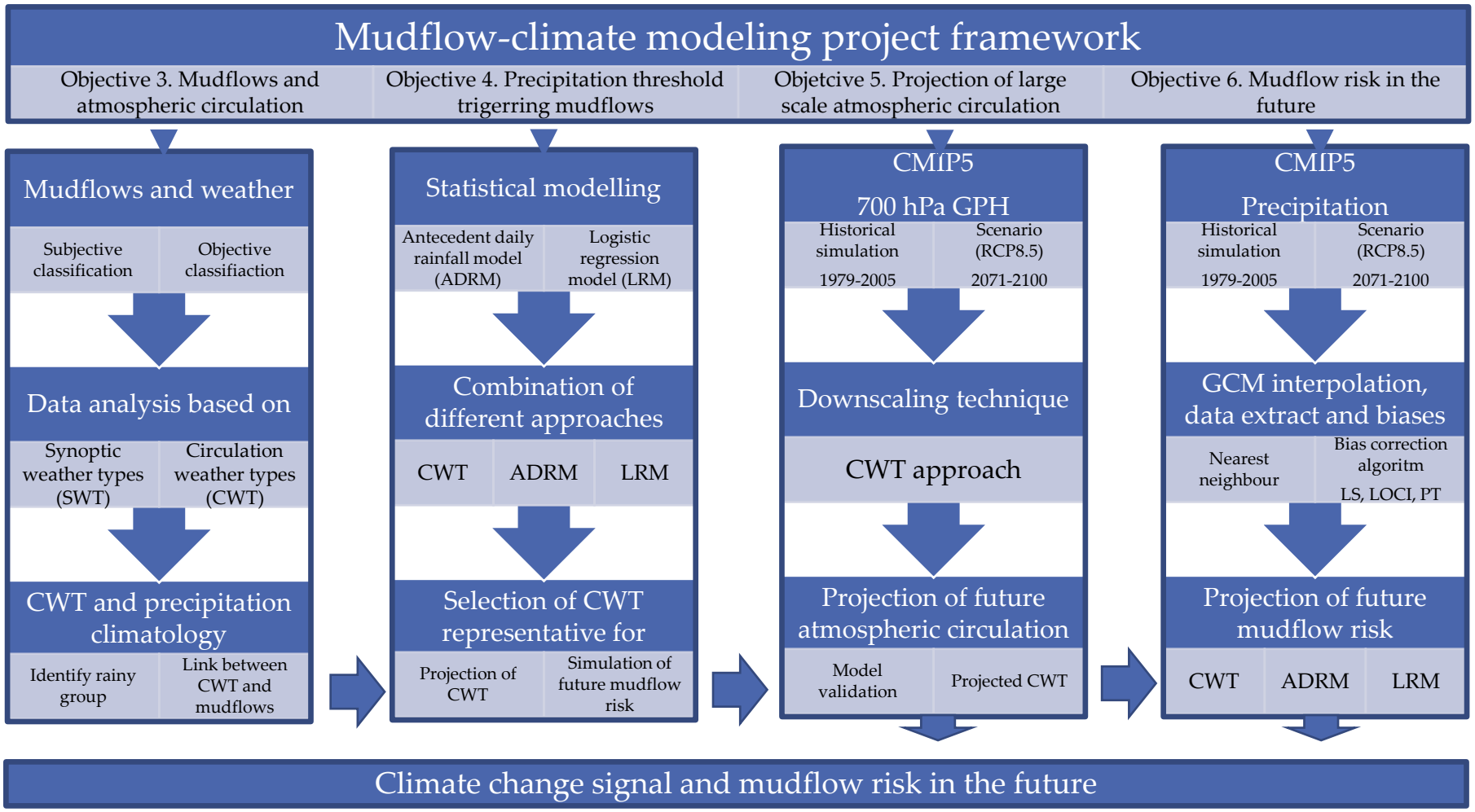

Figure 1.8. The schematic flow-chart of mudflow-climate modeling applied in this thesis.

1.4. Thesis organisation

In order to answer research objectives raised in section 1.3, the thesis content is divided into 7 chapters structured as below.

Chapter 2: Study Area, Data and Methodology. This chapter gives details of the study area along with the descriptions of qualitative data and their sources and describes all adopted methods to investigate the objectives of the thesis.

Chapter 3: Subjective and Objective Circulation Weather Patterns and Mudflow Occurrences. In this chapter, the role of synoptic and large scale atmospheric processes for the formation of mudflow occurrences in Uzbekistan has been investigated. Mudflow inducing weather conditions are identified by two different methods, one is by using subjective Synoptic Weather Types (SWT) classification derived from synoptic charts by national researchers and the second is the automated Circulation Weather Types (CWT) approach based on assessment of large scale atmospheric characteristics over Uzbekistan. Parts of this chapter has been adopted from the article published in NHESS journal.

Chapter 4: Statistical Modelling of Precipitation Thresholds for Triggering Mudflows. In this chapter, empirical-statistical approach of Antecedent Daily Rainfall Model (ADRM) has been applied to investigate precipitation threshold triggering mudflow for the study area. Furthermore, the chapter details the

knowledge gaps and uncertainties related to assessing precipitation threshold triggering mudflows in regional scale. The analysis presented in this chapter forms a part of the paper that has been published in NHESS journal.

Chapter 5: CWT - Analyses of Present and Future Atmospheric Circulation over Uzbekistan.

In this chapter, model outputs from CMIP5 projection are used to assess the abilities of selected 10 GCMs to simulate the present day (1979-2005) pressure field at 700 hPa and precipitation climatology over study area using CWT approach including comparison to model results from the ERA-Interim reanalysis data are presented. Based on RCP8.5 experiments the ensemble outputs of selected GCMs of CMIP5 for the analysis of CWT variability on seasonal timescales to identify the anthropogenic climate change signal.

Chapter 6: Mudflow Risk in Uzbekistan under Anthropogenic Climate Change.

Chapter 6 continues from Chapter 5, where the simulated precipitation outputs from 10 CMIP5 RCP8.5 experiments is projected in order to assess the future mudflow risk in Uzbekistan using a combination of CWT, ADRM and statistical transfer function (logistic regression model). The methodology used in this chapter explains the potential impacts of climate change conditions on

precipitation induced mudflow occurrences in Uzbekistan. Investigations in Chapter 5 and 6 are prepared as a research article for publication in the Journal of Climate.

Chapter 7: Conclusions and Outlook.

This chapter concludes the thesis by revisiting two central core findings of the thesis, namely (1) to explore the association between atmospheric circulation patterns and mudflow occurrences in Uzbekistan and (2) to investigate the anthropogenic changes of air flow directions associated with precipitation patterns as a good indicator on mudflows in the future. The final chapter also summarises the most important findings of the thesis discussed in the earlier chapters and provides recommendations and potential research topics which merit further analysis.

2 Study Area, Data and Methodology

2.1. Study area

2.1.1. General climate conditions

In general, the climate in Uzbekistan is continental and semi-arid with hot and dry summers and cold winters, sometimes severe with snowfall. Due to its geographic location (between 37°-45°N and 56°-73° E), Uzbekistan has three main climate zones: a zone of deserts and dry steppes occupying about 79% of the territory, the foothills or piedmont zone, and the area of high mountains (Figure 2.1) extending over the remaining 21% respectively (Chub, 2007).

Chub (2007) confirms that the long-term climatology based on 50 stations data (some series reach back to 1881) in Uzbekistan (Figure 2.2) shows that the mean air temperature in July varies from 26°C in a greater part of the lowlands to 30°C in the south and desert areas making it the hottest month of the year. The maximum values can reach up to 45°C in the southern part of Uzbekistan. The record temperature of 50°C occurred in Termez and the Kyzylkum Desert. The coldest month is January when the mean air temperature drops to 0°C in the south and can go below -8°C in the north of the country. The minimum

temperature can be well below -40°C in the Ustyurt Plateau in extremely cold years.

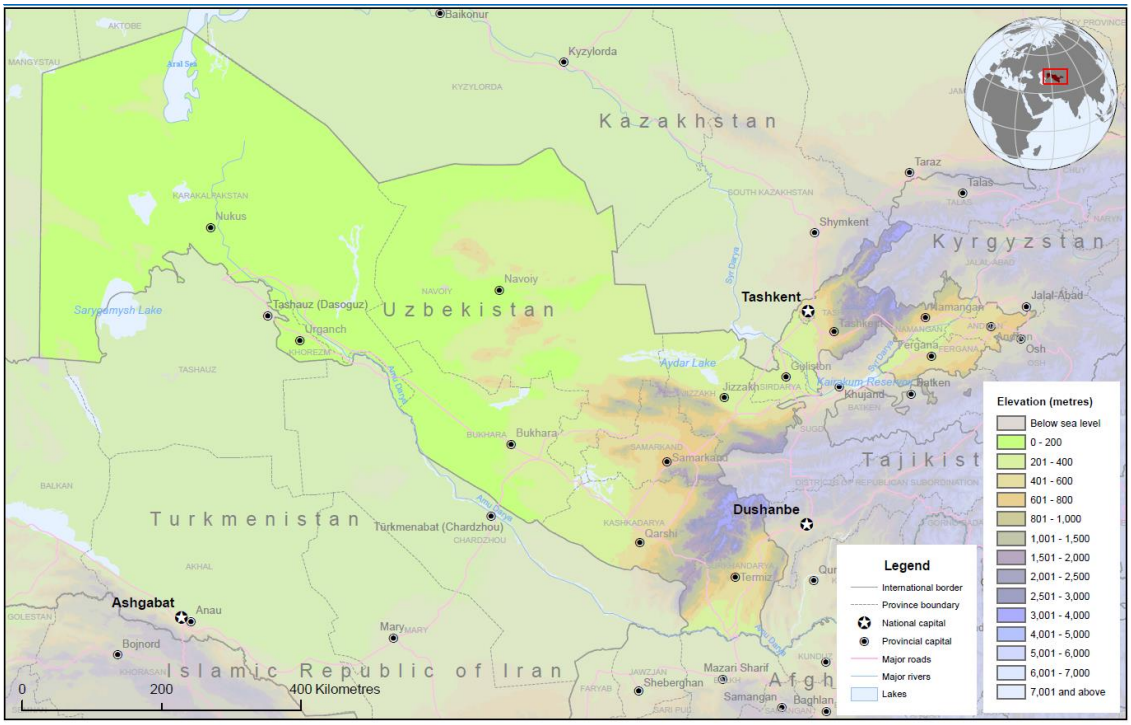

Figure 2.1. Elevation map of Uzbekistan (Source: OCHA – United Nations Office for the Coordination of Humanitarian Affairs).

The air temperature in the piedmont areas at an altitude from 300-400 to 600-1000m is notably warmer during the cold season of the year and cooler in summers than the plain areas of the country. With increasing altitude in the mountainous regions, the air temperature drops 0.6°C per 100 m on average. This is associated with the complex relief of the study area, e.g., cold air flow over low-elevation, radiative cooling and wind speed (Bugayev, 1946, Chub, 2007, Kurbatkin, 2009). However, the temperature may be colder in the bottom of the valleys and intermountain basins due to frequent temperature inversions (Chub,

2007). Figure 2.5 characterises monthly mean temperature patterns and precipitation regime covering the 30-year period of January 1984–December 2013 inclusive, in five representative stations (Figure 2.2) namely: Gallyaaral (574 m), Chimgan (1620 m), Mingchukur (2132 m), Baysun (1241 m) and Sokh (1200 m), located in piedmont and mountain areas in Uzbekistan.

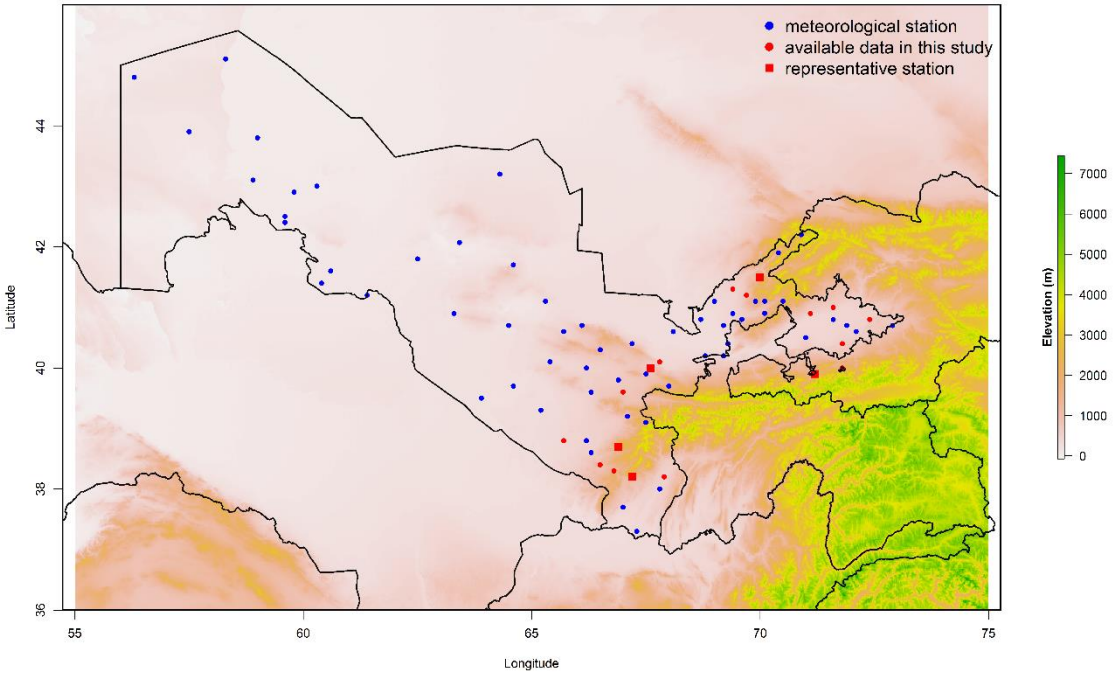

Figure 2.2. Location of 80 meteorological stations in Uzbekistan (blue and red circles) with available data (red circle) and representative 5 stations (red square) in this study. Elevation source[5]: SRTM 90m Digital Elevation Database v4.1.

[5] http://srtm.csi.cgiar.org/srtmdata/

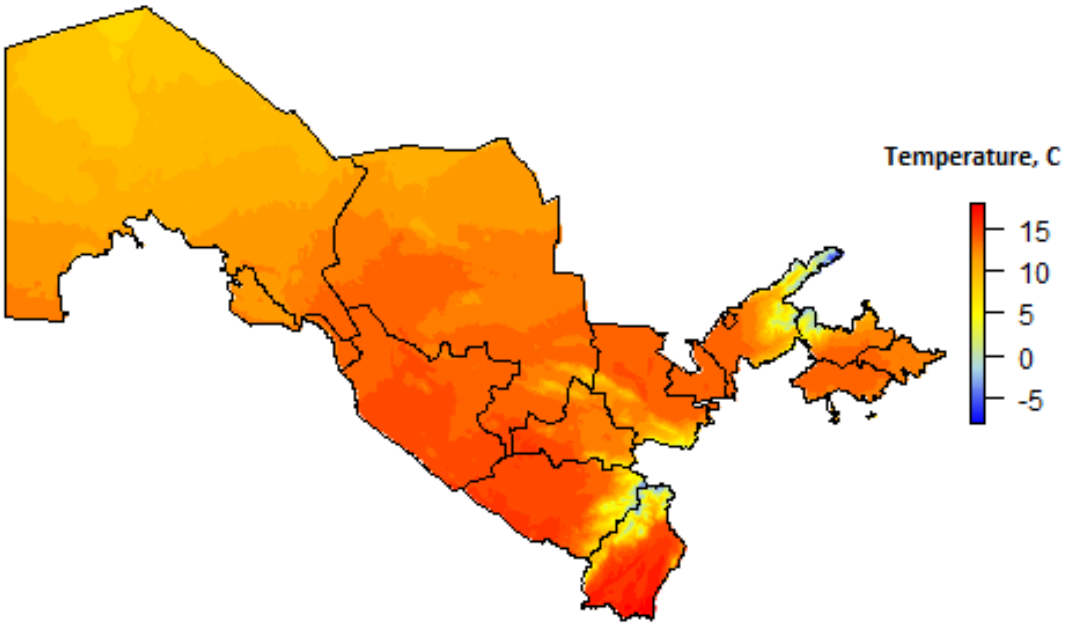

Figure 2.3. Annual mean temperature in Uzbekistan (Source: https://gadm.org/).

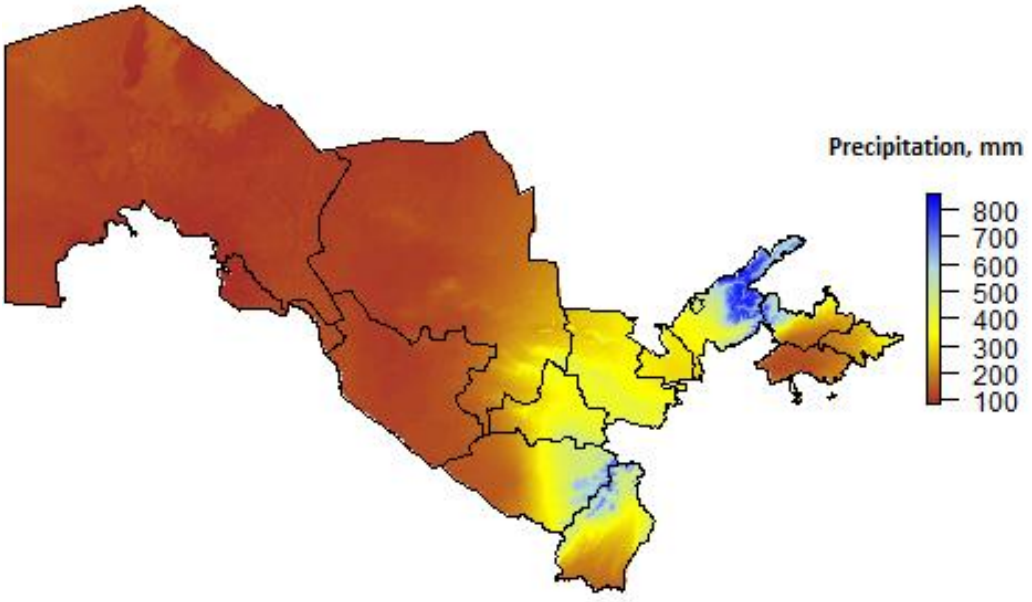

Figure 2.4. Total annual precipitation in Uzbekistan (Source: https://gadm.org/).

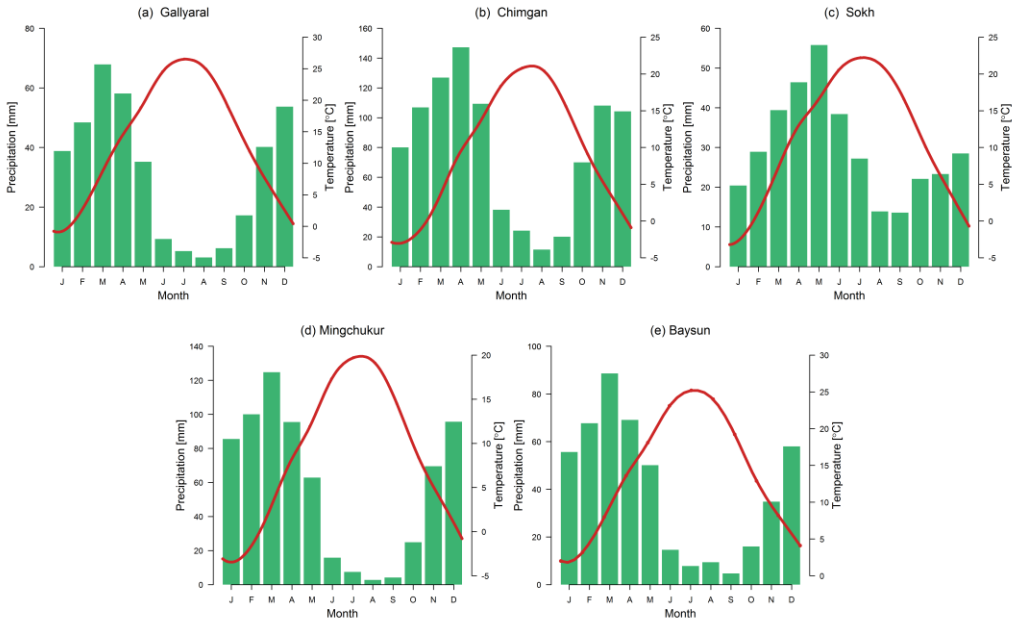

Figure 2.5 The 30-year means (1984–2013) of monthly temperature (°C, red line) and precipitation (mm, green bars) at five selected stations, namely Gallyaaral in the Zerafshan basin (a), Chimgan in the Chirchik–Akhangaran basin (b), Sokh in Fergana Valley (c), Mingchukur representing the Kashkadarya basin (d) and Baysun in the Surkhandarya basin (e) with high occurrences of mudflow in Uzbekistan. The graphs have different scales.

The amount and distribution of precipitation, as well as its seasonal variability, greatly depends on the geographical location of the area (Figure 2.1), topographic features (Figure 2.1, Figure 2.2) and the general characteristics of the atmospheric circulation (Figure 2.6). In fact, several authors have identified moist air from the Atlantic Ocean, the Mediterranean Sea and the Persian Gulf as the main large-scale or regional climate factor for the precipitation regime in the country

(Bugayev, 1946, Small et al., 1999, Inagamova et al., 2002, Chub, 2007, Schiemann et al., 2008). The average precipitation distribution in Uzbekistan has a sharp contrast between the plain and mountain areas (Figure 2.4). Mean annual precipitation in major parts of the plains or deserts and dry steppes (Ustyurt Plateau, Kyzylkum Desert, Karshi, Dalverzin and Golodnaya steppes) is about 80-200 mm. However, precipitation can be significantly greater in some piedmont areas and the mountains, particularly in the north-east and the south-east of the country. In fact, precipitation in areas with an elevation between 600-1000 m or piedmont areas (Tian Shan and Gissar-Alay mountain ranges) can reach up to 500 mm; above 1000 m elevation the annual totals may exceed 500 mm (Figure 2.4). In some hillsides, especially the western slopes of Tian Shan, it may even be greater than 2000 mm (Chub, 2007).

Generally, the precipitation regime in Uzbekistan reveals a seasonal character with wet conditions from October to May and a dry season with little or almost no rainfall during the summer (Figure 2.5). Heavy precipitation events frequently occur during the rainy season, especially in March and April. August represents the driest month with the minimal amount of rainfall throughout the year.

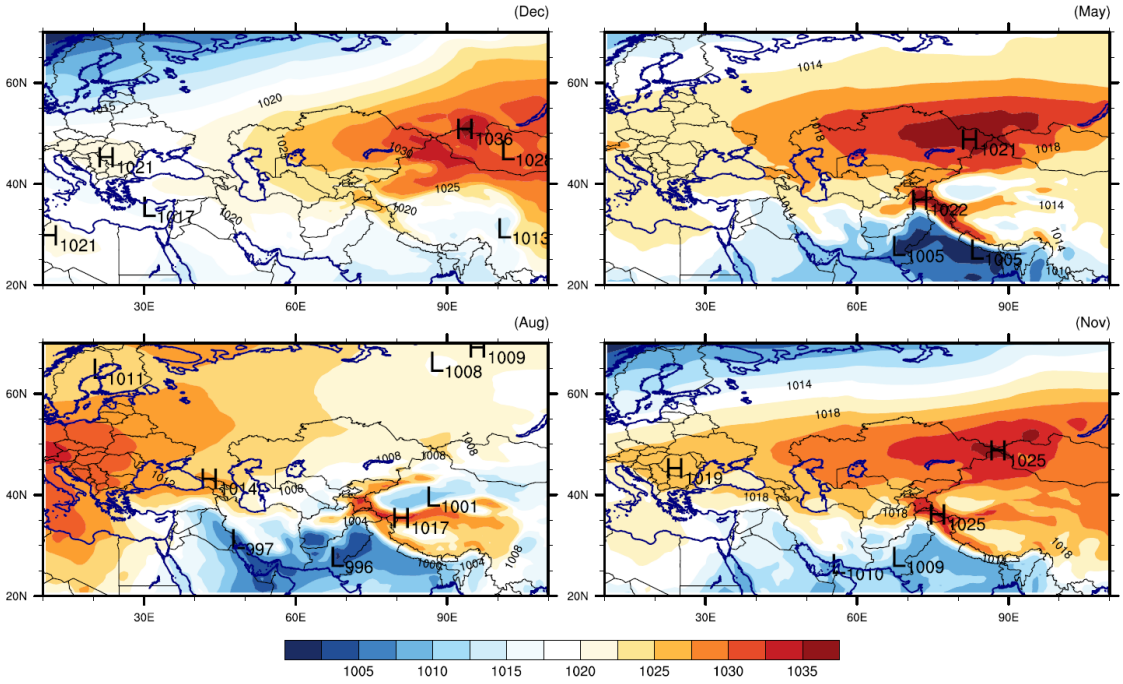

Figure 2.6. Seasonal MSLP (hPa) characteristics over Central Asia for the period 1984-2013.

2.1.2. Mudflows in Uzbekistan

The earliest mudflow event induced by snowmelt and avalanches in Akhangaran river basin was recorded in March 1870 (Lyakhovskaya, 1989, Chub et al., 2007). The archive data of mudflow occurrences in Uzbekistan since then, the Soviet period and after, has been collected and published as catalogues by Uzhydromet.

In this study, a century-long time series of the annual distribution of mudflows was investigated in order to identify key factors contributing to extreme mudflow occurrences. During the observation period (1870-2014) more than 3000 mudflow events have been identified in the river basins in the piedmont areas of

Uzbekistan. Table 2.1 provides comprehensive information on the monthly distribution of mudflows in five regions of the country.

Table 2.1. Monthly distribution of mudflow events in five regions in Uzbekistan.

Basin	Data	Jan	Feb	Mar	Apr	May	Jun	Jul	Aug	Sep	Oct	Nov	Dec	Total	Mean
Fergana	1875-2014	8	21	34	292	605	462	218	67	2	0	2	0	1711	12
Zerafshan	1872-2014	7	36	80	177	157	54	19	10	0	2	1	1	544	3.8
Surkhandarya	1890-2014	0	0	20	151	146	63	7	0	0	2	0	0	389	3
Chirchik-Akhangaran	1870-2014	1	3	31	91	64	17	19	7	0	0	0	0	233	1.6
Kashkadarya	1877-2014	0	3	12	92	42	9	0	6	0	1	0	0	165	1
Total	1870-2014	16	63	177	803	1014	605	263	90	2	5	3	1	3042	21

Mudflows with various magnitudes developing on the slopes of the study area appear several times during the year with an average number of 21 extremes per year (Table 2.1). The highest number of events was observed in 1930 with 167 mudflows followed by 161 mudflows in 1931, 144 episodes in 1963 and 108 events in 2012 (Figure 2.7, Figure 2.8). An interesting point is that the 5, 11 and 21 years moving average of mudflow events features a periodicity of approximately 30-years, which repeated the highest peaks in the 1930s, 1960s and 1990s (Figure 2.7). The last peak period of mudflow activity occurred in the 2010s. This signature of potential natural variability will pose an additional challenge for investigation of mudflow cycles and their variability, under climate change conditions. However, according to Chub (2007), apart from the natural causes the number of recorded mudflows can increase due to several factors which often

interact to generate mudflow occurrences in Uzbekistan. Social-economic factors such as residential and industrial activities below unstable hillslopes accelerate soil creep as well as accumulated materials in channels decrease the roughness condition by overloading with fills which can potentially increase the probability and impact of mudflows.

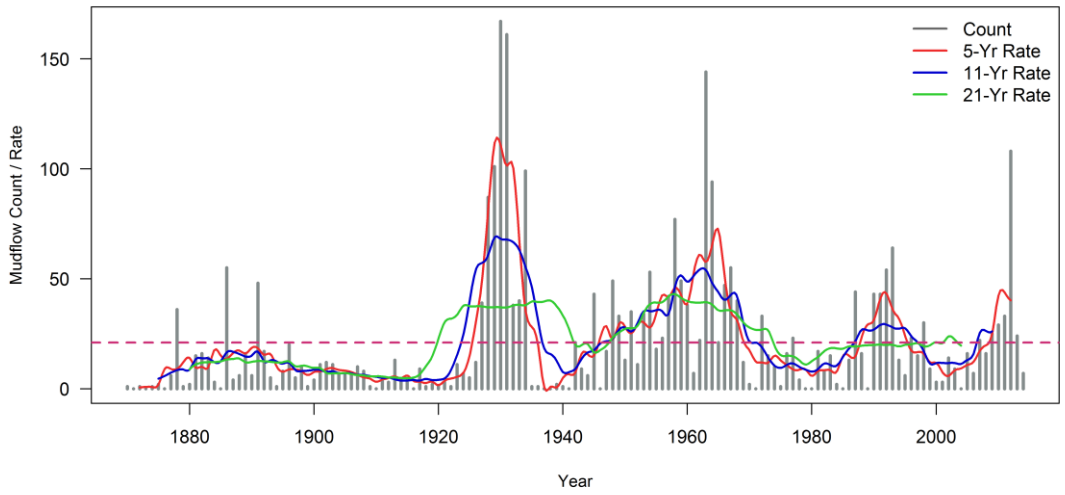

Figure 2.7. Variability in mudflow events in Uzbekistan (1870–2014). Vertical bars present the mudflow observations for each year. The mean annual mudflow count (21) is indicated in a solid continuous horizontal line (pink). Curves (red, blue, green) have been fitted to the distribution for illustrative purposes and denote the 5-, 11- and 21-year rates of mudflow occurrences.

More than 90% of all recorded mudflows were associated with extreme precipitation events, hail and sleet whereas 6% of mudflow episodes were observed during intensive snowmelt events (Figure 2.9) induced by respective temperature and precipitation changes (Chub et al., 2007). Glaciers melting due to increasing temperatures and mountain lakes outbursts (Petrov et al., 2017) and

dam failures has been suggested as possible reasons to trigger further minor mudflows (1.4%) in the study area (Figure 2.9). Approximately 80% of all recorded mudflow episodes with different origins occurred during the period of April-June (Figure 2.10).

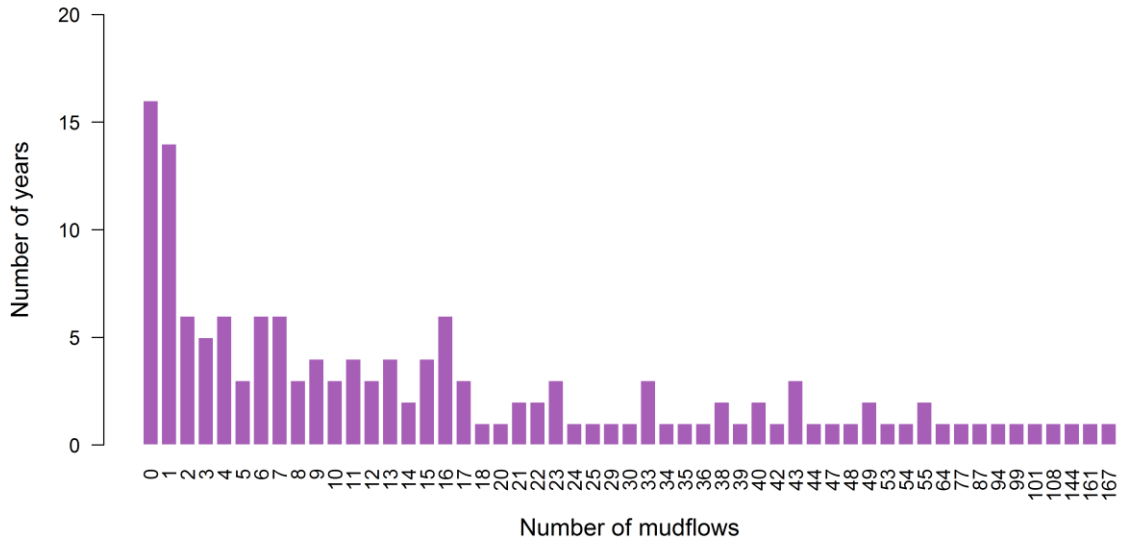

Figure 2.8. Histogram of mudflow occurrences in Uzbekistan.

Records confirm that mudflow events often affected the Fergana Valley indicating the highest event frequency during the investigation period of 12 mudflow occurrences per year on average (Table 2.1). Salikhova (1975) and Lyakhovskaya (1989) interpreted that due to its topographic feature, the Fergana Valley was susceptible to constant mudflow passages. Geologically the uplands in the Fergana Valley are mostly covered with loess loam which minimises water infiltration and makes it receptive for even a small surface runoff to flush off the

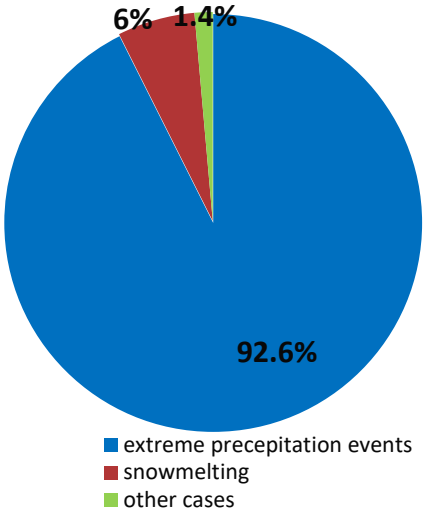

Figure 2.9 Reason for the formation of mudflows in Uzbekistan (after Chub et al. (2007)).

soil easily. This process contributes to soil erosion which ends with the formation of mudflow episodes almost every year from March till August in the valley. In contrast to the Fergana Valley, the geological structure of the mountain areas for the following regions, namely, Zerafshan, Surkhandarya and Kashkadarya basins is formed of effusive or volcanic rocks of the Palaeozoic age, which may cause more debris flows rather than mudflow events (Table 2.2). Geo-morphologic factors

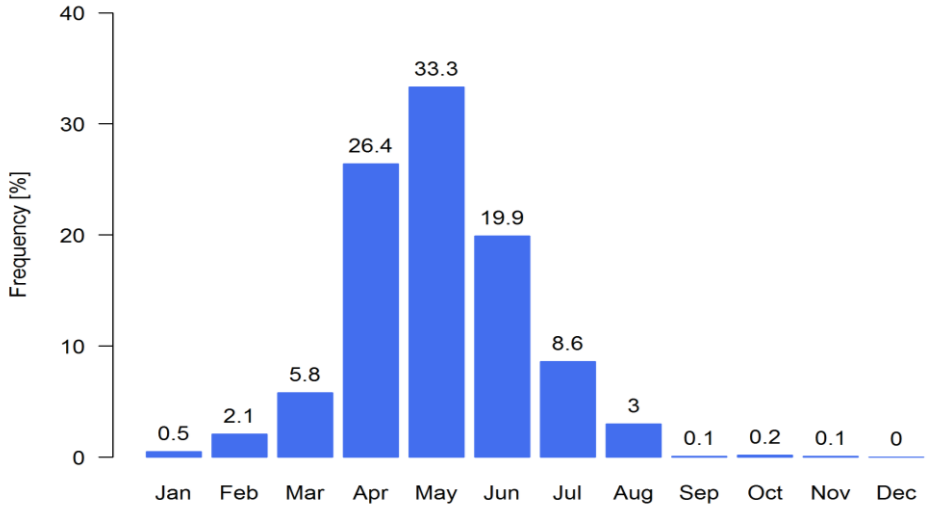

Figure 2.10. Monthly mudflow frequencies (bars) for the years 1870-2014. Values over the bars indicate the percentage of mudflow occurrences in a given month.

can be useful to determine the general susceptibility of various lithologies to landsliding in specific region (Sidle and Ochiai, 2006). There are more than 450 streams located in the river basins in the mountain and foothill areas in Uzbekistan and it is fairly common to observe extreme mudflow occurrences in multiple streams on the same day (Chub et al., 2007). For instance, on 15 April 1964 only in the Samarkand province (Zerafshan Valley) 22 mudflow episodes were recorded in a single day (Lyakhovskaya, 1989). During the period spanning from 1870-2014 up to 24 passage of flows were observed on 18 May 1991 in many parts of the country.

Table 2.2. Physiographic characteristics of the basins located in the study area.

Basin/Region	Highest elevation	Zone of mudflow formation	Geology	Soil	Geomorphology
Fergana Valley	in the north – Chatkal, 4503m (Chatkal range, Uzbekistan); in the east – Fergana, 4940 m (Fergana range, Kyrgyzstan); in the south - Pik Tandykul, 5544 m (Alay mountains, Kyrgyzstan)	1000-2000 m	slate, limestones, granites, schists	conglomerates covered by loess loam	zone of high mountains gradually changes to the hills with 1000-1800 m altitude which surrounds the lowlands in the valley in clockwise direction from north-west to south; the western part is open
Zerafshan	Chakyl-Kalyan, 2835 m (Zerafshan range, Uzbekistan)	900-2000 m	dark phyllite, marble, shale	volcanic ash	
Surkhandarya	Khazret Sultan, 4643 m (Gissar range, Uzbekistan)	1500-2000 m	porphyry, conglomerate, sandstone, shale, limestone	volcanic ash	region is surrounded by high mountains
Chirchik-Akhangaran	Adelung, 4301m (Pskem mountains, Uzbekistan)	1200-3000 m	granites and syenites	pebbly and loess mixture	monotonous and mainly represented by hills, mountains and highlands
Kashkadarya	Gava, 4150 m (Gissar range, Uzbekistan)	1000-2000 m	limestone, marble, crystal formations in shale, granite	sandy clay and other continental deposits	featured by steep slopes reaching maximum elevations

2.3. Data

The investigation is based upon two categories of datasets: ground observation and the state-of-the-art reanalysis and GCMs experiments.

Observed daily meteorological variables recorded by Uzhydromet, such as precipitation and temperature from the five meteorological stations (Gallyaral, Sokh, Chimgan, Mingchukur and Baysun) located in the mountains and the foothills with high mudflow passages were used to produce respective climatologies.

In addition, historical data of Uzhydromet regarding mudflow occurrences in Uzbekistan over the period 1870-2014 were analysed. National scale mudflow database includes information such as the name of the water stream, location, date of passage, the potential reason for the formation of the mudflow, a rough estimate of the volume and major damages.

Data of the daily mean synoptic situation or local classification of Synoptic Weather Types (SWT), which is available at Library Services and the Archive Department of Uzhydromet as catalogues of six hourly (00, 06, 12, 18 GMT) data manually derived from synoptic charts, was calculated to produce relative outputs regarding mudflow inducing weather situations. The period considered in this study is a warm season (March-August) of 1984-2013.

In order to assess potential climatic drivers over Uzbekistan daily mean lower atmospheric flow in 700 hPa geopotential height (GPH) fields by the European Centre for Medium-Range Weather Forecasts (ECMWF) ERA-Interim reanalysis (Dee et al., 2011), spanning the period 1984-2013, was used to estimate the large-scale atmospheric circulation. This gridded data set has 0.75^{o} spatial resolution.

The daily mean Z_{700} outputs from 10 AOGCMs of the CMIP5 (Taylor et al., 2012) projection are used in this study (Table 5.1). The daily outputs for historical (1979-2005) simulation and future experiment (2071-2100) under the RCP8.5 scenario are applied. For all models and experiments, only the first ensemble member (r1i1p1) is considered.

2.4. Methods

2.4.1. Synoptic Weather Type

Investigation of atmospheric circulation over Central Asia first started in 1921 in the Turkestan Synoptic-meteorological Institute in Tashkent (Aksarin and Inagamova, 1993). The complexity and diversity of the regional atmospheric circulation was identified soon after Bugayev and Giorgio developed and simplified a model of airflow advection to explain for synoptic differences in the 1930s and 40s (Giorgio and Bugayev, 1936, Bugayev et al., 1957, Aksarin and Inagamova, 1993). The founders of the Central Asian Tashkent Institute of Weather Forecasters, Bugayev and Giorgio, had supervised research on synoptic meteorology and the impact of orographic factors on CA's climate for many years. In 1947 scientists published the first findings of the statistical characteristics of synoptic situations over the region for the cold period in the newsletters published by the USSR Academy of Science (Sarimsakov et al., 1947). After a decade, researchers summarised the studies on the atmospheric circulation classification scheme for CA and had published it as a fundamental monograph, describing the main atmospheric patterns as 11 SWT over CA (Bugayev et al., 1957). This monograph is still being used as the main literature study and guidelines on synoptic conditions in Central Asian countries mainly in Uzbekistan (G.M.'s personal experience, Aizen et al. (2004)). Figure 2.11 provides a basic illustrative view of SWT classified by Bugayev et al. (1957)

emphasizing the air mass source regions and their path to CA. In the early 1960s, researchers at the Scientific Institute of Hydrometeorological Service of Uzbek SSR (nowadays Uzbekistan) updated Bugayev and Giorgio's classification from 11 to 15 types by including additional weather classes. Subjectively classified weather types for all the years, except 2013-2014, over CA and Uzbekistan have been published as registers of daily sequence of SWT in Ilinova (1968), Voynova and Inagamova (1982) and Inagamova (1993, 2013). Table 2.3 provides comprehensive information for these 15 primary SWT, describing weather conditions on a synoptic scale in CA and particularly in Uzbekistan. Figure 2.12 shows the long-term seasonal distribution (1935-2014) of SWT within CA and Uzbekistan.

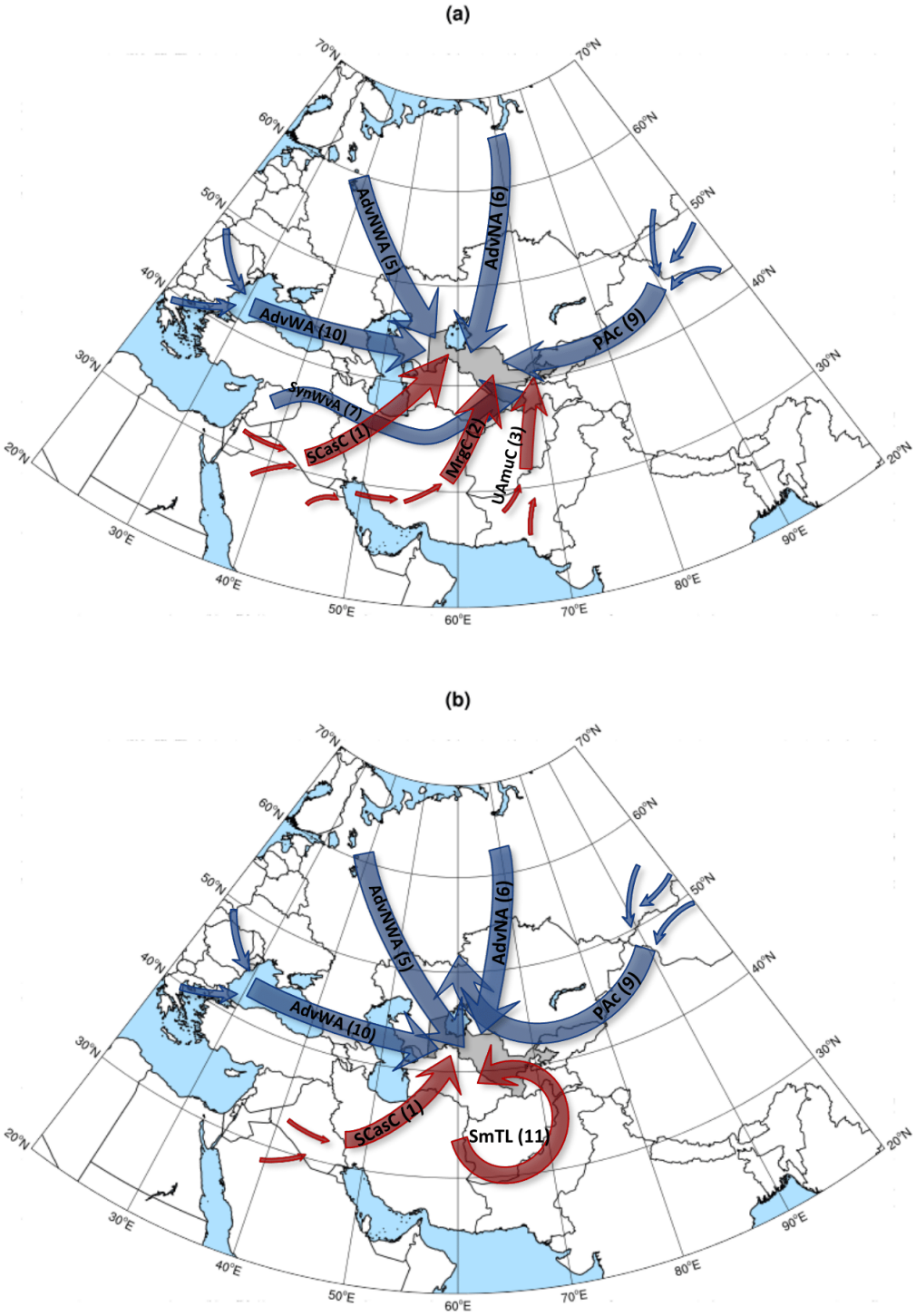

Figure 2.11. Scheme of synoptic weather types in Central Asia and Uzbekistan during the cold (a) and warm seasons (b) of the year (after Inagamova et al., 2002). Blue and red arrows indicate relatively cold and warm air trajectories approaching the investigation area (grey background). Abbreviations and numbers of each weather type are explained in Table 2.3.

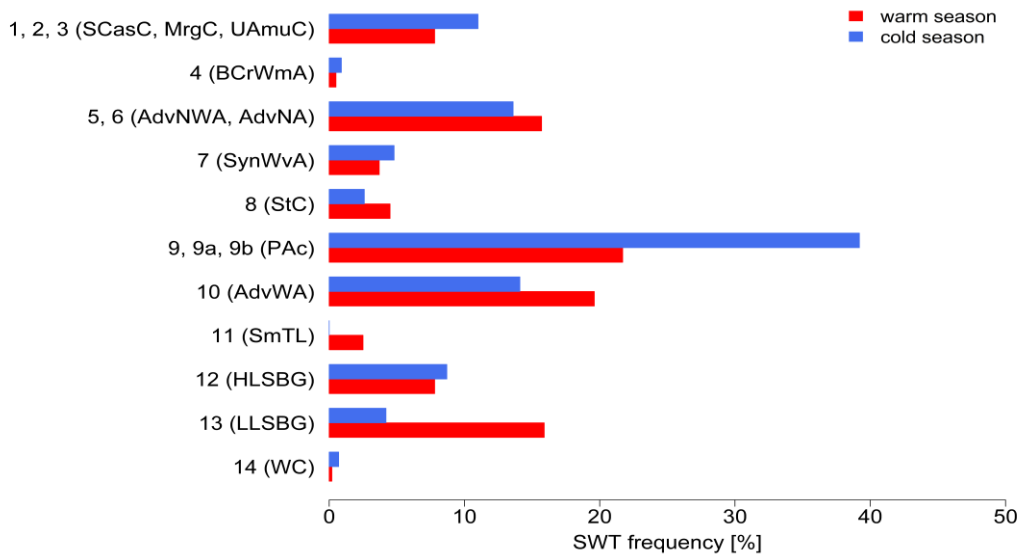

Figure 2.12. Frequency distributions of daily SWT by Bugayev's classification during the cold (September-February) and warm (March–August) seasons in the period of 1935–2014 years. Definitions of SWTs can be seen in Table 2.3.

Table 2.3. Synoptic weather types (SWT) of Central Asia and general weather characteristics over the region and in Uzbekistan. SWT 1-9, 9a and 10-11 was classified by Bugayev et al. (1957); types 9b and 12-15 were added later by the researchers of the Hydrometeorological Scientific Institute in Uzbekistan.

Group	Code	Synoptic Weather Type (SWT)	Source region	Air mass	Characteristics
Group A Cyclones from south and south-west	1	South Caspian Cyclone (SCasC)	Southern part of Caspian Sea, east of Mediterranean Sea, Mesopotamia, Northern part of Arabian Peninsula	tropical	rising temperature in the warm sector of the cyclone in winter, heavy precipitation especially in mountain areas, strong winds, dust storms along the desert areas
	2	Murgab Cyclone (MrgC)	Cyclone forms as a wave in Iraq, Mesopotamia, Iran and approaches to the Southern part of Turkmenistan, Murghab and Tejen Rivers' basins	tropical, continental (temperate zones)	mild and wet in the warm sector of the cyclone, strong winds, heavy precipitation, thunderstorms in spring, floods in the rivers, sometimes radiation fog
	3	Upper-Amudarya Cyclone (UAmuC)	Afghanistan, West Pakistan, Persian Gulf	tropical	warm air flow, cloudy; precipitation may be observed in the territory of Tajikistan; strong winds in the mountain areas, sometimes fog
	4	Broad carrying the warm air (BCrWmA)	South-westerly and southerly flows in the troposphere approach to the Southern part of European Russia, Western Kazakhstan and Central Asia	tropical, continental (temperate zones)	warm, clear, dry weather condition with light winds
Group B Advection of cold airflow from north and north-west	5	Advection of cold north-westerly air flow (AdvNWA)	South-eastern part of European Russia, Western Kazakhstan and Ustyurt	arctic (Siberian sector), continental (temperate zones)	mainly cold in winter with cloudiness, precipitation and strong winds; in summer cool weather, precipitation depends on the orography and convection process; frosts in spring and autumn
	6	Advection of cold northerly air flow (AdvNA)	Ural, Western Siberia, Kazakhstan	arctic (Greenland and the North Sea), continental (temperate zones)	very cold, sometimes severe weather with winds, little precipitation and fog in winter season; thundery and rainfall in summer in the mountain areas; frost in early spring and late autumn
	7	Synoptic wave activity on a cold front (SynWvA)	Eastern Mediterranean, Middle East	Mediterranean, Atlantic (subtropical)	mostly the weather is wet with changeable temperature, sleet showers, winds, occasionally thundery in spring
	8	Stationary Cyclone over the Central Asia (StC)	Regeneration of western or south-western cyclones	Mediterranean, Atlantic, tropical	sleet in cold period; in summer cool and heavy rainfall especially in south-eastern mountain areas, thundery, slight winds

	10	Advection of westerly air flow (AdvWA)		Central and Southern Europe (westerly moist) European Russia and Ukraine (westerly cold)	Atlantic and continental (temperate zones), sometimes arctic	cool, strong winds, precipitation in cold period; in spring and early summer the weather is wet giving most rain, temperature falling, dust storms, thundery
	15	Diving Cyclone (DC)		Norwegian Sea, Barents Sea, Kara Sea	arctic	precipitation, strong winds
Group C Anticyclonic weather	9	Periphery of Anticyclone (PAc)	South-western periphery of Anticyclone (SWPAc)	Siberian High	arctic	in general, it is clear and mostly dry with slight winds; radiation fog in the piedmont and mountain areas in the first phase of the synoptic type, cloudiness and precipitation might be observed in eastern mountain areas of Central Asia
	9a		South-eastern periphery of Anticyclone (SEPAc)	Stationary anticyclone over the Ustyurt, lower Volga or western Kazakhstan (part of Siberian High)	arctic	clear, cold, frost and mist on the plain surface, sometimes precipitation in mountain areas in cold period; in summer, it is cool and slight winds
	9b		Southern periphery of Anticyclone (SPAc)	Siberian High extends to the eastern regions 50-55º N in which Central Asia is on its southern periphery	arctic	mostly this synoptic weather type is cold and dry with foggy days in winter phase; in summer the weather is cool and clear
	11	Summer thermal low (SmTL)		Non frontal low pressure area over southwest Asia	tropical dry	clear, dry, very hot, haze, winds, dust storms
	12	High level of small barometric gradient (HLSBG)		The area of high pressure over the Central Asia which units the Siberian High and the anticyclone over the European Russia	mostly arctic	generally cold, dry and clear weather with light winds; in cold periods it is foggy and little precipitation in south-eastern regions
	13	Low level of small barometric gradient (LLSBG)		Low-pressure area over the Central Asia which aligns in meridional orientation	moderate zones	in most parts of Central Asia there are dry and warm weather conditions; in winter the weather is mostly foggy with slight precipitation; in summer convective clouds and heavy rainfall may be observed in local areas
Group D Mid-latitude cyclone	14	Western Cyclone (WC)		Cyclone tracks from the Mediterranean Sea, sometimes from Northern Africa to the Black Sea or Middle East then reaches to the Central Asia through the Caspian Sea	Mediterranean	strong winds, dust storm in the desert area, precipitation especially in mountain areas

2.4.2. Circulation Weather Type

The circulation weather type (CWT) initially based on the Lamb weather types scheme for the British Isles (Lamb, 1972). Automotive approach developed by Jenkinson and Collison and the basic details of use this classification were provided by Jones et al. in 1993. It is very simple and easy to be applicable regardless of the grid data density for the analysis of air circulation regimes in a wide range of climate studies (e.g., Trigo and DaCamara, 2000, Prudhomme and Genevier, 2011, Pattison and Lane, 2012, Ramos et al., 2014, El Kenawy and McCabe, 2016).

The objective CWT catalogue is illustrated in Figure 2.13 shows how the pressure values can be used to define the atmospheric circulation type on a daily basis for Uzbekistan. Using calculations of total shear vorticity (Z), the resultant flow strength (F), and direction (with an increment of 45◦), the Lamb scheme can provide information on the pure airflow direction (northerly, southerly, easterly, westerly, north-easterly, north-westerly, south-easterly and south-westerly, corresponding to N, S, E, W, NE, NW, SE, and SW) and non-direction type (i.e., cyclonic, anticyclonic) of the flow and hybrid types (CN, CS, CE, CW, CNE, CNW, CSE, CSW, AN, AS, AE, AW, ANE, ANW, ASE, and ASW) and undefined class (U). The southerly flow (SF), westerly flow (WF), total flow (F), southerly shear vorticity (ZS), and westerly shear vorticity (ZW) are computed from

pressure at 700 GPH level at the 16 grid points (1-16) shown in Figure 2.13 using the following formulas:

$$W = \frac{1}{2}(12 + 13) - \frac{1}{2}(4 + 5) \quad (2.1)$$

$$S = 1.74\left[\frac{1}{4}(5 + 2 \times 9 + 13) - \frac{1}{4}(4 + 2 \times 8 + 12)\right] \quad (2.2)$$

$$F = (S^2 + W^2)^{1/2} \quad (2.3)$$

$$ZW = -1.07\left[\frac{1}{2}\left(15 + 16\right) - \frac{1}{2}(8 + 9)\right] - 0.95\left[\frac{1}{2}\left(8 + 9\right) - \frac{1}{2}(1 + 2)\right] \quad (2.4)$$

$$ZS = 1.52\left[\frac{1}{4}\left(6 + 2) \times 10 + 14\right) - \frac{1}{4}(5 + 2 \times 9 + 13\right) - \frac{1}{4}\left(4 + 2 \times 8 + 12\right) + \frac{1}{4}(3 + 2 \times 7 + 11)\right] \quad (2.5)$$

$$Z = ZW + ZS \quad (2.6)$$

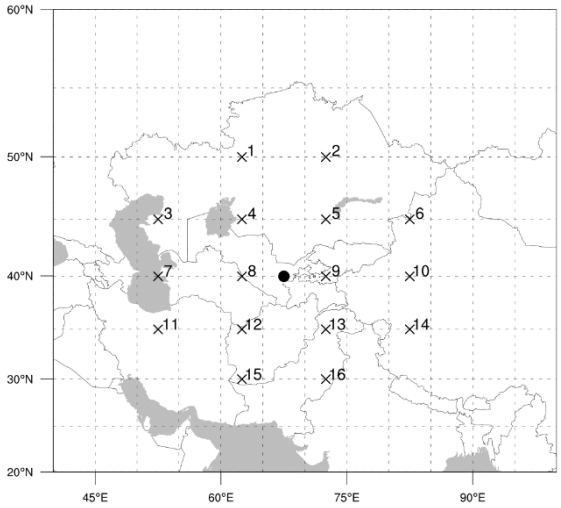

Figure 2.13. Location of the grid points over Uzbekistan and Central Asia used in the calculation of the CWT based on Jenkinson flows and vorticity. The allocated grid point numbers are used in the equations. Black dot is the central grid point (40.0N-67.5E) used in this study. The pressure value of the central grid point is not considered in the equation.

The following rules (Table 2.4) need to be taken into account in order to define the appropriate weather circulation based on Lamb classification scheme.

Table 2.4. Circulation types defined by total shear vorticity (Z) and resultant flow (F).

Weather type acronym	**Calculation**
Directional (N, NE, E, SE, S, SW, W, NW)	$\|Z\| < F$
Cyclonic (C)	$\|Z\| > 2F, Z > 0$
Anticyclonic (A)	$\|Z\| > 2F, Z < 0$
Unclassified cyclonic (UC)	Z < mean annual Z,F < mean annual F,Z > 0
Unclassified anticyclonic (UA)	Z < mean annual Z,F < mean annual F,Z < 0
Cyclonic hybrid (HYC)	$F < \|Z\| < 2F$ and $Z > 0$
Anticyclonic hybrid (HYA)	$F < \|Z\| < 2F$ and $Z < 0$

In this study, the CWT objective method generates a daily circulation database based on ERA-Interim reanalysis for two time periods 1984–2013 (Chapter 3) and 1979-2005 (Chapter 5), as well as selected 10 GCMs from CMIP5 projection for historical run (1979-2005) and future scenario (2071-2100) for 11 basic groups (eight directional, two synoptic and unclassified types). Pressure values at 700 GPH level are considered for this study.

CWT approach is used as perfect prognosis statistical downscaling method (Maraun and Widmann, 2018) to link the large scale predictors (circulation type in this case) to local scale predictands (precipitation and mudflow occurrences) calibrated to observational data. By this way it can be possible to apply to predictors simulated by GCMs.

2.4.3. Antecedent Daily Rainfall Model

In order to estimate the precipitation threshold causing mudflow events in the study area, a combination of an empirical and a statistical models has been applied: 1) Antecedent Daily Rainfall Model (ADRM) as the relationship between antecedent rainfall conditions prior to an actual "rainstorm event" and the rainstorm magnitude itself (Glade et al., 2000); 2) a logistic regression model (LRM) as the relationship between an outcome (dependent or response) variable and a set of independent (predictor or explanatory) variables (Hosmer and Lemeshow, 2000).

The ADRM introduced by Crozier and Eyles (1980) defines landslide triggering rainfall conditions for the Ottago Peninsula during 1977-1978. This model was applied in many parts of the world to obtain the thresholds probability of landslide occurrence on the basis of precipitation conditions (e.g. for New Zealand by Glade et al. (2000), for Portugal by Zêzere and Rodrigues (2002) and Zêzere et al. (2005), for Sao Miguel Island (Azores) by Marques et al. (2008), for Bangladesh by Khan et al. (2012), for China by Bai et al. (2014), etc.). The advantage of this model lays in the substituting of soil moisture storage levels by daily precipitation data. In the absence of real-time soil moisture measurements, this model allows to predict the probability of landslides (Glade et al., 2000). The antecedent rainfall model (Crozier and Eyles, 1980) is expressed by the following formula:

$$ra_0 = kr_1 + k^2r_2 + ... + k^nr_n \qquad (2.7)$$

where ra_0 is the antecedent daily rainfall for day 0; r_1 is the rainfall on the day before day 0; r_n is the rainfall on the n th day before day 0; and k is a constant <1.0. According to Davydov et al. (1973) and Bykov and Vasil'yev (1977) the k parameter depends on the river morphometry and it varies from 0.7 to 0.9, and 0.5 in the case of a slack current. Crozier and Eyles (1980), following Bruce and Clark (1966), used a value of 0.84 for the k factor, which is close to that used in hydrological studies in North America, more precisely Ottawa (United States) streamflow data (Glade et al., 2000). Due to missing data on regional hydrograph recession curves in the study area, the constant decay factor, k in this research was assumed to be 0.84 based on Crozier and Eyles (1980) and Crozier (1986). It was also suggested by specialists at Uzhydromet (personal communication with author) that $k \geq 0.8$ can be used for this study as it is used in the river catchments in the mountain areas of Uzbekistan. Setting k=0.84 worked satisfactorily in the ADRM to assess the triggering thresholds and mudflow probability in the study area.

In the first step, daily rainfall totals of 30 years (1984-2013) recorded in five representative stations (Gallyaaral, Chimgan, Sokh, Mingchukur and Baysun) were used to assess the average probability of mudflow triggering thresholds. The empirical model analysis consists of calculating the antecedent precipitation

for 10 consecutive days. Daily rainfall observations provided by Uzhydromet were used in this study and a period of 24 hrs was taken between 8 a.m. of the previous day to 8 a.m. of the present day.

Finally, the results from the two different investigation strands were integrated to estimate of each weather type as a proxy for the triggering mudflows by applying a combination of CWT, ADRM together with LRM to produce the precipitation threshold per CWT class.

3 Subjective and Objective Circulation Weather Patterns and Mudflow Occurrences

3.1. Introduction and background

Classifications of large and synoptic scale circulation systems have more than a century long history; the earliest classification of the complete pressure pattern over the North Atlantic and Western Europe was developed in 1895 by Van Bebber and Köppen. Through subjective manual procedures, authors distinguished five main weather types and twenty subtypes in relation to the position of anticyclonic and cyclonic movements from the earlier studies of Van Bebber (Barry and Perry, 1973). Since then many regional synoptic classifications of pressure and circulation fields have been developed. Based on the major centre of action and pressure distribution at the surface (Baur, 1936; 1951) and in the middle troposphere (Hess and Brezowsky, 1952), the concept of Grosswetterlagen (GWL, Hess and Brezowsky, 1969) was developed and applied to areas in Europe and eastern part of North Atlantic Ocean. The Grosswetterlagen (GWL) catalogue has a set of 29 synoptic weather patterns each

with a specific definition. Yoshino, in 1968 depicted a weather catalogue including six main circulation types and a total of fifteen subtypes comparable to GWL catalogue for eastern Asia (Barry and Perry, 1973). Another very ambitious endeavour of defining weather circulation based on trajectory of anticyclones along three major axes (normal polar, ultra-polar and Azores normal) to the territory of post-soviet countries has been carried out by Mul'tanovski (1933). Lamb (1972) developed a synoptic scheme calendar of 27 possible weather types and categorised them into seven principle types (anticyclonic, cyclonic, northerly, easterly, southerly, westerly and north-westerly) of weather regime over the British Isles (Jones et al., 2014).

A classification of eleven individual synoptic systems for the Central Asia prepared by Giorgio and Bugayev (1936) and Bugayev et al. (1957) based on overall movement of air masses associated with anticyclone and cyclone tracks in synoptic scale. This classification has been updated to fifteen synoptic weather types and two subtypes in the light of increased amount of information available from satellite images and upper-air data (Inagamova et al., 2002). Daily catalogues of this synoptic weather type (SWT) classification are available from 1938 to the present. The main weather characteristics of this synoptic weather scheme is presented in Table 2.3. The link between SWT and climate variables and associated impacts have been investigated only by a few studies at the

regional scale. Aizen et al. (2004) investigated the link between atmospheric circulation patterns and firn-ice core conditions in Inilchek Glacier located in Tien Shan Mountain system using SWT approach combined with linear regression and correlation methods. These authors inferred that the most precipitation generating weather patterns (SWT 10) as well as synoptic drivers (SWT 5, SWT 11) of dust storm and potential pollutants (ammonium and nitrate) affected to the geochemistry of glaciers. Salikhova (1975) and Lyakhovskaya (1989) used daily SWT classification and identified a direct link between major synoptic patterns with mudflow occurrences in Uzbekistan. Both authors found that westerly (SWT 10) and north-westerly (SWT 5) advections of moist air as well as cyclones tracking from the south and south-west (SWT 1, 2, 3) resulted in extreme mudflow events in the study area.

The advances in computing and increased sophistication in meteorological tools in recent decades have allowed for the development of global reanalysis datasets in a regular grid and these have played a significant role in transfer of manual schemes to automated synoptic classification methods (Sheridan, 2002, Vallorani et al., 2018). Huth et al. (2016) documented fifteen objective classification techniques that were collected in the COST (European Cooperation in Science and Technology) Action 733 database and evaluated the extent to which the classifications could be used to perform the weather system

over the Europe. It is worth saying here that the wide range of automotive algorithms for classifications of weather regime is a key factor for the assessment of their potential applicability (Vallorani et al., 2018) in identification of frequencies of climate variables associated with weather system. Numerous studies have investigated the link between large scale weather circulations and extreme hydrometeorological events including temperature (Vallorani et al., 2018, Linderson, 2001), precipitation (Trigo and DaCamara, 2000, Lorenzo et al., 2008, Raziei et al., 2012, Gevorgyan, 2013, Ramos et al., 2014), atmospheric rivers (Eiras-Barca et al., 2018), wind storms (Donat et al., 2010), floods (Prudhomme and Genevier, 2011, Pattison and Lane, 2012, Teale et al., 2017, Gilabert and Llasat, 2017, Rebelo et al., 2018), droughts (Fleig et al., 2010, Russo et al., 2015), atmospheric pollutants (Laaidi, 2001), and heaths (Vanos et al., 2015, Lee, 2015) in local or regional scale.

The ability of objective weather circulation methods to describe the Central Asian climate have been studied by Reyer et al. (2017) and Gerlitz et al. (2018). Based on Lamb catalogue, the circulation weather types (CWT) algorithm was used to evaluate the relationship between atmospheric circulation and seasonal frequencies of precipitation for Aksu river under climate change conditions (Reyers et al., 2013).

Gerlitz et al. (2018) identified eight weather types (WT) over Central Asia and analysed their relationship with tropical and extratropical drivers and teleconnection modes by utilising k-means-based clustering algorithm applied to mid-troposphere (500hPa GPH). Using this strategy, authors could evaluate the regional circulation characteristics with regards to climate variables such as temperature and precipitation.

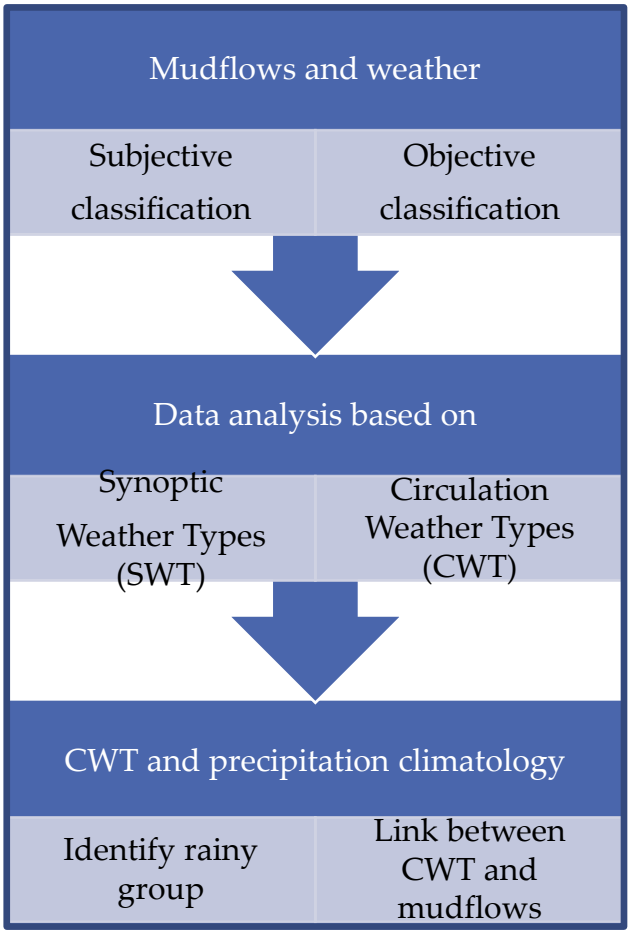

Figure 3.1. Assessment of large scale circulation and mudflow occurrences (Objective 3).

However, there is still lack of investigations for Uzbekistan, when compared to the number and type of studies in Europe, to determine extreme hydro-meteorological events, such as mudflows and mudflow generating weather patterns. Thus, this chapter focus on use of Synoptic Weather Types (SWT) subjective scheme and Circulation Weather Type (CWT) objective approach to examine mudflow inducing

weather patterns in Uzbekistan. Figure 3.1 illustrates the overall methodological approach of this chapter.

The research presented here is novel in that there are no studies which have applied the objective CWT classification scheme to examine what atmospheric conditions (focused on air flow direction) are involved in mudflow occurrences in Uzbekistan. The desired outcome of this chapter is to eventually select representative weather types which can be applicable to a large set of Coupled Model Intercomparison Project Phase 5 (CMIP5) GCMs. That way the influence of precipitation patterns on mudflow occurrences can be studied under climate change scenarios across Uzbekistan and Central Asia in further investigation.

3.2. Data

3.2.1. Observed Data

Observed daily precipitation for the period 1984-2013 recorded by Uzhydromet from the five meteorological stations Gallyaral, Chimgan, Sokh, Mingchukur and Baysun (Table 3.1) located in the mountains and the foothills with high mudflow passages were used to produce respective climatologies (Figure 3.4, Figure 3.5).

In addition, historical data of Uzhydromet regarding mudflow occurrences in Uzbekistan over the period 1984-2013 (March-August) derived from the national scale mudflow database was used to assess the relationship between extreme mudflow events and weather characteristics. This data includes information such

as the name of the water stream, location, date of passage, the potential reason for the formation of the mudflow, a rough estimate of the volume and major damages.

Table 3.1. The main characteristics of the meteorological stations in Uzbekistan used in this study (Source: Uzhydromet)

	Station	WMO	Latitude °N	Longitude °E	Elevation (m)	Established year	Used data for this study
1	Gallyaaral	38577	40.00	67.60	574	1929	1984-2013
2	Chimgan	38706	41.50	70.00	1620	1984	1984-2013
3	Sokh	38749	39.90	71.20	1200	1971	1984-2013
4	Mingchukur	38816	38.70	66.90	2132	1950	1984-2013
5	Baysun	38827	38.20	67.20	1241	1932	1984-2013

Data of the daily mean synoptic situation or local classification of Synoptic Weather Types (SWT), which is available at Library Services and the Archive Department of Uzhydromet as catalogues of six hourly (00, 06, 12, 18 GMT) data manually derived from synoptic charts, was calculated to produce relative outputs regarding mudflow inducing weather situations. The period considered in this study is a warm season (March-August) of 1984-2013.

3.2.2. Reanalysis data

In order to assess potential climatic drivers over Uzbekistan daily mean lower atmospheric flow in 700 hPa geopotential height (GPH) fields by the European Centre for Medium-Range Weather Forecasts (ECMWF) ERA-Interim reanalysis (Dee et al., 2011), spanning the period 1984-2013, was used to estimate the large-scale atmospheric circulation. Additionally, zonal and meridional wind components, specific and relative humidity on the same level have been analysed to understand moisture source on mudflow days. This gridded data set has 0.75^{o} spatial resolution. Detailed description are provided by Dee et al. (2011).

3.3. Methods

3.3.1. Stations and Mudflow Events Selection

Stations namely Gallyaaral (574 m a.s.l.) located in Zerafshan basin, Sokh (1200 m a.s.l.) in Fergana Valley, Chimgan (1620 m a.s.l.) in Chirchik-Akhangaran basin, Mingchukur (2132 m a.s.l.) representing Kashkadarya basin and Baysun (1241 m a.s.l.) in Surkhandarya basin (Figure 2.3, Table 3.1, Figure 3.2 b-c) were considered to investigate regional and local characteristics of the rainfall over each basin with high mudflow passages and its adjustment areas. The investigation area is limited to rain gauges located in the mountain areas, based on the assumption that each station well represents hydro-climatologic conditions of the basin and at the same time station data on rainfall accumulation

process can capture mudflows within the radius of roughly 100 km. Regional and local mudflow data was extracted from the national scale database for the warm season (March-August) of 1984-2013 to evaluate the relationship between mudflows and synoptic and large scale meteorological patterns. There were more than 300 days with mudflow episodes during the investigation period. Each mudflow event was placed within five areas based on information regarding the geographical name of the evidence.

3.3.2. Synoptic Weather Type (SWT)

Subjective scheme of SWT (Bugayev et al., 1957) was adopted in order to manually evaluate the relationship between synoptic weather patterns and recorded mudflow occurrences in five areas with high mudflow passages in Uzbekistan. Therefore, SWT database was created based on SWT daily sequences sources contained in the previously published literature (Ilinova, 1968, Voynova and Inagamova, 1982, Inagamova, 1993, Inagamova, 2013). In addition, daily mean SWT sequence for summer (Mar-Aug) of 1984-2013 was extracted from the database to assess the association between mudflow days and frequency of synoptic scale circulation. R language code is used for calculation of SWT climatological frequencies and its relation with mudflow occurrences over Uzbekistan.

3.3.3. Circulation Weather Type (CWT)

The classification of daily flow patterns was done by the CWT approach. It was developed by Jenkinson and Collison (Jones et al., 1993) based on the original Lamb weather types for the British Isles (Lamb, 1972). The basic method and details of the scheme were provided by Jones et al. in 1993. The objective CWT scheme makes use of three basic variables that define the circulation features at the surface over the study region: direction of mean flow (D), the strength of mean flow (F) and the vorticity (Z). This basic method can be applied to any region with latitude ~30°–70° (Jones et al., 2013). For each day, the direction of the atmospheric flow is determined by considering pressure values at 16 points around the central point at 40.0°N-67.5°E (Figure 3.2 a), and is marked to one of ten CWTs: northeast (NE), east (E), southeast (SE), south (S), southwest (SW), west (W), northwest (NW), north (N), cyclonic (C), and anticyclonic (A). The aim of applying this method is to estimate the impact of airflow on precipitation patterns and its association with extreme mudflow episodes in Uzbekistan. Furthermore, the CWT scheme allows to define atmospheric flow regimes objectively to be applicable for Coupled Model Intercomparison Project Phase 5 (CMIP5) models data.

ERA-Interim reanalysis data on global pressure level at 700 hPa for the climatological period of 1984-2013 was prepared using CDO (Climate Data Operation) tool and was applied as an input data for CWT programme in

FORTRAN code running under the Linux platform. Additionally, more than 300 days of daily mean pressure at GPH 700 hPa related to days with mudflow occurrences in each basin has been selected from the climatological period in order to identify directional air flow on mudflow days by implementing objective scheme. All computational work has been done on LES-Linux Servers for High Performance Computing (HPC) provided by College of Life and Environmental Sciences (LES), University of Birmingham. Selected stations data on daily precipitation provided by Uzhydromet has been used to assess the derived air flow directions impact on precipitation regime in Uzbekistan. This part of the analysis has been done using R core language.

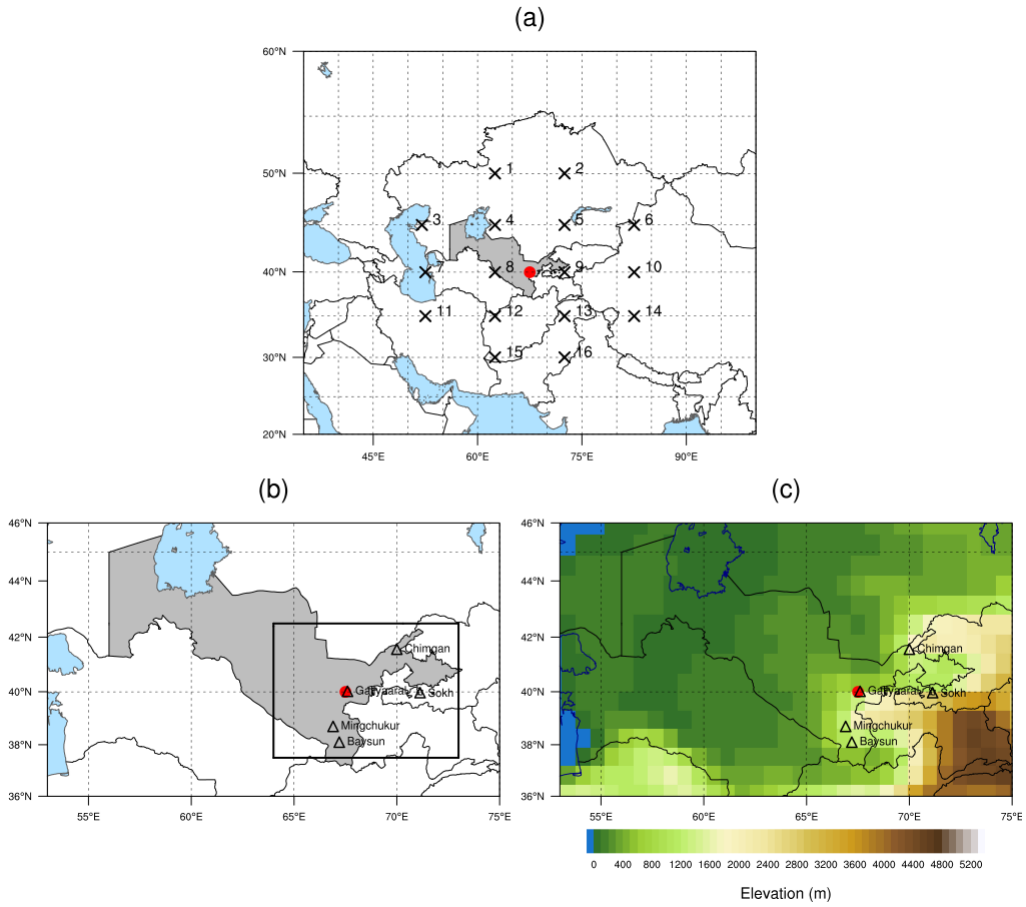

Figure 3.2. Location of the study domain together with the 16 grid points and central grid point (40N-67.5E, red circle) used in the automated weather circulation type (a); Investigation area (b) shown in rectangle and location of selected stations (black triangles) around the central grid point 40.0 N-67.5 E (red circle) of CWT objective method. Stations: Gallyaaral (40.02 N-67.60 E), Chimgan (41.57 N-70.00 E), Sokh (39.97 N-71.13 E) and Mingchukur (38.70N – 66.90 E); (c) ERA-Interim orography map and the location of central grid point (red circle) together with representative five stations (black triangles).

3.4. Results

3.4.1. Synoptic weather types over Uzbekistan and mudflow events

During the investigation period between 1984 and 2013, there were more than 300 days with mudflow occurrences in Uzbekistan. Figure 3.3 shows the

frequencies of mudflow days for each synoptic weather type in five regions (Zerafshan, Chirchik-Akhangaran, Fergana, Kashkadarya and Surkhandarya) with high mudflow passage. According to the results, the majority of mudflows occur during the advection of airflow from *west* (SWT 10) and *low level of small barometric gradient* (SWT 13) in the study area. However, the SWT 13 is the most frequent weather type in Fergana Valley (Figure 3.3 c) as the interaction of frontal circulation with orography as well as the associated effects of condensation and evaporation are assumed to determine the formation of low-level fronts and small-scale rainbands (Buzzi et al., 1998, Inagamova et al., 2002) there. *Stationary cyclone* type (SWT 8) is the second most frequent SWT triggering mudflow events although in some regions it is not as prominent. Purely anticyclonic weather types (SWT 9, 9a, 9b) constitute less than 15% of all events (Figure 3.3) even though this weather type is the most frequent per year on average (Figure 2.12). Cyclones propagating from the *south-west* (SWTs 1 and 2) towards the study area, *advection from north and north-west* (SWTs 6 and 5), *high level of small barometric gradient* (SWT 12) and synoptic wave activity on a cold front (SWT 7) contribute also to significantly unstable weather conditions inducing mud and debris flows (Figure 3.3). While the majority of SWTs were associated with regional or local scale precipitation patterns, the summer thermal low (SWT 11) does not (Figure 3.3 b, c, d). Observations confirmed this SWT has triggered mudflows with origins of snow and glaciers melting due to increasing surface temperatures.

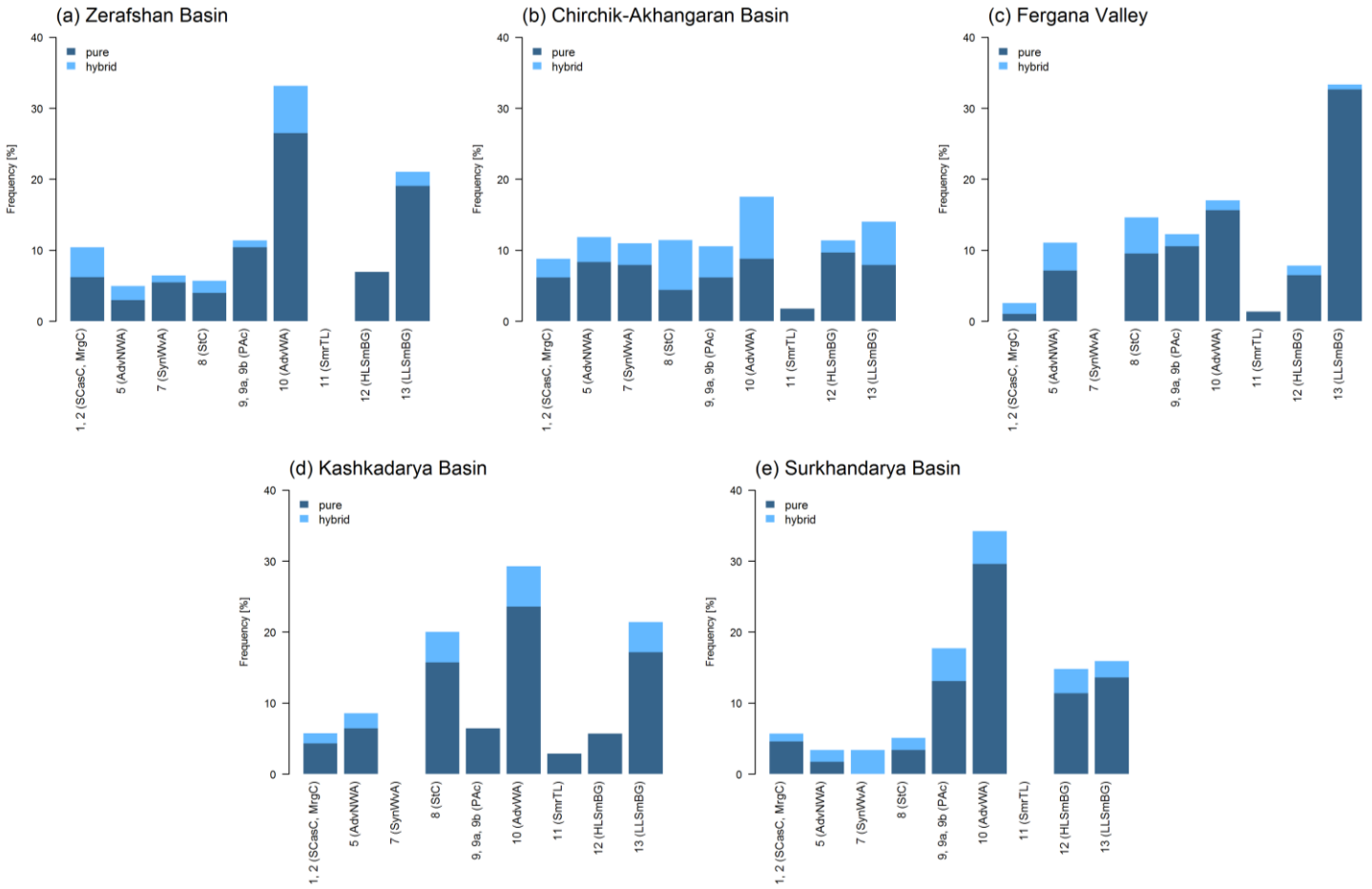

Figure 3.3. Frequency of mudflows under the synoptic weather types (SWT) over Uzbekistan during 1984-2013 (March-August): a) Zerafshan basin (101 days); b) Chirchik-Akhangaran rivers basin (57 days); c) Fergana Valley (147 days); d) Kashkadarya basin (35 days); e) Surkhandarya basin (44 days). Definitions of SWT can be seen in Table 2.3.

3.4.2. Circulation Weather types over Uzbekistan and mudflow occurrences

3.4.2.1. CWT and precipitation climatology

In order to assess the impact of each CWT class on mudflow triggering precipitation regimes, long-term daily circulation types and the corresponding daily values of precipitation were analysed.

Figure 3.4 and Figure 3.5 show the seasonal distribution of the relative frequency of the number of days and precipitation values for each CWT class during 1984–2013 for the five stations (Gallyaaral, Chimgan, Sokh, Mingchukur and Baysun) in total. The column graphs in Figure 3.4 highlight the frequency of each weather class (CWT days, %) as well as the relative contribution of each weather type to the total recorded rainfall values (total precipitation, %) and the average daily precipitation per CWTs (mm/day). The box plots in Figure 3.5 indicates the seasonal rainfall statistics including 90^{th} and 95^{th} percentile of precipitation value within each CWT class.

It is worth noting that on average the large-scale atmospheric circulation over Uzbekistan and Central Asia is mainly dominated by **westerly** (W) weather type throughout the year (Figure 3.4). The frequencies of W type shows the highest value between 22-38%, depending on the season. The percentage of precipitation during the W days ranges from 35% to 75% of the total annual precipitation per station. The

spatial distribution of daily average precipitation up to 3-7 mm/day was associated with the W flow for nearly all the stations (9-12 mm in Chimgan, Figure 3.4 b).

Cyclonic (C) and **anticyclonic** (AC) weather types feature with almost similar frequencies (18%) in summer, however, C flow contributes roughly four times more of the annual precipitation (up to 27%) and daily rainfall values (13 mm/d) compared to the AC class. Even though AC circulation has higher reputation of the circulation days in contrast to C type in the winter half of the year, the C days still indicate higher values of precipitation pattern which makes this CWT one of the wettest airflow. The 90th and 95th percentiles of the precipitation totals confirm this (Figure 3.5).

South-westerly (SW) flow occurs from 6% to 13% during the year and contributes 10-22% of the precipitation totals (5% in Fergana Valley). Seasonal distribution of weather types associated with **easterly** and **southerly** flows (E, SE and S) are up to 1.3 % per season and fairly variable throughout the year and produce little or almost no rainfall, i.e. 0.2-0.5% or less than 1 mm/day. Another minor occurrences associated with **north-westerly** (NW) circulation (1-3%) contributing approximately 3% of the precipitation totals and 4 mm daily rainfall on average depending on the area and the rain gauge data.

In comparison to other stations, the **north-easterly** (NE) and **northerly** (N) weather types have different precipitation patterns at Sokh station, Fergana Valley, during

the warm season of the year (Figure 3.4 c and Figure 3.5 c). This is due to the location and orographic pattern of the area (Figure 3.2 c) which makes these weather types one of the wettest airflow throughout the year with frequent floods and mudflow occurrences.

The impact of small-scale orographic features on weather types and rainfall distribution is assumed to be one of the reasons for the notable seasonal variabilities of the **undefined** weather type throughout the year. For illustrative purposes, an ERA-Interim orography map confirming this has been included (Figure 3.2 c). An important inclusion in this study was the CWT evaluation which highlighted the spatial distribution of precipitation in Uzbekistan on synoptic scale.

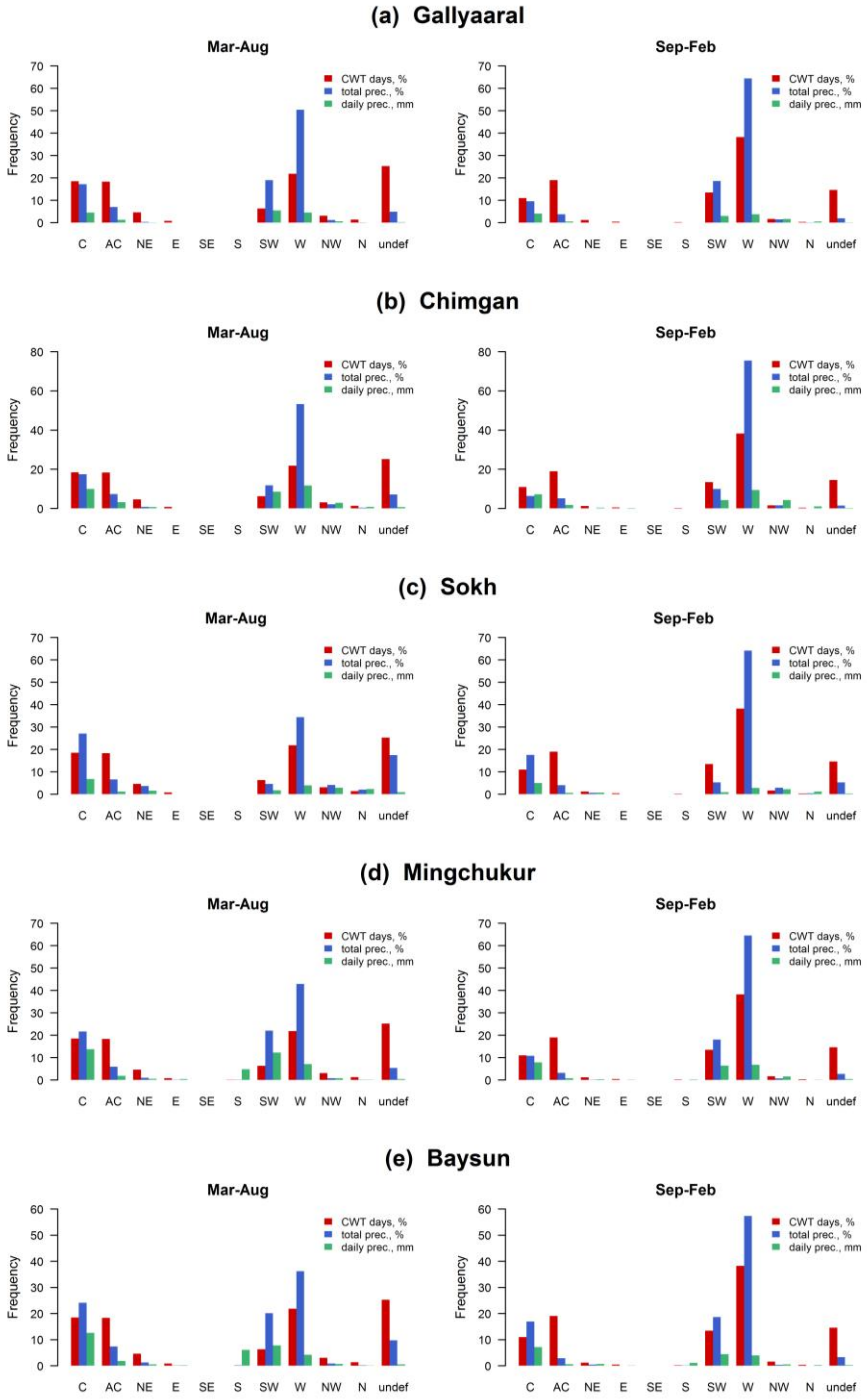

Figure 3.4. Contribution of CWT classes to the observed precipitation over the stations Gallyaaral in the Zerafshan basin (a), Chimgan in the Chirchik-Akhangaran basin (b), Sokh in Fergana Valley (c), Mingchukur representing the Kashkadarya basin (d) and Baysun in the Surkhandarya basin (e) for warm (Mar-Aug) and cold (Sep-Feb) seasons for the years 1984-2013. CWT days - frequency of each class in percentage; % total precipitation - contribution of each class to the overall precipitation; mm/day - daily average precipitation per CWT. The figure has different scales.

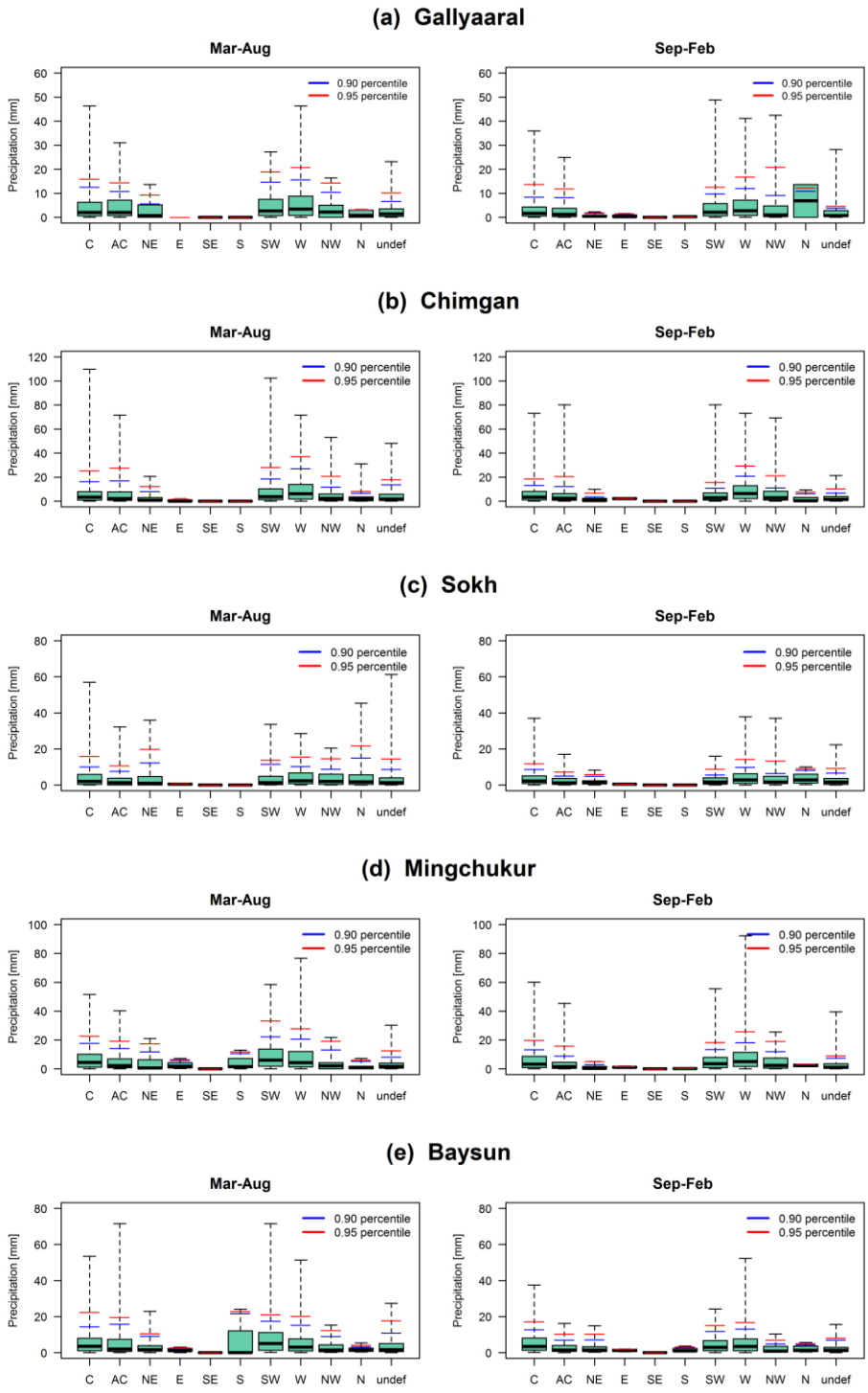

Figure 3.5. Box plots show daily precipitation (1984-2013) per CWT class in five representative stations namely Gallyaaral (Zerafshan basin), Chimgan (Chirchik-Akhangaran basin), Sokh (Fergana Valley), Mingchukur (Kashkadarya basin) and Baysun (Surkhandarya basin). The blue and red lines represent 0.90th and 0.95th percentiles of the precipitation for each class. The graph has different scales.

3.4.2.2. CWT and Mudflows

This section presents the analysis of the relationship between CWT classes and mudflow occurrences in the investigation regions of Uzbekistan. Figure 3.6 shows a comparison between mudflow events with CWT daily frequencies in March-August, 1984-2013. For consistency, the central grid point (40.0N-67.5E) was selected for investigation of 101 days induced mudflow occurrences in Zerafshan basin, 147 days in Fergana Valley, 57 days in Chirchik-Akhangaran, 35 days in Kashkadarya and 44 days in Surkhandarya basins observed in a warm season during the period 1984-2013 (Figure 3.6). Interestingly, the Zerafshan (a), Chirchik (b), Kashkadarya (d) and Surkhandarya (e) regions have similar patterns (Figure 3.6). However, complex orography and complicated topography affect the weather systems and precipitation distribution are assumed to produce slightly different results for Fergana Valley (Figure 3.6 c). The frequencies of W, SW, and C weather types are considered as a "rainy" group with increased mudflow episodes compared to the rest of the CWTs nearly in all five regions. There is also considerable amount of NW circulation type associated with extreme mudflow events in Chirchik and Surkhandarya basins (Figure 3.6 b, e). However, NE days trigger more mudflows in contrast to SW flow which reveals a decrease in Fergana Valley (Figure 3.6 c).

Figure 3.7 confirms that anomalies compared to the average occurrence of mudflow days per C, W and SW classes are higher in comparison to normal CWT climatology

during the warm phases of 1984-2013. The AC weather pattern has a noticeable decline of mudflow frequencies compared to the climatological mean per CWT class. NW flow is also attributed to the mudflow trigger weather class as it was accompanied with heavy rainfall induced extreme mudflow events particularly in the Chirchik-Akhangaran and the Surkhandarya basins and slightly in Fergana Valley. During the investigation period mudflow events in the study area was found to be highly unlikely for E, SE and S resulted, thus representing missing values in the figure.

It is noteworthy here that the variability of C, W, SW and NW days in comparison to all CWT days again show increased trends in mudflow probability and corroborated all results mentioned above. Therefore it can be concluded that appreciable weather classes (C, W, SW, and NW) are the main contributors to observed mudflow occurrences for the study area and is in agreement with the recorded precipitation distribution patterns.

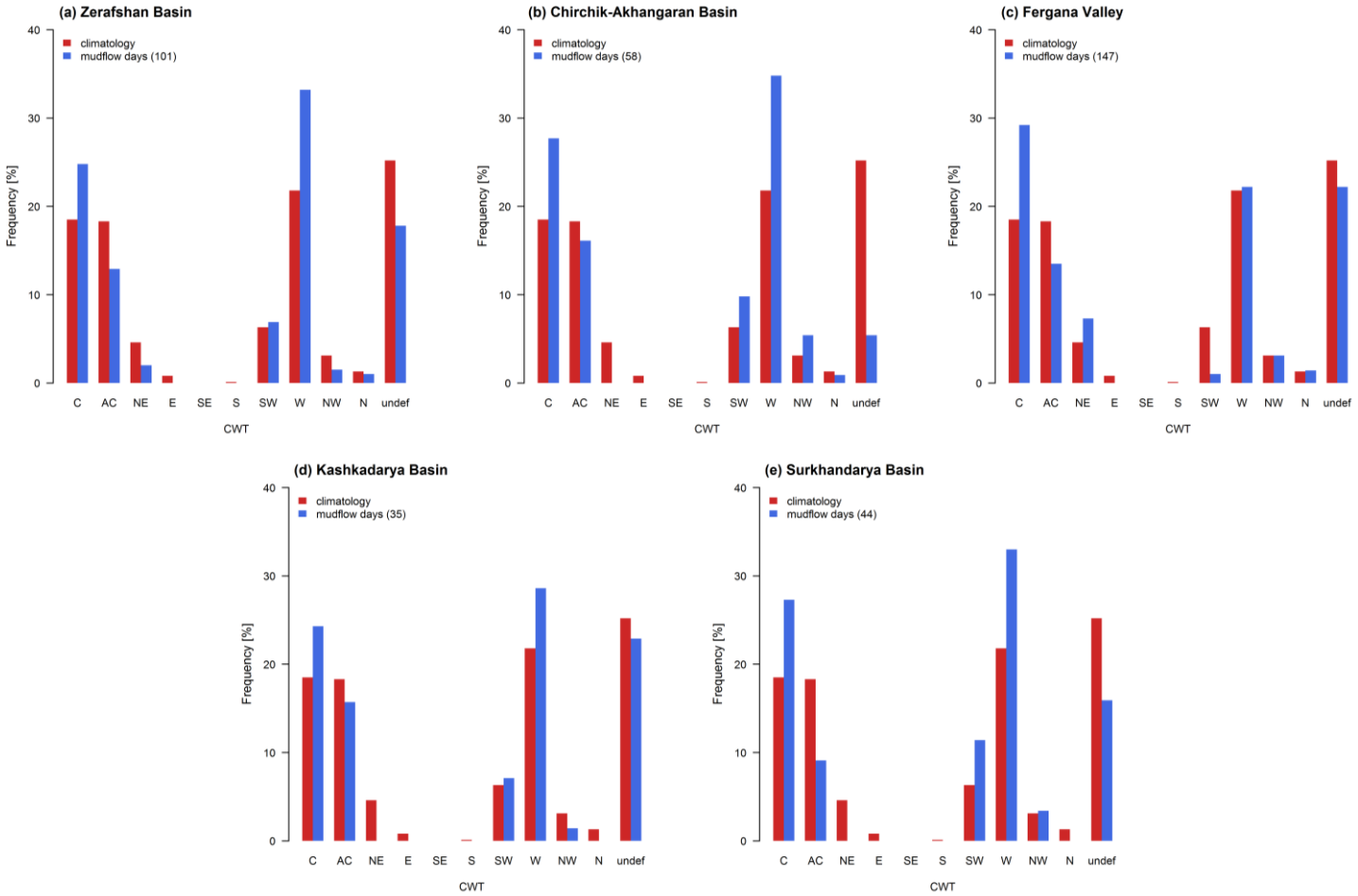

Figure 3.6. Frequency of CWT (700 GPH) climatology for the period March-August, 1984-2013 (red bars) and mudflow days (blue bars) occurred in the Zerafshan basin (a), Fergana Valley (b), the Chirchik-Akhangaran (c), Kashkadarya (d) and Surkhandarya (e) basins in Uzbekistan. Central grid point is 40.0 N - 67.5 E.

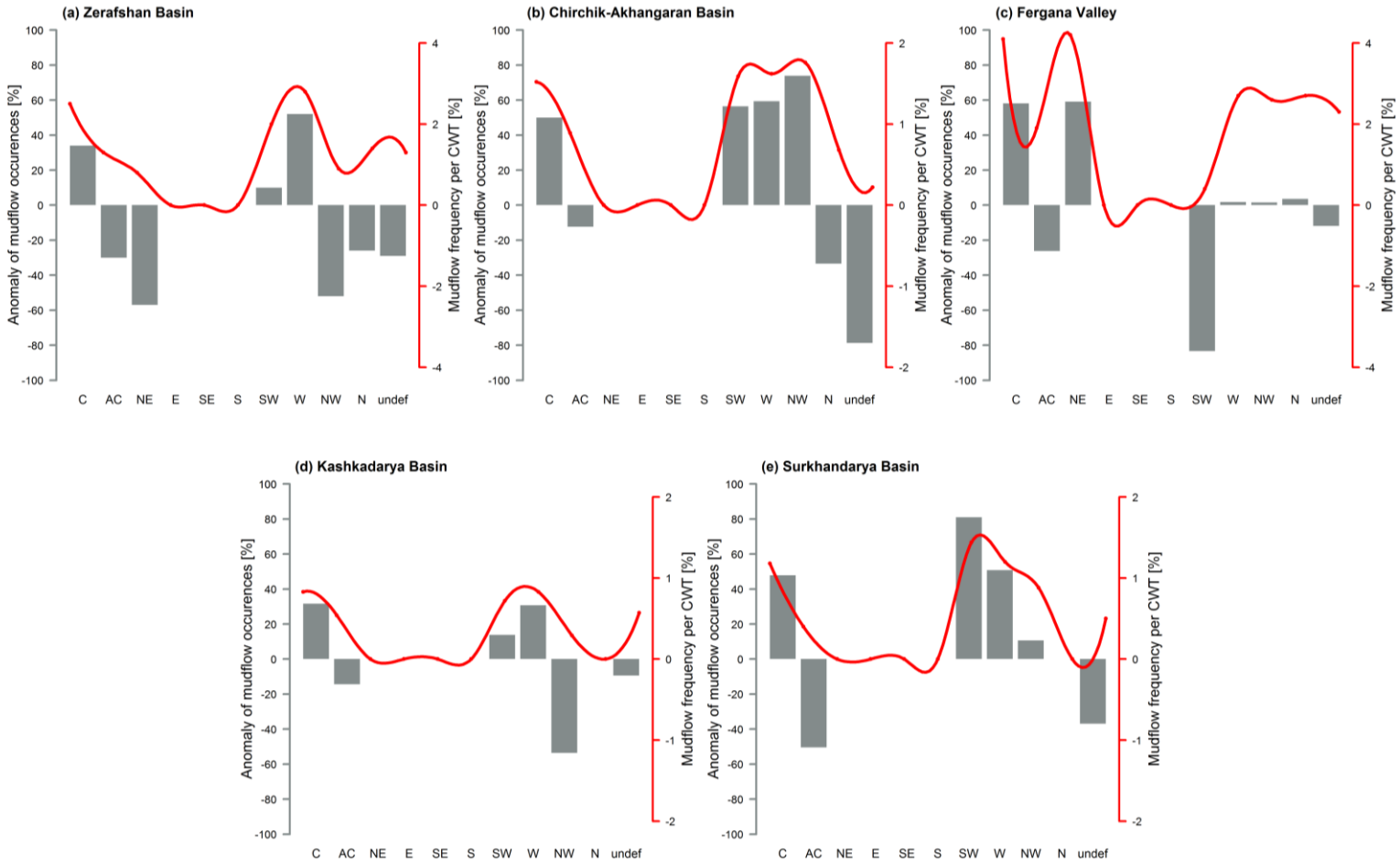

Figure 3.7. Anomaly of mudflow days per CWT class (grey bars, grey axis, %) and CWT classes for mudflow days (red line, red axis, %) for the March-August period between 1984 and 2013 in five regions: a) Zerafshan basin (101 days); b) Fergana Valley (147 days); c) Chirchik-Akhangaran basin (57 days); d) Kashkadarya basin (35 days); e) Surkhandarya basin (44 days). Figure has different scales.

3.4.2.3. Large-scale circulation and hydroclimatological conditions triggering mudflows

The large scale atmospheric flow directions over Uzbekistan have been analysed to understand the synoptic conditions and moisture sources that enhanced rainfall patterns resulting in extreme mudflow occurrences in the study area for the period of 1984-2013.

A strong ridge extending from Central Asia to the Siberia assist in keeping the NE circulation in confined to the study area as well as supported the Atlantic moist air transport from Central Europe to Uzbekistan. At the same time, a trough located downstream of the ridge played a significant role in keeping the moisture budget by feeding with the tropical moist air through the Tibetan Plateau. This mechanism supports persistent extreme rainfall patterns that exacerbated mudflow responses in Zerafshan basin and Fergana Valley (Figure 3.8a, Figure 3.10a).

A subsequent trough sometimes associated with the existence of cyclone over the Aral Sea and with strong SW flow brought moisture from the Mediterranean region, the Arabian Sea and the Persian Gulf into the study area. This mudflow inducing atmospheric pattern was the predominant source of rain associated with the most devastating mudflow events occurred in Uzbekistan (Figure 3.8b, Figure 3.9a, Figure 3.10b, Figure 3.11a, Figure 3.12a).

CWT W days were the direct corridor extending from the Mediterranean region and Central Europe that intensified Atlantic and Mediterranean moisture passage towards the investigation area resulting in the massive formation of mudflows induced by heavy rainfall patterns across Uzbekistan (Figure 3.8c, Figure 3.9b, Figure 3.10c, Figure 3.11b and Figure 3.12b). W airflow direction was characterised to be the dominant circulation weather pattern to trigger extreme mudflow events in the study area.

A following, ridge over the Ural Mountains with extended axis to the northwest supported more NW component and contributed the strongest precipitation intensities in the region (Figure 3.8d, Figure 3.9c, Figure 3.10d, Figure 3.11c and Figure 3.12c). Although, this large-scale atmospheric circulation flow brought highly anomalous moisture from Central Europe and Western Russia into the study area, there was still a chance for tropical moist air to reach the region that played a crucial role during the early stage of the extreme precipitation events.

Furthermore, atmospheric conditions during the CWT N days were characterised by the ridge with meridionally extended axis over the Ural Mountains and a trough on the right side of the ridge with cyclone located over south-eastern Siberia (Figure 3.9d). This synoptic scale weather pattern was associated with precipitation events induced mudflows especially in mountain areas of Zerafshan (Figure 3.8e), the Chirchik-Akhangaran basin (Figure 3.9d) and Fergana Valley (Figure 3.10e).

Strikingly, atmospheric circulation during the C days was influenced by a blocking ridge across western Kazakhstan and a deep trough with low level cyclone existence on the east side of the ridge (Figure 3.9e, Figure 3.10f, Figure 3.11d, Figure 3.12d). The blocking ridge assisted the cyclonic circulation by adding surge of continental and tropical moisture that was able to produce strongest precipitation intensities associated with most mudflow occurrences in the area. However, lower tropospheric precursors during the cyclonic days in the Zerafshan Valley show that the presence of the ridge is less prominent even though cyclonic circulation is highlighted by the wind components (Figure 3.8f).

Anticyclonic weather type condition was characterised by a moderate ridge of high pressure field associated with enhanced westerly and south-westerly flows in the region over Uzbekistan (Figure 3.8g, Figure 3.9f, Figure 3.10g, Figure 3.11e and Figure 3.12e). This hybrid circulation weather pattern persisted to transport tropical-continental moist air towards the study area and was responsible for localising heavy rainfall that contributed mudflow events there.

Inactive frontal zone in lower troposphere on synoptic scale over the region was highlighted during the days with undefined flow direction. Orographic lifting with some embedded deep convection was a key process associated with extreme rainfall triggering mudflows during the days of undefined flow direction (Figure 3.8h, Figure 3.9g, Figure 3.10h, Figure 3.11f and Figure 3.12f).

This section documents large scale climatological aspects of mudflow occurrences in Uzbekistan. Although significant results on atmospheric circulation patterns can be made with CWT approach, it is desirable to investigate moisture source trajectories and detailed analysis of extratropical forcing factors of the extreme precipitation inducing mudflow events in a climatological context in the future.

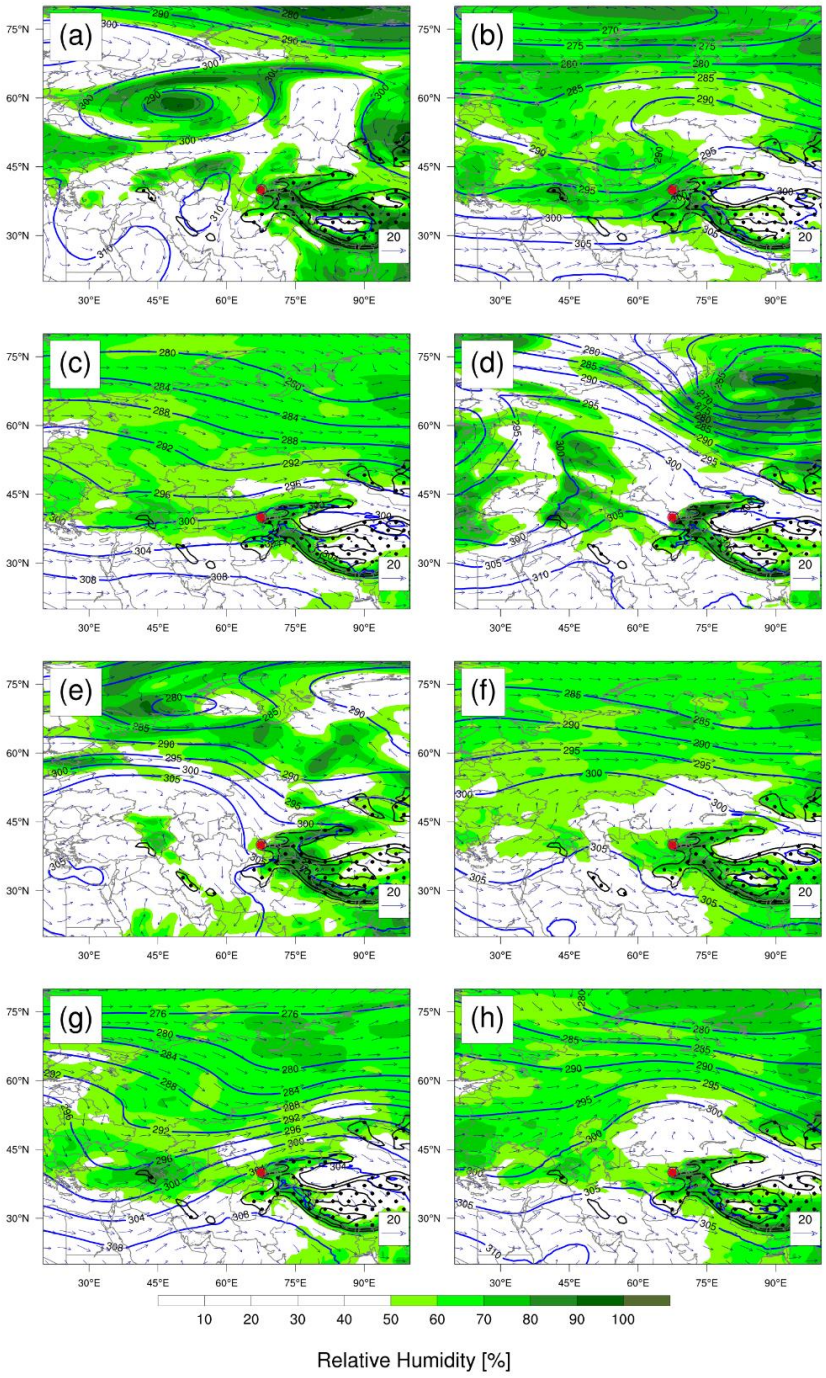

Figure 3.8. CWT north-east (a), south-west (b), west (c), north-west (d), north (e), cyclonic (f), anticyclonic (g) and undefined (h) weather type characteristics on the mudflow days occurring in the Zerafshan basin for the period of 1984–2013. ERA-Interim 700 hPa geopotential height, relative humidity and wind component were used to produce this figure. Red circle indicates the central grid point (40.0°N-67.5°E). Black contour lines together with black dots show the area where the topography is above 2000 m further corresponding 3000 and 4000 m.

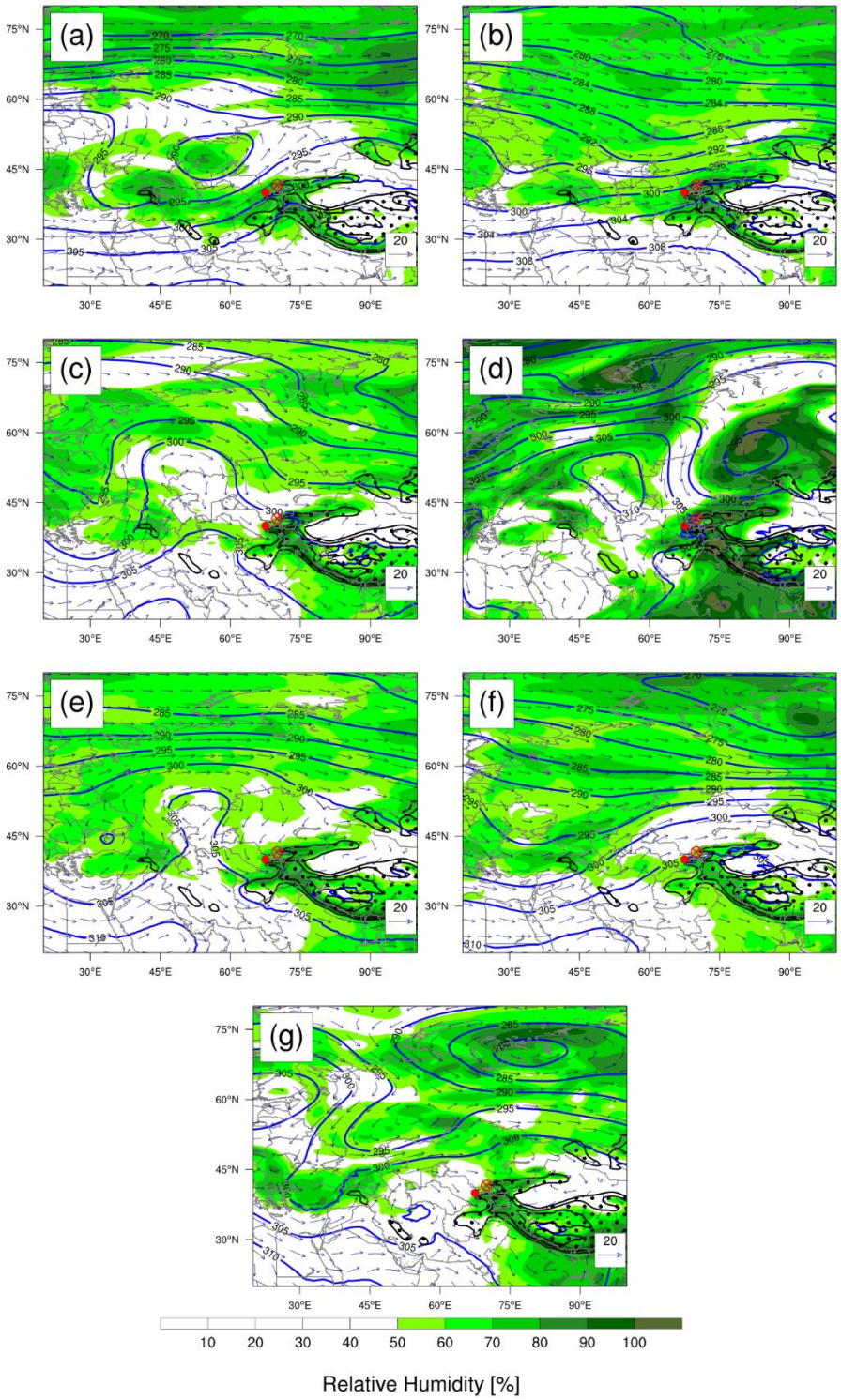

Figure 3.9. Same as Fig 3.8 but in the Chirchik–Akhangaran basin: CWT south-west (a), west (b), north-west (c), north (d), cyclonic (e), anticyclonic (f) and undefined (g) weather type.

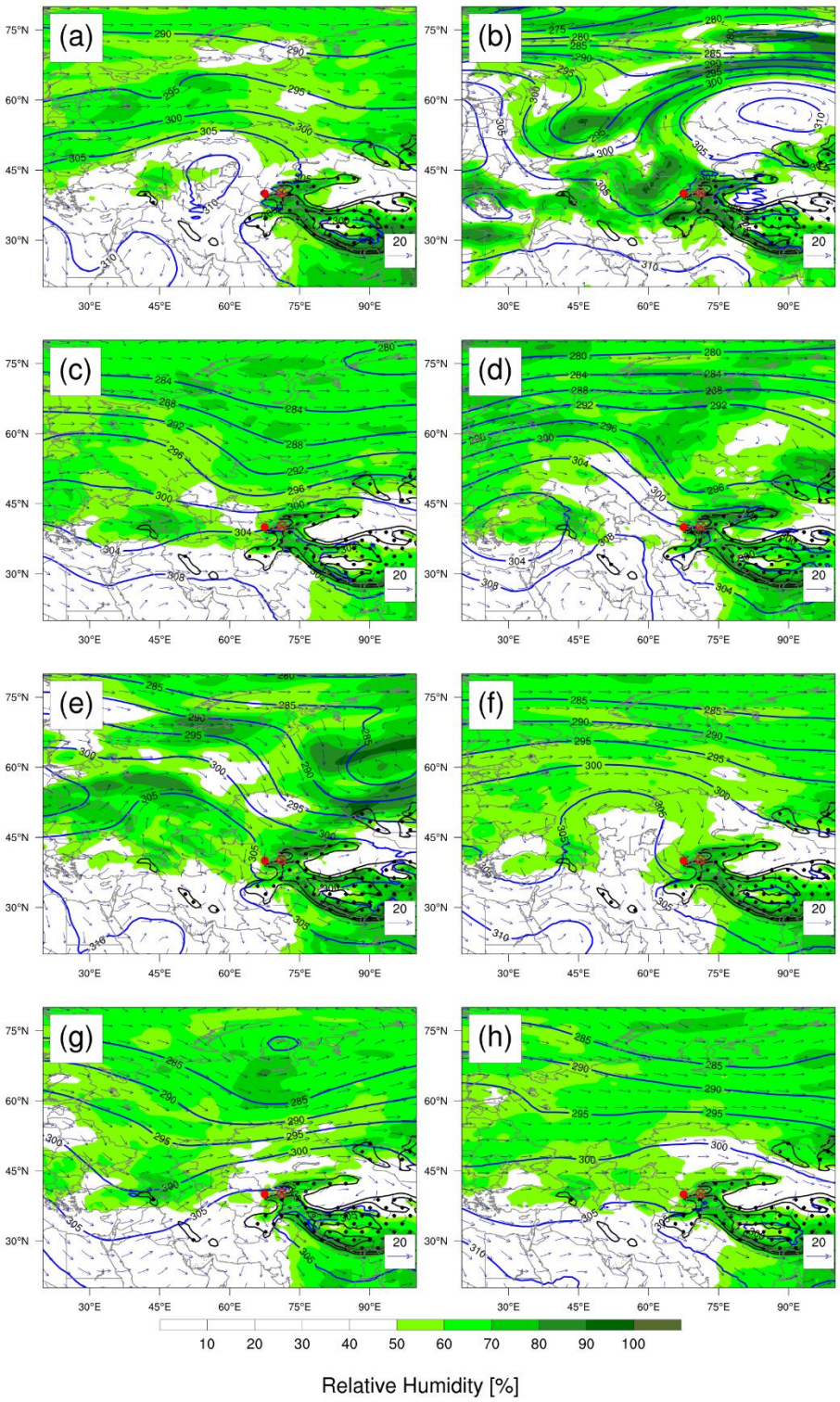

Figure 3.10. Same as Fig 3.8 but in Fergana Valley: CWT north-east (a), south-west (b), west (c), north-west (d), north (e), cyclonic (f), anticyclonic (g) and undefined (h) weather type.

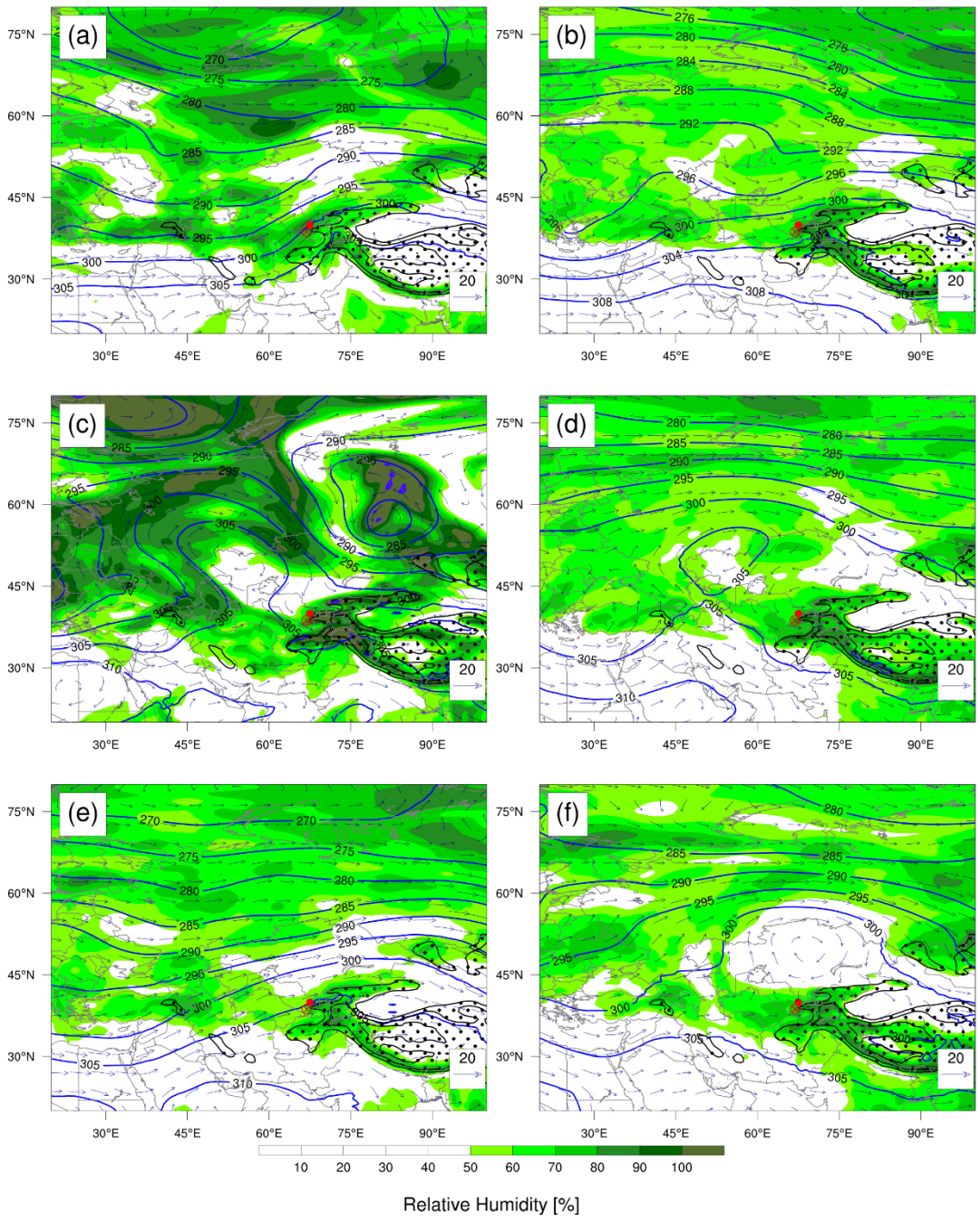

Figure 3.11. Same as Fig 3.8 but in the Kashkadarya basin: CWT south-west (a), west (b), north-west (c), cyclonic (d), anticyclonic (e) and undefined (f) weather type.

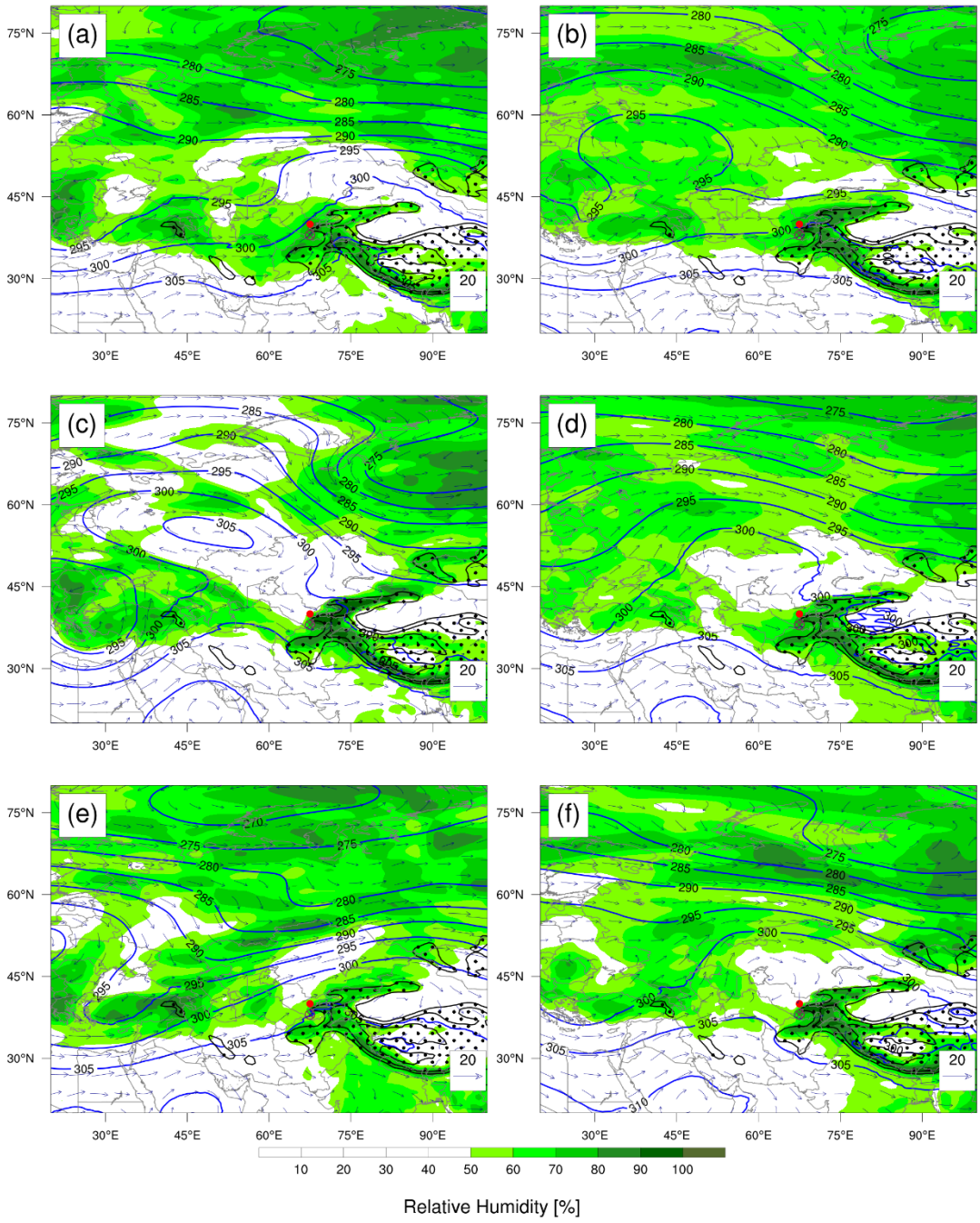

Figure 3.12. Same as Fig 3.8 but in the Surkhandarya basin: CWT south-west (a), west (b), north-west (c), cyclonic (d), anticyclonic (e) and undefined (f) weather type.

3.5. Discussion

3.5.1. Comparisons with previous assessments

3.5.1.1. SWT

Advection of moist and relatively cold air from the west, as classified in the SWT classification by Bugayev et al. (1957), was revealed as the dominant synoptic situation inducing mudflows. This result is consistent with the findings of Aizen et al. (2004), thus confirming that westerly advection is the predominant synoptic scale driver for precipitation climatology in Central Asia. Furthermore, the results presented here complement those of Salikhova (1975) and Lyakhovskaya (1989) who established that mudflow occurrences induced by heavy rainfalls associated with westerly advection as the major synoptic pattern over Uzbekistan. This analysis was done by adopting a manual assessment methodology of mudflow generating weather conditions on synoptic scale based on SWT catalogues. Historical synoptic charts are not yet fully digitised by the Uzhydromet, thus manual assessment was the preferred methodology.

Limitations of SWT

Even though assessment of weather situations by means of SWT may identify plausible synoptic scale flow characteristics triggering mudflows, this subjective approach does not consider any mesoscale conditions over the study area.

Therefore, additional information of smaller scale features such as terrain-induced flow modulations (Stucki et al., 2012) merit further analysis.

3.5.1.2. CWT

The relationships and related variables explaining the spatial distribution of precipitation, obtained by an objective CWT approach, defined the four weather classes westerly (W), south-westerly (SW), cyclonic (C) and north-westerly (NW) as the main drivers of precipitation characteristics on a regional scale. The interesting thing is that similar results have been obtained previously for precipitation generating weather patterns over Portugal and Iberian Peninsula (Trigo and DaCamara, 2000, Ramos et al., 2014) and the most susceptible to causing floods in UK (Longfield and Macklin, 1999, Pattison and Lane, 2012). This allows a positive evaluation of the CWT method in principle.

Furthermore, CWT findings are in line with results from Reyers et al. (2013) who evaluated spatial patterns and annual cycles of precipitation using CWT scheme for Central Asia. Interestingly, the westerly airflow in Reyers et al. (2013) was split into two subgroups, as W1 (distinct zonal flow) and W2 (negative 700 hPa GPH gradient) and NE and E as well as SE and S were combined respectively. In general, it was found that probability of precipitation was much higher for C, CWT W2, N and SW airflows during the summer. However, the highest rainfall probability and

precipitation amount was attributed to the seldom CWT NE/E weather type (Reyers et al., 2013). In our study as well NE weather type despite its low frequency for the selected grid point revealed the high probability of precipitation patterns that could trigger mudflow events in Fergana Valley (Figure 3.4c, Figure 3.7c). Fergana Valley which has a better representation of topography presumably makes a case of particular interest with the findings in previous studies. According to Schiemann et al. (2008) it can be assumed that on smaller spatial scales, the influence of topography on precipitation climatology over Central Asia is paramount. Small et al. (1999) and Reyers et al. (2013) both confirm this.

In addition, this study agrees with findings of Gerlitz et al. (2018), which found a strong positive precipitation anomalies generated by the westerly wind field (WT7 and WT8; T[CA]) associated with westerly moisture flux over all of Central Asia. These authors also confirm that south-westerly flows (WT5) associated with increased advection of moisture tracking from the Arabian Sea, Persia Gulf and Caspian Sea can intensify the spatial variability of precipitation over the target area. North-westerly winds (WT6) mainly associated with dry weather could generate rainfall anomalies in mountain regions of the Tian Shan and Pamir.

Limitations of CWT

Pattison and Lane (2012) reported several limitations in use this classification over the UK while applying this approach to investigate flood generating weather types. Authors experienced that relationship between weather pattern and associated climatological variable such as rainfall records was not always reliable. They also noted that multiple weather types in different regions in UK occurred in a same day and it made the system more complex to use.

In general, the ability of CWT to describe the large scale circulations on lower troposphere over Uzbekistan performed satisfactory results. However, it produces fairly high frequency of undefined weather classes showing a strong seasonality, and particularly during summer relatively large amounts of precipitation (Figure 3.4, Figure 3.7). It could be possible attributed to the impact of mesoscale features such as orographically induced lifting (Gerlitz et al., 2018) and frontogenesis, thus variations of the atmospheric dynamics (Buzzi et al., 1998). Gevorgyan (2013) argued that objective circulation classification scheme does not always identify frontal processes over mountain regions correctly, which makes the objective scheme less suitable to classify differences in the atmospheric circulation in areas with complex topography or when the sub-synoptic scale is effected by the orography in elevated areas, even though the scheme is suitable for large scale circulation patterns. Pattison and Lane (2012) also reported that objective method

has a limitation to identify the details on meso-scale frontal and orographic systems which effects on UK precipitation climatology.

3.6. Conclusion

In this chapter the link between extreme mudflow events in Uzbekistan and atmospheric circulation associated with intense precipitation using multiple and coherent systematic approaches has been examined. This is especially important as only few studies have investigated atmospheric circulation conditions and precipitation variability for different spatial scales over Uzbekistan. This chapter specifically explores the research question: What are the main precipitation supporting weather types inducing mudflows in the study area? The principal findings of this study are as follows:

1. Concerned with basic analysis, rainfall for the period of March-August (1984-2013) delivered by SWT 10 - westerly advection increased the mudflow frequencies over the study area.
2. Objective CWTs that occurred on the days of extreme mudflow events for the warm season of the period 1984-2013 were evaluated and it was found that CWT C, W, SW weather patterns contributed the most to the seasonal precipitation totals resulting in more mudflows in the study area.

Manual assessment of SWT and computational CWT approach when compared with other published papers (Reyer et al., 2017, Gerlitz et al., 2018) indicate that the methodology adopted in this study produced robust results despite the orographic influence on the study area. Overall the methodology developed can be used reliably to examine the potential effects of atmospheric circulation on mudflow events in Uzbekistan and Central Asia. More importantly, selected weather patterns established by an objective CWT method can be a proxy to climate change modelling to investigate how the key factors which influence the mudflow triggering mechanism will change under anthropogenic climate change in the study area.

Significant role of orography on the enhancement of precipitation associated with atmospheric rivers or a seeder feeder mechanism resulting mudflow events in Uzbekistan can be an area of future research.

4 Statistical Modelling of Precipitation Thresholds for Triggering Mudflows

4.1. Introduction and background

Rainfall patterns are responsible for triggering different types of landslides including mudflows. Many investigators have attempted to establish the minimum and/or maximum amount of precipitation which was likely to initiate extreme landslide events for different parts of the world (review by Guzzetti et al., 2008). Nel Caine (1980) did the pioneering work where the author proposed a global rainfall-intensity duration (ID) threshold for shallow landslides and debris flows based on 73 publications from different regions of the world and created generalised standard logarithmic map known as Caine's threshold curve. Thresholds for landslides events using precipitation measurements obtained by physical (process-based, conceptual thresholds) and empirical (historical or statistical) approaches have been systematically reviewed by multiple authors, Guzzetti et al. (1999, 2007, 2008), Wieczorek and Glade (2005) in the last decades. Guzzetti et al. (2007) listed 124 regional and local (Figure 4.1) rainfall thresholds resulting in different types of landslides (debris flows, mudflows, flash-floods etc.) including Caine method (ID)

and normalized ID thresholds which were used for either for research purpose or as a warning alert in operational systems. After a year, these same group of authors updated the existing Caine threshold values (Figure 4.2) based on a global database of 2626 rainfall events inducing shallow landslides and debris flows (Guzzetti et al., 2008).

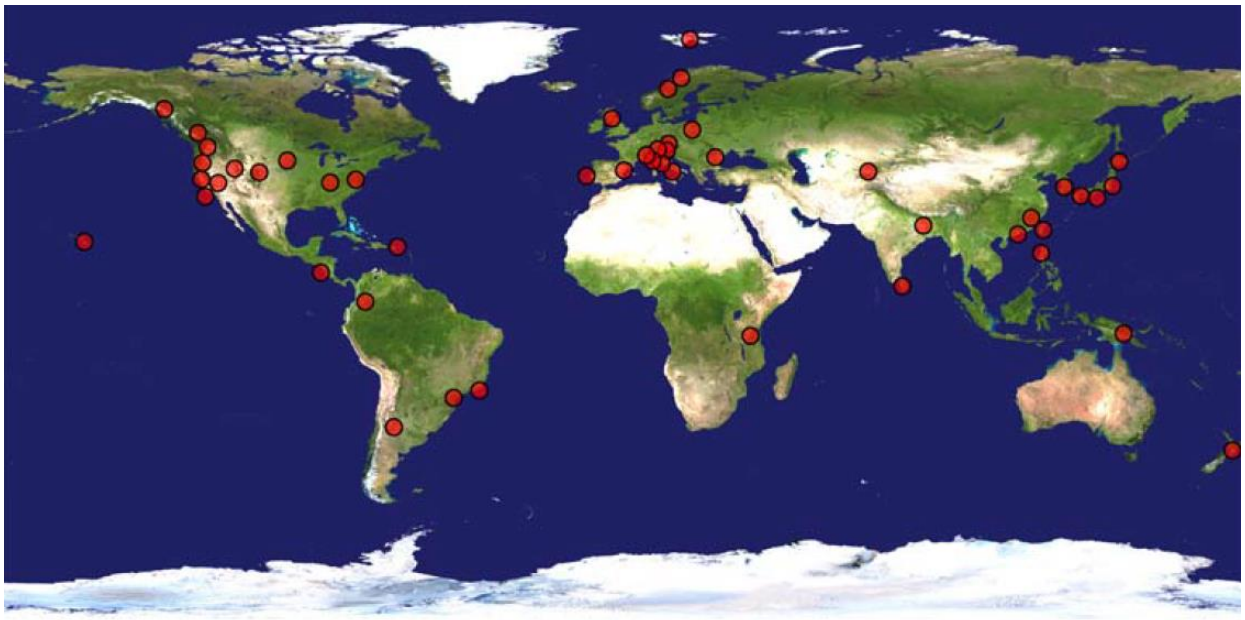

Figure 4.1. Location of areas for which precipitation characteristics initiating shallow landslides or debris flows were available around the world (Source: Guzzetti et al. (2008)).

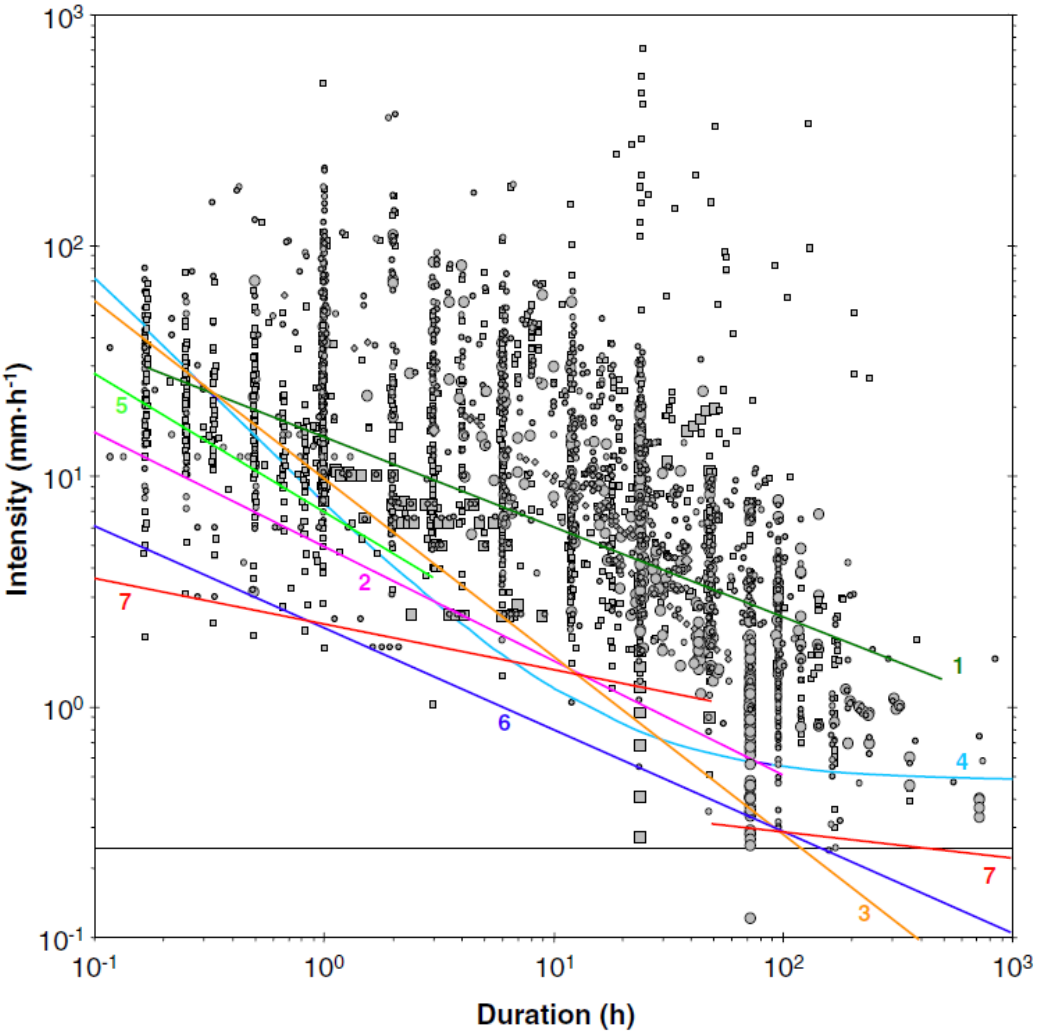

Figure 4.2. Comparison between the global intensity-duration (ID)thresholds defined by: 1 - Caine (1980); 2 - Innes (1983); 3 - Clarizia et al. (1996); 4 - Crosta and Frattini (2001); 5 - Cannon and Gartner (2005); 6 - and 7 - Guzzetti et al. (2008) (Source: Guzzetti et al. (2008)).

A comprehensive list of available rainfall thresholds initiation of landslides and debris flows sorted by continents is given in the website[6] of the Research Institute for Geo-Hydrological Protection.

[6] http://wwwdb.gndci.cnr.it/php2/rainfall_thresholds/thresholds_all.php?lingua=it

Based on literature reviews on precipitation thresholds (Table 4.1) and proposed methods (Table 4.2) the antecedent daily rainfall model (ADRM) was selected as a rainfall threshold model which defines relatively precise threshold and suits the available data and objectives of this thesis. Furthermore, it was assumed that outputs from Chapter 3 could be applicable to ADRM in order to test the most important precipitation generating atmospheric circulation patterns (CWT C, SW and W) resulting mudflows for the purpose of central proxy and preparatory factors for Chapter 6. Figure 4.3 explains the main methodology for assessing the probability of mudflow occurrences in the piedmont areas of Uzbekistan.

Table 4.1. Precipitation threshold triggering shallow landslides in some regions of the world.

Area	Rainfall threshold	Method	Source
Wudu, China	>20 mm/day	Antecedent daily rainfall	Bai et al. (2014)
Lisbon, Portugal	>24 mm/day	Antecedent daily rainfall	Zêzere and Rodrigues (2002)
Abruzzo, Italy	~ 1.6-1.8mm/h	Intensity duration (ID) or Caine method	Brunetti et al. (2010)
Shikoku Island, Japan	40 to 120 mm/day	ID method	Hong et al. (2005)
Chittagong City, Bangladesh	>40 mm/day	ID method	Khan et al. (2012)
Colorado, US	1.0 to 32.0 mm/h	ID method	Cannon et al. (2008)
California, US	1.3 to 20.4 mm/h	ID method	Cannon et al. (2008)
Eastern Jamaica	2 to 93 mm/h	ID method	Ahmad (2003)
Durban Region, South Africa	100-150 mm/2h	Critical Precipitation coefficient	Bell and Maud (2000)
Puerto-Rico	70 mm/h	ID method	Jibson (1989)

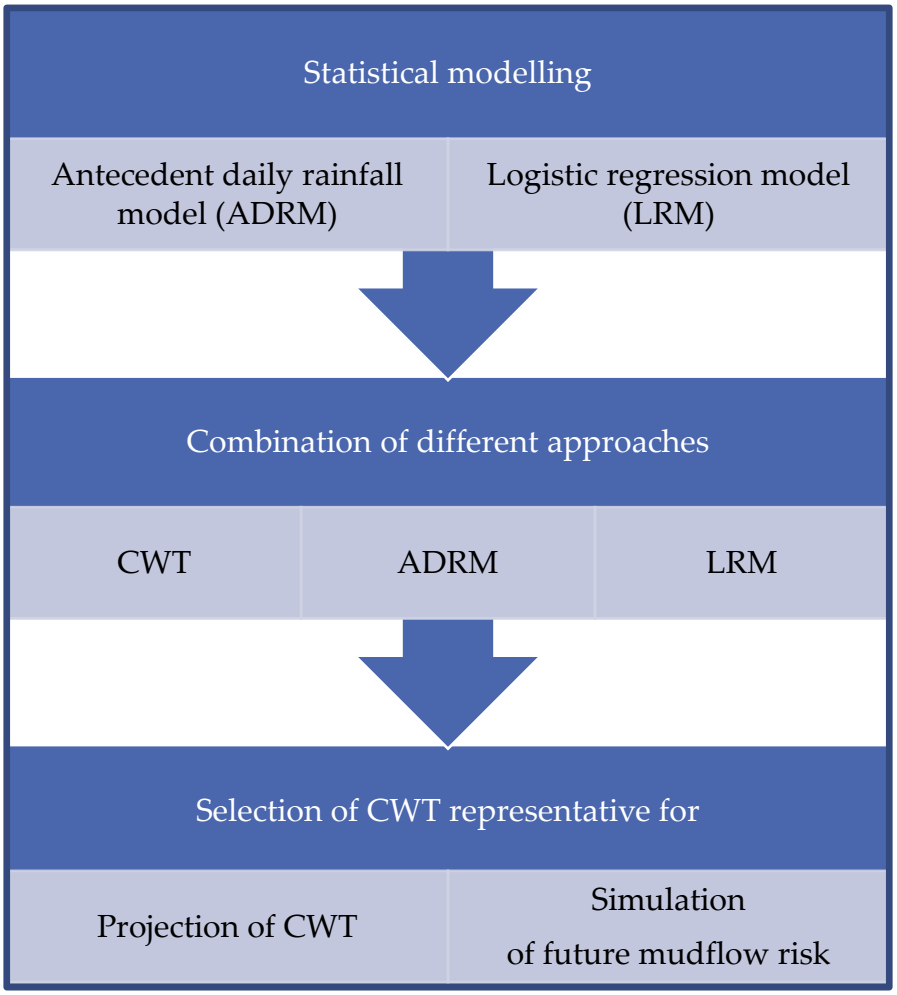

Figure 4.3. Schematic flow-chart of the methodology to define the precipitation threshold triggering mudflows (Objective 4).

Table 4.2. Examples of statistical techniques used to establish precipitation thresholds for the initiation of landslides (types of landslides: A – all, D – debris flow, S – slope, Sh – shallow landslides)

Method	**Area**	**Land slide type**	**Source**	**Input variables**	**Summary of findings**	**Advantages**	**Drawbacks**
Antecedent daily rainfall model using logistic regression approach	North Island of New Zealand	A	Glade et al. (2000)	Antecedent rainfall (mm), daily rainfall (mm)	Calculated thresholds are able to represent the regional probabilities of landslides occurrences on the basis of rainfall conditions	Easily calculated on day-to-day basis of rainfall from meteorological records and can be used an early warning	Model uncertainties due to the quality of landslide records and regional characteristics of the area
Empirical relationship between landslides and precipitation	Dolomites, North-eastern Italy	D	Bacchini and Zannoni (2003)	Rainfall duration (hr), rainfall intensity (mm/h), cumulative rainfall (mm), normalised rainfall (%), normalised intensity on Mean Annual Precipitation (MAP) (%)	Obtained a threshold equation for debris-flow activity shows lower value comparing with the thresholds proposed by other authors	This threshold can be used as an early warning signal in the debris-flow susceptible areas	The threshold cannot be applied as a predictive tool
Independent statistical approaches: Bayesian inference method and Frequentist technique	Italy and Abruzzo Region, central Italy	A	Brunetti et al. (2010)	Rainfall duration D (hr) and the rainfall mean intensity I (mm/h)	The new regional thresholds are lower than the new national thresholds for Italy, and lower than regional thresholds proposed by other studies for the investigation area	The scheme can be applied for the landslide warning systems based on rainfall measurements and forecasts	Heuristic assumption used due to the uncertain events which was not possible to quantify
Intensity–duration threshold method or Caine (1980) method	Yingxiu, Dujiangyan, Qingping, and Beichuan, Wenchuan	D	Ma et al. (2017)	Rainfall duration (in hr)	Debris flows in the seismic areas present different I-D thresholds depending on local mean annual hourly	It could be used as a prototype for debris flows in areas affected earthquake	Thresholds cannot be applied to other regions

	seismic region, Taiwan				precipitation and debris supply conditions		
Probability of rainfall-induced landslide reactivation method and Generalized Extreme Value model	San Donato and La Salsa landslides, Apennine, Italy	S	Floris and Bozzano (2008)	Accumulated rainfall during the 180 days (mm)	Spatial distribution and seasonal characteristic of the precipitation can impact on the pore pressure variation	It can be used to set up early warning system in case of taking into account the return period of the landslide	Model can be applied only in case of defining the threshold for deep-seated landslides
Probabilistic and empirical methods	Huangshan region, China	Sh	Huang et al. (2015)	Accumulated precipitation (mm), rainfall intensity (mm/ h), a numerical constant	Proposed method suggest four early warning levels (zero, outlook, attention, and warning) and a rainfall threshold values resulting shallow landslides in mountainous regions.	It is indeed a suitable approach to investigate shallow landslides induced by rainfall	Due to the limited datasets on landslides and rainfall records, the threshold identified in this study is for a usage in the regional basis
Empirical and theoretical relations between rainfall and landslide initiation	San Francisco Bay region, California, USA	A	Keefer et al. (1987)	average annual precipitation (mm), antecedent precipitation(mm), rainfall duration (hr), rainfall intensity (mm/hr), critical volume of water (mm)	A real time regional warning system has been developed based on complex analysis and real-time monitoring the rainfall records from rain gauges, precipitation forecast from the National Weather System and delineation of areas affected by landslides	It could be used as a benchmark for systems in regions susceptible to landslides	Modifications and additional developments on rainfall duration, soil moisture and pore water pressures as well as geomorphological conditions are needed to consider
A novel algorithm to define landslides using bootstrapping statistical technique	Sicily, Southern Italy	A	Melillo et al. (2016)	number of rainfall events per year (#), rainfall duration (h), cumulated rainfall (mm), mean rainfall	The proposed method identified 29,270 rainfall events (2009-2012) and reconstructed 472 ED (cumulated rainfall duration)	Obtained threshold can be applied in an operational early warning system	Relative uncertainties exist for the shape parameter that defines slope of

and a frequentist method				intensity (mm/h), peak hourly rainfall intensity (mm/h)	rainfall conditions as possible triggers of the observed landslides. Reconstructed rainfall events divided into six categories from “light” to “torrential” that have resulted in slope instabilities.		the power which can effect threshold line
Subjective data analysis	Hungary	A	Szabó (2003)	Winter precipitation (mm), annual precipitation (mm)	A strong correlation between landslide processes and precipitation events is identified. An old landslides reactivated by extreme winter precipitation	Subjective approach is valid mainly for shallow and translational slides in case of insufficient data to apply for the statistical modelling	NA
Intensity–duration thresholds, regression analysis, homogenous slope stability assessment	Kagoshima, southern Kyushu, Japan	A	Yamao et al. (2016)	Rainfall intensity (mm/h), antecedent precipitation index (mm), slope gradient, adjusted for evapotranspiration losses (mm), pore water pressure response (h), wet soil density (mg m^3)	Two scenarios of rainfall triggering landslides were identified: long-term accumulated rainfall and shorter duration with high intensity of storms. Precipitation characteristics and API (adjusted for evapotranspiration losses) affect the hydrogeomorphic processes that can affect landslide occurrences in the study area	A useful tool for predicting landslide occurrences and improving sediment disaster prevention as well as a signal of early warning system	Similarities and differences of landslide triggering mechanisms (climate, slope gradients, porosity, etc.) should be considered before the application of the results to other regions

4.2. Data

4.2.1. Observational data

Daily precipitation totals for the period of 1984-2013 recorded in five representative stations (Gallyaaral, Chimgan, Sokh, Mingchukur and Baysun) were used to assess the average probability of mudflow triggering thresholds. Daily rainfall observations provided by Uzhydromet were used in this study and a period of 24 hrs was taken between 8 a.m. of the previous day to 8 a.m. of the present day. Additionally, observation data on air temperature from the representative stations for 30 years (1984-2013) is used for temperature analysis in this study.

4.3. Methods

4.3.1. Antecedent daily rainfall model (ADRM)

In order to estimate the precipitation threshold causing mudflow events in the study area, a combination of an empirical and a statistical models has been applied: 1) Antecedent Daily Rainfall Model (ADRM) as the relationship between antecedent rainfall conditions prior to an actual "rainstorm event" and the rainstorm magnitude itself (Glade et al., 2000); 2) a logistic regression model (LRM) as the relationship between an outcome (dependent or response) variable and a set of independent (predictor or explanatory) variables (Hosmer and Lemeshow, 2000).

The ADRM introduced by Crozier and Eyles (1980) defines landslide triggering rainfall conditions for the Ottago Peninsula during 1977-1978. This model was

applied in many parts of the world to obtain the thresholds probability of landslide occurrence on the basis of precipitation conditions (e.g. for New Zealand by Glade et al. (2000), for Portugal by Zêzere and Rodrigues (2002) and Zêzere et al. (2005), for Sao Miguel Island (Azores) by Marques et al. (2008), for Bangladesh by Khan et al. (2012), for China by Bai et al. (2014), etc.). The advantage of this model lays in the substituting of soil moisture storage levels by daily precipitation data. In the absence of real-time soil moisture measurements, this model allows to predict the probability of landslides (Glade et al., 2000). The antecedent rainfall model (Crozier and Eyles, 1980) is expressed by the following formula:

$$ra_0 = kr_1 + k^2r_2 + \ldots + k^nr_n \qquad (4.1)$$

where ra_0 is the antecedent daily rainfall for day 0; r_1 is the rainfall on the day before day 0; r_n is the rainfall on the n th day before day 0; and k is a constant <1.0. According to Davydov et al. (1973) and Bykov and Vasil'yev (1977) the k parameter depends on the river morphometry and it varies from 0.7 to 0.9, and 0.5 in the case of a slack current. Crozier and Eyles (1980), following Bruce and Clark (1966), used a value of 0.84 for the k factor, which is close to that used in hydrological studies in North America, more precisely Ottawa (United States) streamflow data (Glade et al., 2000). Due to missing data on regional hydrograph recession curves in the study area, the constant decay factor, k in this research was assumed to be 0.84 based on Crozier and Eyles (1980) and Crozier (1986). It was also suggested by specialists at

Uzhydromet (personal communication with author of the thesis) that $k \geq 0.8$ can be used for this study as it is used in the river catchments in the mountain areas of Uzbekistan. Setting k=0.84 worked satisfactorily in the ADRM to assess the triggering thresholds and mudflow probability in the study area.

In the first step, daily rainfall totals of 30 years (1984-2013) recorded in five representative stations (Gallyaaral, Chimgan, Sokh, Mingchukur and Baysun) were used to assess the average probability of mudflow triggering thresholds. The empirical model analysis consists of calculating the antecedent precipitation for 10 consecutive days. Daily rainfall observations provided by Uzhydromet were used in this study and a period of 24 hrs was taken between 8 a.m. of the previous day to 8 a.m. of the present day.

Finally, the results from the two different investigation strands were integrated to estimate of each weather type as a proxy for the triggering mudflows by applying a combination of CWT, ADRM together with LRM to produce the precipitation threshold per CWT class.

4.3.2. Logistic regression model

In the next step, LRM was developed in order to estimate the relationship between mudflow occurrences and daily rainfall and antecedent rainfall value. The LRM was run in the freely available/open source R software environment. Mudflow occurrence was treated as a dependent variable and 10 days of antecedent rainfall

index and the rainfall value on the day with the mudflow event were used as independent variables. The values of the variables were the input data for the LRM algorithm to calculate the precipitation threshold equation and plot probability (P) curves for P=0.1, P=0.5 and P=0.9. This approach is analogous to the one presented in Glade et al. (2000).

Logistic regression is based on the idea transforming the predictand (mudflow in this case) to a binary (or dummy variable), taking in the values zero and one (Hosmer and Lemeshow, 2000, Wilks, 2011) expressed in equation 4.2:

$$x_2 = \begin{cases} 1, if\ x_1 > c \\ 0, if\ x_2 \leq c \end{cases} \quad (4.2)$$

where x_2 is a binary variable (mudflow occurrence), x_1 predictor (daily precipitation and daily antecedent rainfall index), 1 is presence of mudflows and 0 can be assigned if no mudflow is present.

Logistic regression technique is fit to binary predictands using log-odds, or *logit,* link function $g(p) = \ln[\frac{p}{1-p}]$, yielding the generalized linear function is expressed in the formulation of 4.3 and 4.4.

$$\ln\left(\frac{p_i}{1-p_i}\right) = b_0 + b_1x_1 + \cdots + b_kx_k \quad (4.3)$$

$$p_i = \frac{\exp(b_0+b_1x_1+\cdots+b_Kx_K)}{1+\exp(b_0+b_1x_1+\cdots+b_Kx_K)} = \frac{1}{1+\exp(-b_0-b_1x_1-\cdots-b_Kx_K)} \quad (4.4)$$

where p_i is predicted value from the i th set of predictors, b is slope or gradient, x is predictor variable, K is single predictor case, when $b_0 + b_1 x_1 \rightarrow +\infty$ exponential function approach becoming large than the predicted value p_i, in case $b_0 + b_1 x_1 \rightarrow -\infty$ the p_i approaches zero.

Equation 4.4 can be applied for an S-shaped curve yielding nonlinear function in logistic regression analyses.

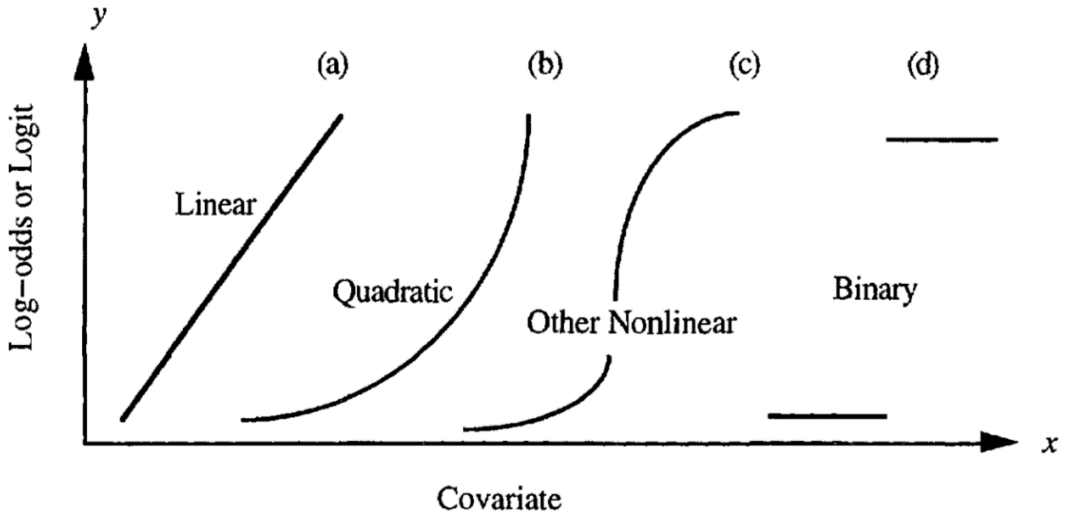

Figure 4.3. Relationship between the logit and a continues variable based on a) linear, b) quadratic, c) other nonlinear or cubic, and d) binary function (adapted from Hosmer and Lemeshow (2000).

Hosmer and Lemeshow (2000) suggested graphs for several different relationships between logit and continues independent variable (Figure 4.3) fitting a linear model which would yield a significant slope.

4.4. Results

4.4.1. Application of ADRM for station data

The model results (Figure 4.4) show that minimum and maximum thresholds boundaries with different probabilities of occurrence exist, but not all rainfall values between the thresholds are associated with mudflow episodes. A daily rainfall value ≥0.1 mm, from March till August (1984-2013), was selected for plots presented in Figure 4.4. Following Glade et al. (2000), all rainfall days were divided into three categories: days associated with mud and debris flows; days with no recorded mudflows; and days with probable mudflow episodes. Events in the third category or probable mudflows were not recorded in historical data. This category is applied to those days when the rainfall value was similar or exceeded the precipitation levels of days with recorded debris and mudflows keeping in mind that mudflow event could occur but it might not be documented in historical records. However, the summary of the daily precipitation value, which is recorded from 8 am till 8 am of the next day might not tally with the day of the mudflow occurrences. Therefore, mudflow passages were also assumed to be a probable variable as the information regarding the exact time of the mudflow occurrence was not existed. Additionally, the air temperature patterns in March-May were analysed for some meteorological stations; for example, Chimgan located at more than 1600 metres altitude, which led to the conclusion that the high precipitation events recorded were likely snowfall periods which leaves very little possibility of mudflow passage. Hence, a probable

mudslide event was not analysed for high altitude areas, even though high precipitation values existed.

According to Figure 4.4, there is a 10% probability of mudflow events if the antecedent rainfall value reaches 40 mm in the Gallyaaral station, approximately 60 mm in Mingchukur and 90 mm in Chimgan stations (Table 4.3). Interestingly, there is always a chance that a rainfall event of sufficient magnitude could induce the mudflows, even when the antecedent index is less than the levels above. The results indicate that a weather type with a high level of relative moisture may provide sufficient rainfall to trigger floods and mudslides even when the cumulative rainfall value is close to 0 or soil moisture storage is in deficit. In contrast, after a long period of accumulation of antecedent rainfall, which weakens the slope gradually, the slope becomes more susceptible to the less value of rainfall on a given day and this could trigger a mudflow event.

Some mudflow events were recorded when the rainfall level and antecedent rainfall index showed less than 10 mm. This could be possibly induced by snowmelt due to a joint occurrence of sudden temperature rises and rainfall. On the other hand, local heavy rainfall events in the adjacent areas of the stations could induce the flows and mudslides in the river catchment and hilly areas.

Figure 4.4 (c) shows that the Sokh station area located in the Fergana Valley is more susceptible to extreme mudflow events; indicating that mudflow events are also

influenced by the geomorphologic structure of the area. The 0.1 probability threshold indicates that 10 mm of rainfall with antecedent conditions of less than 30 mm can trigger flash floods or mudflows in Sokh. It means that the threshold varies in space and it is important to consider the regional characteristics of the research area whilst applying the ADRM.

Table 4.4 provides logistic regression equations to the data from the five stations which can be used to estimate the rainfall thresholds with different probabilities of mudflow occurrences. For Chimgan station a cubic regression and for Mingchukur a quadratic equation with probability curves proved to be the best fit, however, probability envelopes of the linear regression worked satisfactorily for the data of the other stations, namely Gallyaaral, Sokh and Baysun. Associated values of Chi-squared test represented in Table 4.4 show the significance of model fitting for the stations data.

Table 4.3. Threshold probabilities (10%, 50% and 90%) inducing mudflow events in 5 stations (Gallyaaral, Chimgan, Sokh, Mingchukur and Baysun); r_a - antecedent rainfall index (mm), r - daily rainfall value (mm).

Station	10%		50%		90%	
	r_a	r	r_a	r	r_a	r
Gallyaaral	≤ 40	≤ 20	≤ 90	≤ 40	≤ 130	≤ 60
Chimgan	≤ 90	≤ 45	≤ 110	≤ 75	≤ 125	≤ 100
Sokh	≤ 30	≤ 10	≤ 70	≤ 35	≤ 115	≤ 50
Mingchukur	≤ 60	≤ 25	≤ 85	≤ 50	≤ 100	≤ 65
Baysun	≤ 60	≤ 20	≤ 95	≤ 40	≤ 130	≤ 55

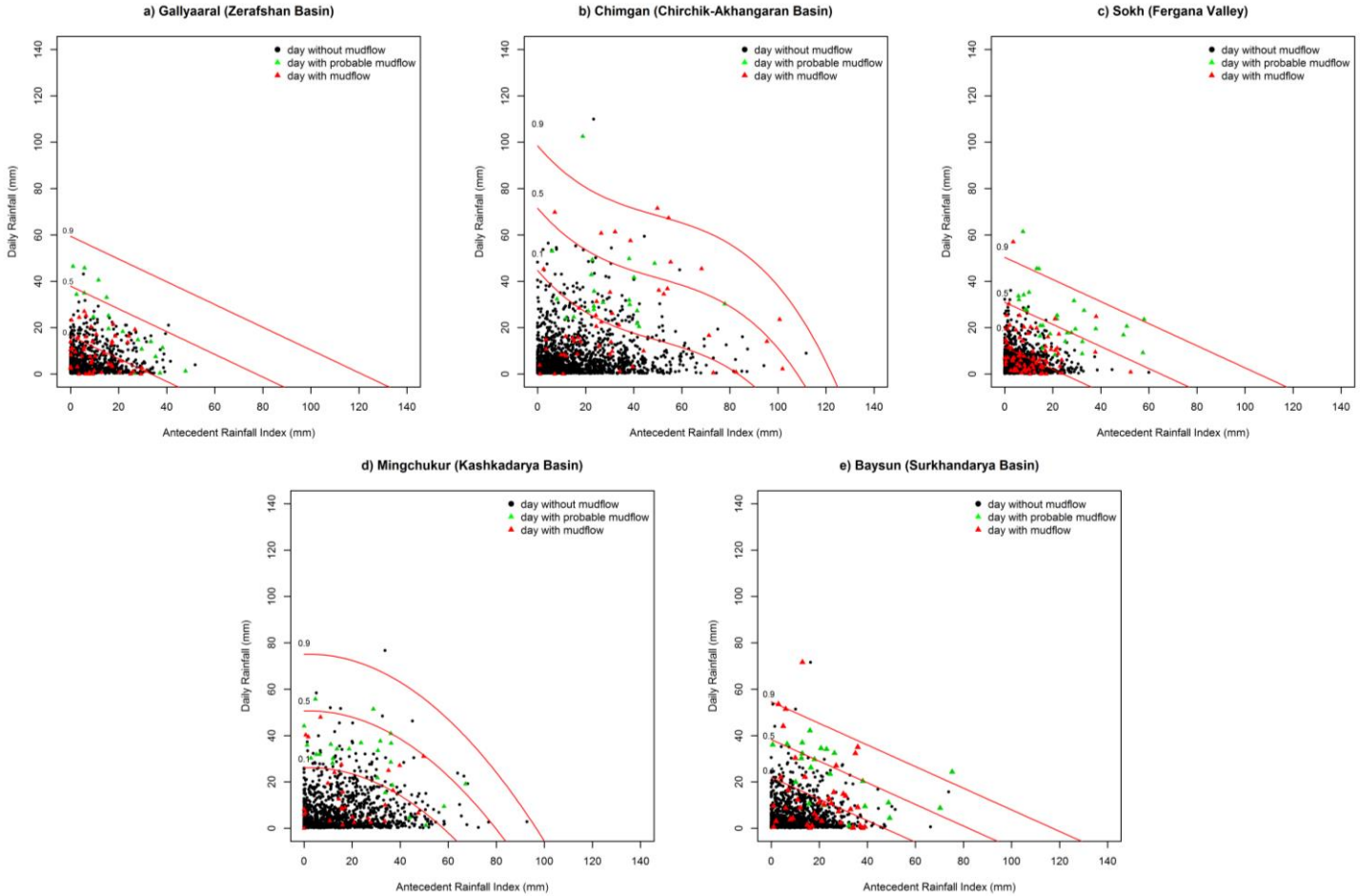

Figure 4.4. Antecedent Daily Rainfall Model applied to the representative stations Gallyaaral (a), Chimgan (b), Sokh (c), Mingchukur (d) and Baysun (e) for the period 1984-2013. Red lines and curves indicate 0.1th, 0.5th and 0.9th probability threshold triggering mudflow occurrences in respective regions. Equations from Table 4.3 used for calculation of the probability lines in selected stations.

Table 4.4. Rainfall threshold probability equations of mudflow occurrences in selected areas (P – probability, r – daily rainfall, r_a- antecedent rainfall, Pr(>Chi) - Chi-squared results to the regions respectively).

Station	Probability equation	Pr(>Chi)
Gallyaaral	$\log\left(\frac{P}{1-P}\right) = -3.87 + 0.10 * r + 0.05 * r_a$	9.402e-05
Chimgan	$\log\left(\frac{P}{1-P}\right) = -5.84 + 0.082 * r + 0.099 * r_a - 0.0015 * r_a^2 + 0.00001 * r_a^3$	1.455e-10
Sokh	$\log\left(\frac{P}{1-P}\right) = -3.50 + 0.11 * r + 0.05 * r_a$	3.285e-07
Mingchukur	$\log\left(\frac{P}{1-P}\right) = -4.54 + 0.89 * r - 0.003 * r_a + 0.0008 * r_a^2$	8.036e-07
Baysun	$\log\left(\frac{P}{1-P}\right) = -5.15 + 0.13 * r + 0.062 * r_a$	8.835e-08

4.4.2. Application of ADRM per CWT

In this section, the ADRM fit for each CWT class is examined in order to identify precipitation thresholds triggering mudflow events under each weather type for the five stations (Gallyaaral, Chimgan, Sokh, Mingchukur and Baysun) located in areas with high probability of mudflow events in Uzbekistan. For this purpose, all rainfall days with an amount of ≥0.1 mm and the calibrated antecedent rainfall was divided into each weather type. Observed mudflow events in areas were marked with the weather types. Data for the summer periods (March-August) of 1984-2013 by using CWT and ADRM together with LRM were used to construct mudflow triggering precipitation threshold per CWT class (Figure 4.5).

The probability envelopes on C, W and SW days in all stations show consistently positive results each resembling regional overlaid threshold to trigger the extreme mudflow event. Following the above named airflows, the antecedent rainfall index associated with the AC circulation has sufficient magnitude to trigger mudflows even when the antecedent index and the rainfall value are less than regional threshold for Gallyaaral, Chimgan and Sokh stations (Figure 4.5). It is assumed that AC hybrid, mainly anticyclonic westerly (ACW) and anticyclonic south-westerly (ACSW) initiate significantly more mudflow probability than purely anticyclonic flow. Another interesting observation is that the overlaid threshold probabilities for mudflow events under the NW airflow in Chimgan, Sokh and Mingchukur indicate that similar or less values of antecedent and daily rainfall records of regional probability can trigger mudflow occurrence there. The NE (except in Fergana Valley, Figure 4.5), E, SE and S flows had little or no precipitation to effect mudflow cases in the study area. Threshold probability tests computed for rainfall data per CWT for five individual stations over the period 1984 to 2013 are given in Table 4.5.

This study attempts to identify more sensitive weather types to trigger mudflow events in Uzbekistan, using the CWT approach and antecedent rainfall model. The relative importance of each CWT to induce mudflows varies considerably, and includes antecedent rainfall index and the daily precipitation value. Results from this study confirm that W, SW, C, NW and AC hybrid (associated with W and SW

flows) are the main drivers of the interannual variability of precipitation patterns and responsible for the rainfall induced mudflow cases depending on the regions in Uzbekistan on a synoptic scale. This confirms the core findings of the synoptic classification by Bugayev. The CWT objective approach proves to be a useful tool to address questions of anthropogenic climate change with model data.

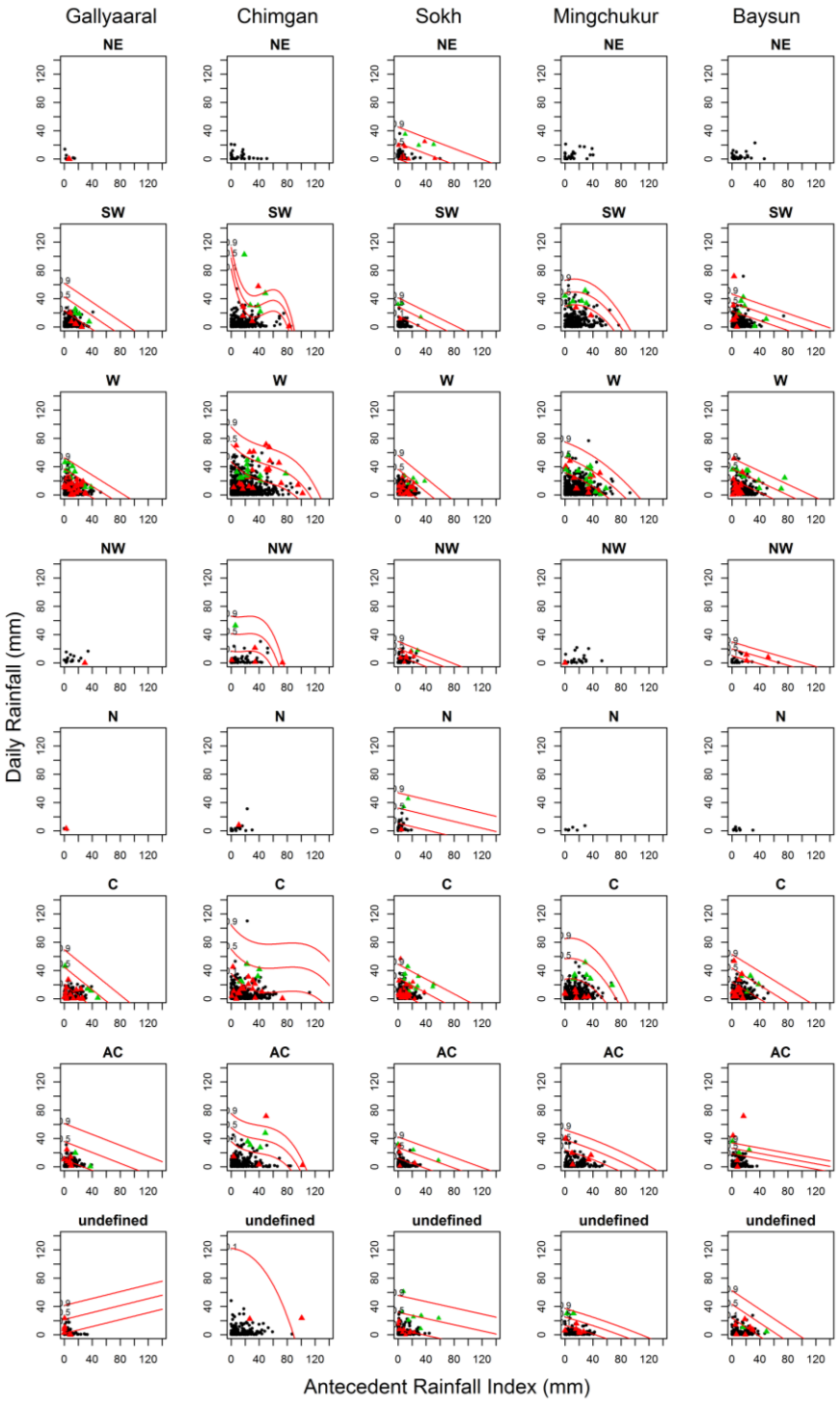

Figure 4.5. Threshold probabilities initiating mudflow occurrencesper CWT class in the stations namely Gallyaaral, Chimgan, Sokh, Mingchukur and Baysun (panel columns) for the period of March-April 1984-2013. Black dot is a day without mudflow, green triangle – days with probable mudflow, red triangle is a day initiated mudflow occurrences in the study area. Red lines and curves indicate 0.1th, 0.5th and 0.9th probability threshold triggering mudflow occurrences per CWT class.

Table 4.5. Threshold probability (10%, 50% and 90%) values initiating mudflow episodes per CWT for individual stations in Uzbekistan; r_a - antecedent rainfall index (mm), r - daily rainfall value (mm).

CWT	Gallyaaral						Chimgan						Sokh						Mingchukur						Baysun					
	10%		50%		90%		10%		50%		90%		10%		50%		90%		10%		50%		90%		10%		50%		90%	
	r_a	r	r_a	r	r_a	r	r_a	r	r_a	r	r_a	r	r_a	r	r_a	r	r_a	r	r_a	r	r_a	r	r_a	r	r_a	r	r_a	r	r_a	r
NE	-	-	-	-	-	-	-	-	-	-	-	-	≤10	≤0.1	≤70	≤20	≤120	≤45	-	-	-	-	-	-	-	-	-	-	-	-
SW	≤40	≤20	≤70	≤45	≤100	≤60	≤80	≤80	≤85	≤100	≤90	≤115	≤40	≤18	≤65	≤30	≤95	≤42	≤70	≤30	≤85	≤50	≤95	≤70	≤80	≤20	≤120	≤35	≤130	≤50
W	≤40	≤20	≤70	≤40	≤95	≤55	≤95	≤50	≤115	≤70	≤130	≤100	≤25	≤18	≤50	≤40	≤75	≤55	≤60	≤30	≤85	≤58	≤108	≤78	≤60	≤20	≤90	≤40	≤120	≤50
NW	-	-	-	-	-	-	≤60	≤20	≤70	≤40	≤75	≤65	≤40	≤10	≤60	≤20	≤85	≤30	-	-	-	-	-	-	≤55	≤10	≤80	≤20	≤120	≤30
N	-	-	-	-	-	-	-	-	-	-	-	-	≤60	≤10	≥120	≤35	≥120	≤55	-	-	-	-	-	-	-	-	-	-	-	-
C	≤30	≤20	≤60	≤50	≤90	≤70	≤130	≤40	≥140	≤75	≥140	≤105	≤25	≤10	≤60	≤30	≤100	≤50	≤58	≤30	≤78	≤60	≤90	≤88	≤45	≤25	≤80	≤45	≤115	≤60
AC	≤40	≤15	≤105	≤40	≤140	≤70	≤85	≤40	≤100	≤60	≤110	≤80	≤40	≤10	≤85	≤28	≤120	≤40	≤78	≤25	≤105	≤40	≤130	≤55	≤125	≤20	≤140	≤25	≤140	≤35
und	-	-	-	-	-	-	≤90	≤120	-	-	-	-	≤55	≤8	≥120	≤35	≥120	≤58	≤60	≤15	≤90	≤25	≤120	≤40	≤40	≤25	≤75	≤44	≤100	≤60

4.5. Discussion and Conclusions

Concept of rainfall thresholds for inducing mudflows based on the daily rainfall and antecedent conditions has been applied for many regions of the world. Bai et al. (2014) suggested that if rainfall intensities and antecedent rainfall index exceed 20 mm then this condition is very likely to trigger debris flows in Wudu mountain region in China. Guzzetti et al. (2008) documented that thresholds for mountain regions generally require lower average of rainfall values that regions with a Mediterranean climate. Glade et al. (2000) justify that ADRM technique applied to Hawke's Bay, Wairarapa and Wellington in New Zeeland indicate negative relationship between daily precipitation and antecedent index (i.e, in the condition of increased wet antecedent index, lower rainfall amount is required to trigger landslides). Conversely, when the amount of rainfall is higher, less antecedent rainfall magnitude is needed to induce landslides. For instance, study authors show that 82 mm of rainfall and zero for antecedent conditions (at P=0.1 confidence interval), as well as, 128 mm for antecedent conditions at zero daily rainfall value required for Wellington; for Hawke's Bay are 258 mm and 201 mm and for Wairarapa the corresponding values are 190 mm and 175 mm.

By means of the antecedent rainfall model presented in this study it was identified the regional differences in the probabilities of precipitation thresholds causing mudflow events (Table 4.3, Table 4.4). However, sparse data on actual mudflows

and uncertainty over probable mudflow occurrences could be the main factors regarding the uncertainty in model building (Glade et al., 2000). Nevertheless, this identified thresholds deliver reasonable and well justified results and forms a benchmark for any further study for this region. The Antecedent Daily Rainfall Model (ADRM) results further corroborate findings by Trofimov (2006) who used Pearson correlations to calculate rainfall thresholds for triggering mudflows in Fergana Valley. For Sokh area, he suggested a 0.5^{th} probability of mudflow events in case daily precipitation reaches 22.3 mm. This value falls in the lower envelope of the 0.5^{th} probability threshold identified for Fergana Valley in this study (Figure 4.4). However, regional thresholds cannot be applied easily to neighbouring areas due to additional natural variables influencing mudflows such as geologic, geomorphologic and hydrologic factors as well as slope aspect and land use. Despite of the limitations, obtained thresholds can be used in local or regional civil defence systems to provide early warning alerts and mitigate damages in currently unprotected areas of Uzbekistan.

A desired focus of future work could be to validate the ADRM model and logistic regression method by comparing the calculated probability values to measured mudflow occurrences in the investigated area. Cross-validation techniques are suitable to measure the performance of the prediction skill of the statistical model (in this case logistic regression) by determining to what extent a training dataset fits

the logistic regression outcome. Additionally, the widely used Brier's "probability score" can be used to evaluate the accuracy and reliability of logistic regression, as it is basically used for binary events (in this case "mudflow happened" = 1, or "no mudflow" = 0).

A combination of three statistical approaches (CWT, ADRM and LRM) revealed that when the W, C and SW directional flow classes occurred over Uzbekistan, the higher precipitation amount (a characteristic of these directional flows) and antecedent rainfall could trigger mudflow episodes and increase its magnitude and probability. The findings of this attempt can be applicable to simulate mudflow risk in Uzbekistan under the global warming conditions in Chapters 5 and 6.

5 CWT – Analyses of Present and Future Atmospheric Circulation over Uzbekistan

5.1. Introduction

For Central Asia, future projections of anthropogenic climate change have mainly been focused on surface temperature and precipitation characteristics over the region, which includes Uzbekistan. For instance, Ozturk et al. (2012, 2017) investigated the impact of climate change results on seasonal variability of precipitation and temperature over Central Asia under the framework of Coordinated Regional Climate Downscaling Experiment (CORDEX) Region 8 by using RegCM4 and RegCM4.3.5. Results obtained from the regional RegCM4 model driven by the ECHAM5 A1B scenario for the future (2070-2100) climatology of Central Asia show relatively high warming trend in temperature (from 3°C up to 11.4°C on average) and a decrease in precipitation, particularly, in the southeastern part of the domain (Ozturk et al., 2012). IPCC's RCP4.5 and RCP8.5 scenario outputs

for the HadGEM2-ES and the MPI-ESM-MR models downscaled by the RegCM4.3.5 climate projection for near future (2011-2040), mid-future (2041-2070) and far future (2071-2100) in Ozturk et al. (2017) also show reasonably good agreement with the outputs of previous study by Ozturk et al. (2012).

The high-resolution regional climate model (RCM) REMO has been implemented over Central Asia by Mannig et al. (2013) in order to better understand the seasonal cycle of precipitation and temperature under the anthropogenic climate change. Downscaled ECHAM5/MPI-OM A1B emission scenario indicates a warming of up to 7°C in the northern part of Central Asia and mountain areas until the end of the twenty-first century. However, climate change scenarios predict dryer summer conditions in a large area of Central Asia and wetter cold seasons over the northern part of the region and for most areas of the Tibetan Plateau.

Huang et al. (2014) projected future change in the annual precipitation over Central Asia for the period 2011-2100 by applying CMIP5 (Taylor et al., 2012) GCMs under the different emission scenarios (RCP2.6, RCP4.5 and RCP8.5). Authors found increasing trends of the annual precipitation (over 3-9 mm per decade) for the northern Central Asia, the Tian-Shan Mountains and northern Tibet by the end of 2100 when they compared with the previous investigations on climate change signals over the Central Asia. The authors suggested that large scale atmospheric water vapour fluxes and surface evaporation over the study region could be the

possible mechanisms of the increasing changes in projected precipitation (Huang et al., 2014).

Using the recent developments in the field of climate modelling, Malsy et al. (2012) and White et al. (2014) investigated the impact of climate change on water resources in Central Asia, including Uzbekistan. Malsy et al. (2012) found an increase in mean annual water availability in most river basins of Central Asia by applying the large-scale hydrology model WaterGAP3 driven by 3 GCMs ECHAM5, IPSL-CM4 and CNRM-CM3 under the two emission scenarios (IPCC-SRES A2 and B1) for the future climate (2071-2100). However, in White et al. (2014) the water discharge is projected to decline by 10-20% in the Amu Darya River basin by running the AMU-WEAP model under the high emission scenario (A2) of CMIP3 GCMs. A warming trend in summer temperatures up to 5°C and seasonal shifts in precipitation cycle may lead to an increase in water demand of agriculture from the existing 10.6% to 16% for the Amu Darya basin by 2070-2099 (White et al., 2014).

Thereafter, Radchenko et al. (2017) projected the potential changes of runoff in Syrdarya river basin in the Fergana Valley, Central Asia, by using dynamically downscaled A1B SRES scenario for the period 2071-2100. An increase in annual temperature from 3.7°C up to 3.9°C and increase in precipitation from 11% up to 13% (71-108 mm) was obtained for the future period 2071-2100 compared to the baseline period 1971-2000 for the 18 investigated river catchments of Syrdarya

basin. The likely cause was attributed to evapotranspiration increase driven by changing trends in the temperature of the region (Radchenko et al., 2017). However, the authors of the study reported that the annual runoff in the Fergana Valley will likely reduce by 10%, even though an increase in runoff is estimated for non-glaciered river catchments in the future. At the same time, a seasonal shift in runoff to earlier phases was projected with an increase of winter-spring runoff between 44% and 107% and a decrease (12-42%) in summer runoff when irrigation water is paramount importance for success agriculture in the Fergana Valley.

In many studies (Sorg et al., 2012, Kure et al., 2013, Sorg et al., 2014) the adverse effects of global warming to the Central Asian glacier zones in the Tien-Shan and the Pamir mountains have been evaluated. Based on glacio-hydrological Glacier Evolution Runoff Model (GERM) and application of downscaled atmospheric data from CMIP5 projection, Sorg et al. (2014) predicted a substantial glacier shrinkage due to the increase of air temperature over the Tien Shan Mountains, considered to be the water tower of Central Asia (Sorg et al., 2012) and its effects on the water availability until the end of the century. Furthermore, Kure et al. (2013) used three GCMs (CCSM3, CSIRO, and ECHAM5) emission scenarios together with watershed hydrology model (HEC-HMS) and concluded that the consequent increase in snow/ice melt rates in glacier-fed Pamirian rivers (Pyandj and Vakhs) is expected

until about 2060 and from about 2080 onward the small glaciers of Pamir Mountains will start to disappear.

Moreover, increased risks due to climate change and its negative consequences on farming and food productivity over Central Asia by application of SRES A1B and A2 greenhouse gas emission scenarios of Intergovernmental Panel on Climate Change (IPCC) have been recently investigated by Sommer et al. (2013) and Bobojonov and Aw-Hassan (2014).

Lioubimtseva and Henebry (2009) and Xenarios et al. (2018) have reviewed the existed literature on anthropogenic climate change impact on Central Asia and adaptation measures considering temperature and precipitation projections for the region.

These studies aside, there have been relatively few investigations focusing on the projected changes in large scale atmospheric circulation as a main driver of precipitation extremes over Central Asia under the global warming conditions. Zhao et al. (2018) simulated subtropical westerly jet (SWJ) stream and its effect on the projected precipitation over Central Asia for the summers for the period 2071-2100 by using of 25 CMIP5 models. By applying the empirical orthogonal function (EOF) method, these authors revealed the strength and position of SWJ in the future over Central Asia. According to the ensemble results from CMIP5, Zhao et al. (2018) explained the SWJ axis shifting further south over Central Asia which will result in

more summer rainfall in most of northern part of the region and northwestern China in the future, however, authors found uncertainties regarding future precipitation changes in the rest of the Central Asia.

Hitherto only Reyers et al. (2013) studied the link between weather system and precipitation frequency and its magnitude for the Aksu river basin in Central Asia, considering CWT approach as a controlling factor for future climate change scenarios. CWT representatives which were dynamically downscaled with the RCM COSMO-CLM4.8 forcing ERA-40 reanalysis for historical simulation coupled with the future scenarios of the ECHAM5/MPI-OM1 models, the authors projected the changes in precipitation climatology over the Aksu basin until 2100. Outputs of statistical-dynamical approach show a decrease in annual precipitation over large parts of the Aksu river basin in Tien Shan Mountains and an opposite sign is defined to the southeast of the investigation area.

In relation to Europe and other continents, many studies have investigated the large scale atmospheric circulation as a main driver of precipitation extremes by employing the weather patterns approach using CMIP5 models for the last few years. Santos et al. (2016) identified eight weather types by simulation with 22 CMIP5 GCMs which were downscaled by weather typing over the Western Europe. Considering the radiative forcing projections under the RCP8.5, authors have inferred the increase (decrease) of a particular weather type frequencies and

associated precipitation over the Western Europe by the end of the century. Similar methodology is applied to simulate and project the changes in French weather pattern seasonal frequencies using 26 GCM ensemble from CMIP5 by Brigode et al. (2017). Authors found strong simulated frequency of WP2 (western oceanic circulation) and WP8 (anticyclonic type) weather patterns that potentially lead to a dryer climate over France. The gradual decrease in the frequency of WP2 which is associated with rainy days and increased occurrence of non-rainy WP8 days are projected for the future summers in the study region.

The projected changes in weather type frequencies over the Arabian Peninsula were performed using different emission scenarios (RCP2.6, RCP4.5, RCP8.5) and multi-model ensemble from the CMIP5 database (El Kenawy and McCabe, 2016). Based on results of emission scenarios, El Kenawy and McCabe (2016) predicted an increase in rainfall patterns associated with cyclonic and easterly weather types and a decrease of anticyclonic circulations with lower amount of precipitation in winter by the end of the century. All studies suggest that projected changes in large scale circulation can be robust indicators to investigate not only the precipitation climatology, but it would be beneficial for a wide range of climate change impact assessments and predictions of extreme events such as frequency and intensity of flooding and droughts, water resources and agricultural production under the global warming trends.

In general, studies indicate that CMIP5 models with higher resolution can better capture the circulation patterns and associated precipitation. The challenging problem of quantifying the effect of large scale circulation on landslides is considered only in few analyses. Schmidt and Dehn (2000) and Schmidt and Glade (2003) using simple statistical downscaling technique named as analog method (Zorita and Storch, 1999), analysed links between climate change and landslides in Wellington, New Zealand. By means of analog approach, the large-scale atmospheric circulation simulated by a GCM is usually compared to the historical observations and by this way the most similar condition is defined as its analog. Based on analog downscaling approach, a local precipitation scenario can be derived from observation data and GCM simulations, in order to apply the analogs to project landslide triggering precipitation scenario.

Large scale atmospheric circulations have been suggested to be the main driver of precipitation extremes in investigations (Reyers et al., 2013, Santos et al., 2016, El Kenawy and McCabe, 2016, Brigode et al., 2017) which used weather patterns approach with application of the CMIP5 models, the results of these studies provide inspiration to postulate that extreme rainy atmospheric circulation type can be a good indicator for mudflow frequency and intensity for the future in Uzbekistan. Taking into account the climate change studies on atmospheric circulation, in this chapter an attempt has been made to construct and analyse the projected changes

of large scale atmospheric circulation defined on a daily basis as a diagnostic tool for a more comprehensive dynamical interpretation of precipitation driving mechanisms and its association with mudflow frequencies in Uzbekistan. General methodology applied in this chapter is illustrated in Figure 5.1.

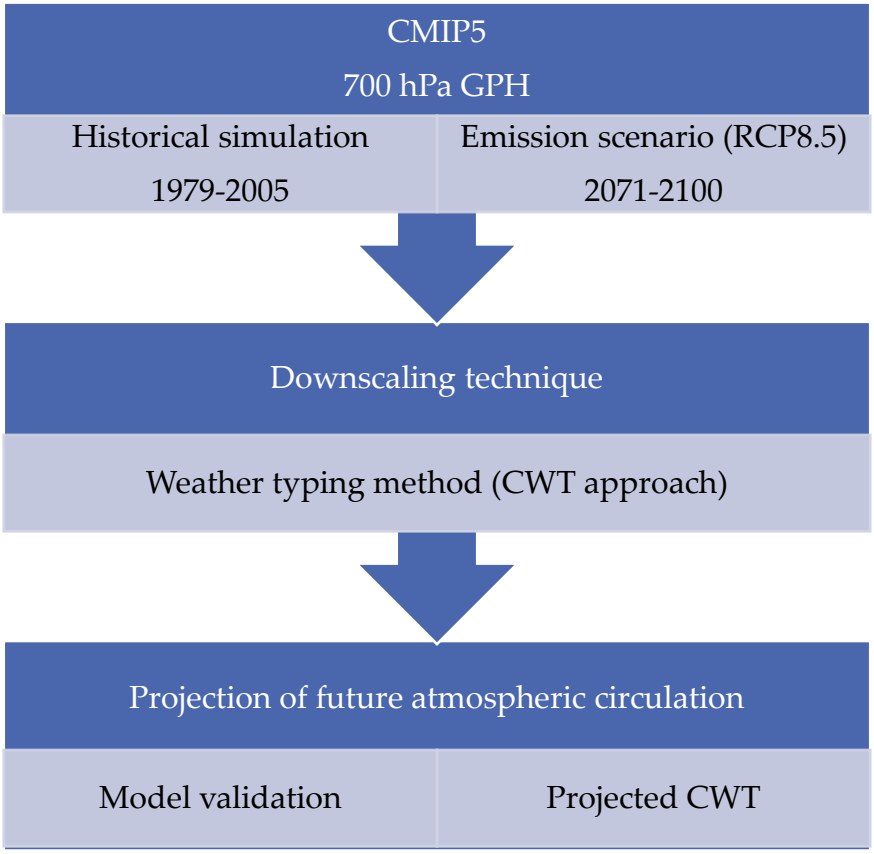

Figure 5.1. Schematic flow chart of the methodology used in this chapter (Objective 5).

5.2. Data

5.2.1. Reanalysis of geopotential height field

The ERA-Interim global atmospheric reanalysis data (Dee et al., 2011) is applied as reference for the historical period, 1979-2005. Only one geopotential height field at

700 hPa (Z_{700} hereafter) is considered in this study. The gridded data set has 0.75° spatial resolution (approximately 80 km) and 12 hr temporal resolution. The daily mean Z_{700} has been considered for the historical period. Reanalysis data is available at ECMWF's meteorological archive[7].

5.2.2. CMIP5 GCM geopotential height field outputs

The daily mean Z_{700} outputs from 10 AOGCMs of the CMIP5 (Taylor et al., 2012) projection are considered in this chapter. Table 5.1 reports main characteristics of each GCM, such as climate centre and acronyms, resolution and representative references, experiment type and covered time period of available outputs.

The daily outputs of two different experiments are applied:

1. The "historical" experiment or a simulation of the recent past under the historical forcing which is available for the years 1950-2005.
2. The Representative Concentration Pathways "RCP8.5" scenario or the high radiative forcing surplus at approximately 8.5 W/m^2 from 2006 to 2100.

For all models and experiments, only the first ensemble member (r1i1p1) is considered in this chapter. The time period for historical simulations evaluated in

[7] https://apps.ecmwf.int/datasets/data/interim-full-daily/levtype=sfc/

this study is 1979-2005 and for the future scenario is 2071-2100. CMIP5 data used in this chapter is available on CEDA[8] and CERA[9] online archives.

5.3. Methods

5.3.1. CWT classification of the historical and future experiments

The daily mean Z_{700} historical and future experiments data from 10 selected GCMs of CMIP5 multi-model projection are interpolated using bilinear interpolation onto the same horizontal resolution as the ERA-Interim reanalysis. Therefore, CMIP5 GCM outputs are statistically downscaled to define the frequency of each weather type by CWT approach (Jones et al., 1993) previously described in Chapters 2 and 3. Daily CWTs are computed using the daily low tropospheric pressure and airflow directions (AC, C, N, NE, E, SE, S, SW, W, NW, undefined) and which are determined by considering 16 grid points around a central point located (40.0°N-67.5E°) over Uzbekistan.

5.3.2. Bias correction and climate change signal

CWT seasonal frequencies of historical experiments from CMIP5 GCMs are substantially biased compared to real climate data (ERA-Interim reanalysis in this

[8] http://data.ceda.ac.uk/badc/cmip5/data/cmip5/output1/
[9] https://cera-www.dkrz.de/WDCC/ui/cerasearch/

case). This is calculated by the following equation (5.1) adopted from Maraun and Widmann (2018):

$$Bias_{\theta}(Z_{700}) = \theta_{mod}(Z_{700}) - \theta_{obs}(Z_{700}) \quad 5.1$$

where, $Bias_{\theta}(Z_{700})$ is a systematic difference between a historical simulation of GCMs $\theta_{mod}(Z_{700})$ for the period of 1979-2005 and an observed data $\theta_{obs}(Z_{700})$ for the same period as a model data.

The CWT projection for the 10 CMIP5 GCMs ensemble scenarios constructed as a seasonal rate per CWT class attributable to climate change signal calculated by the formula (5.2):

$$A_{CWT}(Z_{700}) = CWT_{sce}(Z_{700}) - CWT_{pres}(Z_{700}) \quad 5.2$$

where, $A_{CWT}(Z_{700})$ is burden of CWT frequency attributable to climate change, CWT is a frequency per airflow direction, $CWT_{sce}(Z_{700})$ is the CWT frequency for the years 2071-2100, $CWT_{pres}(Z_{700})$ CWT frequency for the present time period 1979-2005.

Table 5.1. CMIP5 GCMs characteristicsincluding acronyms, modelling centre name, experiment type, time period of data availability, model grid resolution, and a representative reference.

Model name	Model abbreviation	Climate centre	Acronym for the climate centre	Calendar	Experiment	Time period for this study		GCM resolution (lat × lon)	Reference
						control	scenario		
ACCESS1-0	Australian Community Climate and Earth-System Simulator, version 1.0	Commonwealth Scientific and industrial Research Organization/Bureau of Meteorology, Australia	CSIO CAWCR, Australia	proleptic gregorian	RCP8.5 r1i1p1	1979-2005	2071-2100	1.9 × 1.2 L38	Bi et al. (2012)
bcc-csm1-1	Beijing Climate Center, Climate System Model, version 1.1	Beijing Climate Center, China Meteorological Administration, China	BCC, CMA, China	365 day	RCP8.5 r1i1p1	1979-2005	2071-2100	2.8 × 2.8 L26	Wu et al. (2014)
CMCC-CM	CMCC-CM	CMCC - Centro Euro-Mediterraneo per i Cambiamenti, Italy	CMCC, Italia	standard	RCP8.5 r1i1p1	1979-2005	2071-2100	0.75 × 0.75 L31	Scoccimarro et al. (2011)
CNRM-CM5	Centre National de Recherches Météorologiques Coupled Global Climate Model, version 5	Centre National de Recherches Meteorologiques (CNRM), France and Centre Europeen de Recherches et de Formation Avancee en Calcul Scientifique (CERFACS), France	CNRM-CERFACS, France	standard	RCP8.5 r1i1p1	1979-2005	2071-2100	1.4 × 1.4 L31	Voldoire et al. (2013)
GFDL-CM3	Geophysical Fluid Dynamics Laboratory Climate Model, version 3	Geophysical Fluid Dynamics Laboratory (GFDL) at National Oceanic and Atmospheric Administration (NOAA)	NOAA-GFDL, United States	365 day	RCP8.5 r1i1p1	1979-2005	2071-2100	2.5 × 2.0 L48	Donner et al. (2011)
HadGEM2-CC	Hadley Centre Global Environment Model, version 2, Carbon Cycle	Met Office Hadley Centre, United Kingdom	MOHC, UK	360 day	RCP8.5 r1i1p1	1979-2005	2071-2100	1.9 × 1.2 L60	Martin et al. (2011)
HadGEM2-ES	Hadley Centre Global Environment Model, version 2, Earth System	Met Office Hadley Centre, United Kingdom	MOHC, UK	360 day	RCP8.5 r1i1p1	1979-2005	2071-2099		Jones et al. (2011)
IPSL-CM5A-LR	L'Institut Pierre-Simon Laplace Coupled Model, version 5A, low resolution	Institute Pierre Simon Laplace, France	IPSL, France	365 day	RCP8.5 r1i1p1	1979-2005	2071-2100	3.7 × 1.9 L39	Dufresne et al. (2013)
MIROC5	Model for Interdisciplinary Research on Climate, version 5	Atmosphere and Ocean Research Institute (The University of Tokyo), National Institute for Environmental Studies, and Japan Agency for Marine-Earth Science and Technology, Japan	AORI-NIESJAMSTEC, Japan	standard	RCP8.5 r1i1p1	1979-2005	2071-2100	1.4 × 1.4 L40	Watanabe et al. (2011)
MPI-ESM-LR	Max Planck Institute Earth System Model, low resolution	Max Planck Institute for Meteorology, Germany	MPI-N, Germany	proleptic gregorian	RCP8.5 r1i1p1	1979-2005	2071-2100	1.9 × 1.9 L47	Zanchettin et al. (2013)

5.4. Results

5.4.1. Model validation. Historical experiments of seasonal CWT frequencies simulated by CMIP5 GCMs

The effects of large scale atmospheric circulation over Uzbekistan have been examined by evaluating GCMs ensemble to simulate the historical CWT frequencies for the warm and cold periods of 1979-2005. The seasonal frequencies of CWT are generally well simulated by applying statistical downscaling procedure. Figure 5.2 presents ERA-Interim outputs and historical experiments of seasonal distribution for each weather type simulated by the GCM considering RCP8.5 emission scenario. Based on the findings of the statistical downscaling, compared to the observational data (ERA-Interim in this case) most models capture the seasonal frequencies of CWT as same as in observation or with small discrepancies.

Figure 5.3 summarizes the frequency changes calculated between ERA-Interim and GCM historical experiment for the period of 1979-2005. From the ten selected models **ACCESS1-0, HadGEM2-ES**, **HadGEM2-CC** and **MPI-ESM-LR** represent nearly realistic outputs of CWT frequencies for the historical period with less than 5% of changes for each CWTs for the warm and cold periods of the year. Only NE flow (6.5%) in March-August is overestimated by both **HadGEM2** models also C days (7%) in September-February is increased by **MPI-ESM-LR**.

In contrast, **bcc-csm1-1** model performs the CWT frequency differences significantly throughout the year. This model overestimates (10-12%) the frequency of cyclonic days and underestimates (8-18%) the undefined circulation type over the historical period. Therefore, this model overestimates the NE airflow (7.2%) in summer and SW flow (6.7%) in winter period of the year.

The **CCMC-CC** model simulates well and underestimates slightly only the days of undefined flow direction in March-August (7%) and September-February (5.3%). Further remarkable results between observation and biases achieved by simulation of **CNRM-CM5** with minor decreases on C days in summer (6%) and W flow in winter (6%)**.**

GFDL-CM3 overestimates slightly the W days (6.8%) in winter and C days (6.9%) in summer, as well as underestimates AC (5.8%) and SW (6.2%) airflow directions in winter. This model also is similar to most of the models and reproduces the decrease of undefined weather type (5.9%) especially in the warm phase of the year. However, **IPSL-CM5A-LR** underestimates AC (5.9%), undefined weather type (6.7%) in summer and overestimates W airflow during the warm (11.2%) and cold (11.8%) phases of the year. The frequencies of C days (7.2%) in a warm period is underestimated and W days (10.6%) in cold phase of the year is overestimated by **MIROC5**.

The correlation distributions of the CWT frequencies of each GCM for the warm and cold periods of the year show that historical experiments of selected models match well with the observation (Figure 5.4). However, **bcc-csm1-1** differs from the other models and observation and significantly maintains CWT changes and uncertainties, especially in warm season of the year. Therefore, it is reasonable that historical simulation of CWT frequencies of selected models can reproduce accurately, to a great extent, the large scale atmospheric circulation over Uzbekistan and CA.

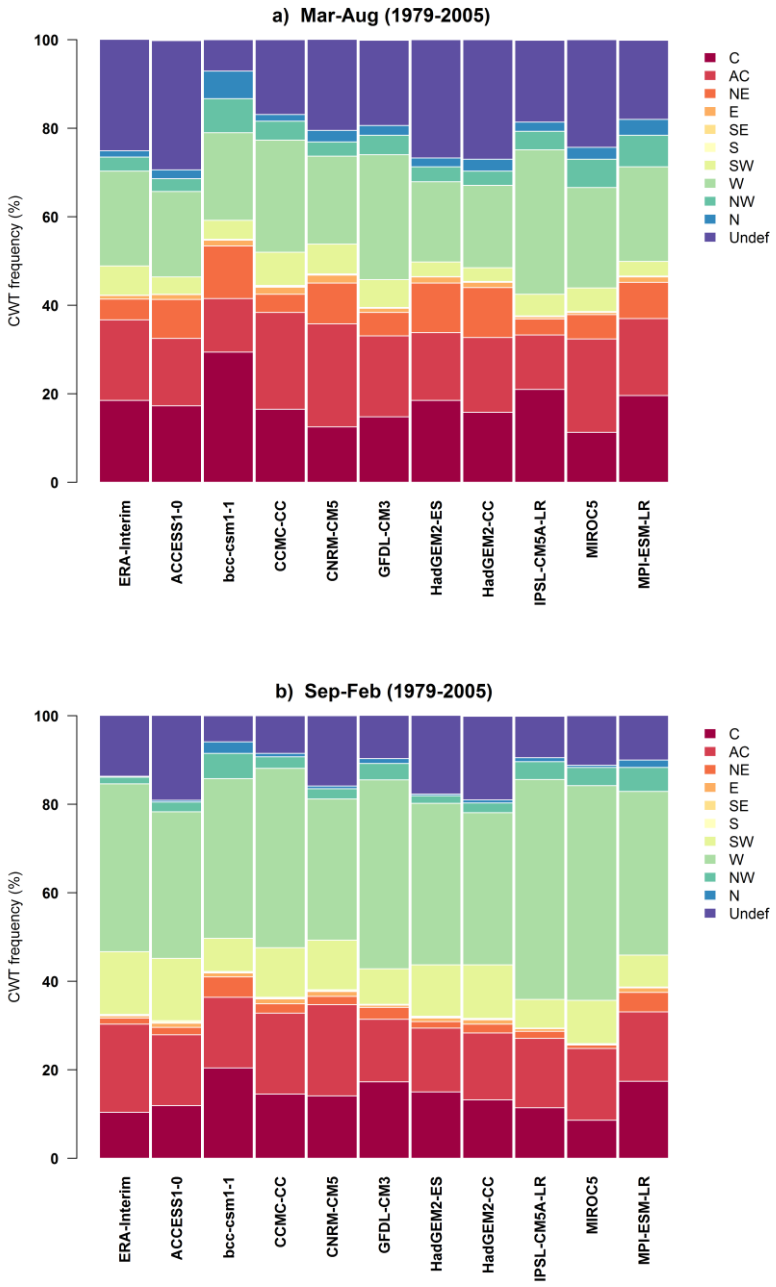

Figure 5.2. Seasonal frequencies of ERA-Interim reanalysis and 10 GCM historical experiments for each CWT for the period of 1979-2005.

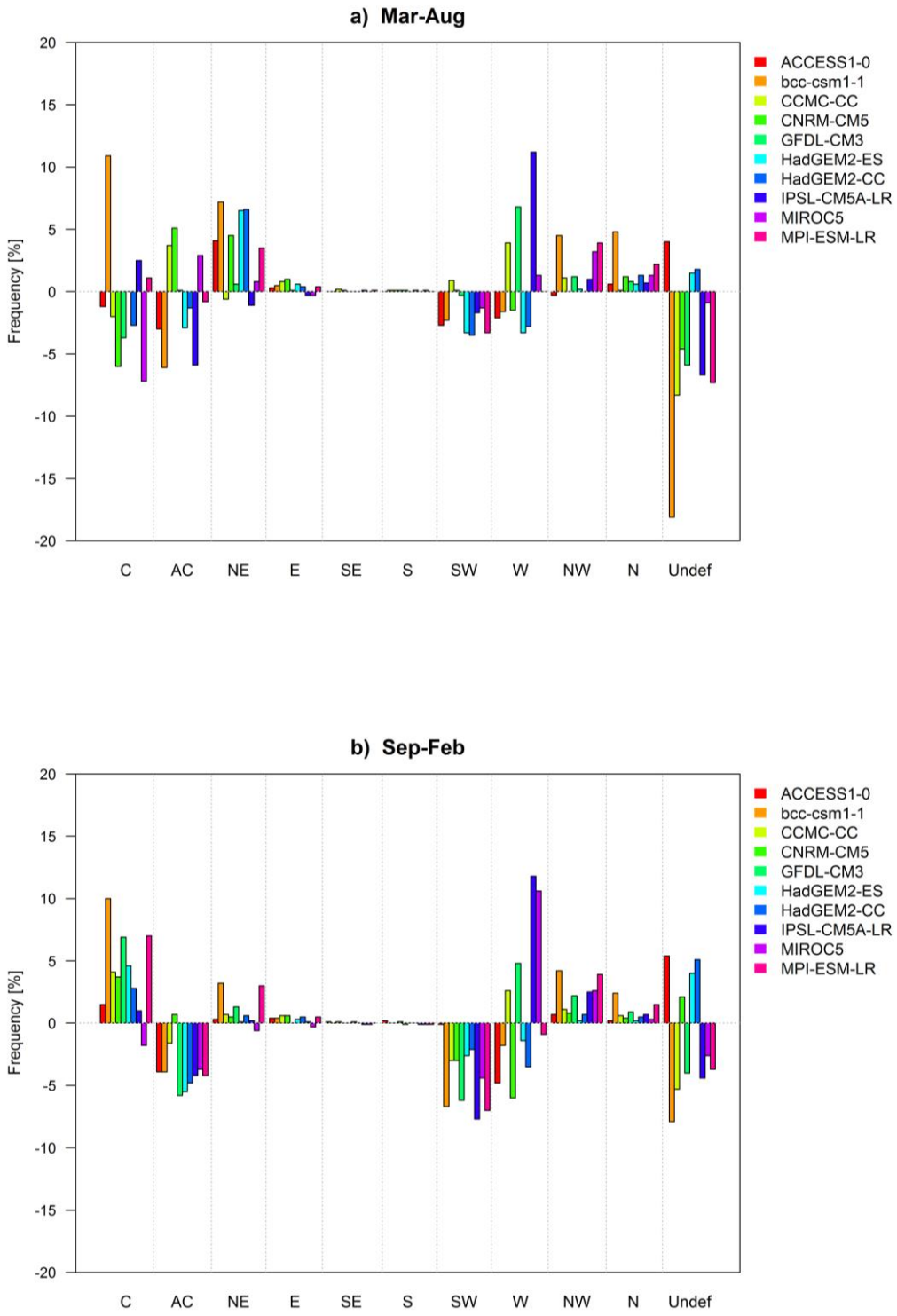

Figure 5.3. Seasonal differences between historical experiments in the selected 10 CMIP5 models and ERA-Interim reanalysis (1979-2005 GCM minus 1979-2005 ERA-Int) over Uzbekistan at 700 hPa GPH.

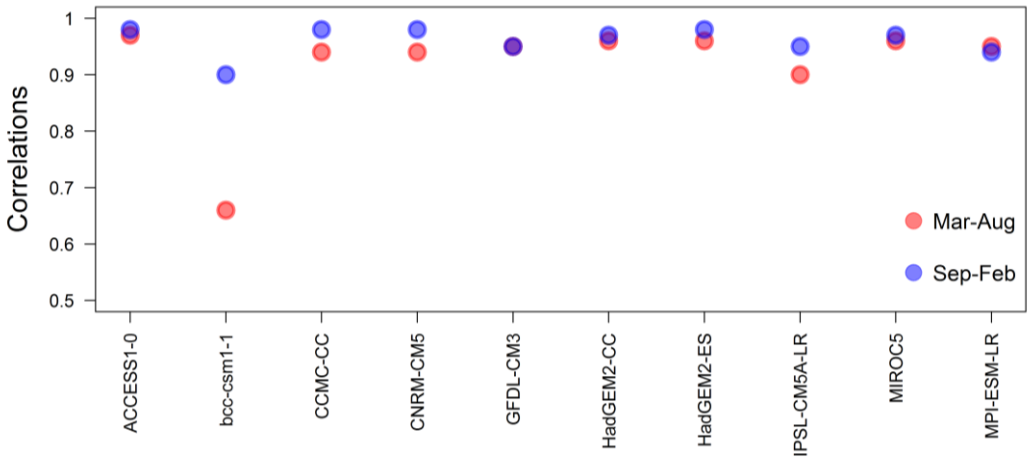

Figure 5.4. Pearson correlations between CWT frequencies of ERA-Interim and selected 10 GCMs historical experiences of CMIP5 projection over the study area for the March-August (red circle) and September-February (blue) of 1979-2005 years.

5.4.2. Future projections of CWT frequencies

The effects of changes in large scale atmospheric circulation frequencies over Uzbekistan and Central Asia the end of this century 2100, under RCP8.5 scenario (Figure 5.5), is explored in this section. Figure 5.6, Table 5.2 and Table 5.3 display the changes in the CWT frequencies in lower troposphere (Z_{700}) over the study area (2071-2100 minus 1979-2005).

The results of CMIP5 GCMs suggest that **CWT W** direction will become more frequent and increase up to 4.5% in the target period of 2071-2100. Of the 10 GCMs selected, only the bcc-csm1-1 model shows that W airflow will decrease (-0.8 %) during the period of September-February in the future.

7 GCMs of the 10 diagnose that the **CWT C** weather will be actively increasing in the warm season up to 2.6%. The bcc-csm1-1 model and IPSL-CM5A-LR show that cyclonic days will be less frequent in summer (-1.9% and -4.4%). In contrast to the warm period, the cyclonic circulation will be less active during the cold season (September-February) in the future; only ACCESS1-0 and HadGEM2-CC models highlight that C days will be stronger by increasing its frequency up to 2.3% in the winter for the 2071-2100 period.

CWT AC days will decrease up to -4.5% in the warm phase, however, there are model uncertainties for the cold period of the year. In contrast to the CWT AC days, the **CWT SW** airflow will decrease in cold season of the year and there are model uncertainties during the warm season in the future. The three models, ACCESS1-0, HadGEM2-ES and HadGEM2-CC show increase (from +0.3% to +1.7%), whereas the remaining seven models show decrease (from -0.4% to -1.9%) in the SW circulation lower troposphere during the summer for the 2071-2100 period.

The projections of the ensemble of CMIP5 models show that **NE** and **N** atmospheric circulations will decrease, especially the NE type show a decrease of up to -2.5% (March-August) over the study area in the future. The **CWT E, SE** and **S** days will remain at the same level or change by ±0.6% in the 2071-2100 years. Model uncertainties exist for the **CWT NW** flow direction with the amount of ±1% in the

future. Due to the topography, the **undefined** weather type is projected to increase (4.3%) notably in warm phase of the year.

In general, based on the CMIP5 GCMs ensemble results it can be predicted that CWT frequencies and magnitudes will not change in some cases (CWT SE and S), as ensemble mean has clear anomalous results with maximum seasonal variation ±2.3% in the diagnostic period of 2071-2100 (Table 5.2 and Table 5.3). However, it can be concluded that CWT C and W directions will be stronger during the warm phase and it is important to link these airflows to mudflow occurrences associated with named circulation patterns in the future.

Table 5.2. Climate change signal for the warm season of March-April (2071-2100 minus 1979-2005) in the CWT frequencies in each weather class and for each model (for the expansions of model abbreviation and acronym see Table 5.1).

Model name	Circulation Weather Type (CWT)										
	C	AC	NE	E	SE	S	SW	W	NW	N	Und
ACCESS1-0	0.3	-2	-2.5	-0.3	0	0	1.2	0.1	0	-0.2	3.6
bcc-csm1-1	-1.9	0.4	-0.8	-0.3	0	-0.1	-0.5	3.3	-0.4	-0.5	0.7
CMCC-CM	1.3	-0.9	-1.2	-0.1	-0.2	0	-1.9	3.7	-0.9	-0.5	0.7
CNRM-CM5	0.9	-0.8	-2.1	-0.7	0	0	-0.7	1.1	-0.1	-0.7	3.2
GFDL-CM3	2.3	-3.6	-2.4	-0.5	0	-0.1	-1.5	2.3	-0.2	-0.4	4.3
HadGEM2-CC	0.9	-1.4	-2.5	-0.6	0.1	-0.1	1.7	-0.2	-0.3	-0.1	2.6
HadGEM2-ES	-0.2	-1.2	-2.4	-0.6	0	-0.1	0.3	0.1	0	0.7	3.4
IPSL-CM5A-LR	-4.4	0.8	-1.9	-0.2	-0.1	-0.1	-0.7	4.5	0.7	-0.8	2.3
MIROC5	1.4	-0.8	-1.7	-0.2	0	-0.1	-0.7	2.2	0.4	0.2	-0.7
MPI-ESM-LR	2.6	-4.5	-1.1	0.1	0	0	-0.4	3.8	0.4	-0.6	-0.2
Ensemble mean	0.3	-1.4	-1.9	-0.3	-0.02	-0.1	-0.3	2.1	-0.04	-0.3	2

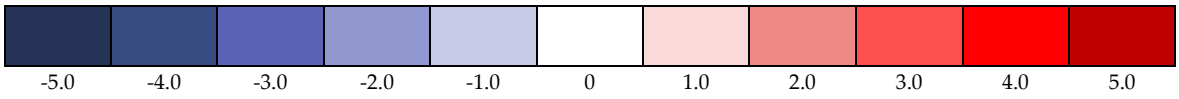

Table 5.3. Same as Table 5.2 but for the period of September-February (2071-2100 minus 1979-2005).

Model name	Circulation Weather Type (CWT)										
	C	AC	NE	E	SE	S	SW	W	NW	N	Und
ACCESS1-0	2.3	-0.8	-0.1	0.4	-0.1	-0.2	-1.4	1.3	0.5	0.1	-2.1
bcc-csm1-1	-0.1	0.3	0.3	0.1	0	-0.1	0	-0.8	-0.5	-0.5	1.2
CMCC-CM	-0.3	-1.4	-0.3	0	-0.2	0	-2	3.3	0.5	-0.1	0.4
CNRM-CM5	-1.6	0.1	-0.1	-0.2	0	-0.1	-1	1.8	0.1	0.1	0.9
GFDL-CM3	-2.5	1	-0.4	0.1	-0.1	0	-0.8	1.8	-0.8	-0.4	1.9
HadGEM2-CC	1.1	-0.7	-0.6	0	0	0	-2.5	4.3	-0.2	-0.3	-1.1
HadGEM2-ES	-1	1	-0.4	0.1	-0.1	-0.1	-0.8	2.8	0.3	-0.2	-1.8
IPSL-CM5A-LR	-1.2	-0.6	-0.7	0.2	0	-0.1	-0.8	3.1	-0.5	-0.4	1
MIROC5	-0.5	-0.3	-0.2	0.1	0	0	-1.8	3	-0.5	-0.2	0.4
MPI-ESM-LR	-0.4	1	-0.9	-0.1	-0.1	0	-0.3	2.4	-1.2	-0.4	0
Ensemble mean	-0.4	-0.04	-0.3	0.1	-0.1	-0.1	-1.1	2.3	-0.2	-0.2	0.1

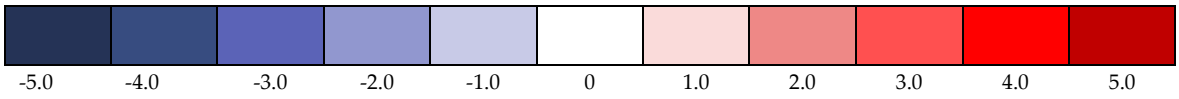

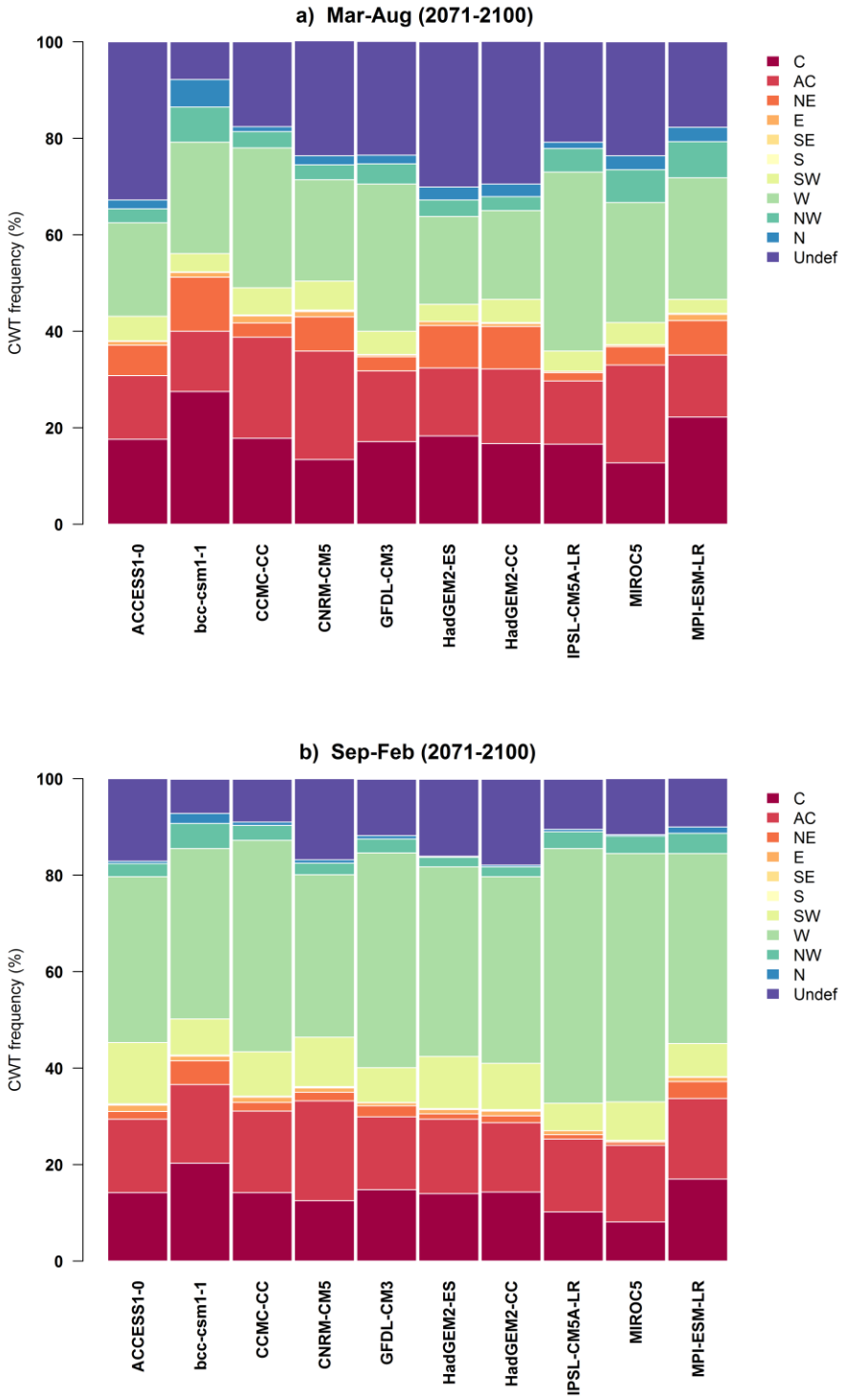

Figure 5.5. Scenario of seasonal frequencies of CWT under the selected 10 GCMs for the period of 2071-2100.

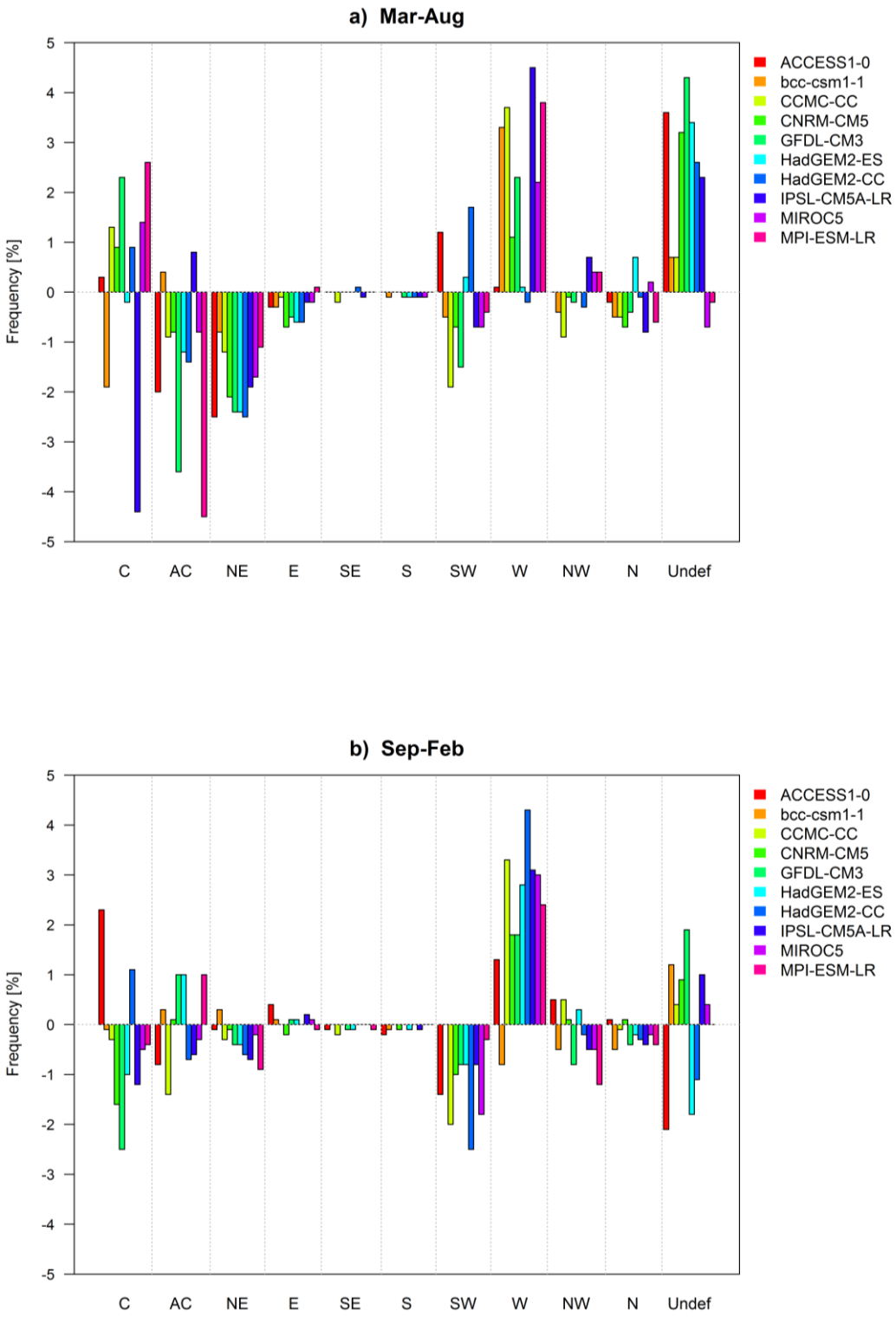

Figure 5.6. Seasonal frequencies of CWT for CMIP5 GCMs scenarios (2071-2100 minus 1979-2005) over Uzbekistan at 700 hPa GPH.

5.5. Discussions

5.5.1. Comparison with other studies

CMIP5 models are used to evaluate CWT frequencies under recent and future climate conditions to enable to link the changes in CWT to mudflow occurrences induced by precipitation associated with specific circulation patterns. Only a limited number of investigations are focused on the projected changes in atmospheric circulation over Central Asia, particularly in Uzbekistan and they must be duly taken into account to compare achieved results in this chapter. No study has examined the relationship between projected large scale circulation and its impact on future mudflow risk in Uzbekistan.

The increased frequency of CWT W airflow is expected to contribute to an overall increase of precipitation by the end of the century. This outcome is corroborated by Reyers et al. (2013) in which ECHAM5/MPI-OM1 ensemble is dynamically downscaled by CWT approach for the Aksu River basin located in Central Asia. Moreover, this weather type gives a climate change signal in mudflow occurrences associated with the mechanism of westerly airflow in lower troposphere over the study area for the future. Conversely, the robust decrease in the occurrence of CWT AC leads to lower precipitation particularly when it is hybrid or associated with W and SW flows. Further, the smaller magnitude of ensemble mean in changes associated with CWT E, SE, S, NW and N circulation patterns show that the

relationship between named weather types and precipitation has a weaker climate change signal and it is assumed to remain invariant (Table 5.2,Table 5.3 and Figure 5.6). Similar results have been obtained by Reyers et al. (2013).

However, model outcomes for the CWT C strongly vary in seasonal frequencies which predict that the climate will be rainy in warm period (March-August) and mudflows associated with cyclonic days will occur frequently in comparison to the cold period (September-February) for Uzbekistan in the future. Therefore, the skill of CMIP5 models projected for CWT SW highlight that significant uncertainties exist over spring and summer even though there is a clear signal that SW will be less frequent in future autumns and winters. Zhao et al. (2018) confirms that subtropical westerly jet centred over Caspian Sea will change its position by shifting further south in the last 50 years of the 21st century and it will affect summer rainfall in Central Asian countries including Uzbekistan. Ensemble mean results in this study also indicate the frequency of CWT SW which brings tropical moist and warm air associated with extreme rainfall to Uzbekistan is more likely to decrease under future climate conditions. However, results in Reyers et al. (2013) show opposite signs in frequency of CWT SW in the future. This disagreement motivates a more detailed investigation in future.

Finally, the significant changes in undefined weather class especially in warm periods can be summarised by regarding the influence of orographic features of the

investigation area. On the other hand it can be attributed to outperform identified biases of individual models along with CMIIP5 projection.

5.5.2. Limitations and future outlook

Concerning the model outputs in this study several factors can be underlined as limitations which needs to be analysed and investigated in the future. First of all, it should be noted that very few studies exist to compare and better understand the projected changes in large scale circulation patterns and underlying mechanisms associated with precipitation in Central Asia, particularly, in Uzbekistan. Simulations of CWT classification with 10 CMIP5 GCMs for recent climate conditions highlight biases in reproducing the variability of observed weather types and their seasonal changes. However, it would be an interesting perspective to try other reanalyses data (e.g. NCEP) and bias correction methods in order to simulate the evolution of CWTs frequencies over Uzbekistan and Central Asia. Nevertheless, simulated frequency of weather circulations and its distribution in this study show a realistic result of particular weather patterns known to potentially lead to extreme rainfall events affecting mudflow occurrences. Correlation analysis between ERA-Interim and CMIP5 models confirm how well observation and model data fit each other for the historical period of 1979-2005 (Figure 5.4). Furthermore, only 10 GCMs from CMIP5 projection have been attempted to assess the links between weather frequencies and mudflow occurrences induced by precipitation associated with large-scale atmospheric circulation for the RCP8.5 scenario over the study area.

However, a more detailed analysis by application of all representative models from CMIP5 projection under different scenarios can be considered for future research. Moreover, dynamical downscaling approach by application of other circulation catalogue, for example, CORDEX RCM and WP (Weather Pattern) classification (Michelangeli et al., 1995), could be a perspective experiment in order to see if similar weather circulations over Uzbekistan are identified for the recent and future climate. Therefore, future research should focus on models contributing to lower the uncertainties since the projection for future large-scale circulation is strongly dependent on the model's ability to represent the physical mechanisms underlying climate variability and change (Santos et al., 2016).

5.6. Conclusions

In this chapter, daily mean Z_{700} outputs from 10 CMIP5 (Taylor et al., 2012) models have been statistically downscaled by application of CWT approach. Only the first member (named r1ip1) from the historical experiment (1979-2005) and future (2071-2100) under the RCP8.5 emission scenario (radiative forcing surplus of 8.5 W/m2 in 2100) has been considered for each GCM. By this way the ability of the CMIP5 models in simulating large scale circulation in lower troposphere and its effect on the projected mudflow risk over Uzbekistan was evaluated.

Comparisons of downscaled historical frequencies of large scale circulation with observational (ERA-Interim in this case) suggest that the statistical downscaling

approach of CWT is appropriate to capture the low tropospheric circulation over Uzbekistan. In general, seasonal frequencies of CWTs do not change significantly as the overall results indicate that spatial frequency of airflow directions have an amplitude up to ±5 percent in the 2071-2100 years. However, the application of CWT methodology reveals that W and C airflows will become stronger during the mudflow occurrences season or in the warm period (March-August) by the end of the century. It means that extreme mudflow events associated with the above named weather types will increase in the period of 2071-2100. However, CWT SW is more likely to decrease under the future climate conditions even though there are model uncertainties in the warm phase by the end of the century.

The implications that achieved results can be linked to impacts on precipitation patterns resulting in mudflow occurrences associated with the important airflows (C, W and SW) detailed in the next chapter.

6 Mudflow Risk in Uzbekistan under Anthropogenic Climate Change

6.1. Introduction

Precipitation plays a major role in mudflow formation and the projected future rainfall could predict such phenomena and help set up warning systems. A number of studies attempted to investigate the impact of climate change on different types of landslide occurrences by application of downscaled precipitation patterns as an input parameter obtained from GCMs (Schmidt and Dehn, 2000, Chiang and Chang, 2011) and RCMs (Schmidt and Glade, 2003). These studies mainly focused on mountain and hilly areas prone to slope failures with the interaction of the climatic variables such as extreme rainfall events. The main drawback in the use of downscaled climate variables such as precipitation from GCMs output for landslide-climate analyses lays in the uncertainty inherent to the downscaled climate projections (Gariano and Guzzetti, 2016). Additionally, raw GCM precipitation simulations may be still biased especially in the mountain regions

(Fowler et al., 2007, Fang et al., 2015). Mannig et al. (2013) concluded that additional model run would be desirable to assess the uncertainties and biases in the precipitation patterns in their study domain such as Central Asia. The authors suggest adoption of dynamical or statistical downscaling approaches to obtain high spatial and temporal resolution in order to examine climate change impacts on precipitation parameters. Inadequate observational/empirical data due to lack of meteorological stations in the study area has been often cited as a limitation (e.g. Ozturk et al. (2017) and Reyers et al. (2013)) to explain the model bias over the mountains and high plateau regions of Central Asia. Huang et al. (2014) note that out of 28 CMIP5 models only 5 models (CanESM2, EC-EARTH, GFDL CM3, MIROC5, and MRI-CGCM3) have better ability to capture a multimodel ensemble mean and simulates well with CRU (Climate Research Unit) rainfall observation over Central Asia and Tibetan Plateau for the historical experiment during 1901–2005. Zhao et al. (2018) identified that only 14 models of the 25 models from CMIP5 projection in which the precipitation distribution matched well with subtropical westerly jet circulation over the Central Asia.

Gariano and Guzzetti (2016) systematically documented the existing investigations world-wide; they detailed the concepts used in the selected studies and associated methodologies and included the results of analyses due to the climate change impact on different types of landslides. Figure 6.1 shows the geographical

distribution of the climate change studies in relation to all type of landslide events for each country reported by Gariano and Guzzetti (2016). Figure 6.1 shows that no investigation regarding landslide (in this case mudflow) – climate has been done in Central Asian countries including Uzbekistan. Therefore, the work presented in this chapter is novel in that it is the first investigation which analyses the potential impacts of global warming on precipitation induced mudflow episodes in the piedmont and mountainous areas of Uzbekistan.

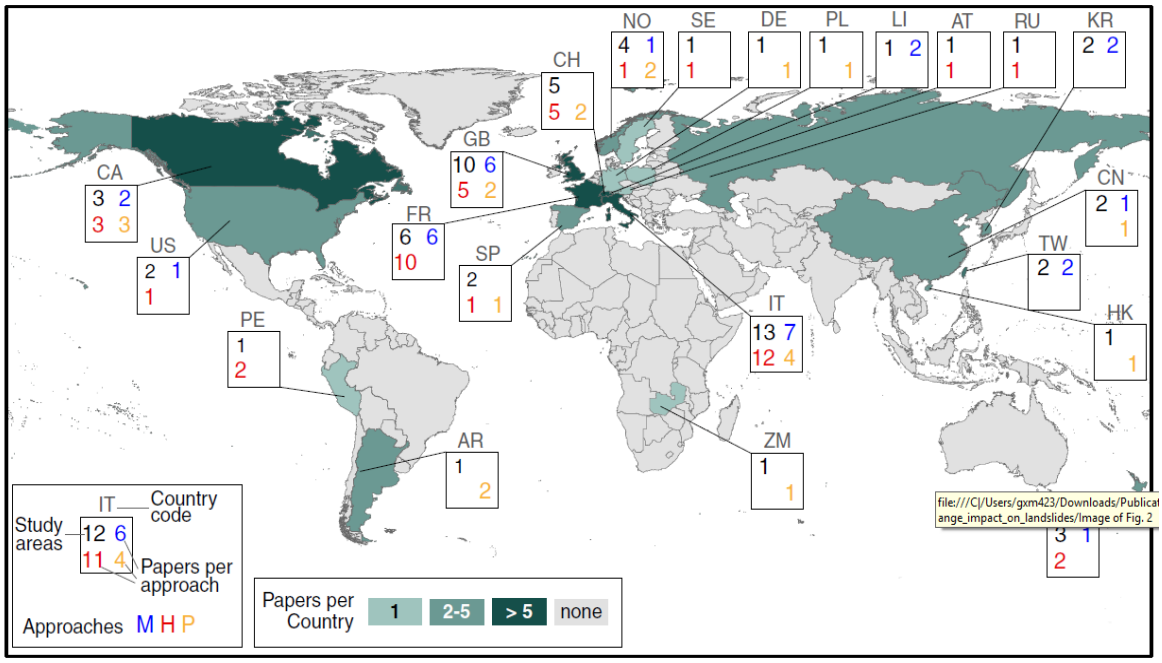

Figure 6.1. Geographical distribution of landslide-climate studies by countries. Green coloured countries with country code show the number of published papers. Coloured numbers indicate the number of different approaches which were investigated by countries. Approaches: M (blue), modelling approach; H (red), historical analysis; P (orange), analysis of paleo landslide evidences. Adapted from Gariano and Guzzetti (2016).

Figure 6.2 presents the systematic approach implemented in this chapter. First of all, an evaluation of the selected 10 GCMs from CMIP5 projection was conducted to be examine the effects of anthropogenic climate changes on precipitation climatology by adopting statistical downscaling or empirical or combined approaches for the recent (1979-2005) and future climate (2071-2100) in Uzbekistan. In the next step, GCM outputs were applied to an empirical-statistical ADRM to assess the effect of anthropogenic emissions of greenhouse gases on precipitation threshold inducing mudflows for the target period of 2071-2100 in the study area. For this purpose, the extracted daily precipitation timeseries from the CMIP5 GCMs for the control run (1979-2005) and future experiment (2071-2100) under the RCP8.5 emission scenario was corrected by bias correction procedure. Then, the CMIP5 GCMs were evaluated by calculating frequency means between the station based climate and the raw precipitation by CMIP5 and bias corrected values. The results of two selected GCMs out of 10 were used to run the ADRM approach. The analysis demonstrates that model outputs for climate change studies are capable to predict mudflow occurrences and is unique to this field of research for Uzbekistan.

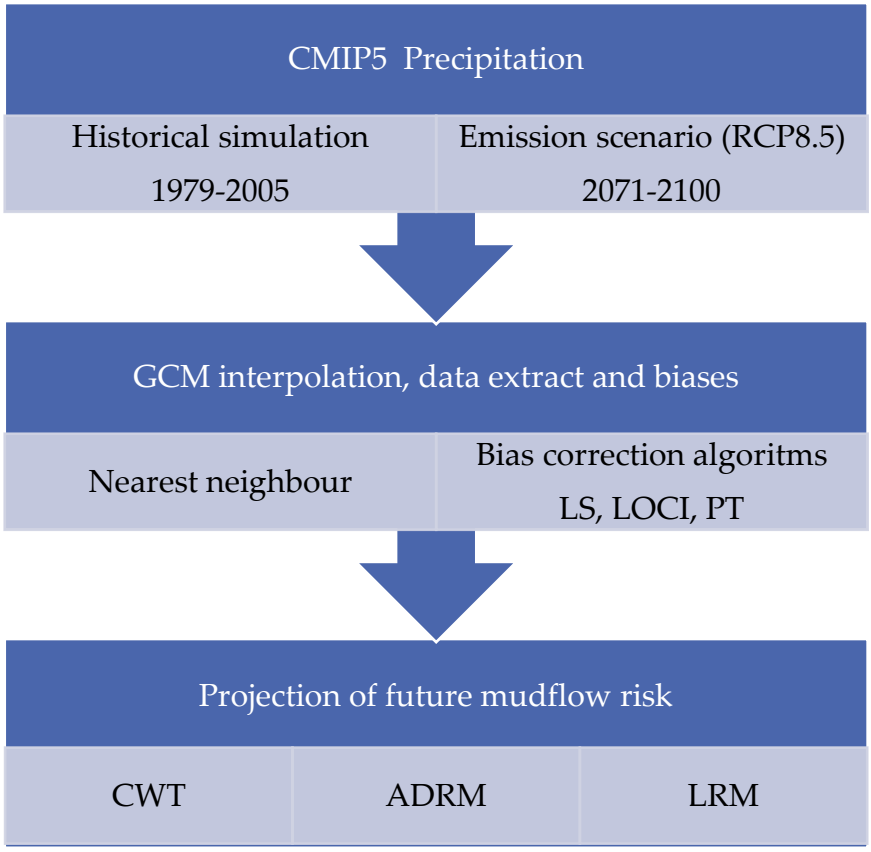

Figure 6.2. Projected mudflow behaviour chain (Objective 6).

6.2. Data

To evaluate the modelling capabilities of 10 selected GCMs from CMIP5 multi-model projection, simulated precipitation from the GCMs are compared to station based observational data for the 27-year period 1979-2005. The main focus is precipitation timeseries for the warm season of the year (March-August) because the application is towards precipitation threshold resulting mudflow occurrences in summer over the study area.

6.2.1. Simulation data

Selected 10 GCMs from the multimodel CMIP5 ensemble for historical run (1979-2005) and future scenarios (2071-2100) of precipitation are used in this chapter. Detailed description of CMIP5 are provided by Taylor et al. (2012). The atmospheric component of horizontal and vertical resolutions for each model is described in Table 5.1 (please see Chapter 5). Simulated data used of the grid-box that includes the location of the weather station used to calibrate the precipitation timeseries for the period of 1979-2005.

6.2.2. Observed data

Daily observed precipitation data for a period of 27 years (1979-2005) of the selected station (Gallyaaral) recorded by Uzhydromet according to WMO standards is used for bias correction of GCM predictors and validation of the historical experiment.

6.3. Methods

6.3.1. Extraction of CMIP5 ensemble daily rainfall timeseries

Before the extraction CMIP5 GCMs precipitation data, selected 10 models were interpolated using bilinear algorithm. Thereafter, the grid box that included the location of the selected weather station (Gallyaaral) used to extract raw precipitation values from CMIP5 GCMs based on nearest grid point interpolation. Daily rainfall values for the 10 selected GCMs for historical simulation (1979-2005) were extracted in order to validate the raw data with the observational timeseries. Daily rainfall

values for future scenario 2071-2100 under the RCP8.5 emission were also extracted at the same grid box.

6.3.2. Bias correction methods for GCM precipitation data

The choice of a bias correction algorithm plays a significant role in assessing the precipitation pattern for recent and future climate conditions. In this study, three bias correction methods such as linear scaling (LS), local intensity scaling (LOCI) and power transformation (PT) are employed for adjusting GCMs outputs. Timeseries of daily precipitation data for the period of 1979-2005 and 2071-2100 are used for bias correction techniques.

6.3.2.1. Linear scaling of precipitation

The linear scaling or simply scaling method introduced by Lenderink et al. (2007) quantifies the bias by application of monthly correction values based on the differences between observed and raw data of the model (Fang et al., 2015). The formula for simple scaling is:

$$P_{cor,m,d} = P_{raw,m,d} \times \frac{\mu(P_{obs,m})}{\mu(P_{raw,m})} \qquad (6.1)$$

$P_{cor,m,d}$ is corrected precipitation on the dth day of mth month, and $P_{raw,m,d}$ is the model raw precipitation on the dth day of mth month. μ represents the expectation

operator (e.g., μ ($P_{obs,m}$) represents the mean value of observed precipitation at given month m).

6.3.2.2. Local intensity scaling of precipitation

Local intensity scaling method presented by Schmidli et al. (2006) consists of three steps (Teutschbein and Seibert, 2012) that can effectively correct for biases during the wet-day frequency and intensity. In a first step, a model precipitation threshold for the mth month ($P_{thres,m}$) is calibrated such that the number of GCM simulated days exceeding this threshold matches the number of observed days with precipitation more than 0 mm (Teutschbein and Seibert, 2012, Fang et al., 2015). Thereafter, the following formula quantifies a scaling factor s from the wet day intensities:

$$s_m = \frac{\mu(P_{obs,m,d} | P_{obs,m,d} > 0)}{\mu(P_{raw,m,d} | P_{raw,m,d} > P_{thres,m})} \qquad (6.2)$$

Finally, GCM simulated precipitation is corrected by the scale parameter:

$$P_{cor,m,d} = \begin{cases} 0, \\ P_{raw,m,d} \times s_m \end{cases} \text{ if } P_{raw,m,d} < P_{thres,m} \qquad (6.3)$$

6.3.2.3. Power transformation of precipitation

The power transformation approach uses an exponential form to further adjust the variance statistics of precipitation time series while the above two algorithms (LS

and LOCI) are limited to correct the differences in the variance (Teutschbein and Seibert, 2012). Following Fang et al. (2015) b_m the exponent for the m th month is estimated (Shresta, 2015) by the LOCI combination approach formula:

$$f(b_m) = \frac{\sigma(P_{obs,m})}{\mu(P_{obs,m})} - \frac{\sigma\left(P_{LOCI,m}^{b_m}\right)}{\mu(P_{LOCI,m}^{b_m})} \quad (6.4)$$

where σ indicates the standard deviation, $P_{LOCI,m}$ is the corrected precipitation by the LOCI algorithm for the m th month. If the exponent factor b is greater than 1 for the m th month it means that the GCMs underestimates the coefficient of variances of observed precipitation timeseries for the m th month. After the identification of the b_m factor, the parameter $s_m = \frac{\mu(P_{obs,m})}{\mu(P_{LOCI,m}^{b_m})}$ (6.5) is adjusted in a stepwise manner to match the mean corrected values to the observed mean. Thereafter, the corrected precipitation timeseries by LOCI approach is used:

$$P_{cor,m,d} = s_m \times P_{LOCI,m,d}^{b_m} \quad (6.6)$$

6.3.3. ADRM method

After the calculation of antecedent rainfall index of bias corrected precipitation from two GCMs (CMCC-CM and MPI-ESM-LR) obtained by PT approach, the daily rainfall value as a driving factor of mudflow occurrences in the study area is applied to ADRM for the control run and future scenario. Calculation antecedent daily rainfall index is based on simple formula:

$$ra_0 = kr_1 + k^2r_2 + ... + k^nr_n \qquad (6.7)$$

where ra_0 is the antecedent daily rainfall for day 0; r_1 is the rainfall on the day before day 0; r_n is the rainfall on the n th day before day 0; and k is a constant <1.0, in this case k=0.84.

6.3.4. Logistic regression model

Logistic equation is developed in order to estimate the relationship between mudflow occurrences (dependent variable) and daily rainfall value and 10 days of antecedent rainfall index (independent variables). Equation is based on the following formula:

$$\log\left(\frac{p}{1-p}\right) = F(r, r_n) \qquad (6.8)$$

where p is the probability (p) of mudflow occurrences on a given day. The probability curves for P=0.1, P=0.5 and P=0.9 are quantified in this study. This method is analogous to the one presented in Glade et al. (2000).

6.3.5. Selection of extreme rainfall events triggering mudflows

Based on results in Chapter 4, the precipitation values for more than 20 mm and antecedent index with ≤40mm during the CWT C, SW and W days have been derived from the bias corrected precipitation data for control run (1979-2005) and future projection (2071-2100) simulated for the Gallyaral station. It was assumed that the chance of mudflow occurrences in case of precipitation below 20 mm is

relatively less, and this assumption has been validated in Chapter 4 whereby it shows that there is only 10% probability of mudflow occurrences for the Gallyaral station when precipitation amount is ≤20mm (Table 4.3, Figure 4.4). However, it should be duly taken into account that higher antecedent rainfall index could trigger mudflow magnitude even though the precipitation amount is less than 20 mm. The limitation of this approach lies with the fact that only daily rainfall values are included as mudflow inducing factor and neglecting temperature patterns.

6.4. Results

6.4.1. Evaluation of bias correction methods applied to precipitation

The evaluation of daily mean precipitation values of GCM simulations before and after bias corrections against the observational variable at the Gallyaral meteorological station is listed in Table 6.1. Time-series based performances of observed precipitation, GCM outputs and corrected data are visualised as 7 days running mean to smooth daily variability of precipitation (Figure 6.3 and Figure 6.4). Additionally, Q-Q plot is used to compare the theoretical distributions of each parameter (Figure 6.5 and Figure 6.6). The time range used for bias correction in this study is 27 years from 1979 to 2005.

Table 6.1 present that the raw data of the models, namely ACCESS1-0, CNRM-CM5, HadGEM2-CC, HadGEM2-ES and IPSL-CM5-LR overestimate the average precipitation (1.84, 1.34, 1.37, 1.38, 1.24 mm each) compared to the observation (1.04

mm) for the investigation period. In contrast, MIROC5 and MPI-ESM-LR GCMs underestimate the precipitation values (0.86 and 0.78 mm), at the same time bcc-csm1-1 (1.09 mm) slightly overestimates precipitation over the Gallyaaral station. It is notable that mean values of raw precipitation data presented by CMCC-CM (1.04 mm) and GFDL-CM3 (1.02 mm) models are similar to the mean value (1.04 mm) of observed timeseries (Table 6.1).

Frequency statistics of mean values at the Gallyaral station after the application of bias correction techniques (LS, LOCI and PT) significantly improved and had a good estimation of bias corrected precipitation values compared to the GCM raw data. Correcting the precipitation timeseries with **LS method** ensures that maximum rainfall never exceeds the raw maximums if the model raw overestimates the observed data. After correction of daily rainfall, the response of corrected values at Gallyaral station by scaling algorithm gives more realistic mean values even though the method underestimates the maximums of observed precipitation (Table 6.1, Figure 6.3, Figure 6.4).

Compared to the LS method, **LOCI algorithm** significantly overestimates the GCM simulation from observation values, likewise frequency statistics of corrected values are higher than the mean values. After the correction by LOCI procedure for the bias in the station, 27 years averaged precipitation data, it was found that it is

insignificant for most of models, however, results from CMCC-CM, CNRM-CM5 and MPI-ESM-LR are more realistic (Table 6.1, Figure 6.3 and Figure 6.4).

The ability of **PT method** to reproduce the precipitation shows robust results amongst bias correction techniques applied in this study. Frequency statistics of mean values (Table 6.1) and visualisation (Figure 6.3 and Figure 6.4) perform that method fits well and improves the GCM raw data achieving close agreement of the mean corrected values with the observed timeseries.

Out of ten selected GCMs the best frequency metrics and bias corrected results are related to CMCC-CM and MPI-ESM-LR models. In a first case, the raw data of CMCC-CM model reveals similar station based timeseries with minor overestimation in the beginning of winter season (Figure 6.3). For the MPI-ESM-LR model, the raw values, after applying bias correction techniques, match the observation variable. Hence, the above named two models' bias corrected outputs, preferably obtained by PT technique, could help to identify precipitation threshold triggering mudflows in the study area for the recent and future climate.

Table 6.1. Frequency based statistics (unit: mm) of daily mean observed precipitation, GCM raw data and bias-corrected values (LS, LOCI, PT) at the Gallyaral station for the historical period (1979-2005) and future scenario (2071-2100).

		standard deviation		mean		median		75th percentile		99th percentile	
		control	**scenario**	**control**	**scenario**	**control**	**scenario**	**control**	**scenario**	**control**	**scenario**
ACCESS1-0	Obs	0.98		1.04		0.84		1.70		3.52	
	Raw	1.54	1.81	1.84	2.18	1.63	2.13	2.68	3.43	5.87	6.74
	LS	0.86	1.12	1.04	1.30	1.02	1.23	1.66	2.09	3.39	3.96
	LOCI	1.40	3.31	1.65	3.87	1.47	3.41	2.69	5.87	4.85	13.32
	PT	0.94	1.52	1.04	1.53	0.90	1.24	1.58	2.47	4.01	6.57
bcc-csm1-1	Obs	0.98		1.04		0.84		1.70		3.52	
	Raw	0.88	0.91	1.09	0.99	1.09	0.84	1.78	1.71	3.07	3.11
	LS	0.84	0.89	1.05	0.95	1.04	0.81	1.64	1.55	2.97	3.24
	LOCI	1.33	1.54	1.65	1.54	1.52	1.03	2.72	2.62	4.93	5.39
	PT	1.02	1.37	1.04	1.13	0.84	0.64	1.61	1.64	3.69	5.95
CMCC-CM	Obs	0.98		1.04		0.84		1.70		3.52	
	Raw	0.97	1.24	1.04	1.7	0.93	0.87	1.68	1.93	3.86	4.57
	LS	0.97	1.35	1.04	1.21	0.92	0.84	1.69	1.89	3.75	5.56
	LOCI	0.99	1.37	1.05	1.22	0.93	0.84	1.67	1.93	3.77	5.72
	PT	0.97	1.41	1.04	1.23	0.91	0.82	1.65	1.98	3.70	6.15
CNRM-CM5	Obs	0.98		1.04		0.84		1.70		3.52	
	Raw	1.19	1.28	1.34	1.42	1.21	1.11	2.09	2.27	4.60	4.74
	LS	0.95	1.08	1.04	1.13	0.91	0.86	1.70	1.78	3.60	4.22
	LOCI	1.08	1.19	1.25	1.31	1.13	1.05	1.89	2.04	4.23	4.49
	PT	1.00	1.18	1.04	1.16	0.85	0.80	1.70	1.79	3.71	4.42
GFDL-CM3	Obs	0.98		1.04		0.84		1.70		3.52	
	Raw	0.79	0.78	1.02	0.94	1.04	0.94	1.63	1.53	2.83	2.83
	LS	0.84	0.85	1.05	0.97	1.05	0.92	1.72	1.64	3.10	3.18
	LOCI	1.33	1.36	1.59	1.47	1.51	1.31	2.59	2.52	4.57	4.90
	PT	0.97	1.22	1.04	1.13	0.89	0.83	1.73	1.77	3.78	4.63
HadGEM2-CC	Obs	0.98		1.04		0.84		1.70		3.52	
	Raw	1.37	1.90	1.50	2.01	1.14	1.64	2.17	3.23	5.47	7.37
	LS	0.88	1.34	1.04	1.46	0.98	1.38	1.68	2.46	2.99	4.89
	LOCI	1.73	2.43	1.74	2.43	1.33	2.00	2.72	3.88	7.33	9.62
	PT	0.99	1.89	1.04	1.82	0.87	1.41	1.68	3.11	3.59	7.60
HadGEM2-ES	Obs	0.98		1.04		0.84		1.70		3.52	
	Raw	1.38	1.74	1.58	1.99	1.30	1.84	2.29	3.18	5.52	6.46
	LS	0.84	1.30	1.04	1.43	0.98	1.37	1.67	2.38	3.13	4.94
	LOCI	1.44	2.01	1.63	2.22	1.42	2.06	2.56	3.56	5.69	7.49
	PT	0.96	1.75	1.04	1.73	0.90	1.42	1.69	2.96	3.80	6.44
IPSL-CM5-LR	Obs	0.98		1.04		0.84		1.70		3.52	
	Raw	1.24	1.06	1.27	0.99	0.93	0.66	2.26	1.65	4.08	3.96
	LS	0.88	0.77	1.04	0.80	1.01	0.70	1.69	1.32	3.15	3.04
	LOCI	1.27	1.09	1.44	1.09	1.31	0.95	2.41	1.82	4.37	4.05
	PT	0.99	0.98	1.04	0.88	0.82	0.63	1.66	1.43	3.67	4.01
MIROC5	Obs	0.98		1.04		0.84		1.70		3.52	
	Raw	0.75	0.89	0.86	0.98	0.64	0.75	1.31	1.54	2.88	3.78
	LS	0.92	1.08	1.04	1.19	0.85	0.95	1.62	1.90	3.46	4.24
	LOCI	1.16	1.38	1.39	1.59	1.16	1.38	2.06	2.45	4.39	5.49
	PT	1.00	1.34	1.04	1.32	0.78	0.93	1.63	2.07	3.94	5.19
MPI-ESM-LR	Obs	0.98		1.04		0.84		1.70		3.52	
	Raw	0.81	0.93	0.78	0.78	0.58	0.48	1.36	1.27	2.80	3.54
	LS	1.10	1.18	1.05	1.01	0.86	0.61	1.74	1.67	3.85	4.71
	LOCI	1.10	1.23	1.04	1.04	0.79	0.61	1.77	1.66	3.87	4.87
	PT	1.00	1.19	1.04	1.06	0.87	0.68	1.76	1.67	3.58	4.74

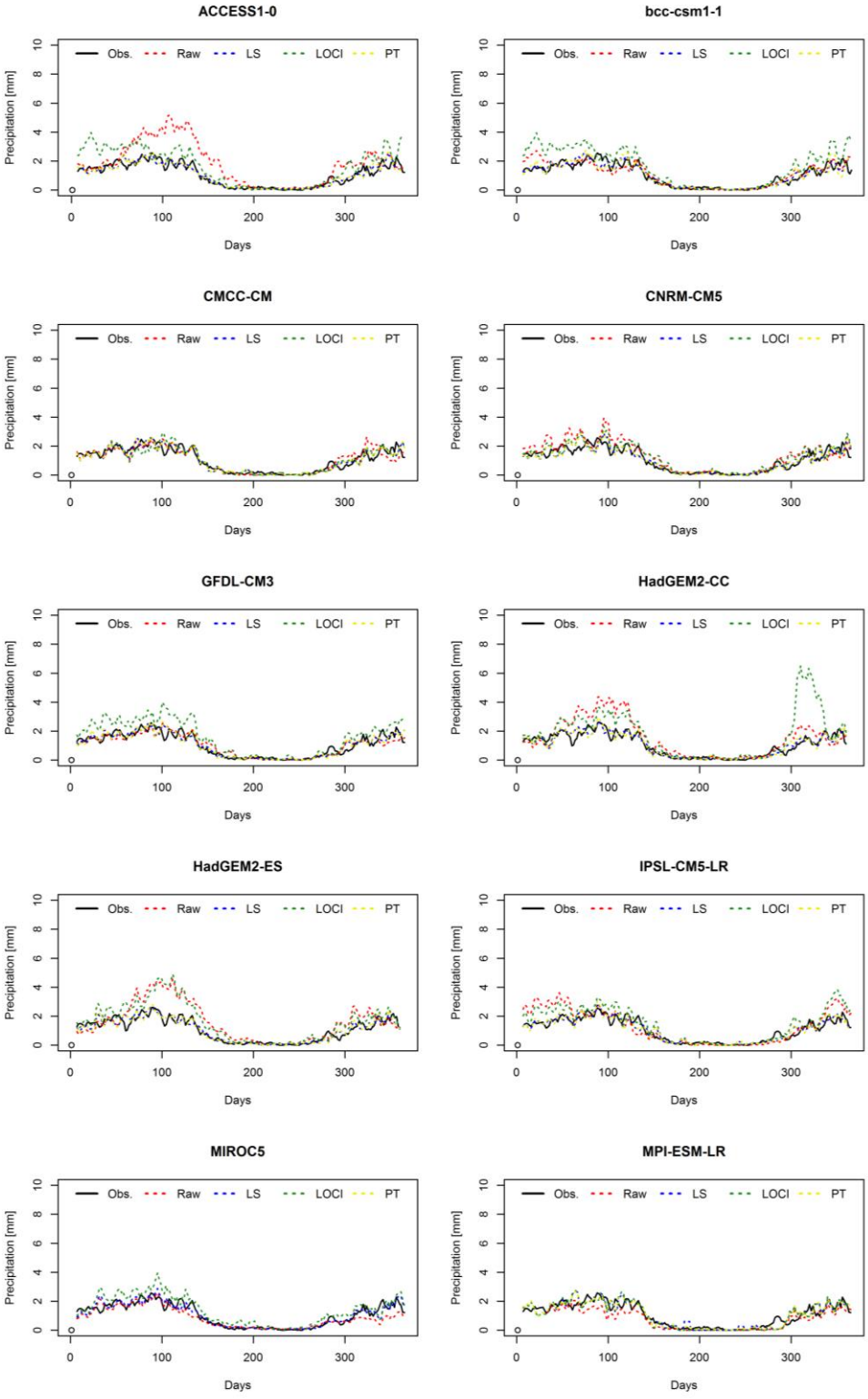

Figure 6.3. Daily mean precipitation of observed, raw GCM-simulated and bias corrected values at the Gallyaaral station with the 7-day smoothed moving average method for the years of 1979-2005.

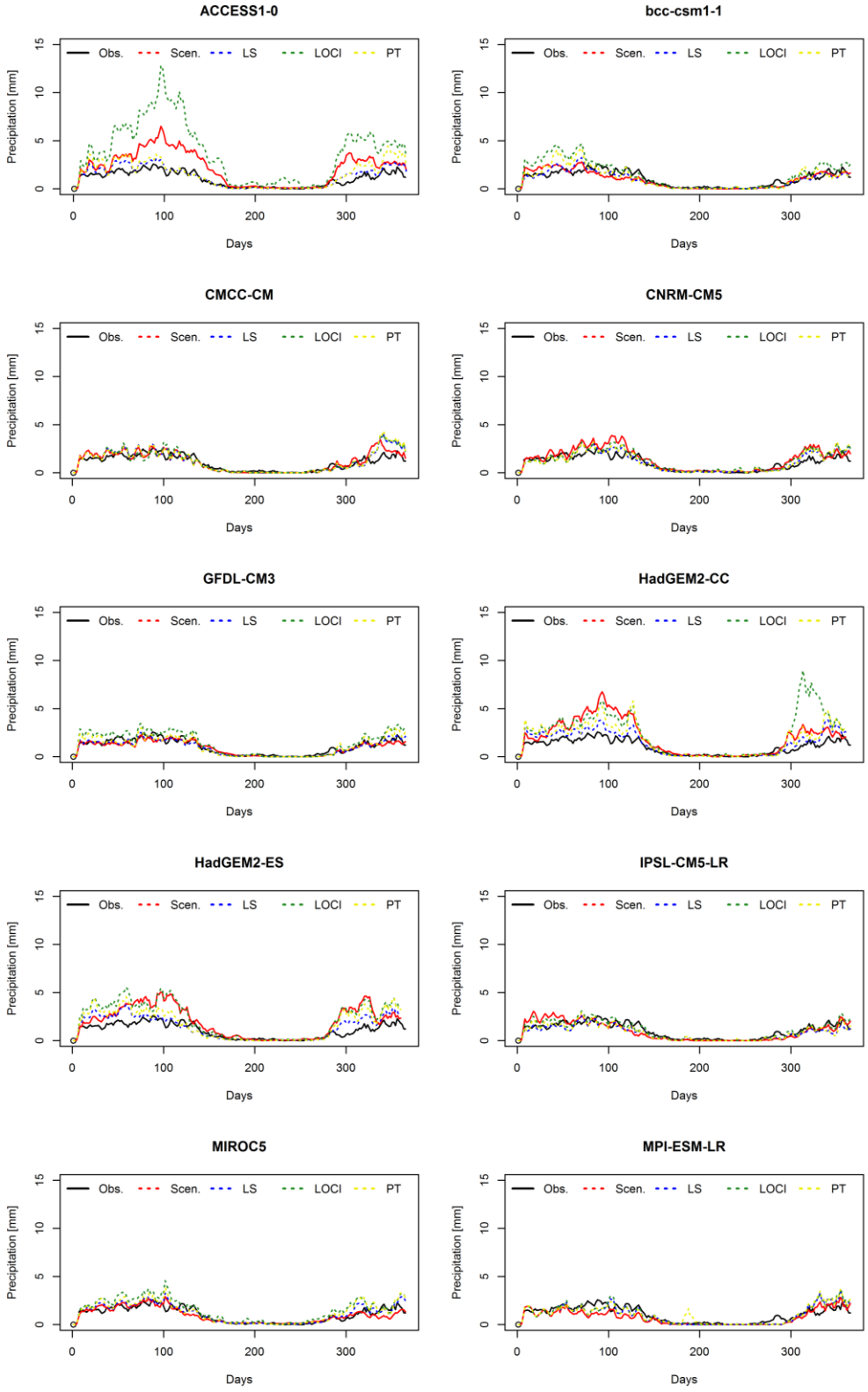

Figure 6.4. Same as Figure 6.3 but for the years of 2071-2100.

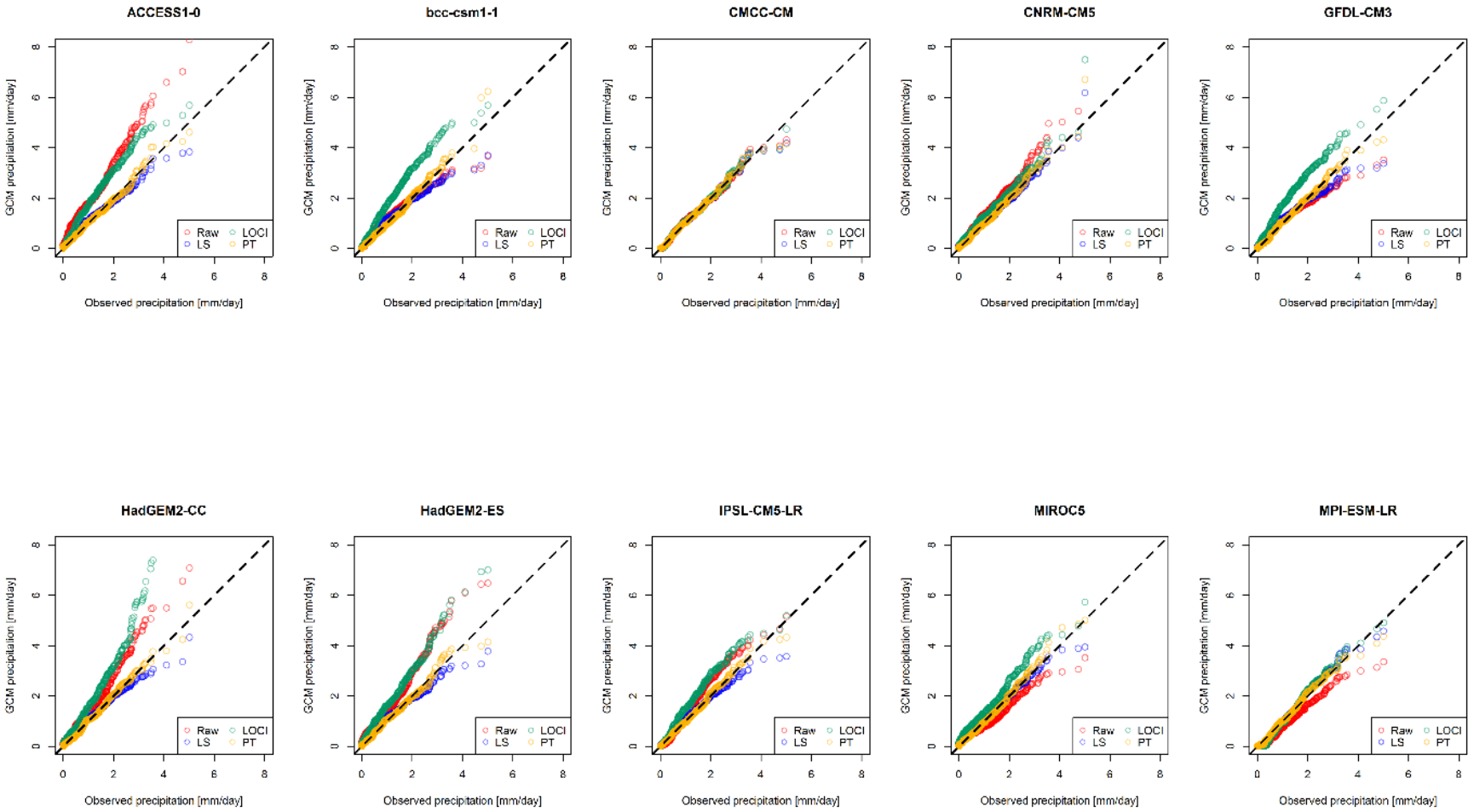

Figure 6.5. Q-Q plot of corrected simulated daily average precipitation against station (Gallyaaral) daily mean precipitation for the period of 1979-2005.

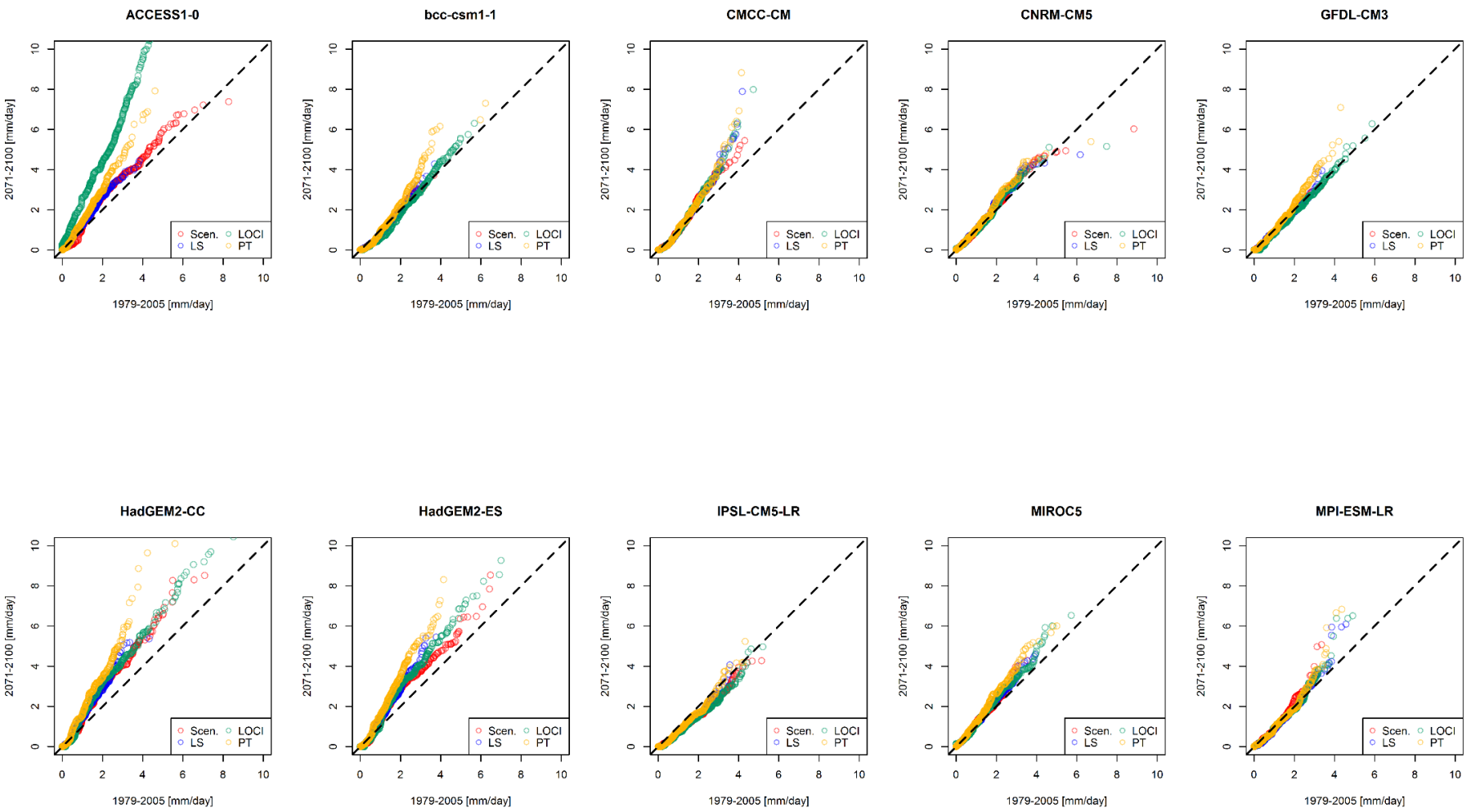

Figure 6.6. Q-Q plot of corrected precipitation from selected GCMs scenarios for the period of 2071-2100.

6.4.2. Linking global circulation model outputs to ADRM

Probabilities of mudflow occurrences using antecedent daily rainfall conditions as an independent factor triggering mudflow events has been analysed here. Equation (6.9) explained for the Gallyaaral station in the Table 4.4 was used to calculate the threshold probability line for control run (1979-2005) and future scenarios (2071-2100) of two selected GCMs (CMCC-CM and MPI-ESM-LR). Model outputs are presented in Figure 6.7.

$$\log\left(\frac{P}{1-P}\right) = -3.87 + 0.10 * r + 0.05 * r_a \qquad (6.9)$$

Probability envelopes of mudflow occurrences based on model data which include antecedent rainfall condition and daily precipitation as input data for ADRM show that results using equation 6.9 works satisfactorily for both GCMs (Figure 6.7). However, calculation of the probability line (Table 6.2) based on the synthetic mudflow occurrences assumed by taking into account the selected rainfall class CWT C, SW and W generating extreme events, show that CMCC-CM underestimates the 0.5 and 0.9 threshold probability lines for control run and future scenario (Figure 6.8). This might be due to exclusion of information on temperature conditions as this is an important parameter to be taken into account while running the ADRM as it was discussed in Chapter 4. The modelling results for MPI-ESM-LR precipitation data suggest that the probability line is underestimated (<0.5 and <0.9) for the control period, however, the probability for the future scenario fits, but has

some uncertainties. This might be due to the very high values of precipitation and antecedent rainfall index projected by MPI-ESM-LR GCM. In general, both GCMs were able to capture probability lines even though the ADRM has some limitations due to the exclusion of temperature conditions. Overall the outputs from the GCMs (CMCC and MPI-ESM-LR) for the threshold probabilities are acceptable as both can capture the antecedent conditions and extreme events evaluated by ADRM taking into account CWT C, SW and NW airflows as a proxy to simulate and project future risk of mudflows in Uzbekistan.

Table 6.2. Rainfall threshold probability equations of mudflow occurrences in the Gallyaaral station established using GCM corrected precipitation data (P – probability, r – daily rainfall, r_a- antecedent rainfall, Pr(>chi) - chi-squared results).

Time period		CMIP5 GCM	Probability equation	Pr(>chi)
Control	1979-2005	CMCC-CM	$\log\left(\frac{\mathrm{P}}{1-\mathrm{P}}\right) = -5.62 + 0.19\mathrm{r} + 0.10 * \mathrm{r_a}$	3.12e-13
		MPI-ESM-LR	$\log\left(\frac{P}{1-P}\right) = -4.43 + 0.17 * r + 0.07 * r_a$	5.25e-10
Scenario	2071-2100	CMCC-CM	$\log\left(\frac{P}{1-P}\right) = -4.61 + 0.15 * r + 0.06 * r_a$	7.99e-09
		MPI-ESM-LR	$\log\left(\frac{P}{1-P}\right) = -3.86 + 0.13 * r + 0.03 * r_a$	0.00082

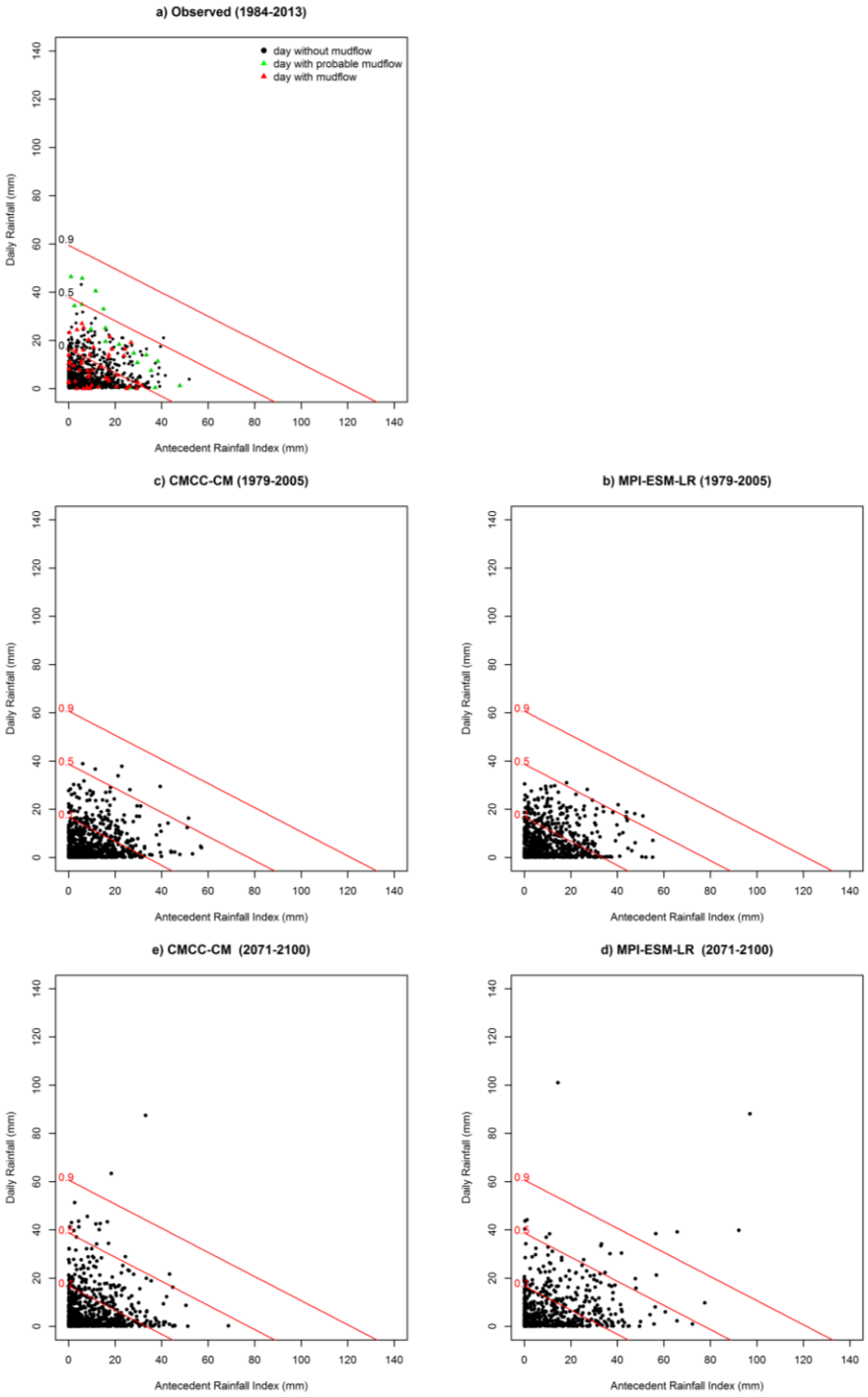

Figure 6.7. An antecedent daily rainfall model applied to the observed and representative CMIP5 GCMs outputs for the Gallyaaral station for the March-August covering three time period: station data 1984-2013 (a), 1979-2005 for the control run (b, c) and 2071-2100 for future scenario (d, e). Red lines indicate the 0.1, 0.5 and 0.9 probability threshold triggering mudflow occurrences. Equation (6.1) from Table 4.2 was used for calculation of the probability lines at the selected station.

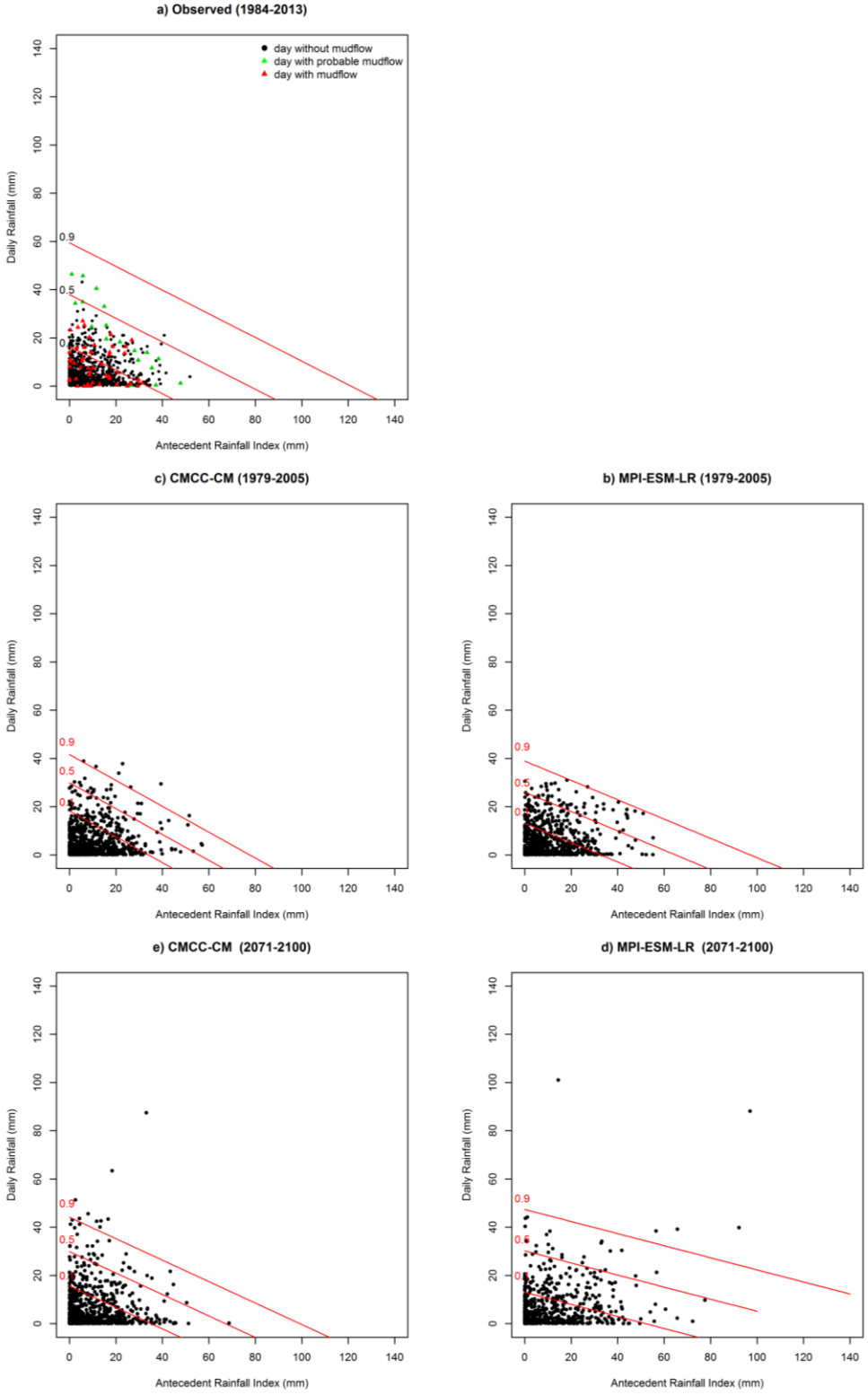

Figure 6.8. Same as Figure 6.7 but calculation of threshold probability lines for control and future scenarios are based on equations given in the Table 6.2.

6.5. Discussion

The research presented in this chapter compared the abilities of 10 selected GCMs from CMIP5 multi-model projections with the aim to investigate precipitation climatology as the main triggering factor of mudflow occurrences in Uzbekistan for the historical period of 1979-2005 and future scenarios under the RCP8.5 for the 2071-2100 period. Simulated precipitation was analysed by applying three bias correction algorithms (LS, LOCI, PT) to select suitable model outputs to run the ADRM model. Precipitation threshold triggering mudflow occurrences for the control period (1979-2005) and future scenario (2071-2100) obtained for the Gallyaaral station were evaluated using logistic approach equation (please see Chapter 4 for details). At the same time threshold probability was identified taking into account mudflow generating weather patterns namely CWT C, SW and W associated with daily rainfall (≤20mm) and antecedent conditions (≤40mm) as central proxies to simulate synthetic mudflow occurrences under the recent and future climate scenarios. Several conclusions can be made from the analysis done in this chapter:

1. Based on the outputs of LS, LOCI and PT bias correction techniques, PT approach has a higher ability to capture the observed precipitation and reproduce more realistic precipitation values from the model raw data for the historical experiments.

2. CMCC-CM and MPI-ESM-LR models, of the 10 selected GCMs of CMIP5 models, show realistic results for the historical experiments of precipitation data. Whereas, CNRM-CM5, GFDL-CM3, IPS-C5M-LR and MIROC5 represent remarkable outputs for future scenarios. The remaining four models overestimate precipitation values over Uzbekistan. This is corroborated with the results presented in Zhao et al. (2018).
3. CMCC-CM and MPI-ESM-LR model outputs corrected by PT bias technique are suitable to investigate changes in precipitation timeseries and its link to mudflow occurrences under recent and future climate conditions for the study area.
4. Threshold probability equation based on observed data works satisfactorily, however equation coefficients which are not derived from the observed data give slightly underestimated threshold lines in both GCMs (CMCC-CM and MPI-ESM-LR).
5. CWT C, SW and W directions can work satisfactorily as proxies to identify precipitation threshold triggering mudflows in the study area.
6. The model outputs show that mudflow occurrences will increase by the end of the century, as the model scenarios show increasing precipitation amount at the selected station.

However, several limitations still exist in this study. First, amongst the ten models used only outputs from two models were applied to establish the precipitation threshold probabilities using ADRM and statistical transfer function by means of logistic regression. It would be desirable to run different GCMs with rainfall data and compare the achieved results in order to better understand future risk of extreme mudflow events and the triggering factors. Second, the synthetic or probable mudflow derived from the rainfall data on relevant day with CWT C, SW and W circulations, which are used as a proxy in this case, cannot be dated exactly for the same day of observational data. Schmidt and Glade (2003) have shared this limitation in their study. Nevertheless, the results from the use of two GCMs demonstrate reasonable outputs when compared with the thresholds obtained from observational data.

Despite all weaknesses, it can be concluded that CMIP5 GCMs precipitation timeseries with efficient downscaling and bias correction techniques can link precipitation extremes and rainfall induced landslide types using antecedent rainfall model together with logistic regression function for any region with available rainfall and landslides data.

7 Conclusions and Outlook

7.1. Research findings and conclusion

Extreme mudflow occurrences during the warm phase of the year (mainly March to August), especially in the piedmont areas of Uzbekistan, are a major threat to human life and property, infrastructure, land use and natural resource base. In the last decades, research rooted in engineering and environmental sciences as well as the advances in computing resources have greatly increased the ability to understand the main causes, triggers and the driving mechanisms of different types of landslides in worldwide (Clague and Roberts, 2012). Most of the research activities conducted mudflows and other landslide types occurring in Central Asia and Uzbekistan deal with geological and topographical factors (Havenith et al., 2006, Juliev et al., 2017 and 2019) affecting slope stability, however, high impact of weather and climate variables on landslide types including mudflows have been not yet fully understood or explored. To the best of knowledge, no study attempted to analyse the impact of large scale atmospheric circulation patterns in generating mudflows in springs-summer transition seasons in Uzbekistan using weather

typing algorithm by applying data analysis based on in situ or archive records on mudflow and daily climate variables (precipitation and temperature) combining with state-of-the-art in the field, such as the ECMWF reanalysis dataset and AOGCMs from CMIP5 multi-model projection.

The main purpose of this thesis is to understand the atmospheric drivers of mudflow variability on local and synoptic to hemispheric scales and how these factors will change periodically considering global warming conditions on longer time scales. To fulfil this purpose, as a first step **historical data of mudflow occurrences** in Uzbekistan provided by the Centre of Hydrometeorological Service of the Republic of Uzbekistan (Uzhydromet) for more than 140 years are statistically analysed **in Chapter 2**. During the investigation period a total of around 3000 mudflow events were observed with about 21 events per year on average and a maximum of 168 mudflows in 1930. The most frequent mudflow occurrences was assigned to Fergana Valley in the eastern part of Uzbekistan due to its geomorphological settings, while central (Zerafshan basin), north-eastern (Chirchik-Akhangaran basin) and southern (Kashkadarya and Surkhandarya basins) regions show lower values of annual mudflow distribution.

In **Chapter 3 synoptic and large scale circulation systems and its link to the mudflow occurrences in Uzbekistan** for a period of 30 year (1984-2013) have been

analysed by using subjective weather classification (SWT, synoptic weather type) and objective (CWT, circulation weather type) approaches.

SWT 10 or westerly advection from the seventeen weather patterns from Bugayev et al. (1957) synoptic scheme is classified as a dominant synoptic circulation generating mudflow occurrences in the study area for the years 1984-2013. This agrees with the findings of Salikhova (1975) and Lyakhovskaya (1989) that heavily precipitating synoptic circulation especially when it is hybrid or accompanied with cyclones from south-western (SWT 1, 2, 3) can potentially increase mudflows occurrences and heavy floods in rivers. Similarly, Aizen et al. (2004) found that westerly weather system (SWT 10) out of the 17 synoptic circulation types was strongly associated with precipitation climatology observed in Tian Shan Mountains of Central Asia.

Objective weather type classification approach showed a significant relationship between CWT cyclonic (C), westerly (W), south-westerly (SW) airflow directions and mudflow events comparable with the other CWT classes for the warm phase (March-August) of 1984-2013 in the study area. Additionally, these weather classes together contributed to more than two thirds of the recorded precipitation in Uzbekistan. Interestingly, the structure of results of individual weather classes, for instance, CWT north-westerly (NW) airflow suggested that the advection of moist air is also connected to precipitation events and resulting in mudflows in the two

river basins (Chirchik-Akhangaran and Surkhandarya) in the study area. Additionally, due to the orographic effect, the CWT north-easterly (NE) days could trigger more mudflows in Fergana Valley. It is worth mentioning that main results of objective circulation patterns characterising precipitation climatology are similar to comparable investigation that have been carried out previously by Reyers et al. (2013) and Gerlitz et al. (2018).

Hence, the notable performances of CWT approach to detect the climatic drivers of mudflow occurrences recorded in Uzbekistan has robust results and has major implications for analyses of mudflows under the climate change conditions in **Chapters 5 and 6.**

Rainfall thresholds for the initiation of mudflow occurrences in Uzbekistan are investigated in Chapter 4. Empirically based antecedent daily rainfall model (ADRM, Glade et al., 2000) and statistical logistic regression (LRM) analysis have been applied in order to define the rainfall thresholds as the best separators of precipitation conditions (Guzzetti et al., 2007) that induced mudflow events over the study area. Calculations were performed for daily precipitation records from five selected meteorological stations (Gallyaaral, Chimgan, Sokh, Mingchukur and Baysun) for the period of March-August, 1984-2013. Considering 10 days period of cumulative rainfall together with daily precipitation values and mudflow records, the probability thresholds for the initiation of mudflows have been derived within

the study area. The established thresholds and probabilities are regionally based (Glade et al., 2000) which is explained by the lithological and geomorphological as well as the climatic conditions of each basin. The uncertainty in model construction is due to the quality of mudflow data and mudflow's timing as well as rainfall values stored in the database. Nevertheless, an obtained threshold could be used as a benchmark for the relevant studies at a regional scale as well as an early warning signal in the mudflow susceptible areas in Uzbekistan.

One of the objectives was to combine different strands (CWT, ADRM and LRM) to identify a proxy based on selection of mudflow inducing weather class by clustering antecedent index, precipitation values and mudflows and these were assigned to a CWT class. Results obtained from this attempt confirmed that significant rainfall values and antecedent conditions on CWT C, SW and W days could initiate mudflows frequencies and magnitudes compared to other circulation patterns in the study area.

Coupled Model Inter-Comparison Project Phase 5 (CMIP5) multi model ensemble climate change projections for large scale atmospheric conditions are analysed in **Chapter 5: by statistical downscaling of present and future atmospheric circulation over Uzbekistan**. In order to better understand the driving mechanisms of mudflow induced precipitation, well-established Circulation Weather Types (CWT) classification is applied for the recent (1979-2005) and future (2071-2100)

climate considering RCP8.5 emission scenario of 10 GCM ensemble. Ten circulation types (C, AC, NE, E, SE, S, SW, W, NW and N) with conspicuous distribution and seasonality are identified in the selected geographical sector covering Uzbekistan and Central Asia with grid point located at 40.0N-67.5E. Historical simulation of an ensemble of 10 GCMs from the CMIP5 with respect to changes in the atmospheric circulation shows realistic outputs with some minor discrepancies of individual models against observation based ERA-Interim reanalyses dataset. However, the pertinent results of the effects of important large-scale circulations modulating precipitation, such as CWT C, SW and W, identified to trigger mudflow occurrences over the study area have been described in previous chapters 3 and 4. CMIP5 outcomes suggest that changed frequencies of cyclonic C and westerly W airflow directions will potentially contribute to more extreme mudflow occurrences during the warm season (March-August) by up to 5% near the end of the century. However, the ensemble results show uncertainties regarding the CWT SW airflow associated with the most devastating mudflow events in Uzbekistan for the projected period of March-August in 2071-2100. The clear advantage of the CWT approach applied in this study is that the climate change signals for precipitation generating mechanism impact on mudflow occurrences are significantly coherent and it is consistent with the results in previous studies (Reyers et al., 2013).

The assessment of effects of global warming on mudflow occurrences using statistically downscaled precipitation series from 10 GCM of CMIP5 as an input of the triggering factor for **future mudflow risk in Uzbekistan** has been elaborated in **Chapter 6**. Considering the historical simulations over 1979-2005 and following the projections of RCP8.5 emission scenario for the target period of 2071-2100, precipitation climatology have been evaluated using bias correction techniques. The results of the selected two models (CMCC-CM and MPI-ESM-LR) on precipitation for the period March-August have been assigned per CWT class in order to run control and future scenarios. By this way, the synthetic rainfall series were linked to a central proxy – a mudflow generating weather types (CWT C, SW and W) in order to diagnose potential changes in mudflow occurrences given the changed CWT characteristics by running the statistical-empirical algorithm of ADRM. Results for the important weather types (C, W and SW) confirm that mudflow activity will increase in the selected region as precipitation values associated with the CWT C, W and SW flows in CMIP5 projections are expected to increase in the warm season for the target period of 2071-2100.

The ultimate goal of this chapter was to use simulated future frequencies of precipitation known to trigger potential mudflow occurrences in Uzbekistan especially in the Zerafshan basin. However, the significance of rainfall threshold values vary geographically which gives uncertainty associated with rainfall

projections for the remaining basins which are needed to produce projected threshold within the framework of mudflow-climate chain for further studies. Nevertheless, this methodology can be considered to be a first attempt to identify the relationship between GCM and extreme mudflow hazards for the future in Uzbekistan in regional scale. Additionally, the outputs could be linked to economic models (Schmidt and Glade, 2003) for more detailed investigations in order to diagnose probable damages and evaluate direct and indirect impacts and implications for designing preventive interventions over the study area.

7.2. Limitations and reservations

The major limitations of the approaches used in this thesis lie in the well-known inherent incompleteness of the following procedures. These limitations are listed below:

- **First** of all, data issues regarding mudflow timing impeded derivation of useful information and restricted understanding the essential influences of diurnal and nocturnal rainfall variations to mudflow occurrences.
- **Second**, station based observation data does not include hourly rainfall intensity and duration information. These are essential for the selection and application of the statistic based rainfall threshold models used to identify the triggers for initiating mudflow in regional scale; for example, most of the existing models use the rainfall intensity as an input data to establish the regional threshold (Caine, 1980). These two major drawbacks in the empirical data prompted the use of the ADRM model with combination of logistic regression algorithm to obtain the rainfall threshold inducing mudflows to fulfil the objectives of the research.
- The **third** limitation is that the local synoptic classification SWT is subjective although it allows mudflow occurrences to be linked to synoptic scale atmospheric circulation over the study period.

- The **fourth** limitation is related to the effect of the topographic heterogeneity of the area, orographic lifting and frontal system which raised the issues regarding high frequencies of undefined weather class while determining the large scale circulation by CWT approach in lower troposphere over the study area.
- **Fifth,** some significant climate model biases have been identified due to overestimation or underestimation of CWT frequencies and precipitation climatology suggesting the low skills and model limitations in simulating mudflow risk under the climate change conditions.

However, despite the above mentioned limitations, this thesis work successfully demonstrates that objective circulation weather patterns is useful to predict future mudflows. The combination of methodological approaches adopted to circumvent the problems regarding empirical data for study area is a novel contribution to the field of atmosphere sciences and climatology over Uzbekistan and Central Asia. There is a lack of peer-reviewed literature for the study area, a limitation that this thesis attempts to overcome.

7.3. Forward outlook

Each of the chapters of this thesis make a significant contributions towards the assessment of atmospheric circulation weather patterns generating mudflow

occurrences for the observed and simulated future climate conditions for Uzbekistan. However, to comprehensively understand the mudflow-climate processes and related dynamics, the following add on research topics would be interesting future work to study the potential impact of mudflow hazards in Uzbekistan.

- The insufficient representation of elevation dependencies of precipitation necessitates further studies which focus on exploring the effect of topography and heterogeneous surface on precipitation process in combination with relevant atmospheric circulation, such an analysis will provide further insight into the causes of extreme mudflow occurrences over the study area. Thus, the use of regional climate models and dynamical downscaling techniques to elaborate future risk of mudflow from climate change in regional scale could be interesting future research area. As the traditional coarse–resolution climate models do not have the ability to project reliable future changes in rainfall intense, the experiments at very high (<5-km grid spacing) resolution (Kendon et al., 2014, Kendon et al., 2017) or convection permitting climate model simulations (e.g. COSMO-model) would be beneficial to examine orographically induced convective precipitation (Fosser et al., 2015) causing flash-floods and mudflows over the study area.

- Since the influence of large-scale teleconnection modes (Hurrell and Van Loon, 1997, Polonsky et al., 2004, Bueh and Nakamura, 2007) on the frequency of precipitation resulting in mudflows have not been investigated yet, this could be another interesting area of research as a next step.
- Furthermore, the assessment of atmospheric rivers (Ralph et al., 2006, Hughes et al., 2014, Eiras-Barca et al., 2018, Ramos et al., 2018), which is relevantly new subject area, needs to be studied for the investigation area, in order to understand the significant impact of atmospheric rivers on precipitation generating mudflow hazards and its geospatial distribution.
- Moreover, taking account of geological factors in the input data would likely provide more advanced and robust results regarding threshold probabilities for the initiation mudflows.
- Finally, the methodology applied in this thesis proves that CWT is an advanced tool which could be used to define and better understand the significant relationship between the large scale circulation patterns and extreme hydrometeorological hazards, such as droughts, floods, glacial conditions as well as, agriculture and other climate dependent livelihoods and infrastructure losses, in addition to, risks to human life.

Appendix A

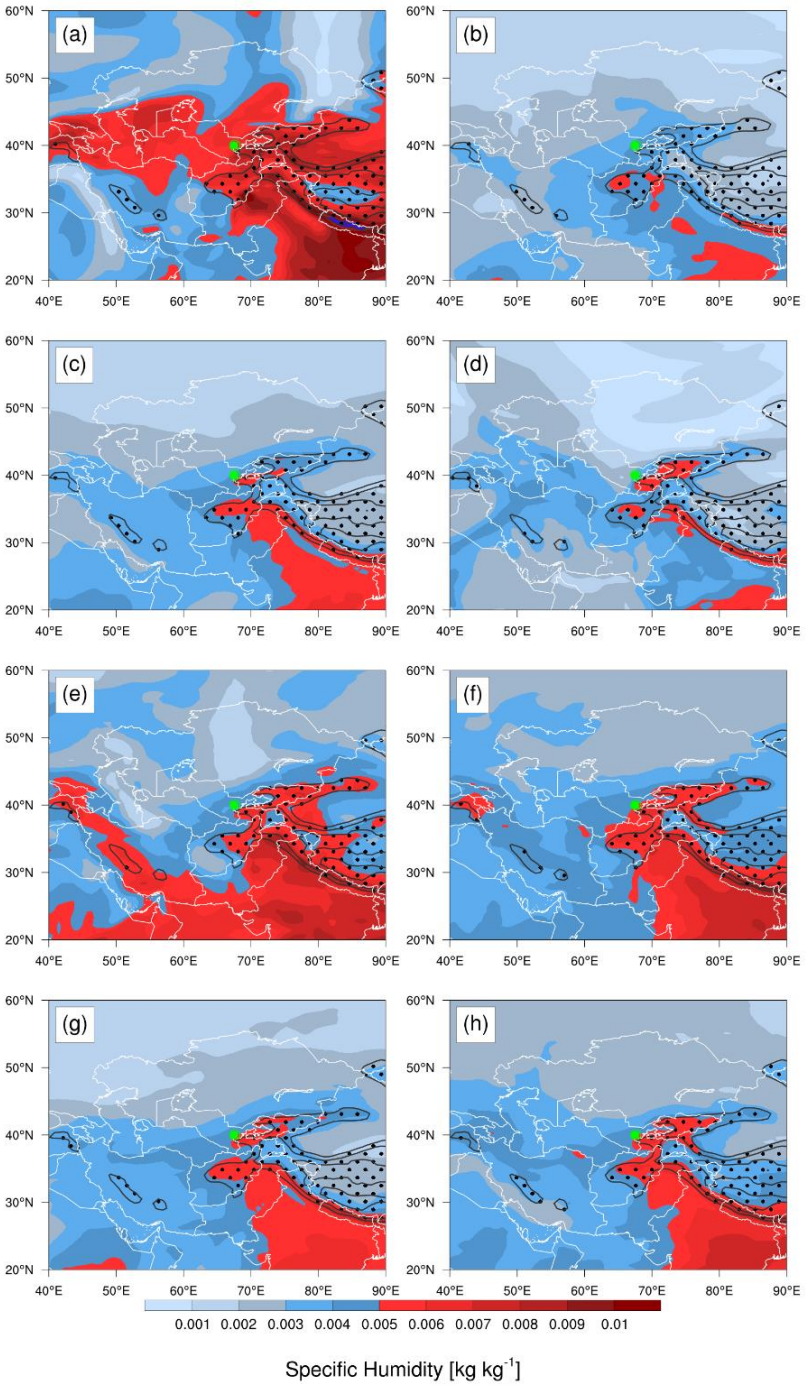

Figure A 1. ERA-Interim average specific humidity at 700 hPa GPH on mudflow days occurred in the Zerafshan basin for the period of 1984–2013: CWT north-east (a), south-west (b), west (c), north-west (d), north (e), cyclonic (f), anticyclonic (g) and undefined (h) weather days. Black contour lines together with black dots show the area where the topography is above 2000m further corresponding 3000 m and 4000m.

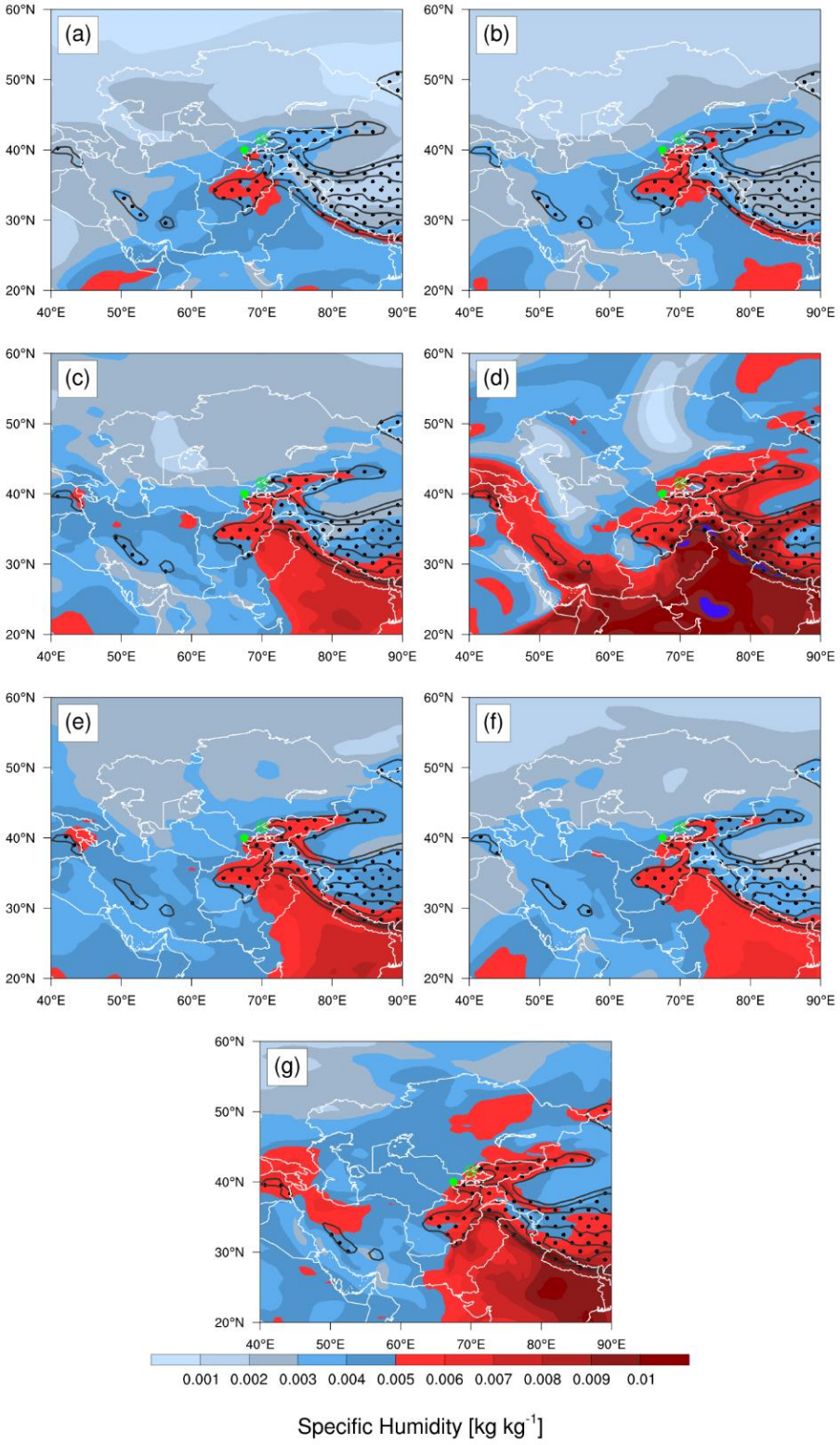

Figure A 2. Same as Figure A1 but for Chirchik-Akhangaran basin: CWT south-west (a), west (b), north-west (c), north (d), cyclonic (e), anticyclonic (f) and undefined (g) weather type.

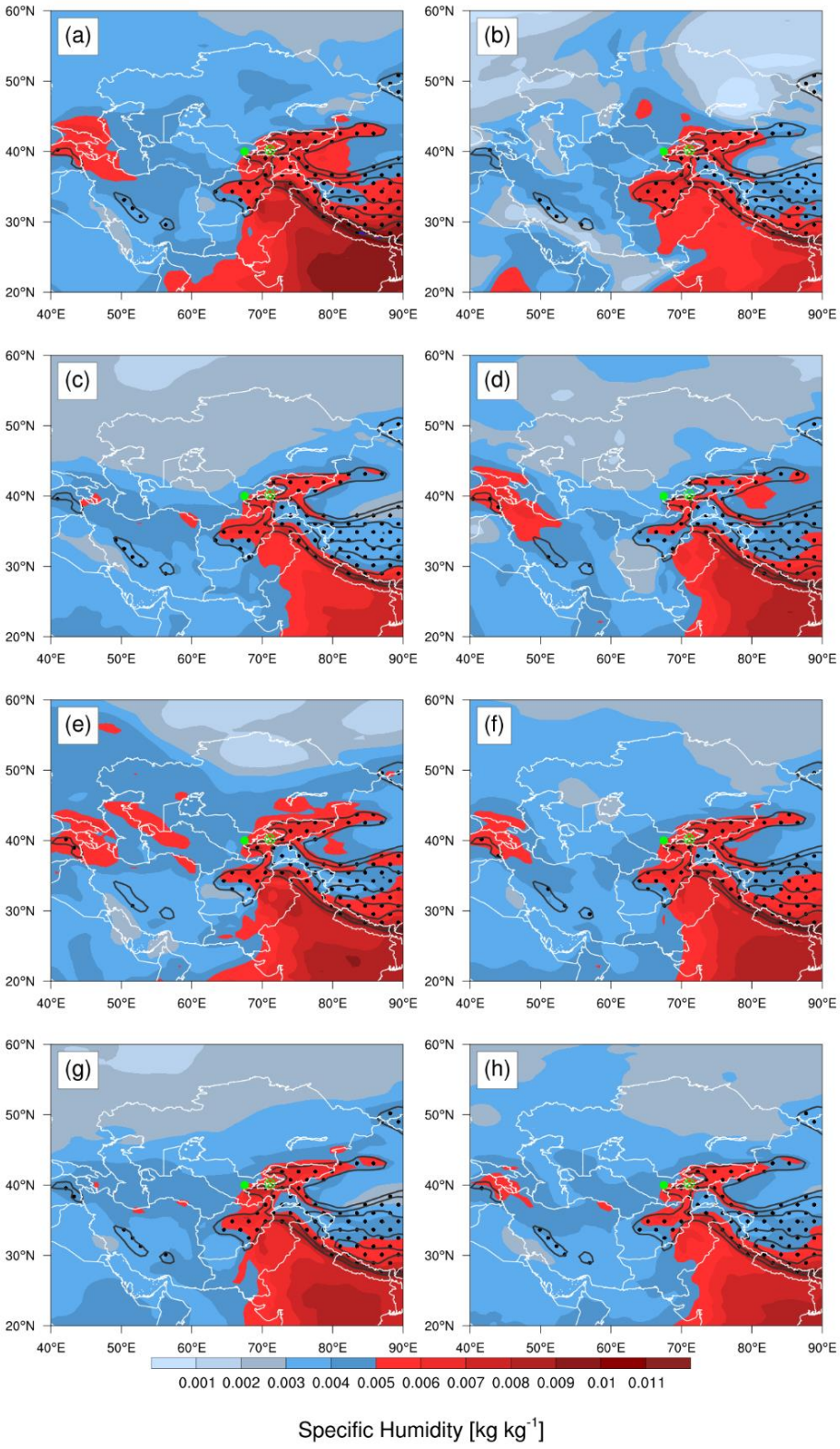

Figure A 3. Same as Figure A1 but for Fergana Valley: CWT north-east (a), south-west (b), west (c), north-west (d), north (e), cyclonic (f), anticyclonic (g) and undefined (h) weather type.

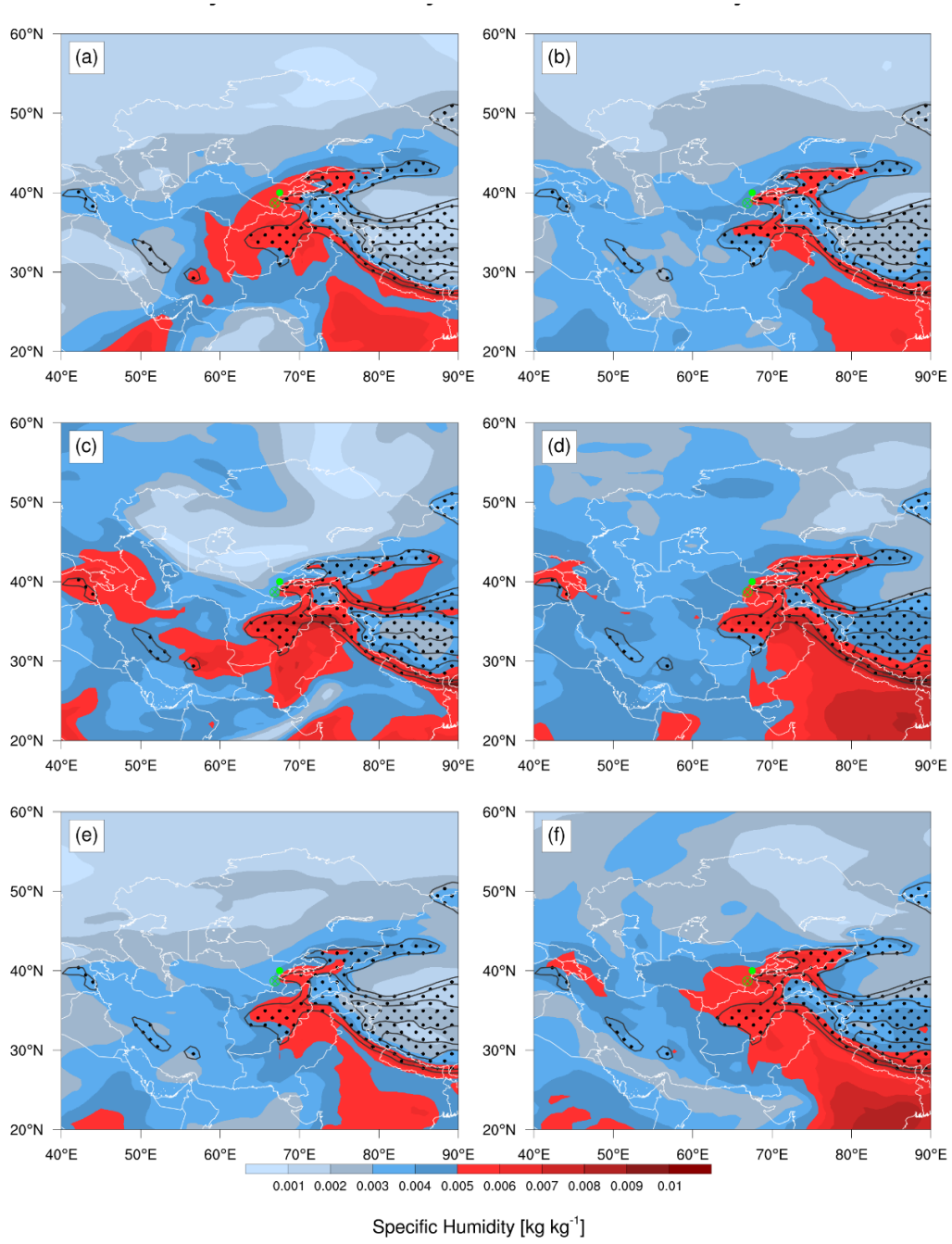

Figure A 4. Same as Figure A1 but for Kashkadarya basin: CWT south-west (a), west (b), north-west (c), cyclonic (d), anticyclonic (e) and undefined (f) weather type.

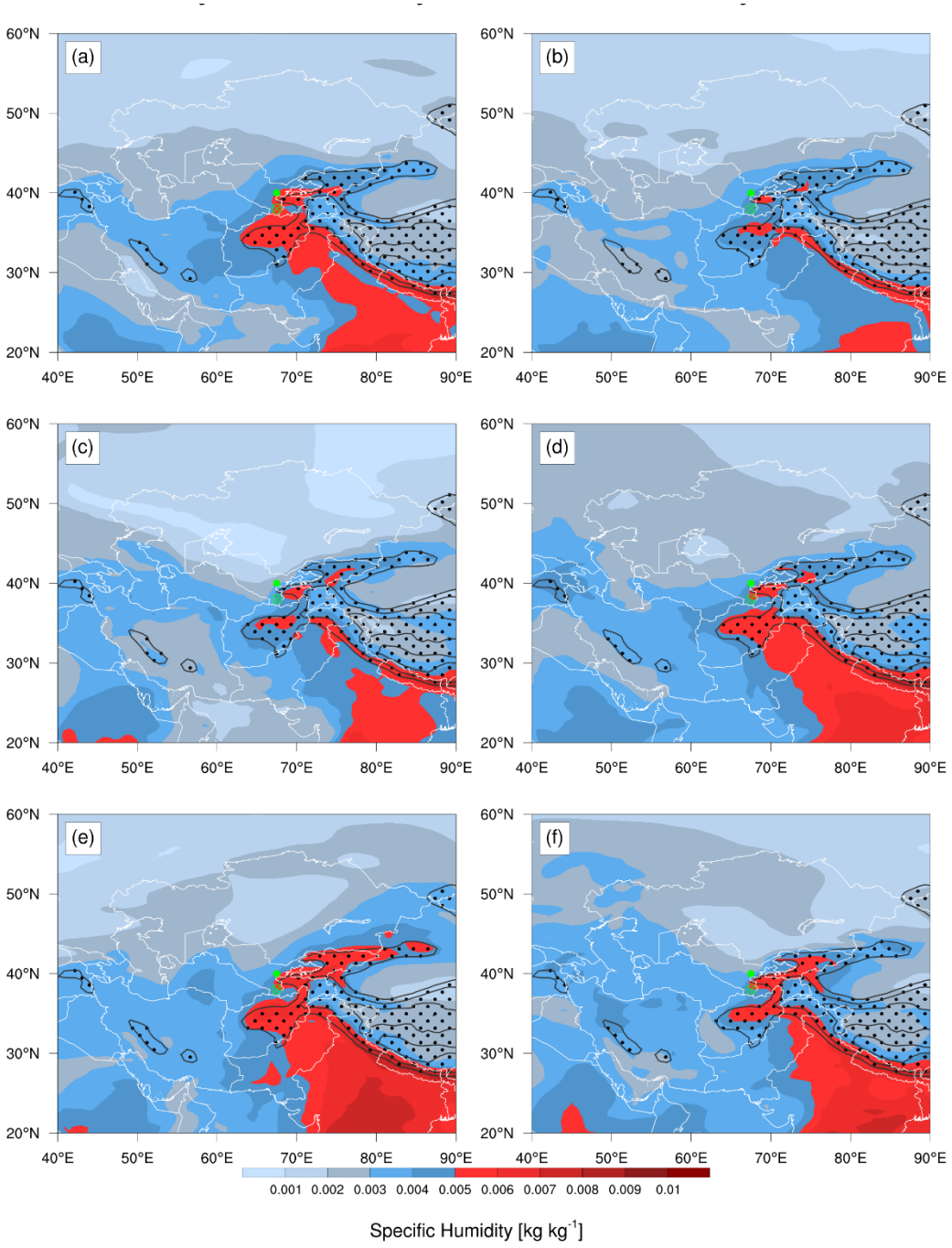

Figure A 5. Same as Figure A1 but for Surkhandarya basin: CWT south-west (a), west (b), north-west (c), cyclonic (d), anticyclonic (e) and undefined (f) weather type.

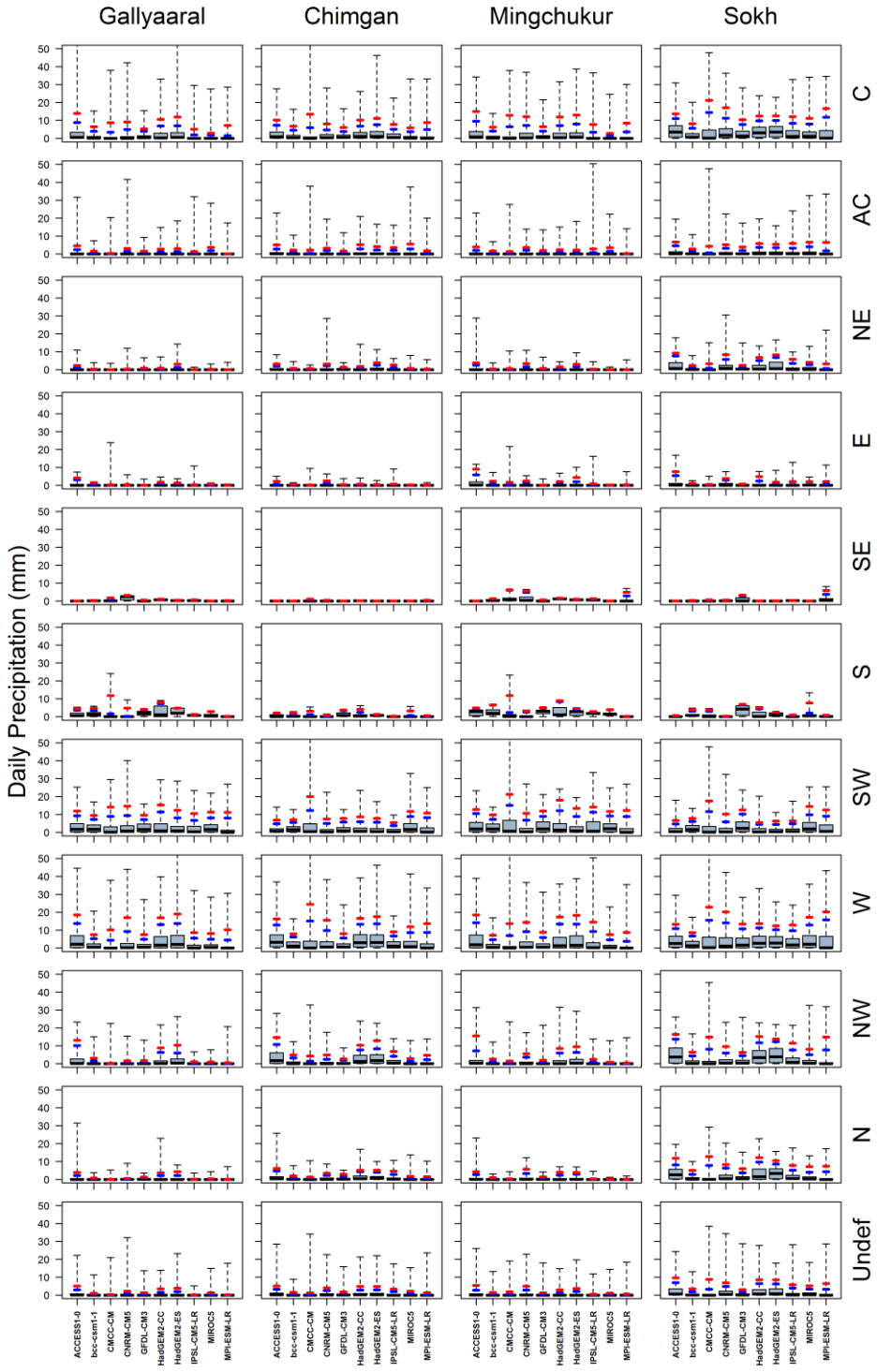

Figure A 6. Box plots show daily precipitation for the warm phase (March-August) of control period 1979–2005 for each CWT class at four representative stations, namely Gallyaaral (Zerafshan, basin), Chimgan (Chirchik–Akhangaran basin), Mingchukur (Kashkadarya and Surkhandarya basins) and Sokh (Fergana Valley) simulated by the 10 GCM from CMIP5 multi-model without bias correction. The blue and red lines represent percentiles 0.90 and 0.95 of the precipitation for each class.

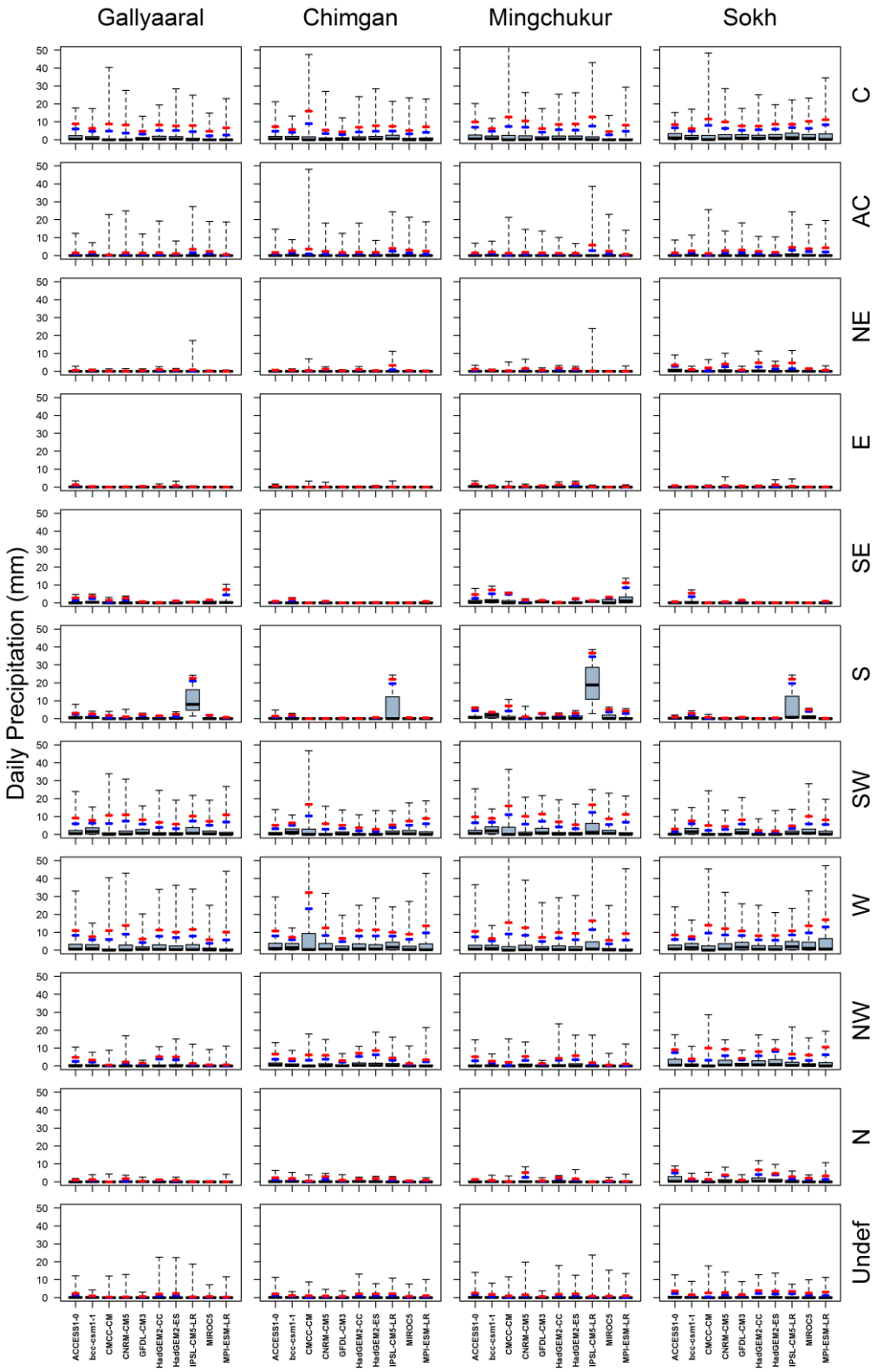

Figure A 7. Same as Figure A6 but for the period of September-February, 1979-2005.

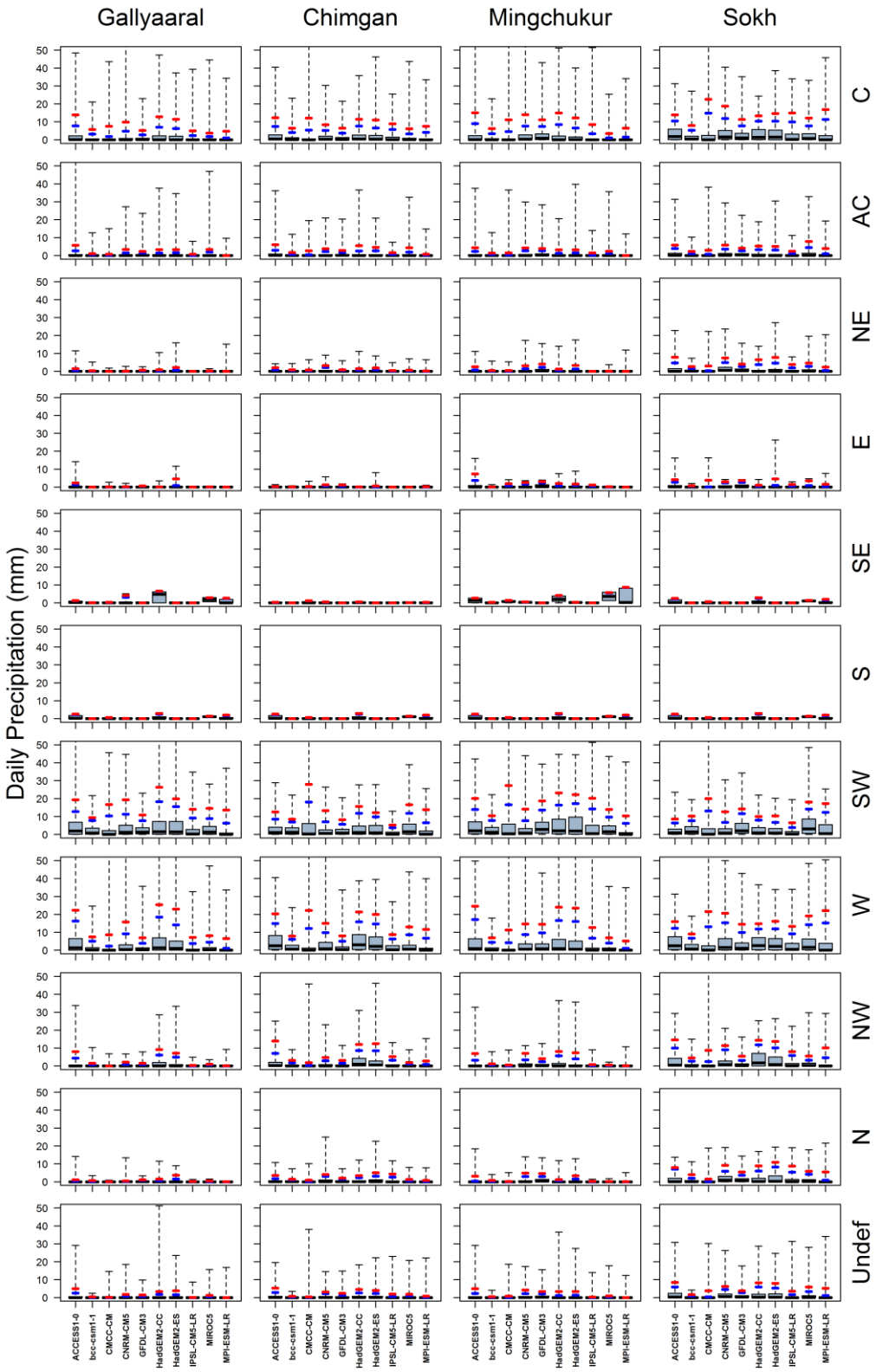

Figure A 8. Same as Figure A6 but for future scenario of March-August, 2071-2100.

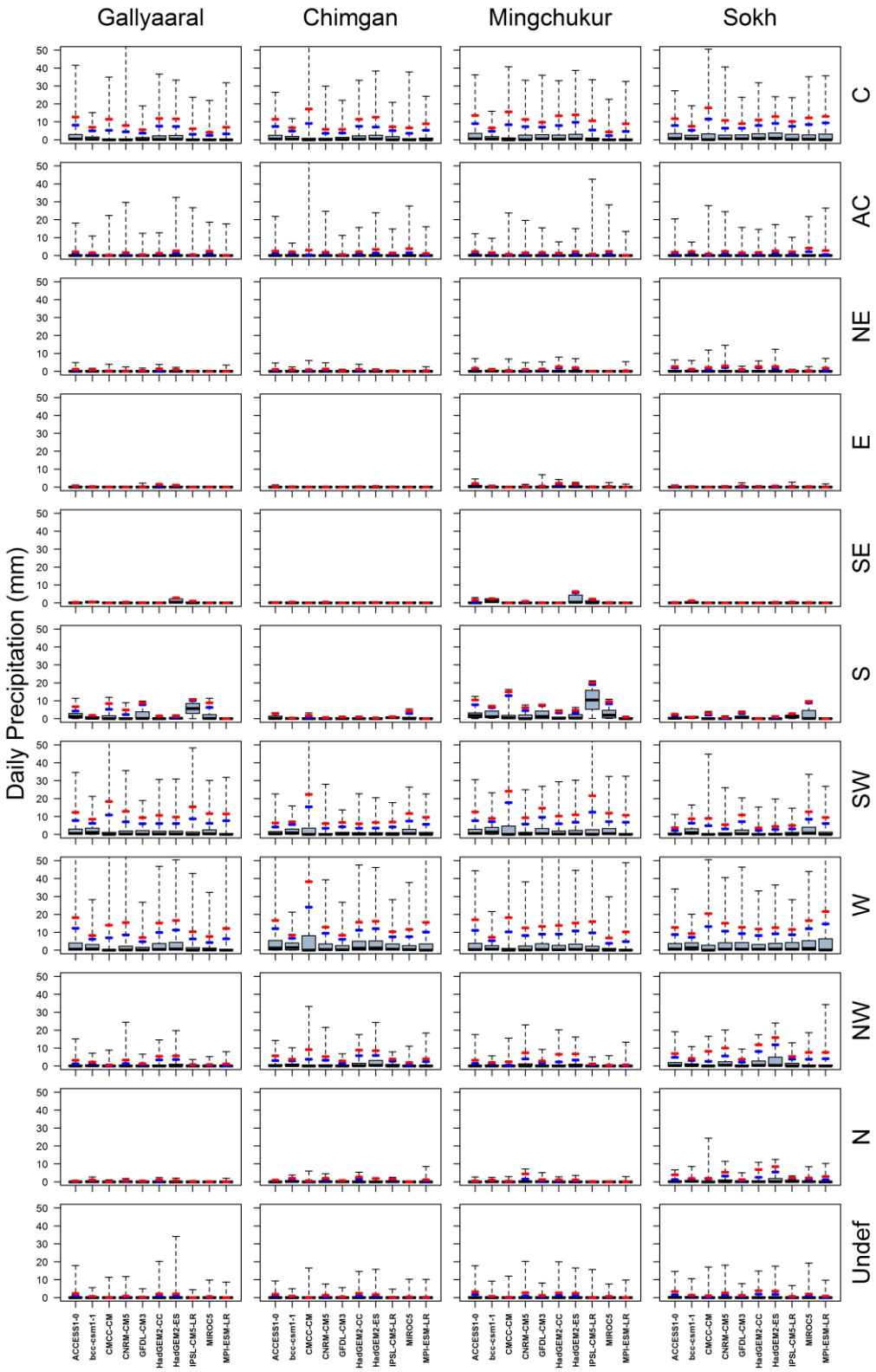

Figure A 9. Same as Figure A6 but for future scenario of September-February, 2071-2100

References

Ahmad, R. 2003. Developing early warning systems in Jamaica: rainfall thresholds for hydrological hazards. *National Disaster Management Conference.* Ocho Rios, St Ann, Jamaica, 9-10 September 2003.

Aizen, V. B., Aizen, E. M., Melack, J. M., Kreutz, K. J. & Cecil, L. D. 2004. Association between atmospheric circulation patterns and firn-ice core records from the Inilchek glacierized area, central Tien Shan, Asia. *Journal of Geophysical Research: Atmospheres,* 109**,** n/a-n/a.

Aksarin, S. I. & Inagamova, S. I. 1993. *Sketches of Hydrometeorology in Central Asia (in Russian),* Saint-Petersburg, Gidrometeoizdat.

Altinsoy, H., Ozturk, T., Turkes, M. & Kurnaz, M. L. 2013. Simulating the Climatology of Extreme Events for the Central Asia Domain Using the RegCM 4.0 Regional Climate Model. *In:* HELMIS, C. G. & NASTOS, P. T. (eds.) *Advances in Meteorology, Climatology and Atmospheric Physics.* Berlin, Heidelberg: Springer Berlin Heidelberg.

Babko, V. L. 1978. Mudflow hazards in Uzbekistan. *Proceedings of XV scientific conference on debris flows.* Tashkent, 27-29 September.

Bacchini, M. & Zannoni, A. 2003. Relations between rainfall and triggering of debris-flow: case study of Cancia (Dolomites, Northeastern Italy). *Nat. Hazards Earth Syst. Sci.,* 3**,** 71-79.

Bai, S., Wang, J., Thiebes, B., Cheng, C. & Yang, Y. 2014. Analysis of the relationship of landslide occurrence with rainfall: a case study of Wudu County, China. *Arabian Journal of Geosciences,* 7**,** 1277-1285.

Barry, R. G. & Perry, A. H. 1973. *Synoptic Climatology. Methods and Applications.,* Methuen&Co Ltd. London. 555pp.

Baur, F. 1936. Wetter, Witterung, Groswetter und Weltwetter. *Z. angew. Met. 53, 377-81.*

Baur, F. 1951. Extended-Range Weather Forecasting. *In:* MALONE, T. F. (ed.) *Compendium of Meteorology: Prepared under the Direction of the Committee on the Compendium of Meteorology.* Boston, MA: American Meteorological Society.

Bell, F. G. & Maud, R. R. J. E. G. 2000. Landslides associated with the colluvial soils overlying the Natal Group in the greater Durban region of Natal, South Africa. 39**,** 1029-1038.

Bi, D., Dix, M., Marsland, S., O'Farrell, S., Rashid, H., Uotila, P., Hirst, Kowalczyk, E., Golebiewski, Sullivan, A., Yan, Hannah, Franklin, C., Sun, Vohralik, Watterson, Zhou, K., Fiedler, R., Collier, M. & Puri, K. 2012. *The ACCESS coupled model: Description, control climate and evaluation*.

Blackwelder, E. 1928. Mudflow as a Geologic Agent in Semiarid Mountains. *GSA Bulletin,* 39**,** 465-484.

Bobojonov, I. & Aw-Hassan, A. 2014. Impacts of climate change on farm income security in Central Asia: An integrated modeling approach. *Agriculture, Ecosystems & Environment,* 188**,** 245-255.

Brigode, P., Gérardin, M., Bernardara, P., Gailhard, J. & Ribstein, P. 2017. Changes in French weather pattern seasonal frequencies projected by a CMIP5 ensemble. *International Journal of Climatology,* 10.1002/joc.5549.

Bruce, J. P. & Clark, R. H. 1966. *Introduction to Hydrometeorology*, Pergamon Press, 319 pp.

Brunetti, M. T., Peruccacci, S., Rossi, M., Luciani, S., Valigi, D. & Guzzetti, F. 2010. Rainfall thresholds for the possible occurrence of landslides in Italy. *Nat. Hazards Earth Syst. Sci.,* 10**,** 447-458.

Bueh, C. & Nakamura, H. 2007. Scandinavian pattern and its climatic impact. *Quarterly Journal of the Royal Meteorological Society,* 133**,** 2117-2131.

Bugayev, V. A. 1946. *Climate in Central Asia and Kazakhstan (in Russian),* Tashkent, Academy of Sciense of the Uzbek SSR.

Bugayev, V. A., Giorgio, V. A., Kozik, E. M., Petrosyants, M. A., Pshenichniy, A. Y., Romanov, N. N. & Chernisheva, O. N. 1957. *Synoptic processes of Central Asia (in Russian),* Tashkent, Academy of Science of Uzbek SSR.

Bull, W. B. 1964. Alluvial fans and near-surface subsidence in western Fresno County, California. *Professional Paper.* - ed.: 10.3133/pp437A.

Bulmer, M. 2012. Landslides on other planets. *In:* STEAD, D. & CLAGUE, J. J. (eds.) *Landslides: types, mechanisms and modelling.*: Cambridge Univ. Press, Cambridge.

Buzzi, A., Tartaglione, N. & Malguzzi, P. 1998. Numerical Simulations of the 1994 Piedmont Flood: Role of Orography and Moist Processes. *Monthly Weather Review,* 126**,** 2369-2383.

Bykov, V. D. & Vasil'yev, A. V. 1977. *Hydrometry (in Russian),* Leningrad, Gidrometeoizdat.

Caine, N. 1980. The Rainfall Intensity: Duration Control of Shallow Landslides and Debris Flows. *Geografiska Annaler. Series A, Physical Geography,* 62**,** 23-27.

Cannon, S. H. & Gartner, J. E. 2005. Wildfire-related debris flow from a hazards perspective. *Debris-flow hazards and related phenomena.* Springer.

Cannon, S. H., Gartner, J. E., Wilson, R. C., Bowers, J. C. & Laber, J. L. J. G. 2008. Storm rainfall conditions for floods and debris flows from recently burned areas in southwestern Colorado and southern California. 96**,** 250-269.

Chiang, S.-H. & Chang, K.-T. 2011. The potential impact of climate change on typhoon-triggered landslides in Taiwan, 2010–2099. *Geomorphology,* 133**,** 143-151.

Chub, V. Y. 2007. *Climate change impacts on hydrometeorological processes, agro climatic and water resources of the Republic of Uzbekistan (in Russian),* Tashkent, Voris Nashriyot.

Chub, V. Y., Trofimov, G. N. & Merkushkin, A. S. 2007. *Mudflows in Uzbekistan (in Russian),* Tashkent, Uzhydromet.

Clague, J. J. & Roberts, N. J. 2012. Landslide hazard and risk. *In:* STEAD, D. & CLAGUE, J. J. (eds.) *Landslides: Types, Mechanisms and Modeling.* Cambridge: Cambridge University Press.

Clarizia, M., Gullà, G. & Sorbino, G. Sui meccanismi di innesco dei soil slip. International conference Prevention of hydrogeological hazards: the role of scientific research, 1996. 585-597 (in Italian).

Coussot, P. 1997. *Mudflow Rheology and Dynamics,* A.A.Balkema/Rotterdam/Brookfield. 272 pages.

Crosta, G. B. & Frattini, P. Rainfall thresholds for triggering soil slips and debris flow. Proceedings of the 2nd EGS Plinius Conference on Mediterranean Storms, edited by: Mugnai, A., Guzzetti, F., and Roth, G., Siena, Italy, 2001. 463-487.

Crozier, M. J. 1986. *Landslides: Causes, Consequences and Environment,* London, CROOM HELM.

Crozier, M. J. & Eyles, R. J. 1980. Assessing the probability of rapid mass movement. *Third Australia - New Zealand Conference on Geomechanics.* Wellington: New Zealand Institution of Engineers, 2.47-2.51.

Davydov, L. K., Dmitriyeva, A. A. & Konkina, N. G. 1973. *General Hydrology,* Leningrad, Gidrometeoizdat.

Dee, D. P., Uppala, S. M., Simmons, A. J., Berrisford, P., Poli, P., Kobayashi, S., Andrae, U., Balmaseda, M. A., Balsamo, G., Bauer, P., Bechtold, P., Beljaars, A. C. M., van de Berg, L., Bidlot, J., Bormann, N., Delsol, C., Dragani, R., Fuentes, M., Geer, A. J., Haimberger, L., Healy, S. B., Hersbach, H., Hólm, E. V., Isaksen, L., Kållberg, P., Köhler, M., Matricardi, M., McNally, A. P., Monge-Sanz, B. M., Morcrette, J.-J., Park, B.-K., Peubey, C., de Rosnay, P., Tavolato, C., Thépaut, J.-N. & Vitart, F. 2011. The ERA-Interim reanalysis: configuration and performance of the data assimilation system. *Quarterly Journal of the Royal Meteorological Society,* 137**,** 553-597.

Deser, C., Knutti, R., Solomon, S. & Phillips, A. S. 2012. Communication of the role of natural variability in future North American climate. *Nature Climate Change,* 2**,** 775.

Donat, M. G., Leckebusch, G. C., Pinto, J. G. & Ulbrich, U. 2010. Examination of wind storms over Central Europe with respect to circulation weather types and NAO phases. *International Journal of Climatology,* 30**,** 1289-1300.

Donner, L. J., Wyman, B. L., Hemler, R. S., Horowitz, L. W., Ming, Y., Zhao, M., Golaz, J.-C., Ginoux, P., Lin, S.-J., Schwarzkopf, M. D., Austin, J., Alaka, G.,

Cooke, W. F., Delworth, T. L., Freidenreich, S. M., Gordon, C. T., Griffies, S. M., Held, I. M., Hurlin, W. J., Klein, S. A., Knutson, T. R., Langenhorst, A. R., Lee, H.-C., Lin, Y., Magi, B. I., Malyshev, S. L., Milly, P. C. D., Naik, V., Nath, M. J., Pincus, R., Ploshay, J. J., Ramaswamy, V., Seman, C. J., Shevliakova, E., Sirutis, J. J., Stern, W. F., Stouffer, R. J., Wilson, R. J., Winton, M., Wittenberg, A. T. & Zeng, F. 2011. The Dynamical Core, Physical Parameterizations, and Basic Simulation Characteristics of the Atmospheric Component AM3 of the GFDL Global Coupled Model CM3. *Journal of Climate,* 24**,** 3484-3519.

Dufresne, J.-L., Foujols, M.-A., Denvil, S., Caubel, A., Marti, O., Aumont, O., Balkanski, Y., Bekki, S., Bellenger, H., Benshila, R., Bony, S., Bopp, L., Braconnot, P., Brockmann, P., Cadule, P., Cheruy, F., Codron, F., Cozic, A., Cugnet, D., de Noblet, N., Duvel, J.-P., Ethé, C., Fairhead, L., Fichefet, T., Flavoni, S., Friedlingstein, P., Grandpeix, J.-Y., Guez, L., Guilyardi, E., Hauglustaine, D., Hourdin, F., Idelkadi, A., Ghattas, J., Joussaume, S., Kageyama, M., Krinner, G., Labetoulle, S., Lahellec, A., Lefebvre, M.-P., Lefevre, F., Levy, C., Li, Z. X., Lloyd, J., Lott, F., Madec, G., Mancip, M., Marchand, M., Masson, S., Meurdesoif, Y., Mignot, J., Musat, I., Parouty, S., Polcher, J., Rio, C., Schulz, M., Swingedouw, D., Szopa, S., Talandier, C., Terray, P., Viovy, N. & Vuichard, N. 2013. Climate change projections using the IPSL-CM5 Earth System Model: from CMIP3 to CMIP5. *Climate Dynamics,* 40**,** 2123-2165.

Eiras-Barca, J., Lorenzo, N., Taboada, J., Robles, A. & Miguez-Macho, G. 2018. On the relationship between atmospheric rivers, weather types and floods in Galicia (NW Spain). *Nat. Hazards Earth Syst. Sci.,* 18**,** 1633-1645.

El Kenawy, A. M. & McCabe, M. F. 2016. Future projections of synoptic weather types over the Arabian Peninsula during the twenty-first century using an ensemble of CMIP5 models. *Theoretical and Applied Climatology,* https://doi.org/10.1007/s00704-016-1874-y**,** 1-17.

Elsner, J. B. & Jagger, T. H. 2013. *Hurricane Climatology. A Modern Statistical Guide Using R*, Oxford University Press.

Fang, G. H., Yang, J., Chen, Y. N. & Zammit, C. 2015. Comparing bias correction methods in downscaling meteorological variables for a hydrologic impact study in an arid area in China. *Hydrol. Earth Syst. Sci.,* 19**,** 2547-2559.

Fleig, A. K., Tallaksen, L. M., Hisdal, H., Stahl, K. & Hannah, D. M. 2010. Inter-comparison of weather and circulation type classifications for hydrological drought development. *Physics and Chemistry of the Earth, Parts A/B/C,* 35**,** 507-515.

Fleishman, S. M. 1978. *Debris flows,* Leningrad, Gidrometeoizdat. (In Russian).

Floris, M. & Bozzano, F. 2008. Evaluation of landslide reactivation: A modified rainfall threshold model based on historical records of rainfall and landslides. *Geomorphology,* 94**,** 40-57.

Fosser, G., Khodayar, S. & Berg, P. J. C. D. 2015. Benefit of convection permitting climate model simulations in the representation of convective precipitation. 44**,** 45-60.

Fowler, H. J., Blenkinsop, S. & Tebaldi, C. 2007. Linking climate change modelling to impacts studies: recent advances in downscaling techniques for hydrological modelling. *International Journal of Climatology,* 27**,** 1547-1578.

Gariano, S. L. & Guzzetti, F. 2016. Landslides in a changing climate. *Earth-Science Reviews,* 162**,** 227-252.

Gerlitz, L., Steirou, E., Schneider, C., Moron, V., Vorogushyn, S. & Merz, B. 2018. Variability of the Cold Season Climate in Central Asia. Part I: Weather Types and Their Tropical and Extratropical Drivers. *Journal of Climate,* 31**,** 7185-7207.

Gevorgyan, A. 2013. Main types of synoptic processes and circulation types generating heavy precipitation events in Armenia. *Meteorology and Atmospheric Physics,* 122**,** 91-102.

Gheusi, F. & Davies, H. C. 2004. Autumnal precipitation distribution on the southern flank of the Alps: A numerical-model study of the mechanisms. *Quarterly Journal of the Royal Meteorological Society,* 130**,** 2125-2152.

Gilabert, J. & Llasat, M. C. 2017. Circulation weather types associated with extreme flood events in Northwestern Mediterranean. *International Journal of Climatology,* 10.1002/joc.5301**,** n/a-n/a.

Giorgi, F., Coppola, E., Solmon, F., Mariotti, L., Sylla, M., Bi, X., Elguindi, N., Diro, G., Nair, V. & Giuliani, G. 2012. RegCM4: model description and preliminary tests over multiple CORDEX domains. *Climate Research,* 52**,** 7-29.

Giorgi, F., Jones, C. & Asrar, G. R. 2009. Addressing climate information needs at the regional level: the CORDEX framework. *World Meteorological Organization (WMO) Bulletin,* 58**,** 175.

Giorgio, V. A. & Bugayev, V. A. 1936. Classification of the atmospheric circulation in Central Asia (in Russian). *Meteorology and Hydrology* 6**,** 72-74.

Glade, T. 1998. Establishing the frequency and magnitude of landslide-triggering rainstorm events in New Zealand. *Environmental Geology,* 35**,** 160-174.

Glade, T., Crozier, M. & Smith, P. 2000. Applying Probability Determination to Refine Landslide-triggering Rainfall Thresholds Using an Empirical "Antecedent Daily Rainfall Model". *Pure and applied geophysics,* 157**,** 1059-1079.

Gravina, T., Figliozzi, E., Mari, N. & De Luca Tupputi Schinosa, F. 2017. Landslide risk perception in Frosinone (Lazio, Central Italy). *Landslides,* 14**,** 1419-1429.

Guzzetti, F., Carrara, A., Cardinali, M. & Reichenbach, P. 1999. Landslide hazard evaluation: a review of current techniques and their application in a multi-scale study, Central Italy. *Geomorphology,* 31**,** 181-216.

Guzzetti, F., Peruccacci, S., Rossi, M. & Stark, C. P. 2007. Rainfall thresholds for the initiation of landslides in central and southern Europe. *Meteorology and Atmospheric Physics,* 98**,** 239-267.

Guzzetti, F., Peruccacci, S., Rossi, M. & Stark, C. P. 2008. The rainfall intensity–duration control of shallow landslides and debris flows: an update. *Landslides,* 5**,** 3-17.

Havenith, H. B., Torgoev, I., Meleshko, A., Alioshin, Y., Torgoev, A. & Danneels, G. 2006. Landslides in the Mailuu-Suu Valley, Kyrgyzstan—Hazards and Impacts. *Landslides,* 3**,** 137-147.

Hawkins, E. & Sutton, R. 2009. The potential to narrow uncertainty in regional climate predictions. *Bulletin of the American Meteorological Society,* 90**,** 1095-1108.

Hayhoe, K., Edmonds, J., Kopp, R. E., LeGrande, A. N., Sanderson, B. M., Wehner, M. F. & Wuebbles, D. J. 2017. Climate models, scenarios, and projections. *In:* WUEBBLES, D. J., FAHEY, D. W., HIBBARD, K. A., DOKKEN, D. J., STEWART, B. C. & MAYCOCK, T. K. (eds.) *Climate Science Special Report: Fourth National Climate Assessment, Volume I.* Washington, DC, USA: U.S. Global Change Research Program.

Hess, P. & Brezowsky, H. 1952. Berichte des Deutschen Wetterdienst in der US-Zone 33. *Katalog der Großwetterlagen Europas*.

Hess, P. & Brezowsky, H. 1969. Katalog der Grosswetterlagen Europas, 2. neubearbeitete und ergänzte Aufl *Berichte des Deutschen Wetterdienstes 113. Bd. 15, Deutscher Wetterdienst, Offenbach am Main*.

Hong, Y., Hiura, H., Shino, K., Sassa, K., Suemine, A., Fukuoka, H. & Wang, G. J. L. 2005. The influence of intense rainfall on the activity of large-scale crystalline schist landslides in Shikoku Island, Japan. 2**,** 97-105.

Hosmer, D. & Lemeshow, S. 2000. *Applied Logistic Regression,* New York, John Wiley & Sons, Inc.

Huang, A., Zhou, Y., Zhang, Y., Huang, D., Zhao, Y. & Wu, H. 2014. Changes of the Annual Precipitation over Central Asia in the Twenty-First Century Projected by Multimodels of CMIP5. *Journal of Climate,* 27**,** 6627-6646.

Huang, J., Ju, N. P., Liao, Y. J. & Liu, D. D. 2015. Determination of rainfall thresholds for shallow landslides by a probabilistic and empirical method. *Nat. Hazards Earth Syst. Sci.,* 15**,** 2715-2723.

Huggel, C., Khabarov, N., Korup, O. & Obersteiner, M. 2012. Physical impacts of climate change on landslide occurrence and related adaptation. *In:* CLAGUE, J. J. & STEAD, D. (eds.) *Landslides, Types, Mechanisms and Modelling*.: Cambridge University Press, Cambridge UK, 121-133.

Huggel, C., Salzmann, N., Allen, S., Caplan-Auerbach, J., Fischer, L., Haeberli, W., Larsen, C., Schneider, D. & Wessels, R. 2010. Recent and future warm extreme events and high-mountain slope stability. *Philosophical Transactions*

of the Royal Society A: Mathematical, Physical and Engineering Sciences, 368**,** 2435-2459.

Hughes, M., Mahoney, K. M., Neiman, P. J., Moore, B. J., Alexander, M. & Ralph, F. M. 2014. The Landfall and Inland Penetration of a Flood-Producing Atmospheric River in Arizona. Part II: Sensitivity of Modeled Precipitation to Terrain Height and Atmospheric River Orientation. 15**,** 1954-1974.

Hungr, O., Evans, S. G., Bovis, M. J. & Hutchinson, J. N. 2001. A review of the classification of landslides of the flow type. *Environmental and Engineering Geoscience,* 7**,** 221-238.

Hungr, O., Leroueil, S. & Picarelli, L. 2014. The Varnes classification of landslide types, an update. *Landslides,* 11**,** 167-194.

Hurrell, J. W. & Van Loon, H. 1997. DECADAL VARIATIONS IN CLIMATE ASSOCIATED WITH THE NORTH ATLANTIC OSCILLATION. *Climatic Change,* 36**,** 301-326.

Hutchinson, J. N. & Bhandari, R. K. 1971. Undrained Loading, A Fundamental Mechanism of Mudflows and other Mass Movements. *Géotechnique,* 21**,** 353-358.

Huth, R., Beck, C. & Kučerová, M. 2016. Synoptic-climatological evaluation of the classifications of atmospheric circulation patterns over Europe. *International Journal of Climatology,* 36**,** 2710-2726.

Ilinova, E. S. 1968. *A register of synoptic processes over Central Asia, 1935-1967 (in Russian),* Tashkent, Central Asian Hydrometeorological Scientific Research Institute.

Inagamova, S. I. 1993. *A register of synoptic processes over Central Asia, 1979-1991 (in Russian),* Tashkent, Central Asian Hydrometeorological Scientific Research Institute.

Inagamova, S. I. 2013. *A register of synoptic processes over Central Asia, 1992-2012 (in Russian),* Tashkent, Uzhydromet.

Inagamova, S. I., Mukhtarov, T. M. & Mukhtarov, S. T. 2002. *General features of synoptic processes of Central Asia (in Russian),* Tashkent, Central Asian Hydrometeorological Scientific Research Institute.

Innes, J. 1983. Debris flows. *Prog Phys Geogr 7:469–501.*

Isakova, A. Y., Trofimov, G. N. & Mamadjanova, G. 2009. Study and mapping of mudflows in Uzbekistan. *Scientific-methodological Foundations of Making the National Atlas of Uzbekistan (in Russian).*

Iverson, R. M. 2014. Debris flows: behaviour and hazard assessment. 30**,** 15-20.

Jibson, R. W. 1989. Debris flows in southern Puerto Rico. *Landslide processes of the eastern United States Puerto Rico, Geological Society of America special paper,* 236**,** 29-55.

Jones, C. D., Hughes, J. K., Bellouin, N., Hardiman, S. C., Jones, G. S., Knight, J., Liddicoat, S., O'Connor, F. M., Andres, R. J., Bell, C., Boo, K. O., Bozzo, A.,

Butchart, N., Cadule, P., Corbin, K. D., Doutriaux-Boucher, M., Friedlingstein, P., Gornall, J., Gray, L., Halloran, P. R., Hurtt, G., Ingram, W. J., Lamarque, J. F., Law, R. M., Meinshausen, M., Osprey, S., Palin, E. J., Parsons Chini, L., Raddatz, T., Sanderson, M. G., Sellar, A. A., Schurer, A., Valdes, P., Wood, N., Woodward, S., Yoshioka, M. & Zerroukat, M. 2011. The HadGEM2-ES implementation of CMIP5 centennial simulations. *Geosci. Model Dev.,* 4**,** 543-570.

Jones, P. D., Harpham, C. & Briffa, K. R. 2013. Lamb weather types derived from reanalysis products. *International Journal of Climatology,* 33**,** 1129-1139.

Jones, P. D., Hulme, M. & Briffa, K. R. 1993. A comparison of Lamb circulation types with an objective classification scheme. *International Journal of Climatology,* 13**,** 655-663.

Jones, P. D., Osborn, T. J., Harpham, C. & Briffa, K. R. 2014. The development of Lamb weather types: from subjective analysis of weather charts to objective approaches using reanalyses. *Weather,* 69**,** 128-132.

Juliev, M., Mergili, M., Mondal, I., Nurtaev, B., Pulatov, A. & Hübl, J. 2019. Comparative analysis of statistical methods for landslide susceptibility mapping in the Bostanlik District, Uzbekistan. *Science of The Total Environment,* 653**,** 801-814.

Juliev, M., Pulatov, A. & Hübl, J. 2017. *Natural hazards in mountain regions of Uzbekistan: A review of mass movement processes in Tashkent province*.

Karpov, P. M. & Pushkarenko, V. P. 1968. Geological zonation of mudflow areas in the river basins of Uzbekistan. *Conference proceedings (in Russian).* Samarkand.

Karpov, P. M., Pushkarenko, V. P., Umarov, A. Y. & Xodjayev, S. K. 1976. *Mudflow hazards in Uzbekistan,* Tashkent, Fan, 134 page. (in Russian).

Keefer, D. K., Wilson, R. C., Mark, R. K., Brabb, E. E., Brown III, W. M., Ellen, S. D., Harp, E. L., Wieczorek, G. F., Alger, C. S. & Zatkin, R. S. 1987. Real-time landslide warning during heavy rainfall. *Science,* 238**,** 921-926.

Kendon, E. J., Ban, N., Roberts, N. M., Fowler, H. J., Roberts, M. J., Chan, S. C., Evans, J. P., Fosser, G. & Wilkinson, J. M. 2017. Do Convection-Permitting Regional Climate Models Improve Projections of Future Precipitation Change? 98**,** 79-93.

Kendon, E. J., Roberts, N. M., Fowler, H. J., Roberts, M. J., Chan, S. C. & Senior, C. A. 2014. Heavier summer downpours with climate change revealed by weather forecast resolution model. *Nature Climate Change,* 4**,** 570.

Khan, Y. A., Lateh, H., Baten, M. A. & Kamil, A. A. 2012. Critical antecedent rainfall conditions for shallow landslides in Chittagong City of Bangladesh. *Environmental Earth Sciences,* 67**,** 97-106.

Kim, H. J., Sidle, R. C., Moore, R. D. & Hudson, R. 2004. Throughflow variability during snowmelt in a forested mountain catchment, coastal British Columbia, Canada. *Hydrological Processes,* 18**,** 1219-1236.

Knutti, R. & Sedláček, J. 2012. Robustness and uncertainties in the new CMIP5 climate model projections. *Nature Climate Change,* 3**,** 369.

Knutti, R., Sedláček, J., Sanderson, B. M., Lorenz, R., Fischer, E. M. & Eyring, V. 2017. A climate model projection weighting scheme accounting for performance and interdependence. 44**,** 1909-1918.

Kudishkin, V. A., Trofimov, G. N., Bondar, V. A. & Ashurbayev, B. A. 1967. Catalogue of mudflow hazards river basins in Kazakhstan, Central Asia and Eastern Siberia. *In:* KAZNIGMI (ed.). Alma-Ata

Kumar, D., Arya, D. S., Murumkar, A. R. & Rahman, M. M. 2014. Impact of climate change on rainfall in Northwestern Bangladesh using multi-GCM ensembles. *International Journal of Climatology,* 34**,** 1395-1404.

Kurbatkin, V. P. 2009. *The Role of the geographical features of Central Asia for the formation of precipitation processes,* Tashkent, Uzhymet.

Kure, S., Jang, S., Ohara, N., Kavvas, M. L. & Chen, Z. Q. 2013. Hydrologic impact of regional climate change for the snowfed and glacierfed river basins in the Republic of Tajikistan: hydrological response of flow to climate change. *Hydrological Processes,* 27**,** 4057-4070.

Laaidi, K. 2001. Predicting days of high allergenic risk during Betula pollination using weather types. *International Journal of Biometeorology,* 45**,** 124-132.

Lamb, H. H. 1972. *British Isles Weather Types and a Register of the Daily Sequence of Circulation Patterns, 1861–1971,* London HMSO.

Lee, C. C. 2015. A systematic evaluation of the lagged effects of spatiotemporally relative surface weather types on wintertime cardiovascular-related mortality across 19 US cities. *International Journal of Biometeorology,* 59**,** 1633-1645.

Lenderink, G., Buishand, A. & van Deursen, W. 2007. Estimates of future discharges of the river Rhine using two scenario methodologies: direct versus delta approach. *Hydrol. Earth Syst. Sci.,* 11**,** 1145-1159.

Linderson, M.-L. 2001. Objective classification of atmospheric circulation over southern Scandinavia. *International Journal of Climatology,* 21**,** 155-169.

Lioubimtseva, E. & Henebry, G. 2009. *Climate and environmental change in arid Central Asia: Impacts, vulnerability, and adaptations*.

Longfield, S. A. & Macklin, M. G. 1999. The influence of recent environmental change on flooding and sediment fluxes in the Yorkshire Ouse basin. *Hydrological Processes,* 13**,** 1051-1066.

Lorenzo, M. N., Taboada, J. J. & Gimeno, L. 2008. Links between circulation weather types and teleconnection patterns and their influence on precipitation

patterns in Galicia (NW Spain). *International Journal of Climatology,* 28**,** 1493-1505.

Lyakhovskaya, L. F. 1989. *Mudflow hazards and its short-term forecasting in the piedmont areas of Uzbekistan (in Russian).* Dissertation on the candidate of Geographical Sciences, Central Asian Hydrometeorological Scientific Research Institute.

Ma, C., Wang, Y., Hu, K., Du, C. & Yang, W. 2017. Rainfall intensity–duration threshold and erosion competence of debris flows in four areas affected by the 2008 Wenchuan earthquake. *Geomorphology,* 282**,** 85-95.

Malsy, M., Aus der Beek, T., Eisner, S. & Flörke, M. 2012. Climate change impacts on Central Asian water resources. *Adv. Geosci.,* 32**,** 77-83.

Mannig, B., Müller, M., Starke, E., Merkenschlager, C., Mao, W., Zhi, X., Podzun, R., Jacob, D. & Paeth, H. 2013. Dynamical downscaling of climate change in Central Asia. *Global and Planetary Change,* 110**,** 26-39.

Maraun, D., Wetterhall, F., Ireson, A. M., Chandler, R. E., Kendon, E. J., Widmann, M., Brienen, S., Rust, H. W., Sauter, T., Themeßl, M., Venema, V. K. C., Chun, K. P., Goodess, C. M., Jones, R. G., Onof, C., Vrac, M. & Thiele-Eich, I. 2010. Precipitation downscaling under climate change: Recent developments to bridge the gap between dynamical models and the end user. *Reviews of Geophysics,* 48**,** n/a-n/a.

Maraun, D. & Widmann, M. 2018. *Statistical Downscaling and Bias Correction for Climate Research,* Cambridge, Cambridge University Press.

Marques, R., Zêzere, J., Trigo, R., Gaspar, J. & Trigo, I. 2008. Rainfall patterns and critical values associated with landslides in Povoação County (São Miguel Island, Azores): relationships with the North Atlantic Oscillation. *Hydrological Processes,* 22**,** 478-494.

Martin, G. M., Bellouin, N., Collins, W. J., Culverwell, I. D., Halloran, P. R., Hardiman, S. C., Hinton, T. J., Jones, C. D., McDonald, R. E., McLaren, A. J., O'Connor, F. M., Roberts, M. J., Rodriguez, J. M., Woodward, S., Best, M. J., Brooks, M. E., Brown, A. R., Butchart, N., Dearden, C., Derbyshire, S. H., Dharssi, I., Doutriaux-Boucher, M., Edwards, J. M., Falloon, P. D., Gedney, N., Gray, L. J., Hewitt, H. T., Hobson, M., Huddleston, M. R., Hughes, J., Ineson, S., Ingram, W. J., James, P. M., Johns, T. C., Johnson, C. E., Jones, A., Jones, C. P., Joshi, M. M., Keen, A. B., Liddicoat, S., Lock, A. P., Maidens, A. V., Manners, J. C., Milton, S. F., Rae, J. G. L., Ridley, J. K., Sellar, A., Senior, C. A., Totterdell, I. J., Verhoef, A., Vidale, P. L. & Wiltshire, A. 2011. The HadGEM2 family of Met Office Unified Model climate configurations. *Geosci. Model Dev.,* 4**,** 723-757.

McGee, W. J. 1896. Sheetflood Erosion. *GSA Bulletin,* 8**,** 87-112.

Melillo, M., Brunetti, M. T., Peruccacci, S., Gariano, S. L. & Guzzetti, F. 2016. Rainfall thresholds for the possible landslide occurrence in Sicily (Southern Italy)

based on the automatic reconstruction of rainfall events. *Landslides,* 13**,** 165-172.

Michelangeli, P.-A., Vautard, R. & Legras, B. 1995. Weather Regimes: Recurrence and Quasi Stationarity. *Journal of the Atmospheric Sciences,* 52**,** 1237-1256.

Mul'tanovski, B. P. 1933. *The synoptic method of long-term weather forecasting. (in Russian),* Moscow : Izdatel'stvo CUEGMS, 140pp.

Niyazov, R. & Nurtaev, B. 2014. Landslides of Liquefaction Caused by Single Source of Impact Pamir-Hindu Kush Earthquakes in Central Asia. *In:* SASSA, K., CANUTI, P. & YIN, Y. (eds.) *Landslide Science for a Safer Geoenvironment: Volume 3: Targeted Landslides.* Cham: Springer International Publishing.

Niyazov, R. A. & Nurtaev, B. S. 2013. Evaluation of Landslides in Uzebekistan Caused by the Joint Impact of Precipitation and Deep-focus Pamir-Hindu Earthquakes. *In:* SASSA, K., ROUHBAN, B., BRICEÑO, S., MCSAVENEY, M. & HE, B. (eds.) *Landslides: Global Risk Preparedness.* Berlin, Heidelberg: Springer Berlin Heidelberg.

Nobles, L. H. & Sharp, R. P. 1953. Mudflow of 1941 at Wrightwood, Southern California. *GSA Bulletin,* 64**,** 547-560.

Ozturk, T., Altinsoy, H. A., Türkeș, M. & Kurnaz, M. L. 2012. Simulation of temperature and precipitation climatology for the Central Asia CORDEX domain using RegCM 4.0. *Climate Research,* 52**,** 63-76.

Ozturk, T., Turp, M. T., Türkeş, M. & Kurnaz, M. L. 2017. Projected changes in temperature and precipitation climatology of Central Asia CORDEX Region 8 by using RegCM4.3.5. *Atmospheric Research,* 183**,** 296-307.

Parker, W. S. 2006. Understanding pluralism in climate modeling. *Foundations of Science,* 11**,** 349-368.

Pattison, I. & Lane, S. N. 2012. The relationship between Lamb weather types and long-term changes in flood frequency, River Eden, UK. *International Journal of Climatology,* 32**,** 1971-1989.

Perov, V. F. 2012. *Selevedenie (in Russian)*, Moscow State University Press. 274 page.

Petrov, M. A., Sabitov, T. Y., Tomashevskaya, I. G., Glazirin, G. E., Chernomorets, S. S., Savernyuk, E. A., Tutubalina, O. V., Petrakov, D. A., Sokolov, L. S., Dokukin, M. D., Mountrakis, G., Ruiz-Villanueva, V. & Stoffel, M. 2017. Glacial lake inventory and lake outburst potential in Uzbekistan. *Science of The Total Environment,* 592**,** 228-242.

Polonsky, A., Basharin, D., Voskresenskaya, E., Worley, S. & Yurovsky, A. 2004. Relationship between the North Atlantic oscillation, Euro-Asian climate anomalies and Pacific variability. *Pacific Oceanography,* 2**,** 52-66.

Prior, D. B., Suhayda, J. N., Lu, N. Z., Bornhold, B. D., Keller, G. H., Wiseman, W. J., Wright, L. D. & Yang, Z. S. 1989. Storm wave reactivation of a submarine landslide. *Nature,* 341**,** 47-50.

Prudhomme, C. & Genevier, M. 2011. Can atmospheric circulation be linked to flooding in Europe? *Hydrological Processes,* 25**,** 1180-1190.

R Core Team 2017. *R: A language and environment for statistical computing. R Foundation for Statistical Computing,* Vienna, Austria.

Radchenko, I., Dernedde, Y., Mannig, B., Frede, H.-G. & Breuer, L. 2017. Climate change impacts on runoff in the Ferghana Valley (Central Asia). *Water Resources,* 44**,** 707-730.

Ralph, F. M., Neiman, P. J., Wick, G. A., Gutman, S. I., Dettinger, M. D., Cayan, D. R. & White, A. B. 2006. Flooding on California's Russian River: Role of atmospheric rivers. 33.

Ramos, A., Trigo, R., Tomé, R. & Liberato, M. 2018. Impacts of Atmospheric Rivers in Extreme Precipitation on the European Macaronesian Islands. *Atmosphere,* 9**,** 325.

Ramos, A. M., Cortesi, N. & Trigo, R. M. 2014. Circulation weather types and spatial variability of daily precipitation in the Iberian Peninsula. *Frontiers in Earth Science,* 2.

Raziei, T., Mofidi, A., Santos, J. A. & Bordi, I. 2012. Spatial patterns and regimes of daily precipitation in Iran in relation to large-scale atmospheric circulation. *International Journal of Climatology,* 32**,** 1226-1237.

Rebelo, L., Ramos, M. A., Pereira, S. & Trigo, M. R. 2018. Meteorological Driving Mechanisms and Human Impacts of the February 1979 Extreme Hydro-Geomorphological Event in Western Iberia. *Water,* 10.

Reyer, C. P. O., Otto, I. M., Adams, S., Albrecht, T., Baarsch, F., Cartsburg, M., Coumou, D., Eden, A., Ludi, E., Marcus, R., Mengel, M., Mosello, B., Robinson, A., Schleussner, C.-F., Serdeczny, O. & Stagl, J. 2017. Climate change impacts in Central Asia and their implications for development. *Regional Environmental Change,* 17**,** 1639-1650.

Reyers, M., Pinto, J. G. & Paeth, H. 2013. Statistical–dynamical downscaling of present day and future precipitation regimes in the Aksu river catchment in Central Asia. *Global and Planetary Change,* 107**,** 36-49.

Rickmers, W. R. 1913. *The Duab of Turkestan: a Physiographic Sketch and Account of Some Travels,* Cambridge - 2010, Cambridge University Press.

Rosi, A., Peternel, T., Jemec-Auflič, M., Komac, M., Segoni, S. & Casagli, N. 2016. Rainfall thresholds for rainfall-induced landslides in Slovenia. *Landslides,* 13**,** 1571-1577.

Russo, A. C., Gouveia, C. M., Trigo, R. M., Liberato, M. L. R. & DaCamara, C. C. 2015. The influence of circulation weather patterns at different spatial scales on drought variability in the Iberian Peninsula. *Frontiers in Environmental Science,* 3.

Salikhova, D. H. 1975. *Aero synoptic conditions of trigerring floods in mountain rivers and prediction the floods for Fergana Valley and Kashkadarya Basin (in Russian).*

Dissertation on the candidate of Geographical Sciences, Central Asian Hydrometeorological Scientific Research Institute.

Santos, J. A., Belo-Pereira, M., Fraga, H. & Pinto, J. G. 2016. Understanding climate change projections for precipitation over western Europe with a weather typing approach. *Journal of Geophysical Research: Atmospheres,* 121**,** 1170-1189.

Sarimsakov, T. A., Giorgio, V. A. & Bugayev, V. A. 1947. Statistical characteristics of synoptic situations for the cold period over the Central Asia (in Russian). *Newsletter of USSR Academy of Science,* 6**,** 451-464.

Schiemann, R., Lüthi, D., Vidale, P. L. & Schär, C. 2008. The precipitation climate of Central Asia—intercomparison of observational and numerical data sources in a remote semiarid region. *International Journal of Climatology,* 28**,** 295-314.

Schmidli, J., Frei, C. & Vidale, P. L. 2006. Downscaling from GCM precipitation: a benchmark for dynamical and statistical downscaling methods. *International Journal of Climatology,* 26**,** 679-689.

Schmidt, M. & Dehn, M. 2000. Examining Links between Climate Change and Landslide Activity Using GCMS. *In:* MCLAREN, S. J. & KNIVETON, D. R. (eds.) *Linking Climate Change to Land Surface Change.* Dordrecht: Springer Netherlands.

Schmidt, M. & Glade, T. 2003. Linking global circulation model outputs to regional geomorphic models: a case study of landslide activity in New Zealand. *Climate Research,* 25**,** 135-150.

Scoccimarro, E., Gualdi, S., Bellucci, A., Sanna, A., Fogli, P. G., Manzini, E., Vichi, M., Oddo, P. & Navarra, A. 2011. Effects of Tropical Cyclones on Ocean Heat Transport in a High-Resolution Coupled General Circulation Model. *Journal of Climate,* 24**,** 4368-4384.

Sheridan, S. C. 2002. The redevelopment of a weather-type classification scheme for North America. *International Journal of Climatology,* 22**,** 51-68.

Shresta, M. 2015. Data analysis relied on Power Transformation of rainfall bias correction (V.2.0) Microsoft Excel file.

Sidle, R. C. & Ochiai, H. 2006. *Landslides: processes, prediction, and land use,* Washington, DC, American Geophysical Union.

Small, E. E., Giorgi, F. & Sloan, L. C. 1999. Regional climate model simulation of precipitation in central Asia: Mean and interannual variability. *Journal of Geophysical Research: Atmospheres (1984–2012),* 104**,** 6563-6582.

Smid, M. & Costa, A. C. 2018. Climate projections and downscaling techniques: a discussion for impact studies in urban systems. *International Journal of Urban Sciences,* 22**,** 277-307.

Sommer, R., Glazirina, M., Yuldashev, T., Otarov, A., Ibraeva, M., Martynova, L., Bekenov, M., Kholov, B., Ibragimov, N., Kobilov, R., Karaev, S., Sultonov, M., Khasanova, F., Esanbekov, M., Mavlyanov, D., Isaev, S., Abdurahimov, S., Ikramov, R., Shezdyukova, L. & de Pauw, E. 2013. Impact of climate change

on wheat productivity in Central Asia. *Agriculture, Ecosystems & Environment,* 178**,** 78-99.

Sorg, A., Bolch, T., Stoffel, M., Solomina, O. & Beniston, M. 2012. Climate change impacts on glaciers and runoff in Tien Shan (Central Asia). *Nature Clim. Change,* 2**,** 725-731.

Sorg, A., Huss, M., Rohrer, M. & Stoffel, M. 2014. The days of plenty might soon be over in glacierized Central Asian catchments. *Environmental Research Letters,* 9**,** 104018.

Stucki, P., Rickli, R., Brönnimann, S., Martius, O., Wanner, H., Grebner, D. & Luterbacher, J. 2012. Weather patterns and hydro-climatological precursors of extreme floods in Switzerland since 1868. *Meteorologische Zeitschrift,* 21**,** 531-550.

Szabó, J. 2003. The relationship between landslide activity and weather: examples from Hungary. *Nat. Hazards Earth Syst. Sci.,* 3**,** 43-52.

Takahashi, T. 2007. *Debris Flow: Mechanics, Prediction and Countermeasures*, Taylor & Francis, London.

Taylor, K. E., Stouffer, R. J. & Meehl, G. A. 2012. An Overview of CMIP5 and the Experiment Design. *Bulletin of the American Meteorological Society,* 93**,** 485-498.

Teale, N. G., Quiring, S. M. & Ford, T. W. 2017. Association of synoptic-scale atmospheric patterns with flash flooding in watersheds of the New York City water supply system. *International Journal of Climatology,* 37**,** 358-370.

Teutschbein, C. & Seibert, J. 2012. Bias correction of regional climate model simulations for hydrological climate-change impact studies: Review and evaluation of different methods. *Journal of Hydrology,* 456-457**,** 12-29.

Trigo, R. M. & DaCamara, C. C. 2000. Circulation weather types and their influence on the precipitation regime in Portugal. *International Journal of Climatology,* 20**,** 1559-1581.

Trofimov, G. N. 2006. *Mudflows in Uzbekistan, prediction of catastrophic failure and repeatability of mudflows in the region under climate changes and adaptation measures (in Russian).* National University of Uzbekistan.

Trzaska, S. & Schnarr, E. 2014. A review of downscaling methods for climate change projections. *United States Agency for International Development by Tetra Tech ARD*, 1-42.

Tulyaganov, S. H. 1988. *Formation of mudflows and calculation of the main characteristics of mudflows in the piedmount zone of the Fergana Valley* Doctoral dissertation (in Russian), MGMI.

UN 2017. World Population Prospects: The 2017 Revision, Key Findings and Advance Tables. Working Paper No. ESA/P/WP/248**,** 46.

Vallorani, R., Bartolini, G., Betti, G., Crisci, A., Gozzini, B., Grifoni, D., Iannuccilli, M., Messeri, A., Messeri, G., Morabito, M. & Maracchi, G. 2018. Circulation

type classifications for temperature and precipitation stratification in Italy. *International Journal of Climatology,* 38**,** 915-931.

Van Bebber, W. J. & Köppen, W. 1895. *Die Isobarentypen des Nordatlantischen Ozeans und Westeuropas, ihre Beziehung zur Lage und Bewegung der Barometrischer Maxima und Minima. Archiv deutsch. Seewarte.,* Hamburg, 18(4), 27pp.

Vanos, J. K., Kalkstein, L. S. & Sanford, T. J. 2015. Detecting synoptic warming trends across the US Midwest and implications to human health and heat-related mortality. *International Journal of Climatology,* 35**,** 85-96.

Varnes, D. J. 1958. Landslide types and processes. *Landslides and engineering practice,* 24**,** 20-47.

Voldoire, A., Sanchez-Gomez, E., Salas y Mélia, D., Decharme, B., Cassou, C., Sénési, S., Valcke, S., Beau, I., Alias, A., Chevallier, M., Déqué, M., Deshayes, J., Douville, H., Fernandez, E., Madec, G., Maisonnave, E., Moine, M.-P., Planton, S., Saint-Martin, D., Szopa, S., Tyteca, S., Alkama, R., Belamari, S., Braun, A., Coquart, L. & Chauvin, F. 2013. The CNRM-CM5.1 global climate model: description and basic evaluation. *Climate Dynamics,* 40**,** 2091-2121.

Voynova, T. A. & Inagamova, S. I. 1982. *A register of synoptic processes over Central Asia, 1968-1978 (in Russian),* Tashkent, Central Asian Hydrometeorological Scientific Research Institute.

Watanabe, S., Hajima, T., Sudo, K., Nagashima, T., Takemura, T., Okajima, H., Nozawa, T., Kawase, H., Abe, M., Yokohata, T., Ise, T., Sato, H., Kato, E., Takata, K., Emori, S. & Kawamiya, M. 2011. MIROC-ESM 2010: model description and basic results of CMIP5-20c3m experiments. *Geosci. Model Dev.,* 4**,** 845-872.

White, C. J., Tanton, T. W. & Rycroft, D. W. 2014. The Impact of Climate Change on the Water Resources of the Amu Darya Basin in Central Asia. *Water Resources Management,* 28**,** 5267-5281.

Wieczorek, G. F. & Glade, T. 2005. Climatic factors influencing occurrence of debris flows. *Debris-flow Hazards and Related Phenomena.* Berlin, Heidelberg: Springer Berlin Heidelberg.

Wilby, R. L. & Wigley, T. M. L. 2000. Precipitation predictors for downscaling: observed and general circulation model relationships. *International Journal of Climatology,* 20**,** 641-661.

Wilby, R. L., Wigley, T. M. L., Conway, D., Jones, P. D., Hewitson, B. C., Main, J. & Wilks, D. S. 1998. Statistical downscaling of general circulation model output: A comparison of methods. *Water Resources Research,* 34**,** 2995-3008.

Wilks, D. S. 2011. *Statistical methods in the atmospheric sciences,* Academic press.

Wu, T., Song, L., Li, W., Wang, Z., Zhang, H., Xin, X., Zhang, Y., Zhang, L., Li, J., Wu, F., Liu, Y., Zhang, F., Shi, X., Chu, M., Zhang, J., Fang, Y., Wang, F., Lu, Y., Liu, X., Wei, M., Liu, Q., Zhou, W., Dong, M., Zhao, Q., Ji, J., Li, L. & Zhou, M. 2014. An overview of BCC climate system model development and

application for climate change studies. *Journal of Meteorological Research,* 28**,** 34-56.

Xenarios, S., Gafurov, A., Schmidt-Vogt, D., Sehring, J., Manandhar, S., Hergarten, C., Shigaeva, J. & Foggin, M. 2018. Climate change and adaptation of mountain societies in Central Asia: uncertainties, knowledge gaps, and data constraints. *Regional Environmental Change,* 10.1007/s10113-018-1384-9.

Yamao, M., Sidle, R. C., Gomi, T. & Imaizumi, F. 2016. Characteristics of landslides in unwelded pyroclastic flow deposits, southern Kyushu, Japan. *Nat. Hazards Earth Syst. Sci.,* 16**,** 617-627.

Yincan, Y. & et al. 2017. Chapter 6 - Submarine Landslides. *In:* YINCAN, Y. & ET AL. (eds.) *Marine Geo-Hazards in China.* Elsevier.

Zanchettin, D., Rubino, A., Matei, D., Bothe, O. & Jungclaus, J. H. 2013. Multidecadal-to-centennial SST variability in the MPI-ESM simulation ensemble for the last millennium. *Climate Dynamics,* 40**,** 1301-1318.

Zêzere, J. & Rodrigues, M. 2002. Rainfall thresholds for landsliding in Lisbon Area (Portugal). *Rybar J, Stemberk J, Wagner P(eds) Landslides***,** 333-338.

Zêzere, J. L., Trigo, R. M. & Trigo, I. F. 2005. Shallow and deep landslides induced by rainfall in the Lisbon region (Portugal): assessment of relationships with the North Atlantic Oscillation. *Nat. Hazards Earth Syst. Sci.,* 5**,** 331-344.

Zhao, Y., Yu, X., Yao, J. & Dong, X. 2018. Evaluation of the subtropical westerly jet and its effects on the projected summer rainfall over central Asia using multi-CMIP5 models. *International Journal of Climatology,* 10.1002/joc.5443**,** n/a-n/a.

Žic, E., Arbanas, Ž., Bićanić, N. & Ožanić, N. 2015. A model of mudflow propagation downstream from the Grohovo landslide near the city of Rijeka (Croatia). *Nat. Hazards Earth Syst. Sci.,* 15**,** 293-313.

Zorita, E. & Storch, H. v. 1999. The Analog Method as a Simple Statistical Downscaling Technique: Comparison with More Complicated Methods. *Journal of Climate,* 12**,** 2474-2489.